EVOLUTION OF FIRE INDUCED RESTRAINT FORCES AND THEIR EFFECT ON THE FIRE RESPONSE OF PRESTRESSED CONCRETE BEAMS

By

Puneet Kumar

A DISSERTATION

Submitted to
Michigan State University
in partial fulfillment of the requirements
for the degree of

Civil Engineering – Doctor of Philosophy

2023

ABSTRACT

Precast prestressed concrete (PC) construction provides numerous advantages over traditional reinforced concrete (RC) construction, in terms of speed of construction, better quality control, cost-effectiveness, better space utilization, and optimized production. Owing to these advantages, the use of PC construction in the built environment has increased significantly in recent decades. While the structural behavior of PC members is well understood at ambient temperatures, there is a lack of understanding on the evolution of fire induced restraint forces in PC beams and their effect on the fire resistance of PC beams. Further, the fire resistance of PC members is currently evaluated using prescriptive design approaches which do not account for all critical factors governing the fire response of PC beams, including realistic restraint conditions, and therefore, current fire resistance provisions may not provide realistic predictions of fire performance.

Therefore, a detailed experimental and numerical study is conducted to evaluate the evolution of fire induced restraint forces and to quantify their effect on the fire response of PC beams. Fire resistance tests were conducted on four PC beams under restrained and unrestrained end conditions. Test variables included fire exposure, restraint conditions, load level, and concrete strength. The fire response of the beams was traced throughout the fire exposure duration by measuring sectional temperatures, beam deflections, and fire induced restraint forces. All four beams were designed as per current building code recommendations to have a fire resistance of 4 hours, however, all four beams attained failure within 2 hours of fire exposure. A numerical model was developed for tracing the fire response of PC beams under specified fire, loading, and restraint conditions. The model accounts for critical factors governing the fire response of PC beams including fire-induced restraint forces, cracking and crushing of concrete, spalling, material and geometric non-linearity, and geometry of the beam. For modeling fire-induced restraint forces a

new efficient spring idealization framework for connections is implemented. Also, the cracking and crushing of concrete is captured by developing a new modified adaptive temperature-dependent failure envelope.

The developed numerical model was validated by comparing response predictions from the model with measured data in fire tests. Results from these comparisons show that the model can capture the fire response of PC beams with reasonable accuracy in both thermal and structural domains. The validated numerical model is applied to carry out a series of parametric studies on the effect of fire-induced restraint forces on the response of PC beams. The effect of cross-sectional shape, support conditions, the gap in connection, level of prestress, and concrete cover thickness on the evolution of fire induced restraint forces is studied for PC and equivalent RC beams. Results from parametric studies show that current prescriptive codes and standards may over-predict fire resistance of PC beams by as high as 100%, PC beams develop 5% to 20% lower restraint forces than equivalent RC beams, and for PC beams with gaps of more than 50 mm experience minimal restraint forces. Also, the fire-induced restraint forces can be either beneficial or detrimental and can significantly alter the fire response of the PC beam, and therefore, should be included in the design process. Based on the results from the fire tests and parametric studies, simplified recommendations are proposed for evaluating the fire resistance of PC beams.

Dedicated to all lives lost to fire.

ACKNOWLEDGEMENTS

I would like to express my deepest gratitude to my Ph.D. advisor, Dr. Venkatesh Kodur for his invaluable guidance, constant support, and encouragement. He has continuously supported me to achieve my academic and professional goals, and I truly appreciate his wisdom and advice. Also, I want to sincerely thank the members of my committee Dr. Weiyi Lu, Dr. Roozbeh Dargazany, and Dr. Andre Benard for their insightful comments, suggestions, guidance, and support.

I would like to thank my peers and friends; Mohannad Naser, Svetha Venkatachari, Ankit Agrawal, Saleh Alogla, Pratik Bhatt, Roya Solhmirzaei, Shrishti Banerji, Augusto Gil, and Derek Hibner for their help and support. I would like to express my gratefulness to Charles Meddaugh, Siavosh Ravanbakhsh, and Brian Gietzel for their support and kindness during the fire tests in the laboratory. I would like to thank Laura Post, Laura Taylor, Margaret Conner, and Bailey Weber for their administrative assistance. I am grateful for the support from the Department of Civil and Environmental Engineering and the College of Engineering for providing several resources during my graduate studies. In addition, I acknowledge the funding from PCI Jenny P fellowship which allowed me to pursue this thesis. Also, I would like to thank Kerkstra Precast Inc. for allowing me to fabricate PC beams at their plant and helping me throughout the fabrication and shipping process. Last but not the least, I would like to thank my family, for years of patience, love, unwavering support, and encouragement.

TABLE OF CONTENTS

CHAPTER 1

1 Introduction

1.1 General

Precast prestressed concrete (PC) is a new form of construction utilizing concrete and high strength steel strands which is highly efficient and economical in buildings and bridge applications. PC members are fabricated in factory under controlled conditions (precast) as per design requirements, are shipped to the construction site after curing (typically 28 days) and are then assembled on site using cranes to construct buildings at rapid speeds. This has many benefits over traditional concrete construction which utilizes reinforced concrete (RC), where steel reinforcement is assembled in formworks on site as per design requirements, and the concrete is poured into the formwork on site. Since concrete curing is done on site, the construction of higher floors cannot be started till the floors below have attained required strength, thus, making it relatively slower construction process as compared to PC construction. Also, due to high strength of prestressing steel strands (ultimate tension strength of 1860 MPa) and prestressing technique used in PC construction, often much smaller member size is needed to resist the same level of load as compared to a RC structural

member. This leads to a better space utilization, reduces the cost of construction, and faster construction times.

Owing to these advantages, use of PC construction in buildings has increased in recent decades. However, there is relatively limited studies on realistic fire behavior of PC members as compared to RC counterparts. Due to different characteristics of PC members, the fire response of PC members is different from that of RC members. Further, the severity of fires has increased in modern buildings due to high level of combustible contents and open concept architecture. In the past two decades, a total of 104.2 million fire incidents have caused more than 1.1 million fire deaths [1], and total annual loss from global fire hazard accounts for about 1% of the world GDP [2] (approximately $961 billion US dollars [3]).

Therefore, with rising severity of fires and increasing use of PC construction in recent decades, it is critical to develop a good understanding on the response of PC members under realistic fire, loading, and restraint conditions. Specially, there is a lack of comprehensive understanding on the effect of restraint on fire resistance of PC beams. To address this, a numerical and experimental study is undertaken herein to evaluate the influence of fire induced restraint forces on fire response of PC beams which can allow designers to account for complex fire behavior of PC beams; thus, improving fire safety in PC buildings.

1.2 Behavior of concrete beams under fire exposure

In buildings, beams are an integral part of moment frame systems for facilitating the load transfer from slabs (or floor systems) to columns. Under fire exposure, sectional temperatures within RC and PC beams increases due to heat transfer between fire and beam (convective and radiative heat transfer) and within beam itself (conduction heat transfer). This heat transfer is primarily governed by thermal properties (thermal conductivity, specific heat, density etc.) of concrete and

reinforcement which vary significantly at elevated temperatures [4]. Variation in fire temperatures and thermal properties at elevated temperatures lead to highly non-linear sectional temperatures within RC and PC beams throughout fire exposure duration. However, due to similar variation in thermal properties of concrete and steel reinforcement (rebars and strands) at elevated temperatures, RC and PC beams undergo a similar thermal response under same fire exposure.

On the other hand, there are significant differences in their corresponding thermo-mechanical response under fire exposure. As the sectional temperatures increase with fire exposure time, mechanical properties of concrete and reinforcement undergo a significant degradation (loss of strength, elastic modulus etc.) which causes a reduction in the strength and stiffness for both RC and PC beams. However, unlike thermal properties, mechanical properties of steel rebars (used in RC beams) and prestressing strands (used in PC beams) vary significantly differently at elevated temperatures. Prestressing strands lose their strength at a relatively rapid rate as compared to rebars (prestressing strands lose 54% of yield strength at 400^{o}C and 90% of yield strength at 600^{o}C) whereas the degradation in the elastic modulus for strands is slightly slower than in rebars, as shown in Figure 1.1. The rapid loss in strength of strands causes PC beams to lose capacity at a faster rate than as compared to equivalent RC beam. Also, the prestress in PC beams is designed to carry most of the applied moment to achieve desired camber or deflection in the beam. However, when a PC beam is exposed to fire exposure, the prestress in strands is lost due to degradation in strength and modulus of strands, and this causes a relatively faster rate of deflection in PC beams. Another factor that influences the structural response of both PC and RC beams is the fire induced restraint forces. Under fire exposure, PC and RC beams experience significant thermal expansion due to increase in thermal strains in concrete and reinforcement as a result of rising sectional temperatures. When this thermal expansion of the beam is restrained due to support conditions,

then an equivalent fire induced restraint force is developed at the beam ends. Since typical RC beams have continuous connections at ends, the restraint forces start developing from the start of fire exposure itself depending on the stiffness of the connection at ends. Whereas, for PC beams, the typical connections at ends are simply supported connections with a gap of 0 mm to 50 mm. Therefore, the restraint forces do not develop until the gap between the beam and the framing elements is overcome by thermal expansion of the PC beam. Such restraint forces can have positive or negative effect on the fire response of the PC and RC beams depending on the location of restraint relative to the centroidal axis of beam and is discussed in detail in Section 1.3.

To illustrate the differences between typical RC and PC beams under fire exposure, a comparison of deflection response in a typical simply supported PC beam and an equivalent RC beam under standard fire exposure is illustrated in Figure 1.2. Note that these results are taken from numerical studies from Chapter 6 for illustration purposes only and are discussed in detail in Chapter 6. As can be seen from Figure 1.2, the deflection response of both PC and RC beams is similar in the first 50 minutes of fire exposure, then deflections in PC beam increase at a much rapid pace and the beam undergo failure at 112 minutes. On the other hand, RC beam deflections increase at a relatively slower pace and the RC beam undergo failure at 212 minutes. It should be noted that both beams undergo similar thermal response. Therefore, beams undergo similar deflection response as long as there is not significant difference in material degradation of prestressing strands and rebars. However, as the reinforcement temperatures reach 400^{o}C, prestressing strands undergo rapid degradation in strength as compared to rebars, causing a faster failure of the PC beam at 112 minutes. Fire response of PC and RC beams under different end conditions is discussed in detail in Chapter 6.

1.3 Critical factors influencing fire response

As discussed above, PC and RC beams exhibit a highly intricate thermo-mechanical response under fire exposure, and this is due to several factors influencing the behavior. These factors include material and geometric non-linearity, material degradation, stiffness of connection, and magnitude and location of restraint force. Of these, the effect of connection stiffness and fire induced restraint forces are not well studied in the literature. Under restrained end conditions, significant restraint forces can develop at beam ends (depending on the connection stiffness) which can have both positive and/or negative effect on load carrying capacity of beam under fire exposure.

If restraint force is acting below centroidal axis of beam, then it mitigates effect of external loading on beam by inducing resistive moment in beam. Whereas, if restraint force acts above centroidal axis of beam then it adds on to applied moment on beam which exacerbates degradation in load carrying capacity. These positive and negative effects of restraint on beams are illustrated for the case of a restrained beam subjected to uniformly distributed loading and exposed to fire in Figure 1.3. Under unrestrained conditions, beam will be subjected to only sagging bending moment from applied loading which causes downward deflection in beam.

Under restrained conditions, when restraint is acting below centroidal axis, it develops a resisting (hogging) bending moment in the beam which causes upward deflection in beam, thus, countering bending moment from applied loading. This decreases the maximum bending moment at mid span from $-WL^2/8$ to $-WL^2/8 + Ry$ (see Figure 1.3(a)) where W is applied uniformly distributed load, L is clear span of beam, R is magnitude of restraint, and y is distance between restraint and centroidal axis. Whereas, when restraint is acting above centroidal axis, it causes sagging bending moment in beam which further adds on to applied bending moment and increases maximum

bending moment at mid span from $-WL^2/8$ to $-WL^2/8 - Ry$ (see Figure 1.3(b)). Therefore, effect of restraint on fire resistance of beam is directly dependent on the magnitude and location of restraint force which further adds to complexity in thermo-mechanical analysis of restrained PC and RC beams, as both magnitude and location of restraint vary throughout fire exposure.

However, the development of restraint force can be generalized into 4 stages for typical PC and RC beams, and this is illustrated in Figure 1.4. In buildings with RC beams, often continuous/flexible connections without gap are used, whereas buildings with PC beams mostly utilize simply supported (roller) connections with 0 mm to 50 mm gap between beam and connecting column. Such gaps influence the onset of fire induced restraint forces, and are therefore, important to account for in the realistic development of restraint forces. On the other hand, development of restraint is significantly different for flexible connection without gap (typical RC beams), therefore, typical evolution of restraint for both RC and PC beams is illustrated in Figure 1.4. In Figure 1.4, Stage 1 represents initial fire exposure when beam pulls inwards due to increase in deflection from material degradation and thermal expansion of beam is either less than the gap between beam and framing elements or is not significant enough to overcome material degradation.

Therefore, typical PC beams do not experience any restraint forces in this stage as there is no contact between beam and the framing elements and roller connections can only develop compressive forces only (apply force against the face of beam). It should be noted that often structural integrity joints are also provided on the top of PC beams to ensure structural stability during erection. However, these connections have minimal strength and are not designed to withstand fire exposure. Therefore, for simplicity, the structural contribution from such connections is ignored in the present generalization shown in Figure 1.4. Whereas, flexible

connections can develop both compressive and tensile forces, and therefore, develop restraint forces to counter the inward pull of the beam. It should be noted that restraint forces are marked negative if they are acting in the direction away from the face of beam (tensile forces in connection) and positive if they are acting towards the face of the beam (compressive forces in connection). Therefore, restraint forces in Stage 1 are marked negative in Figure 1.4.

Stage 2 represents growth stage as restraint force overcomes material degradation effects. Therefore, in this stage, the beam expansion is dominant, and the beam is pushing against the connection, thus, developing compressive restraint forces. This is shown by the change in restraint forces from negative in stage 1 for RC beams to positive in stage 2 and increase in compressive restraint forces for PC beam. It should be noted that the increase in the magnitude of restraint forces in this stage is primarily dependent on the fire exposure, thermal expansion of beam, connection stiffness, material properties, and beam geometry. As fire exposure progresses, material degradation becomes more prominent and causes increased mid span deflection which again causes inward pull on beam joints. Such inward pull counteracts the thermal expansion of the beam which mitigates the compressive restraint forces, and this marks decay stage of restraint, Stage 3. This can be observed by plateau of restraint force in stage 2, and then followed by decay of restraint forces for both PC and RC beams in Stage 3.

Stage 4 starts when material degradation completely overcomes thermal expansion of beam, and it causes beam ends to pull inwards again as in Stage 1, thus, making restraint negative again for RC beams and negligible for PC beams. It should be noted that beam can undergo failure at any stage when the capacity of the beam falls under applied loading. Further, it should be noted that key difference in development of restraint for roller (typical PC beam connection) and continuous/flexible connections (typical RC beams connection) is that no restraint is developed

for PC beams with roller supports in Stage 1 and Stage 4 as there is no physical contact between PC beam and framing elements in these stages. Hence, there can be significant difference in the fire behavior of PC and RC beams due to difference in type of connections. These factors are given due consideration in this study and a new approach is developed to idealize typical connections to capture realistic magnitude and location of restraint forces.

1.4 Current approaches for fire resistance assessment

The fire resistance provisions for PC and RC beams in current codes and standards (ACI, PCI, ASTM) are based on prescriptive approaches [5–7]. The tables used in prescriptive approaches are developed based on fire tests, under standard fire exposure in a furnace. Fire resistance measured from such fire tests is then converted to fire resistance rating which is defined as the fire resistance of a structural member reduced to the nearest hour or half an hour (1, 1.5, 2, 3 or 4 hour fire rating). For example, beams with fire resistance between 121 and 179 minutes are taken as 2 hours fire rated beams which is part of a conservative and simplified process for fire design. The results from standard fire tests are interpolated to similar structural members, and prescriptive guidelines have been developed in terms of minimum clear cover to main reinforcement, member dimensions, and type of concrete to achieve desired fire resistance rating. Also, there are multiple simplified rational approaches as well in various codes and standards [4], and such rational or simplified design approaches can be referred to the literature [8].

In case of restrained RC or PC beams, beam are first classified as restrained or unrestrained based on the vague qualitative guidelines from ASTM E119-18 [5] as shown in Table 1.1. Once the beam is classified as restrained or unrestrained, the prescriptive guidelines are provided in terms of required concrete cover for desired fire rating as shown in Table 1.2. It should be noted that fire resistance rating using prescriptive approach is based on strength (failure temperature in strands to

carry 50% of loading) failure criterion. For PC beams, strength criterion is applied by limiting the temperature in prestressing strands below critical temperature of 427^{o}C (temperature at which strands lose more than 50% of their strength) which is achieved by recommending minimum concrete clear cover to strands based on restraint conditions, beam dimensions, and type of concrete (calcareous, siliceous, or light weight). Therefore, restraint force effects in prescriptive based approach are accounted through a binary classification wherein PC beams are grouped as either fully restrained or unrestrained. This prescriptive classification is more qualitative than quantitative; and does not account for magnitude of restraint and its location relative to centroidal axis which are vital in determining the fire resistance of a PC beam as discussed in Section 1.3.

For example a PC structural beam is considered to be restrained if the space between the end of PC element and framing elements does not exceed 0.25% of the length for members made with normal-weight concrete and 0.10% of the length for members made with structural lightweight-aggregate or sand-lightweight concrete [6]. Similar qualitative guidelines are provided for other structural members as well; and for both PC and RC beams, restrained members are predicted to have higher fire resistance than their unrestrained counterparts by prescriptive approach based building codes [5–7]. Depending on restrained or unrestrained classification, the clear cover requirements for reinforcement are recommended to achieve a specified fire resistance rating as illustrated in Table 1.2 as per PCI manual 124 [6].

Evaluating fire resistance using prescriptive approach have numerous drawbacks which primarily include inability to account for realistic restraint and support conditions; unrealistic failure criteria; inability to account for critical factors governing fire response of PC beams; vague guidelines to classify restrained and unrestrained beams; considering only positive effect of restraint, and use of fire resistance ratings. While all these drawbacks are equally important, among these, one of the

biggest drawbacks in current prescriptive approach based codes and standards remain their assumption that restrained PC beams exhibit higher fire resistance than their unrestrained counterparts and there are no negative effects of restraint on fire resistance. For example, for a beam with width of 300 mm and clear cover of 38 mm, PCI manual 124 [6] predicts a fire resistance rating of 1 hour for unrestrained and 3 hours (200% increase) for restrained conditions as shown in Table 1.1. Therefore, this assumption alone can cause fire resistance predictions to be off by as high as 200% in cases where the level of restraint cannot be properly determined.

This significant increase in fire resistance is based on three assumptions as: (1) restraint acts below centroidal axis and therefore induces resisting moment only, (2) resisting moment arising from restraint significantly mitigates degradation in moment capacity, and (3) beam do not fail under additional stresses arising from restraint. However, due to lack of studies on PC beams under fire exposure, there is no strong experimental or numerical evidence to support these assumptions for PC beams. Further, PCI manual 124 [6] provides a rational design approach where the load carrying capacity of PC beams can determined under fire conditions by reducing the strength parameters at elevated temperatures. However, this approach does not account for magnitude and location of restraint forces.

In reality, fire behavior of PC beams can indeed be very different from RC beams under fire exposure especially due to effect of prestress, higher design loads, relatively rapid degradation of strength in strands as compared to rebars, and differences in development of restraint force due to difference in commonly used connection types in buildings employing PC and RC beams. Therefore, it is important to capture realistic fire response of PC beams specially under restrained conditions.

1.5 Research hypothesis

It is evident from the discussion above that behavior of PC beams under fire exposure is highly intricate and there is a lack of understanding on this behavior of PC beams. Currently, this behavior is oversimplified, specifically under restrained conditions, by current building codes of practice where only positive effects of restraint are considered. To overcome these knowledge gaps, it is important to establish proper understanding of thermo-mechanical behavior of PC beams under fire exposure using both numerical and experimental studies. Therefore, to close these knowledge gaps research is undertaken based on the following hypothesis:

"Significant fire induced restraint forces can develop under fire exposure, and their magnitude and location can vary throughout fire exposure. Such fire induced restraint forces can have positive or negative effect on the fire resistance of the PC beams depending on the location of the restraint force. Therefore, it is important to account for the realistic fire induced restraint forces in fire resistance assessment of PC beams."

1.6 Research objectives

This study aims to develop an understanding on the fire behavior of PC beams under fire exposure using an advanced numerical model. Special emphasis will be given to account for restraint by using non-linear springs based on generic connection idealizations developed in this study, cracking and crushing using a new adaptive failure envelope, and spalling of concrete using a new framework. As part of this study, following specific objectives will be addressed:

1. Undertake a state-of-the-art review on fire resistance of PC and RC concrete beams to identify the knowledge gaps in literature.
2. Develop a generic three-dimensional (3D) finite element (FE) based numerical model in ANSYS to trace the fire response of PC and RC in the entire fire exposure duration.

This model is to account for critical factors governing fire response of PC beams as magnitude and location of restraint, cracking and crushing of concrete, spalling, connection type and stiffness, material degradation, geometry, and realistic fire loading and restraint scenarios.

3. Conduct full scale fire tests on PC beams under different conditions to generate experimental data to validate the above developed numerical model. Sectional temperatures will be compared to validate heat transfer capabilities of the model. Most importantly, efficacy in capturing the effect of restraint will be tested by comparing deflections and restraint forces from test and model.
4. Conduct parametric studies using the validated model to quantify effect of critical factors affecting fire resistance of PC beams, specifically the variation of restraint forces in different types of beams with different combinations of connections.

1.7 Scope and outline of thesis

The scope of this study covers the fire response of all PC and RC beams under any end conditions and fire and loading scenarios. Specifically, this study provides new data on evolution of restraint forces in PC and RC beams and quantify the effect of restraint forces on fire resistance of PC and RC beams. The new connection idealization procedure developed herein can be extended for other structural members as well. The research conducted in this study is presented in seven chapters.

Chapter 1 provides a general background to the problem and status of current codes and standards. It also provides the research hypothesis and objectives of the study along with scope and outline. Chapter 2 provides a state-of-the-art review on fire response of PC and RC beams and identifies key knowledge gaps. Chapter 3 deals with the fire resistance tests conducted to understand the effect of fire induced restraint forces on PC beams and develop required experimental data to

validate the numerical model. Also, a detailed discussion is provided on the experiment design, instrumentation, methodology, and trends in results.

Chapter 4 provides the details on the numerical model from a new procedure to idealize connections using springs to efficiently capture realistic restraint forces and their location to all discretization and analysis details. A detailed analysis procedure is provided along with a flow chart to help researchers implement numerical model in their studies. Then results from Chapter 3 and results from fire tests on RC beams from literature are used to validate the developed numerical model developed in Chapter 4, and the efficacy of the model validation is discussed in Chapter 4. In Chapter 5, details are provided on how a total of 76 numerical studies were designed and analyzed using the advanced numerical model developed in Chapter 4 to understand the fire response of restrained PC and RC beams. Based on the results from the parametric studies in chapter 5, simplified guidelines are proposed for the design of restrained PC beams in Chapter 6. Then based on the discussion provided in Chapters 1 to 6, future studies are identified in Chapter 7 along with conclusions from this study.

Table 1.1 ASTM E119-18 guidance for restrained and unrestrained classification of structural members [5]

Type of Construction	Restraint Classification
I. Wall Bearing:	
1. Single span and simply supported end spans of multiple bays: [A]	
(1) Open-web steel joists or steel beams, supporting concrete slab, precast units, or metal decking	unrestrained
(2) Concrete slabs, precast units, or metal decking	unrestrained
2. Interior spans of multiple bays:	
(1) Open-web steel joists, steel beams or metal decking, supporting continuous concrete slab [B]	restrained
(2) Open-web steel joists or steel beams, supporting precast units or metal decking	unrestrained
(3) Cast-in-place concrete slab construction [B]	restrained
(4) Precast concrete construction [B,C]	restrained
II. Steel Framing: [B]	
(1) Steel beams welded, riveted, or bolted to the framing members	restrained
(2) All types of cast-in-place floor and roof construction (such as beam-and-slabs, flat slabs, pan joists, and waffle slabs) where the floor or roof construction is secured to the framing members	restrained
(3) All types of prefabricated floor or roof construction where the structural members are secured to the framing members [C]	restrained
III. Concrete Framing: [B]	
(1) Beams fastened to the framing members	restrained
(2) All types of concrete cast-in-place floor or roof construction (such as beam-and-slabs, flat slabs, pan joists, and waffle slabs) where the floor or roof construction is cast with the framing members	restrained

Table 1.1 (cont'd)

(3) Interior and exterior spans of precast construction with cast-in-place joints resulting in restraint equivalent to that which would exist in condition III (1)	restrained
(4) All types of prefabricated floor or roof construction where the structural members are secured to such construction [C]	restrained
IV. Wood Construction:	
(1) All types	unrestrained

[A] Floor and roof construction may be considered restrained where they are tied (with or without tie beams) into walls designed and detailed to resist thermally induced forces from the floor or roof construction exposed to fire.

[B] To provide sufficient restraint, the framing members or contiguous floor or roof construction should be capable of resisting the potential thermal expansion resulting from a fire exposure as described in X3.5 and X3.6 of ASTM E119-18.

[C] Resistance to potential thermal expansion resulting from fire exposure may be achieved when one of the following is provided:

(1) Continuous structural concrete topping is used,

(2) The space between the ends of precast units or between the ends of units and the vertical face of supports is filled with concrete or mortar, or

(3) The space between the ends of precast units and the vertical faces of supports, or between the ends of solid or hollow core slab units does not exceed 0.25 % of the length for normal weight concrete members or 0.1 % of the length for structural lightweight concrete members.

Table 1.2 Prescriptive fire resistance requirements based on concrete cover for restrained and unrestrained prestressed concrete beams as per PCI manual 124 [6]

Fire resistance (hours)	**Minimum concrete cover for siliceous and calcareous aggregate (mm)**			
	Beam Width = 203 *mm*		**Beam width > 203 *mm***	
	Unrestrained*	**Restrained***	**Unrestrained***	**Restrained**
1	38	38	38	38
1.5	44	38	38	38
2	64	38	48	38
3	127‡	44†	64	38
4	n/a	64†	76	48†

* Direct interpolation for cover is permitted for beam widths between 203 and 305 mm

† Values are based on beams spaced at more than 1219 mm on center. For beam spacing less than 1219 mm on center, the minimum concrete cover is permitted to be reduced to 19 mm for 4 hour ratings or less.

‡ This value is not possible for 8 in. (203 mm) beam widths but is shown for interpolation purposes.

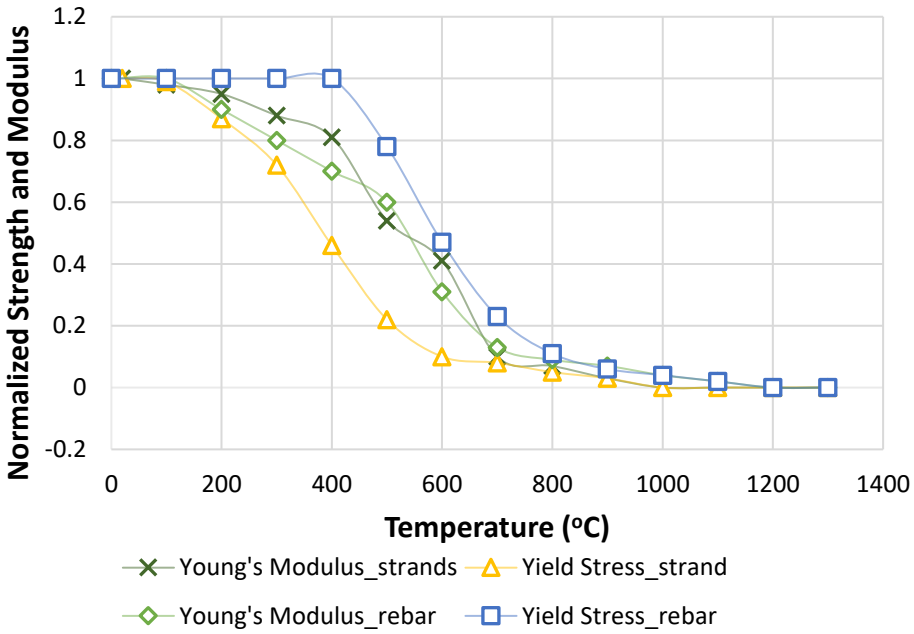

Figure 1.1 Comparison of variation in strength and modulus of prestressing strands and rebars at elevated temperatures

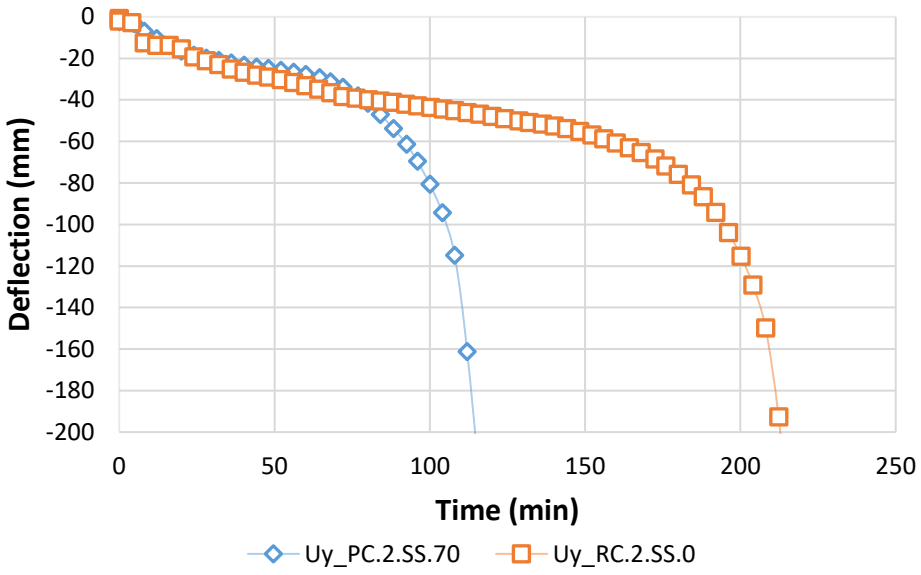

Figure 1.2 Comparison of deflections for PC and equivalent RC beam

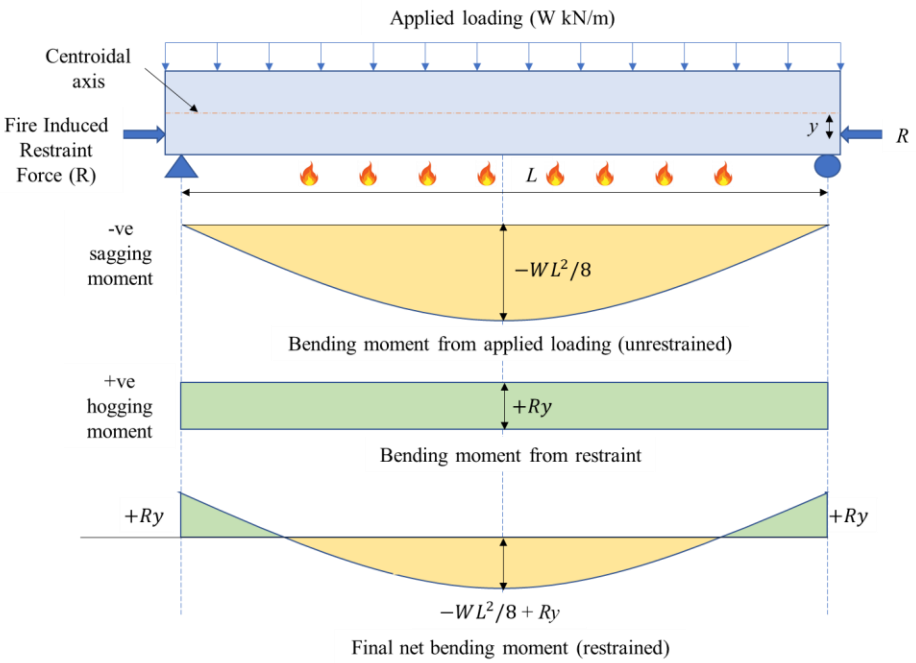

(a)

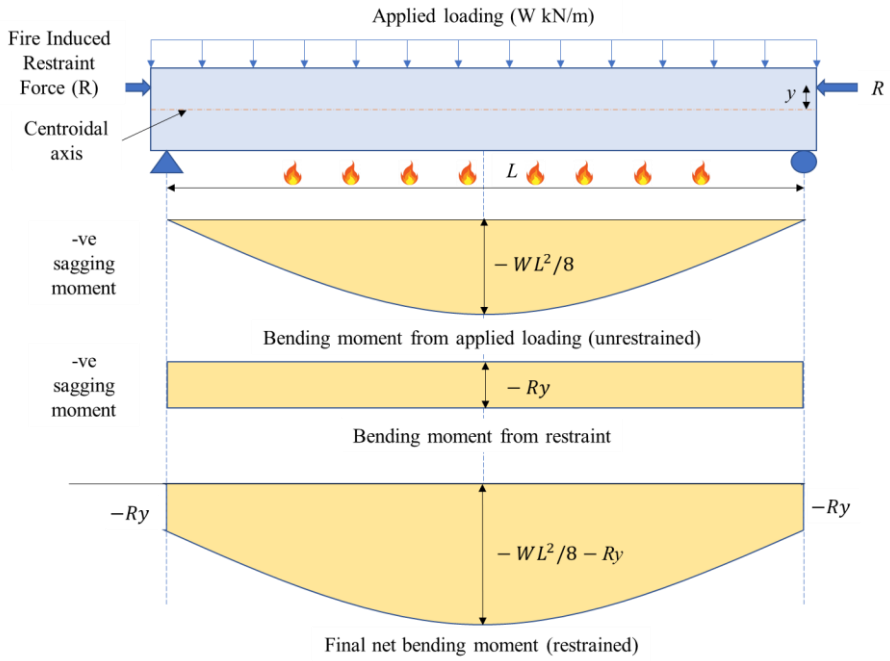

(b)

Figure 1.3 Effect of fire induced restraint force and its location on net bending moment in PC and RC beams (a) restraint below centroidal axis, (b) restraint above centroidal axis

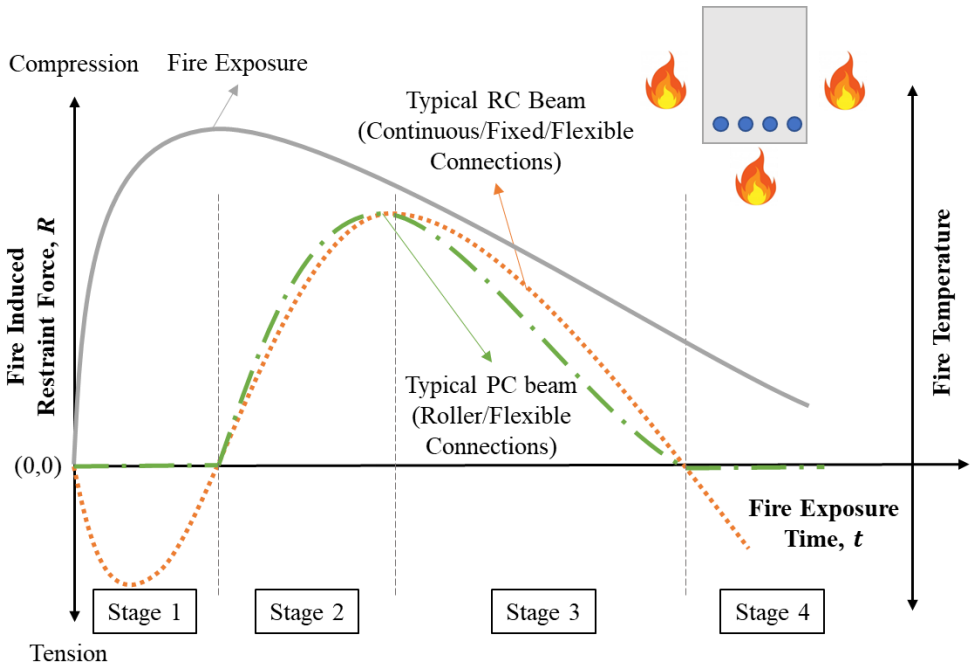

Figure 1.4 Evolution of fire induced restraint force in typical restrained PC and RC beam

CHAPTER 2

2 State-of-the-art Review

2.1 General

To identify the knowledge gaps on the fire behavior of PC and RC beams, a detailed review is provided on the available information relating to experimental and numerical studies, followed by design provisions in codes and standards. While there are numerous experimental and numerical studies on fire behavior of RC beams, only studies with emphasis on restraint effects are reviewed herein to set the context. On the other hand, due to limited studies on fire behavior of PC beams, most of the key historic and recent studies are reviewed in detail. For every study, hypothesis, approach, methodology, and main findings are provided in the review to set the context for current state-of-the-art. Then a detailed discussion is provided on the current treatment of fire resistance evaluation for RC and PC beams by current codes and standards, and their key shortcomings are identified. Further, to understand the challenges for numerical modeling of PC and RC beams, variation in material properties of concrete and reinforcement at elevated temperatures is reviewed.

Also, based on the literature review, key knowledge gaps are identified, and a summary is provided to understand the current state-of-the-art.

2.2 Experimental studies

Dwaikat and Kodur [9] tested a total of six RC beams under standard and design fire exposure to quantify the effect of restraint on fire resistance of RC beams. All beams were of 3960 x 254 x 406 mm dimensions (length x width x depth), and design variables in fire tests included concrete strength (58.2 to 106 MPa), axial restraint (0 to 100%), fire exposure (two design and one standard fire exposure), and load level (55% to 65%). A summary of fire tests is provided in Table 2.1. All beams were tested under four point loading for 4 hours (see Figure 2.1 for fire exposure) or till failure with restraint acting at center of beams to constrain axial thermal expansion of beam. Fire response of beams was measured in terms of developed restraint force, sectional temperatures, deflections, and failure modes. A consistent increase in restraint was observed for both restrained beams till it reached 120 kN and afterwards it was manually calibrated to keep it below 120 kN to ensure safety of load bearing frame of testing furnace, as shown in Figure 2.2. Due to the presence of restraint forces, no failure was observed for restrained beams as compared to unrestrained counterparts, and it can be seen from the deflection response in Figure 2.3. Based on the results from this study, authors reported that developed restraint in HSC beam is relatively less than NSC beam throughout fire exposure, and restraint force increased fire resistance of NSC beams by 33.3% and by 64.4% for HSC beams.

Albuquerque et. al. [10] tested a total of twelve NSC RC beams under restrained and unrestrained fire conditions and three RC beams at ambient temperature as the baseline case. Main variables in their tests included support conditions (axially restrained, rotationally restrained, and simply supported) and concrete strength (26.2 MPa to 31.3 MPa). Details of the tests and applied support

conditions is provided in Table 2.2. All tested beams had same dimensions of 100 x 250 x 4200 mm (width x depth x length) and were tested under four point loading with a load ratio of 50% under ISO 834 standard fire exposure [11] till failure (maximum failure duration occurred at 187 minutes). Axial and rotational restraint was applied by using steel beams attached to the entire face of beam at ends. Development of restraint forces and corresponding deflection response for all tested beams is shown in Figures 2.4 and 2.5.

It can be observed from the Figure 2.4 that restraint forces increased gradually and decayed after attaining peak. This is due to the degradation of material properties at elevated temperatures which increases the deflection of beam due to decrease in load carrying capacity. Increase in midspan deflection causes an inward pull at the ends which mitigates the thermal expansion of the beam, thus, causing a decay in the restraint forces. Summary of the measured fire resistance for tested beams is provided in Table 2.3. Based on the results of this study, Albuquerque et. al. [10] concluded that restraint increased fire resistance for all tested beams from 16% to 100% as compared to their unrestrained counterparts. Highest increase in fire resistance (100%) was observed when both axial and rotational restraint was applied simultaneously to the beam.

However, Fan et. al. [12] showed through an experimental study that the restraint can have positive and negative effects on the fire resistance of short span RC beams under fire exposure. Fan et. al. [12] tested a total of seven RC short beams (1 under ambient temperature and 6 under design fire exposure) to investigate the effect of axial restraint and shear span to effective depth ratio (a/d) on fire resistance of restrained RC short beams. All beams measured 150 x 500 x 2600 mm (width x depth x length) and were fabricated with concrete with a compressive strength of 39 MPa NSC and steel reinforcement with a tensile strength of 537 MPa. Beams were tested under a design fire exposure and subjected to four point loading and variable a/d ratio. Based on the results of this

study Fan et. al. [12] concluded that regardless of a/d ratio, restraint changed failure mode of short RC beams from diagonal splitting ductile failure to brittle sudden failure. Also, authors reported that for beams with $a/d < 2$, axial restraint increased mid-span deflections and cracking. However, for deeper beams ($a/d > 2.5$) restraint mitigated increase in mid span deflections. Therefore, based on the section's aspect ratio restraint forces had positive or negative effect on the fire response of the beams.

Similar trends on the restraint effects are reported for other restrained RC flexural members and can be referred to the literature [13,14]. Also, unlike PC beams, fire behavior of RC beams is well studied under unrestrained conditions. Most of the contemporary experimental studies on fire behavior of RC beams under unrestrained conditions are focused on understanding use of new types of concrete and reinforcement in RC beams [15–18], strengthening using composites [19,20], continuity [21–23], post-fire residual capacity [24,25], or restoration of fire damaged RC beams [26–28]. While detailed review of these studies is beyond the scope of current research project, some key findings which are applicable to fire behavior of RC beams are reviewed herein.

On the other hand, there is only a handful of experimental studies on fire behavior of PC beams under both restrained and unrestrained conditions. One of the early and extensive experimental study on fire resistance of PC beams was conducted by Ashton and Malhotra [29], where they tested a total of 37 post-tensioned beams with emphasis on investigating the effect of shape (two rectangular and one I section), end conditions (axially restrained and unrestrained), load (0 to 1.5 times design load), type of aggregate, specified concrete strength (47.2 MPa to 82.4 MPa), concrete cover to cable (25.4 mm to 51 mm), and additional insulation (o to 63.5 mm) on fire resistance of PC beams. A total of three sections were selected as: Type A (rectangular beam of size 127 mm x 228.6 mm with a 50 mm clear cover to strands), Type B (rectangular beam of size 127 mm x 228.6

mm with two strand groups at clear cover of 25.4 mm and 171.5 mm), and Type C (I section of variable width and 228.6 mm depth). All sections constituted a 508 mm x 76.2 mm slab on top to represent realistic conditions in the buildings. A total of 17 unprotected Type A sections, 9 protected Type A sections, 7 Type B sections, and 4 Type C sections were tested at period of 6 months to 15 months from the day of casting under standard fire exposure for a duration of 2 to 4 hours.

Based on the results from experiments, Ashton and Malhotra [29] reported that for three restrained beams of section Type A, effect of restraint on fire resistance varied from 58% increase to -16% decrease as span of beams increased by 100%. For beam with a span of 1.5 m restraint increased the fire resistance by 58%, for beam with a span of 2.3 m restraint increased fire resistance by 26%, and for beam with a span of 3 m restraint decreased the fire resistance by -16% as compared to simply supported counterparts. It should be noted that all these beams were tested under identical loading and fire conditions and only key difference is span of beam. Also, they concluded that full scale post-tensioned beams with 63.5 mm cover should give only 2 hours of fire resistance and attaining 4 hour fire resistance will require additional fire protection for strands in terms of 25.4 mm thick vermiculite insulation to increase fire resistance by 2 hours. However, PCI manual [6] predicts a fire resistance of 4 hours for restrained PC beams with clear cover of 48 mm and width greater than 203 mm without any additional fire protection which completely contradicts conclusions from this experimental study.

Ryan [30] extended the above work by conducting six more tests on post-tensioned beams at U.S. National Bureau of Standards. The main aim of this experimental study was to supplement additional parameters which were not accounted for in the original study of Ashton and Malhotra [29]. For this purpose, Type A section (T-section of size 127 mm x 228.6 mm with single cable)

was selected from Ashton and Malhotra [29], and six more variables were introduced as: identical and 60% longer span in first two tests, 60% longer span with 25.4 mm vermiculite insulation on three sides of beam and slab bottom, 60% longer span with higher concrete cover, and 60% longer span without top slab. All beams were tested under standard fire exposure only, and based on the combined results from this and study of Ashton and Malhotra [29], Ryan [30] concluded that clear cover is one of the main factor to consider for fire resistance. Also, Ryan [30] recommended use of some light reinforcement in terms of wire mesh for clear cover requirements greater than 76.2 mm to prevent cracking and spalling in cover concrete. However, no further insights were provided by Ryan [30] in terms of effect of restraint on fire resistance of beams. Therefore, it should be noted that restraint was not included into design process till 1971 even though significant positive and negative effects of restraint were well established by experimental studies in 1953 only [31].

Recently, Hou et. al. [32] conducted fire tests on PC beams where the focus was to understand effect of continuity on fire resistance of PC beams. Hou et. al. [32] tested a total of nine continuous two-span bonded PC beams under fire exposure to identify critical factors governing their fire resistance. The test variables included concrete cover thickness (39 mm to 64 mm), load level (47% to 62% of room temperature capacity), degree of prestressing (38% to 74%), and effective prestress (600 MPa to 900 MPa). Summary of fire tests and variables is provided in Table 2.4. All beams measured 5300 mm x 150 mm x 200 mm (length x width x depth) and were tested in continuous two-span support system with a clear span of 2550 mm each. The strength of concrete in tested beams varied from 23 MPa to 62 MPa, and all specimens were tested between 55 to 77 days of casting. Main prestress reinforcement in beams varied from 2 to 4 strands of 5 mm diameter with a tensile strength of 1772 MPa. All beams were tested under standard ISO 834 fire exposure

for a duration of 60 minutes under simultaneous loading and fire exposure, and the thermal and structural response of beams was measured in terms of sectional temperatures and deflections.

The development of sectional temperatures for all tested PC beams can be referred to literature [32]. It can be seen from temperature results reported by Hou et. al. [32] that sectional temperatures increase uniformly at fire exposed surface and a plateau is observed at 100^{o}C for more insulated depths. Hou et. al. [32] attributed the plateau to the evaporation of free water at around 100^{o}C, and suggested moisture migrated from exposed face to insulated depths under fire exposure and thus no plateau is observed near fire exposed surface. After the plateau at around 100^{o}C, sectional temperatures increased consistently at more insulated depths as well. Also, Hou et. al. [32] inferred that load level, effective prestress, and degree of prestressing had minor effect on the evolution of sectional temperatures in the PC beams. Corresponding structural response of these beams is illustrated in Figure 2.6. It can be observed from the Figure 2.6 that deflections increased consistently throughout fire exposure due to loss of prestress and degradation of material properties. Based on the results of this study, it was concluded that load level and cover thickness have significant effect on fire resistance of PC beams, and fire resistance of continuous PC beams is higher than simply supported PC beams.

To further illustrate effect of restraint under fire exposure, results from PC double-tee beams tested under restrained conditions are reviewed herein. Selvaggio and Carlson [33] tested a total of six double-tees under standard fire exposure and variable restraint to quantify the effect of restraint on fire resistance. The dimensions of tested specimen measured at 5.48 × 1.27 × 0.38 m (length x width x depth), and their cross-section is illustrated in Figure 2.7 and summary of test results is illustrated in Table 2.5. The ultimate strength of the strands was 1723 MPa, and they were tensioned to 1206 MPa, 70% of the ultimate strength, during the fabrication of specimen. Tested

double-tees contained calcareous coarse aggregate in concrete and had a compressive strength ranging from 34.5 MPa to 42.9 MPa. The tested specimen was loaded to 55% of their flexural capacity and were tested under standard fire exposure for 4 hours with variable axial restraint. The fire response of the double-tees was measured in terms of cross-sectional temperatures, developed axial thrust, and midspan deflection.

Significant restraint forces were developed in all tested DT beams and development of restraint with respect to fire exposure is shown in Figure 2.8. It can be observed from Figure 2.8 that maximum restraint was experienced under highest degree of axial restraint. However, measured restraint force decreased exponentially when the permissible axial displacement was increased from 3.2 to 31.75 mm, as shown in Figure 2.9. Also, it can be observed from Figure 2.10 that location of restraint relative to neutral axis keeps on changing throughout fire exposure, which imparts variable resisting or adverse moment to PC double-tees. While in the present study, restraint location is mostly under the neutral axis of the double-tees, same may not be the case for all PC structural members under all fire scenarios. It can be clearly observed from Figure 2.11 that for beams with small permissible axial displacement, higher restraint thrust was developed which mitigated the experienced deflection under fire test.

Based on the discussion above, it can be inferred that there is not ample experimental evidence to support the hypothesis that fire induced restraint forces always increase the fire resistance of restrained RC and PC beams under all fire and loading scenarios. Some different relevant studies on PC flexural members can be referred to literature [34–36].

2.3 Numerical studies

Fire behavior of reinforced concrete beams is well researched using numerous numerical models, and a detailed review on evolution of numerical models for tracing fire response of RC beams can

be referred to literature [8,37]. Most of the contemporary numerical studies on fire behavior of RC beams focused on developing simplified models [38,39], and refining existing models [40,41]. Also, the focus of recent studies have been on understanding behavior of composite RC beams [42–58], post-fire residual capacity [59–65], effect of other hazards on fire resistance [66], or behavior of RC beam or similar structural members under varying fire and loading conditions [67–82]. While detailed review of all studies on RC beams is beyond the scope of this study, relevant numerical studies with focus on fire behavior of restrained RC beams are reviewed herein.

Dwaikat and Kodur [83] developed a 2D moment curvature based numerical model to simulate fire behavior of RC beams. Heat transfer was simulated using 2D FE based analysis and then average section temperatures were transferred to moment curvature based structural model to capture corresponding thermo-mechanical response. Developed model was validated by comparing predicted sectional temperatures and deflections against data measured in full scale fire tests and a good correlation between the two was reported by Dwaikat and Kodur [83]. Validated numerical model was utilized to conduct parametric studies to evaluate effect of the magnitude of restraint, and authors concluded that restraint magnitude had significant effect on fire resistance of RC beams. Dwaikat and Kodur [83] concluded that fire induced restraint forces had significant influence on the fire resistance of the RC beams, and it is important to account for the actual stiffness of connection to capture realistic restraint. Kodur and Dwaikat [84] further utilized the results from these parametric studies and proposed a simplified design equation for evaluating fire resistance of RC beams.

A similar numerical approach was followed by Wu and Lu [85] where they developed a 2D virtual work based beam-element for RC beams under fire exposure along with 2D FE based heat transfer model. Developed model was validated by comparing predicted sectional temperatures and

measured axial force and moment against data from fire tests, and Wu and Lu [85] reported a good correlation between the predictions and measurements. They also conducted a series of parametric studies to investigate effect of span, load ratio, and magnitude of axial and rotational stiffness on fire resistance of RC beams. Based on the results, Wu and Lu [85] concluded that axial restraint may increase deflection (negative effect) in beams due to high amount of axial restraint generated in beam and resulting P-delta effects. Also, they reported that rotational stiffness has minor effect on developed axial restraint in RC beams, and while rotational restraint adds hogging resisting moment in the initial heating phase for RC beams these gains are soon lost once sectional temperatures increase and P-delta effects become more predominant under high magnitude axial restraint.

Albrifkani and Wang [86] developed one of the first 3D explicit FE based numerical model in ABAQUS to simulate fire response of RC beams under fire exposure. An explicit numerical model was selected in this study to minimize convergence hurdles arising from material and geometric non-linearities, local failures, and long computation time. While solid elements were utilized for discretizing concrete and reinforcement in both thermal and structural domains, spring elements with multi point constraints were used to simulate axial and rotational restraint. Developed model was validated by comparing predicted axial force-displacement and gravity load-displacement curves with measured data from fire tests, and a reasonable correlation between the two is reported by Albrifkani and Wang [86]. Albrifkani and Wang [86] concluded that the explicit numerical model may be used to model a statis process if the total loading does not fall below 20 times the lowest natural period for 60 minutes of real heating duration. Also, they recommended a damping ratio of 25% to 30% to avoid premature failure from dynamic effects.

Albrifkani and Wang [87] further utilized this model to conduct a more detailed numerical study on axially and rotationally retrained RC beams. Key variables investigated in this study include different level of axial and rotational restraint, bending failure, transition from compression to tension in beam under catenary action, and fracture of reinforcement at ultimate failure. Based on the results from this study, Albrifkani and Wang [87] concluded that multiple failures in beam can occur under restrained conditions as middle span sagging failure, end hogging failure from fracture of tensile reinforcement, and end hogging failure due to crushing. Also, they inferred that if concrete crushing occurs near beam ends then catenary action will develop in RC beams at large deflections.

On the other hand, there are very limited numerical studies focused on tracing fire behavior of PC beams. Franssen and Bruls [34] developed one of the earlier numerical model for PC double-tee beams using computer program SAFIR. In this study, a 2D thermal analysis was conducted to get the sectional temperatures and these temperatures were coupled to structural analysis using Bernoulli beam elements. Franssen and Bruls [34] applied this simplified numerical model to identify potential failure modes for tested double-tees under fire exposure and improved design of the same to enhance fire resistance. Franssen and Bruls [34] concluded that if the geometry of the double-tees is different from the one for which graphs or tables are given then a more refined numerical analysis is required.

Kodur and Hatinger [88] applied a performance based approach for evaluating fire resistance of PC double-tee beams using a 2D finite element based numerical model in SAFIR. Developed model was validated by comparing the predicted fire resistance and midspan deflections with results from full scale experimental data, and a good correlation between the same was reported by authors. Validated model was then utilized to conduct a series of parametric studies to

understand the effect of realistic fire exposure, load ratio, concrete strength, clear cover thickness, aggregate type, and axial restraint on fire resistance of PC double-tees. Based on the results of parametric studies, authors concluded that axial restraint can significantly increase the fire resistance of PC double-tees and magnitude of developed restraint force depends on type of restraint, support conditions, and variable stiffness offered by adjoining members. Also, authors inferred that fire resistance of slender PC double-tees is often limited by strand temperatures whereas for PC double-tees with bulkier stems heat transmission is the key failure mode.

Okasha and Pessiki [89] developed an analytical model to understand the effect of fire induced restraint force on fire resistance of PC double-tees. Analytical model consisted of nonlinear uncoupled finite element analysis in thermal and structural domains, and then the load carrying capacity of double-tees was determined using fiber-based computer model. Authors considered a total of four support conditions in the study as simply supported, fully restrained on ends, flange restrained, and web restrained. Restraint was simulated by applying displacement boundary conditions and measuring developed reactions at constrained nodes. Based on the results of this study, authors concluded that restraint had significant effect on load carrying capacity, and double-tees with restrained flange had less fire resistance than fully restrained or restrained web cases. Also, flexural strength of double-tee restrained by spandrels and inverted tee girders was found to be equal to corresponding simply supported beam, and flange connectors had minimal effect on fire resistance of double-tees. Based on the discussion above, it is evident that there is a lack of understanding on developing generic numerical models for PC beams.

2.4 Design provisions in codes and standards

Currently, there are both prescriptive and rational design provisions in codes and standards [4–7] for evaluating fire resistance of RC and PC beams. For prescriptive approaches desired fire rating

of the RC beam is correlated to the beam width and clear cover to the reinforcement and such specific prescriptive provisions can be referred to literature [4–7]. For simplified approaches, most common one is provided by ACI 216 [7] and PCI manual [6] where the moment capacity of the RC beam is evaluated by temperature dependent strength parameters to account for degradation of material properties in the load carrying capacity at elevated temperatures. Therefore, this approach allows users to calculate temperature dependent moment capacity of RC beam for a given standard fire exposure duration by reading sectional temperatures and material degradation factors from the given charts. Further, Eurocode 2 [4] provides a 500^{o}C isotherm method to calculate the moment capacity of the beam at elevated temperatures. In this approach, the section with temperatures higher than 500^{o}C is considered structurally inadequate and the beam capacity is calculated based on the reduced section (everything with temperatures below 500^{o}C) properties. Therefore, unlike ACI 216 [7] and PCI manual [6] this approach does not account for the actual material degradation at specific temperatures.

Similar prescriptive and rational design procedures are available for PC beams as well, and usually PC beams require higher clear cover in the prescriptive approaches due to rapid strength loss in strands. However, evaluating fire resistance using prescriptive approach have numerous drawbacks which primarily include inability to account for realistic restraint and support conditions; unrealistic failure criteria; inability to account for critical factors governing fire response of PC beams; vague guidelines to classify restrained and unrestrained beams; considering only positive effects of restraint; and use of fire resistance ratings. Inability to represent realistic restraint and support conditions in buildings arise due to experimental constraints as only individual scaled members can be tested in furnace and restraint is applied from load bearing frame of furnace and not from actual connections in buildings. Often due to limits on maximum restraint

force, and use of scaled members, it becomes very complicated to correlate restraint conditions in a furnace to actual buildings [31].

Also, the failure criterion applied to determine fire resistance in prescriptive approach based building codes is very divorced from reality in buildings. In most prescriptive approach based building code, strength criterion is implemented for PC beams by limiting temperature in main reinforcement to remain below critical temperature (temperature at which reinforcement lose 50% of strength) [4–7]. Rationale behind this implementation is that main reinforcement is the main contributor to load carrying capacity of member, and at critical temperature when reinforcement loses 50% of its strength, failure is highly likely. However, structural members fail through excessive deflection through intricate thermo-mechanical response under fire exposure which is governed by a multitude of governing factors which are not accounted for in prescriptive approach based codes and standards. On the other hand, some prescriptive codes do provide simplified rational design equations which account for moment capacity degradation at a critical section in beam [6]. However, these equations do not account for the secondary P-delta effects, cracking, spalling, or restraint force which limits their applicability. Therefore, failure criterion applied by prescriptive approach do not represent realistic member failure in buildings, as it does not account for the effect of all governing factors; thus, leading to inaccurate fire resistance assessment.

Moreover, prescriptive approach based building codes [4–7] do not provide a precise method for defining in situ restrained vs unrestrained classification as shown in Table 1.1. Although some commentary is given on identifying restrained members in buildings, unrestrained members are often defined by exclusion only. Often, it comes to the discretion of fire protection or structural engineer to make the final decision for classifying member as restrained or unrestrained based on their experience and judgment. As restrained classification allows to achieve higher fire resistance

with much smaller clear cover, dimensions, and without fire protection; it becomes significantly more cost-effective to classify members as restrained. Due to these significant economic benefits, often, designers are under pressure to choose a restrained classification for most building structural members. Unfortunately, those designers that choose not to (for example, those with more advanced knowledge of structural behavior under fire exposure) are easily subject to perceptions by other project stakeholders as being obstructionist or overconservative [31]. Thus, this lack of clear guideline for classification from prescriptive approach based building codes creates significant confusion and conflict for designers and building authorities which can lead to unsafe designs.

Another limitation of current codes and standards is their assumption that restraint does not have any negative effect on fire resistance of PC beams. Restrained and unrestrained classification was formally adopted in ASTM E119 standard in 1971 (based on the proposal of 1969) [31]. One of the key factors for this acceptance was the experimental study conducted on protected steel beam floor and roof assemblies under variable restraint at Ohio State University [90]. In this experimental study, a total of 12 beam-slab assemblies with varying composite action were tested, where each beam-slab assembly constituted 102 mm concrete slab (914 mm wide) cast over a 22 gage steel deck supported by a 12WF27 ASTM A36 steel beam. Length of beam slabs measured at 4.57 m for unrestrained and 4.42 m for restrained beam-slabs. Variable restraint conditions were simulated using bolted clip angle connections and welded plate connections. All slabs were loaded to design allowable stresses during fire tests, and it was observed that restraint increased the fire resistance of beam-slab assemblies by an average of 25%.

However, several numerical and experimental studies have demonstrated that fire induced restraint forces can indeed reduce the fire resistance of structural members. Therefore, it can be argued that

the origin of binary classification in terms of “restrained” and “unrestrained” in building codes is an oversimplification of much intricate and less understood problem. Hence, due to these limitations current prescriptive codes and standards do not capture realistic fire response of PC beams.

2.5 High temperature material properties

Thermal and mechanical material properties of concrete, reinforcing steel, and prestressing strands vary significantly at elevated temperatures. Thermal material properties include thermal conductivity, specific heat capacity, density, emissivity, and coefficient of convection. These properties control the heat transfer between fire and beam, and within the beam section itself. On the other hand, mechanical properties include compressive and tensile yield strength, elastic modulus, stress-strain relations, thermal strain, and creep. These properties control the corresponding thermo-mechanical response of the beam. Variation in these properties for concrete and steel (rebar and prestressing steel) is well studied by multiple researchers and can be referred to the literature [8,91,92]. Therefore, only variation in material properties as per provisions in codes and standards is reviewed herein to set the context.

2.5.1 Concrete

Thermal conductivity of concrete varies between 0.5 to 2.5 W/m-^{o}C and its variation as per different codes and test results is illustrated in literature [91]. The variation is primarily attributed to moisture content, type of aggregate, test conditions, and measurement techniques used in experiments. Thermal conductivity of the concrete undergoes a consistent decrease with increasing temperatures which is mainly due to reducing moisture content in concrete. Therefore, typically, thermal conductivity of high strength concrete (HSC) is higher than normal strength concrete (NSC) due to lower moisture content in HSC. Also, while Eurocode 2 [4] provides a upper and

lower limit variations, ASCE [93] provides variation depending on type of concrete aggregate. The variation in specific heat of concrete is illustrated in literature [91]. The specific heat variation is primarily attributed to the vaporization of free water at 100^{o}C, dissociation of $Ca(OH)_2$ into CaO and H_2O between 400-500^{o}C, and the quartz transformation of some aggregates above 600^{o}C [91]. For mechanical properties, the variation in relative compressive strength of NSC and HSC is shown in literature [91]. It can be observed from literature [91] that compressive strength of concrete undergoes significant variation at elevated temperatures and about 80% of strength is lost at temperatures above 800^{o}C. The main reason for strength reduction of concrete is the development of microcracks at elevated temperatures arising from pore pressure buildup and thermal strain in concrete. Other factors that directly affect the strength degradation of concrete include initial curing, moisture content at the time of testing, and presence of admixtures. Further, the strength loss is usually more rapid in HSC concrete due to presence a dense microstructure which significantly increases the pore pressure build-up within concrete. A more detailed discussion on the stress-strain relationships of concrete can be referred to the literature [8,91,92].

2.5.2 Reinforcing and prestressing steel

For reinforcing and prestressing steel, variation in thermal properties follow very similar trend and can be referred to the literature [91]. However, there is significant variation in the high temperature mechanical properties of reinforcing and prestressing steel. This can be observed from Figure 1.1 where the variation in strength and modulus of reinforcing and prestressing steel is provided. It can be observed from Figure 1.1 that till 400^{o}C there is no degradation in the strength of reinforcing strands. Whereas prestressing strands lose about 50% of their room temperature strength at 400^{o}C. Similarly, reinforcing steel lose about 50% of their strength at 600^{o}C, whereas prestressing strands lose about 90% of their strength at 600^{o}C. This high and rapid degradation in the strength of strands

is the primarily cause of relatively faster loss of load carrying capacity in PC beams as compared to RC beam counterparts.

2.6 Knowledge gaps

Based on the literature review, following knowledge gaps are identified as below:

(1) Fire behavior of restrained PC beams is highly intricate and there is lack of advanced analysis approach (models) which can account for full effects of all governing factors such as: fire induced restraint forces, material degradation at elevated temperatures, cracking and crushing of concrete, spalling, material and geometric non-linearity, connection type and stiffness, any geometry, and realistic fire exposure.

(2) There is evidence from experimental and numerical studies that fire induced restraint forces can increase or decrease fire resistance of PC beams.

(3) There are only limited fire tests on PC beams, and there is a lack of reliable fire test data which can be used to validate numerical models.

(4) In prescriptive based approach, extrapolating results from standard fire tests on restrained PC beams to other PC beams using just clear cover and member dimensions as main parameters will not provide an accurate assessment of fire resistance as it does not fully account for all governing factors.

(5) Lack of validated numerical models for tracing the fire behavior of PC beams is constraining researchers from developing simplified rational design framework for PC beams under fire exposure.

(6) There is a lack of parametric studies on restrained PC beams to identify key differences in their fire behavior.

2.7 Summary

A detailed review of the experimental and numerical studies on fire response of PC beams shows that there is limited understanding on the fire behavior of restrained PC beams. Some of the initial experimental studies conducted on PC beams and members showed that significant restraint forces can develop in PC members when the thermal expansion is constrained. This restraint force can have positive or negative effect on the fire resistance of member depending on its location relative to centroidal axis. Also, an exponential decay is reported in the fire induced restraint force as allowed thermal expansion is increased. Further, there is a scarcity of numerical models capable of tracing fire response of restrained PC beams. This is limiting the codes and standards to account for all factors governing the fire response of restrained PC beams.

Table 2.1 Summary of fire tests conducted by Dwaikat and Kodur [9]

Beam	Test No.	Fire Exposure	Concrete Type	Support*	Load (kN)	Moisture Content (kg/m^3)	Fire Resistance (min)		Extent of Spalling
							Measured	Predicted	
B1	I	ASTM E119	NSC	SS	50	74.7	180	180	Minor
B2	II	SF	NSC	AR	50	74.4	No Failure	No Failure	Minor
B3	I	ASTM E119	HSC	SS	50	61.9	160	153	Moderate
B4	II	SF	HSC	SS	50	61.3	No Failure	No Failure	Moderate
B5	III	LF	HSC	SS	60	65	146	147	Severe
B6	III	LF	HSC	AR	50	65.5	No Failure	No Failure	Severe

*SS = Simply Supported, AR = Axially Restrained

Table 2.2 Summary of axial and rotational restraint stiffness ratios in fire tests conducted by Albuquerque et. al. [10]

Test Reference	**Axial restraint ratio ($k_{ax}\ EA/L$)**	**Rotational restraint ratio ($k_{rx}\ EJ/L$)**
T1_k_a0_k_r0	0	0
T2_k_a1_k_r0	0.02	0
T3_k_a1_k_r1	0.02	1
T4_k_a1_k_r2	0.02	2
T5_k_a2_k_r0	0.04	0
T6_k_a2_k_r1	0.04	1

Table 2.3 Summary of fire resistance in fire tests conducted by Albuquerque et. al. [10]

Designation of tested beam	**Fire resistance based on failure criterion in terms of resistance (min)**		**Fire resistance based on failure criterion in terms of deformation (min)**
	$t_{N,mdx}$	$t_{cr,r}$	$t_{cr,d}$
T1_k_a0_k_r0			78
T2_k_a1_k_r0	74	93	89
T3_k_a1_k_r1	97	138	142
T4_k_a1_k_r2	100	150	147
T5_k_a2_k_r0	84	101	98
T6_k_a2_k_r1	109	160	154

Table 2.4 Summary of fire tests conducted by Hou et. al. [32]

Specimens	$cp1/cp2$ **(mm)**	**PPR**	σ_{pe} **(MPa)**	**Load level**	A_p	A_s	f_{cu} **(MPa)**	w **(%)**	**Age at test (days)**
B1	49/39	0.38	600	0.54	$2\Phi^P5$	2Φ14	41	2.77	67
B2	49/39	0.55	750	0.48	$3\Phi^P5$	2Φ12	23	1.83	55
B3	49/39	0.74	900	0.57	$3\Phi^P5$	2Φ8	52	2.36	67
B4	59/39	0.38	750	0.47	$2\Phi^P5$	2Φ14	48	3.5	63
B5	59/39	0.55	900	0.54	$3\Phi^P5$	2Φ12	62	2.1	70
B6	59/39	0.74	600	0.59	$3\Phi^P5$	2Φ8	52	3.29	75
B7	64/39	0.38	900	0.47	$2\Phi^P5$	2Φ14	47	3.49	57
B8	64/39	0.53	600	0.62	$2\Phi^P5$	2Φ10	41	2.67	77
B9	64/39	0.74	750	0.6	$4\Phi^P5$	1Φ10+1Φ8	52	3.84	76
Note: all beams have cross section size of 150 x 200 mm									

Table 2.5 Summary of test results on effect of restraint on fire resistance of prestressed concrete double-tee slabs by Selvaggio and Carlson [33]

Test Parameter	Test Specimen					
	S19	**S11**	**S10**	**S12**	**S13**	**S17**
Allowed thermal expansion (mm)	3.1	7.3	14	19.1	25.4	30.7
ASTM Fire Exposure Duration (min)	250	250	250	250	250	250
Maximum Restraint (kN)	1994.3	1212.4	772.7	591.4	324.5	210.7
Time of attaining maximum restraint (min)	90	180	180	210	250	120
Location of maximum restraint from bottom (mm)	270.5	280.9	207	174.5	156.9	67.31
Average final stand temperature (^{o}C)	846	815	926	815	807	829
Midspan deflection at end of test (mm) *	-3.8	6.4	8.9	30.5	44.2	57.2
* Negative represents movement upward and positive represents downward deflection						

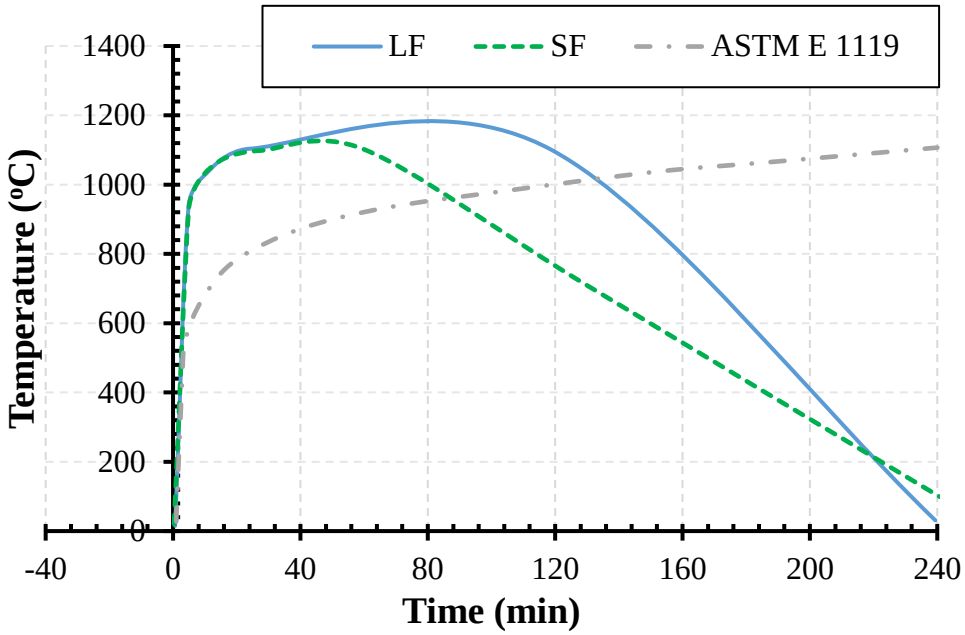

Figure 2.1 Fire exposure used in fire tests on RC beams by Dwaikat and Kodur [9]

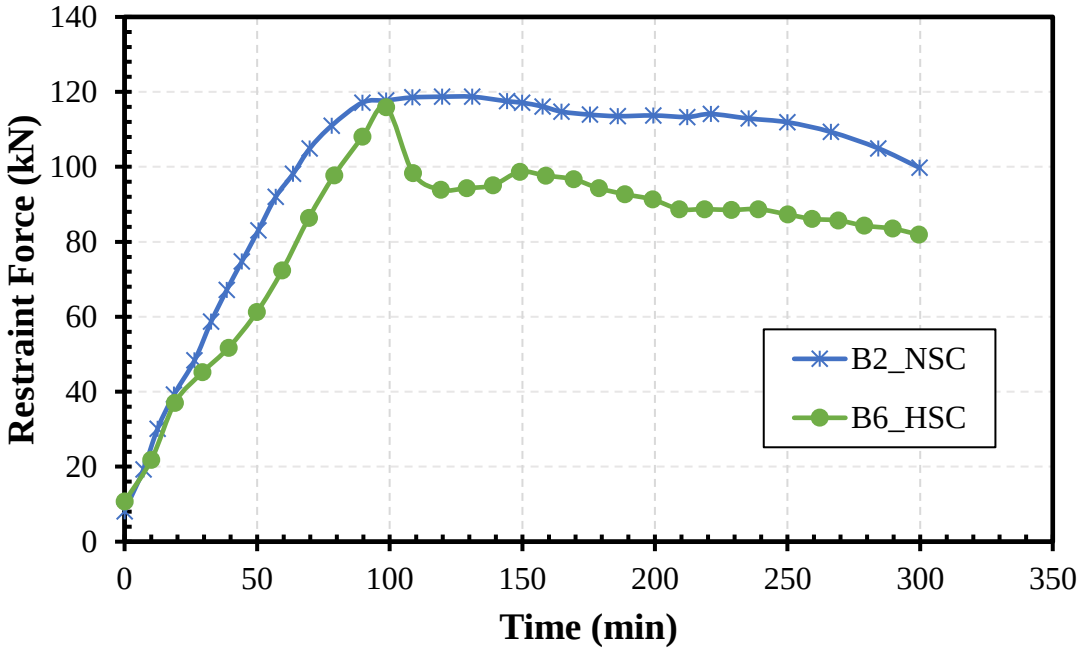

Figure 2.2 Development of restraint force in restrained RC beams in fire tests on RC beams by Dwaikat and Kodur [9]

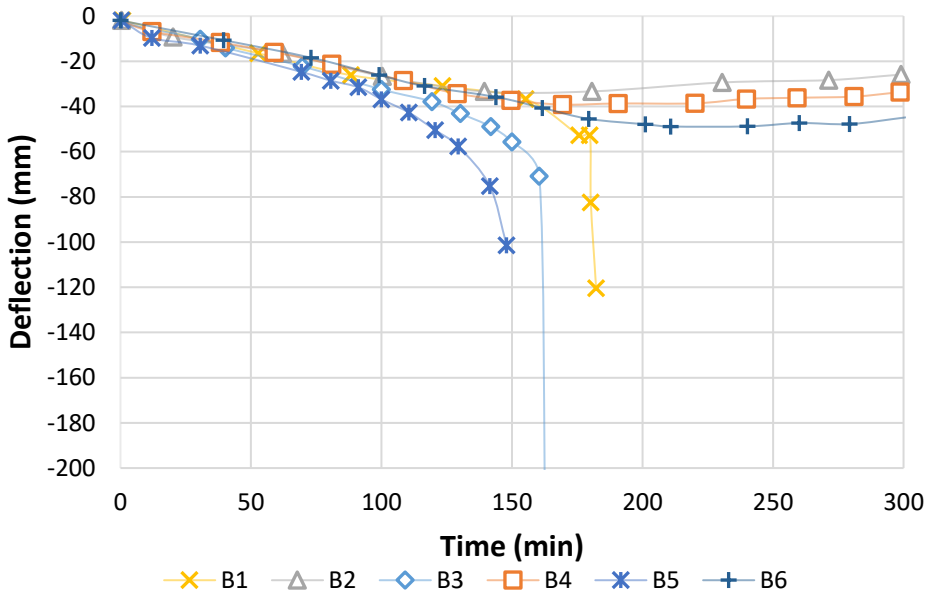

Figure 2.3 Measured midspan deflection in fire tests on RC beams by Dwaikat and Kodur [9]

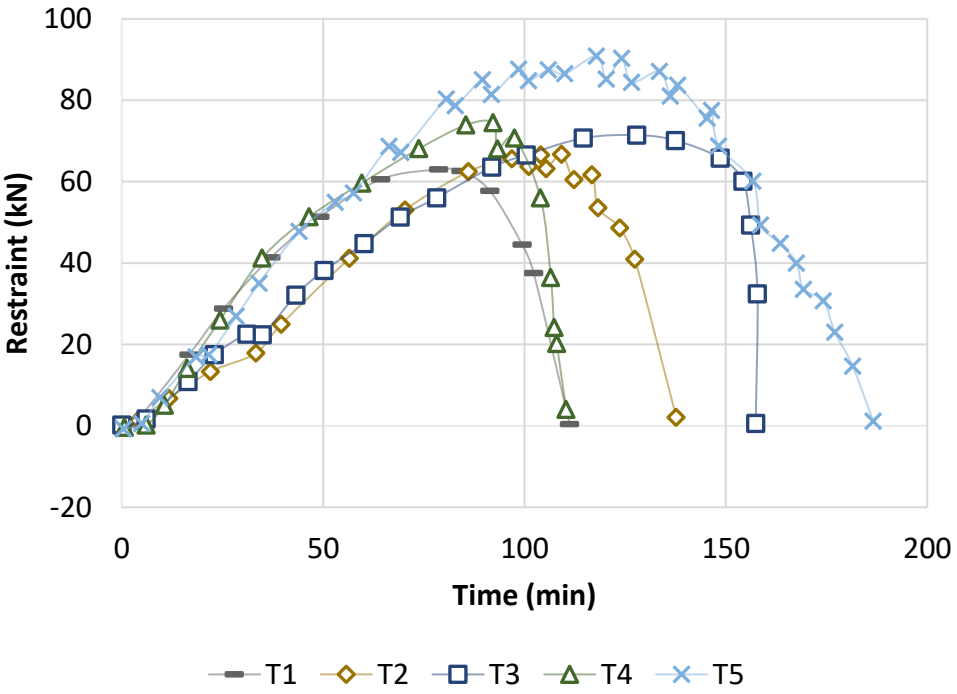

Figure 2.4 Development of restraint force in restrained RC beams in fire tests by Albuquerque et. al. [10]

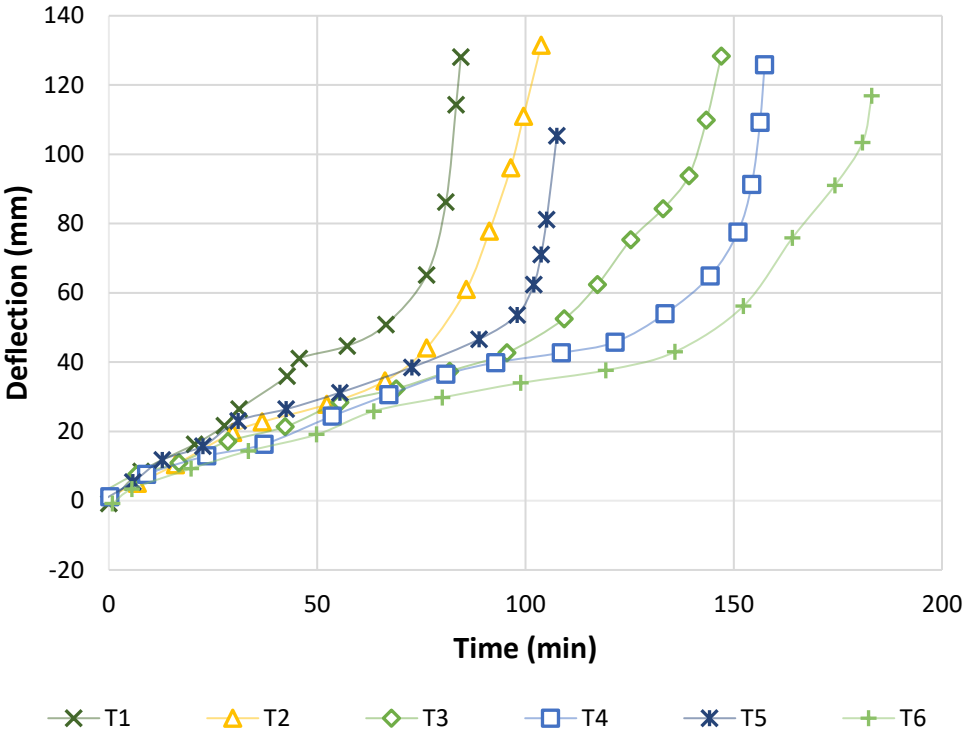

Figure 2.5 Measured midspan deflection in fire tests on RC beams by Albuquerque et. al. [10] (Note: positive y, deflection represents downwards deflection)

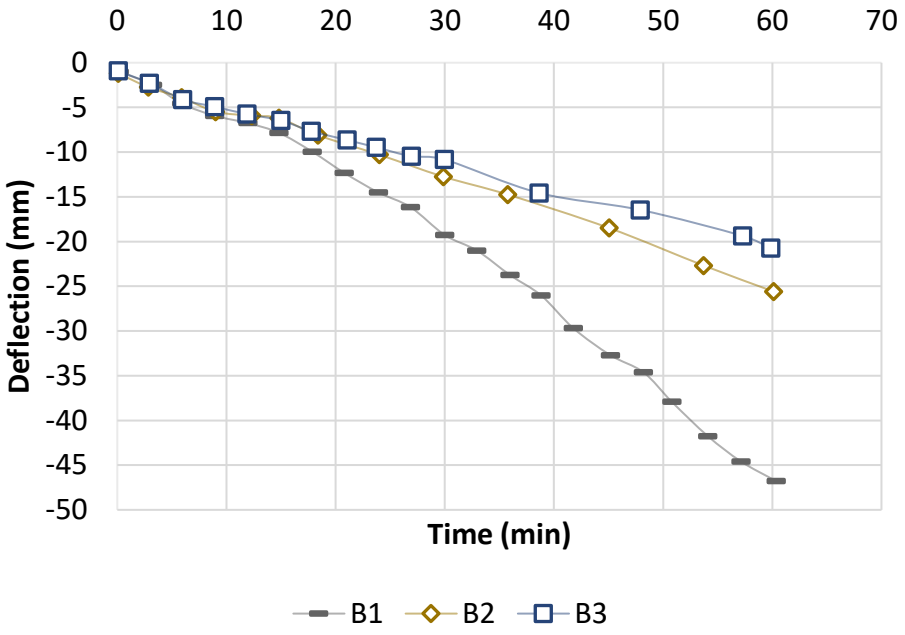

(a)

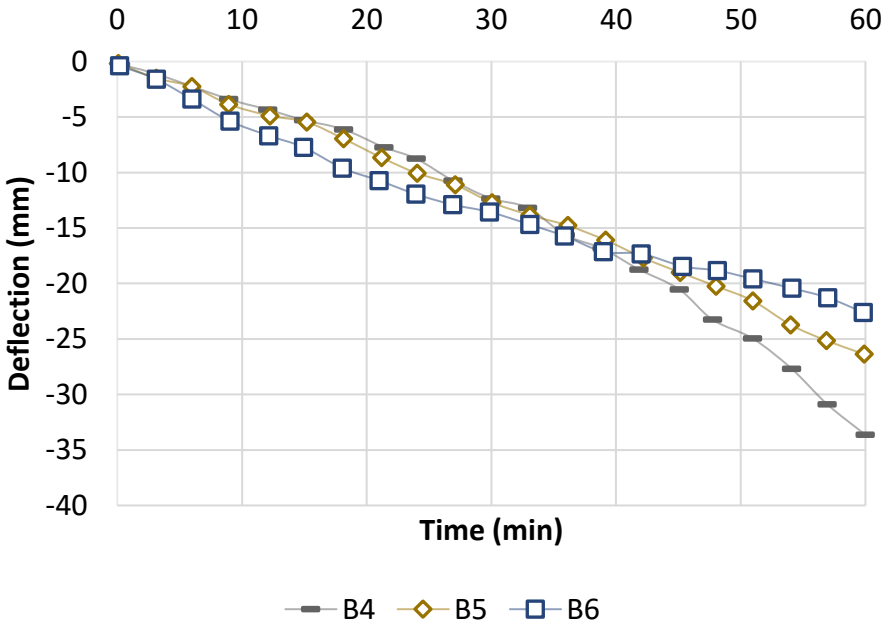

(b)

Figure 2.6 Measured deflections for tested PC beams (a) Beams B1 to B3, (b) Beams B4 to B6, and (c) Beams B7 to B9 in fire tests by Hou et. al. [32]

Figure 2.6 (cont'd)

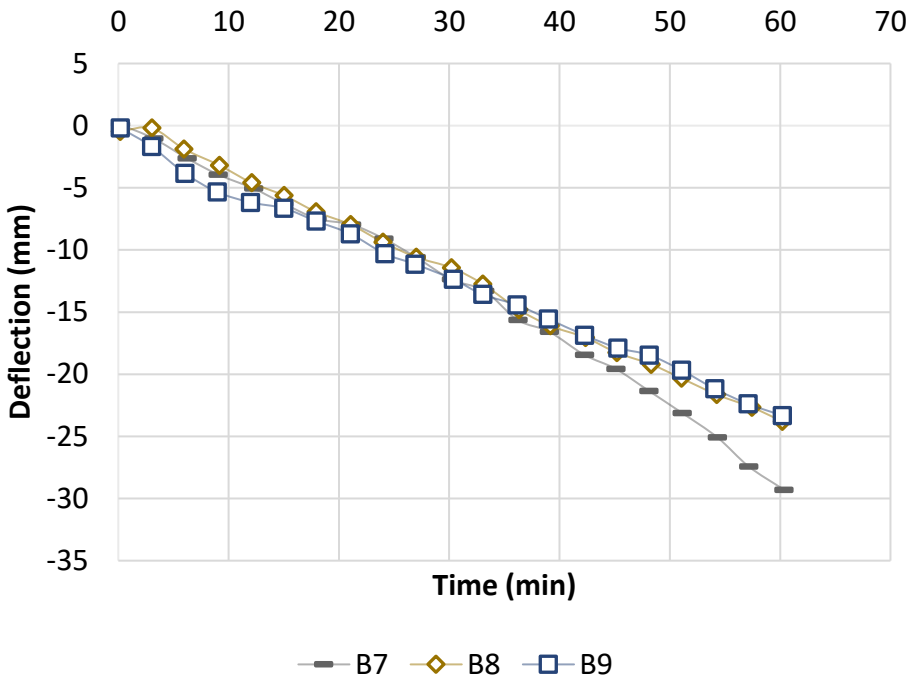

(c)

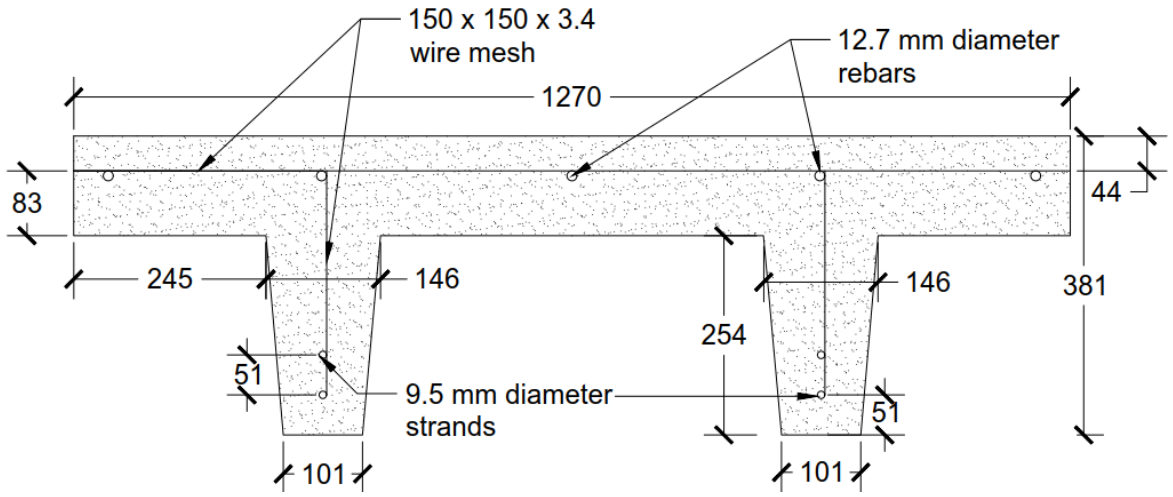

Figure 2.7 Geometry of tested PC double-tee beams in an experimental study by Selvaggio and Carlson [33]

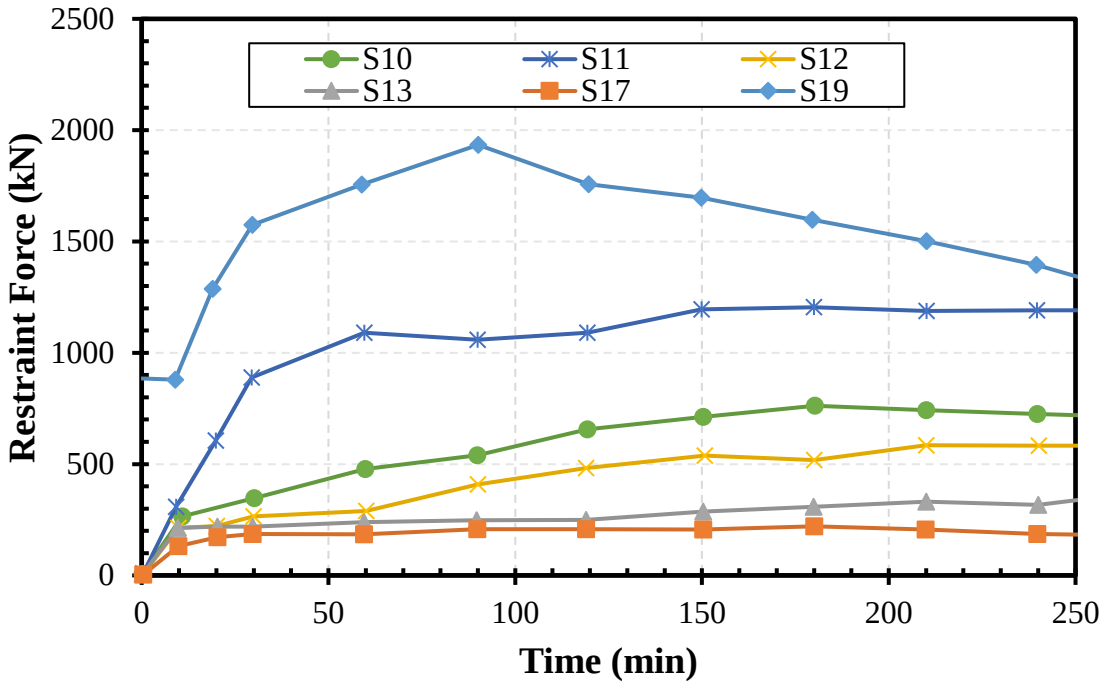

Figure 2.8 Magnitude of fire induced restraint force throughout fire exposure in restrained PC double-tee beams [33]

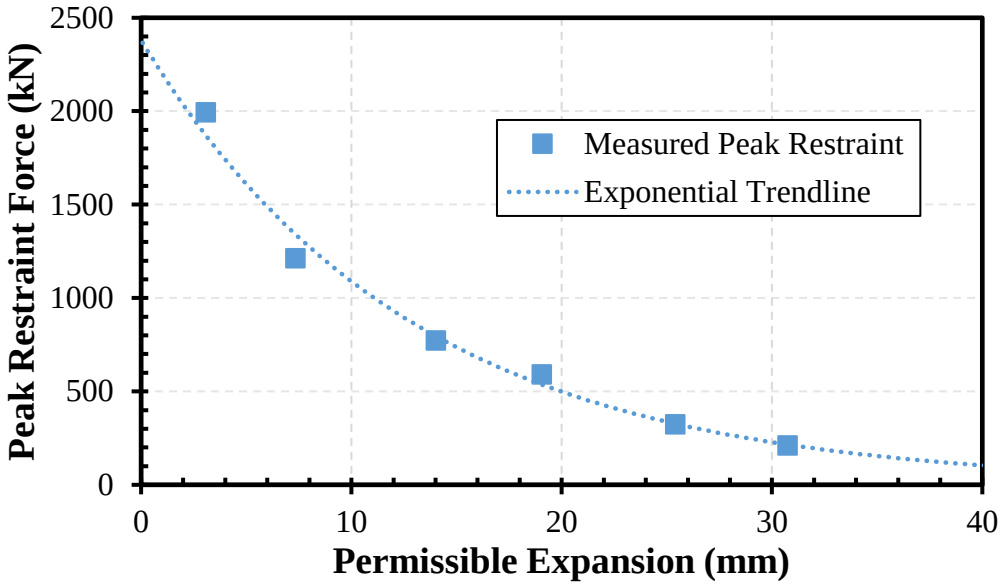

Figure 2.9 Maximum fire induced restraint force corresponding to permissible longitudinal expansion in restrained PC double-tee beams [33]

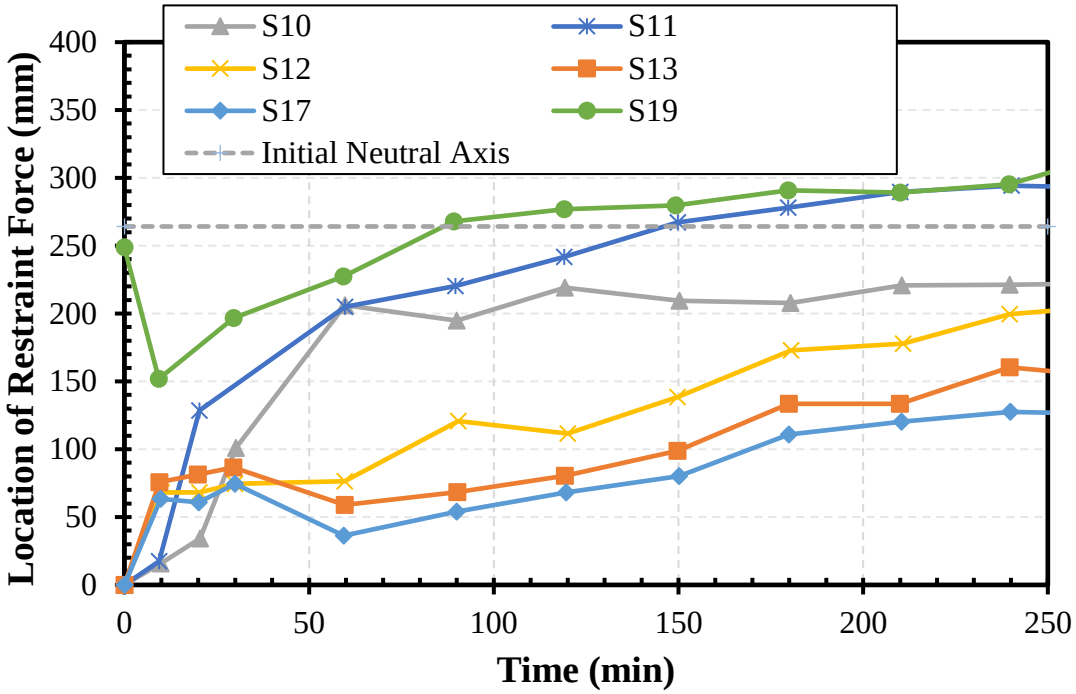

Figure 2.10 Location of fire induced restraint force from bottom of specimens relative to initial neutral axis throughout fire exposure in PC double-tee beams [33]

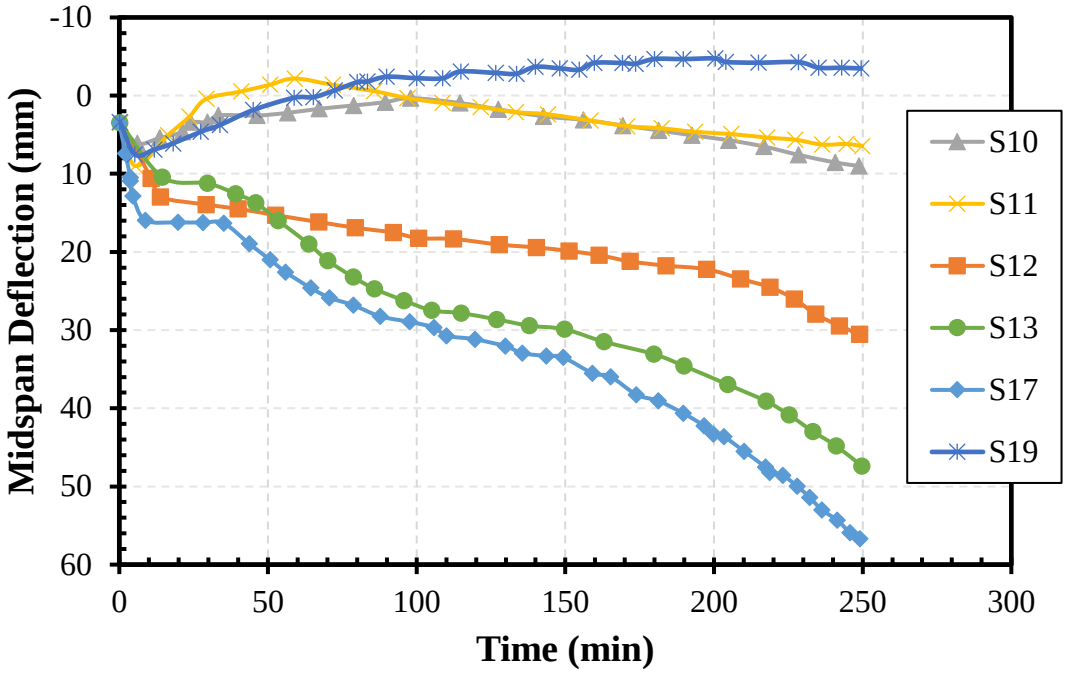

Figure 2.11 Midspan deflection of restrained PC double-tee beams [33] (+ve values represents downward deflection and -ve values upward)

CHAPTER 3

3 Fire Resistance Experiments

3.1 General

As discussed in previous chapter there is a lack of experimental studies on PC beams under fire exposure, especially under restrained conditions. Most of the experimental studies focus on unrestrained fire response of PC beams, and there is a lack of experimental data on evolution of fire induced restraint forces in PC beams. Also, three is a scarcity of experimental studies where identical PC beams were tested simultaneously, one under restrained and other under unrestrained conditions while exposing both to identical fire and loading conditions. This causes a lack of baseline data for fire response of unrestrained PC beams, which can be compared to their identical restrained counterparts. This limits the applicability of experimental data for validation as there is lack of baseline unrestrained response to fully gauge the effect of fire induced restraint forces on fire resistance of PC beams. Thus, there is a lack of reliable experimental data which can be used to validate the numerical models.

Therefore, to study the fire response of PC beams under restrained and unrestrained conditions, a detailed experimental study is designed and undertaken herein. The experimental program consisted of conducting two fire resistance tests on four PC beams under varying fire, loading, and restraint conditions. NSC beams N1 and N1R are tested in fire Test 1, and HSC beams H1 and H1R are tested in fire Test 2. In each fire test, two identical beams were tested simultaneously, one under simply supported and other under restrained end conditions. Fire tests were conducted till failure of beams and their thermo-mechanical response was recorded in terms of sectional temperatures, deflections, and developed restraint force. The data generated from experiments is crucial for understanding fire response of restrained and unrestrained PC beams and is vital for validation of numerical models. These results have been published by author and can be found in the literature [94], however, a more detailed discussion on the same is provided below. Full details on the design of beams, fabrication of beams, test equipment, instrumentation, and test conditions and procedure are presented below.

3.2 Design of beams

All tested beams (labeled as N1, N1R, H1, and H1R) were designed as per PCI design handbook specifications to represent commercially used beams in practice. To minimize number of variables, all beams had identical reinforcement detailing and rectangular cross-section with dimensions of 3962 x 305 x 406 mm (length x width x depth). Detailed dimensions, reinforcement, and instrumentation detailing for tested beams are illustrated in Figure 3.1. Main reinforcement in all beams constituted of 5 low relaxation 12.7 mm diameter strands with an ultimate tensile strength of 1860 MPa and were prestressed to 70% of ultimate strength (1302 MPa). According to ACI 318 [95], a minimum shear reinforcement was provided using 9.5 mm diameter stirrups (ultimate tensile strength of 415 MPa) spaced at 254 mm center to center. To hold the stirrups in place (form

rebar skeleton), two 12.7 mm diameter rebars were provided on top and one at bottom with an ultimate tensile strength of 415 MPa. Also, two lift loops were embedded in all beams at 305 mm from beam end to ensure smooth stripping of the beams from casting bed. Further, to have a fire resistance rating of 4 hours under restrained and unrestrained conditions, all beams were designed with a concrete cover of 76 mm as per PCI manual 124 (see Table 1.2).

3.3 Fabrication of beams

All beams were cast at a local fabrication plant (Kerkstra Precast Inc., Grandville, MI), where a long formwork with partitions was fabricated to cast all beams with same continuous prestressed strands to ensure identical prestress in all beams as shown in Figure 3.2. Once the rebar skeleton was ready in the formwork, corresponding instrumentation was installed in terms of thermocouples and strain gauges in beams prior to pouring of concrete. A total of 18 Type-K chromel-alumel thermocouples were installed at three different sections in each beam for measuring concrete and rebar temperatures. Three sections for thermocouple installation were selected as mid length of beam, and two sections at 762 mm each on both sides of mid-section (see Figure 3.1). This provided sectional temperatures in entire fire exposed region for PC beams and provided better insights on heat transfer within beam under fire exposure. Also, three strain gauges were provided in all beams, one at middle strand and other two at holder rebars. Detailed location of thermocouples and strain gauges is illustrated in Figure 3.1.

After installation of instrumentation, beams N1 and N1R were cast with NSC Mix 1 concrete and beams H1 and H1R were cast with HSC Mix concrete. NSC Mix 1 measured 28 days and test day compressive strength of 28 and 28.1 MPa, respectively. Whereas HSC Mix measured 28 days and test day compressive strength of 56 MPa and 78.4 MPa, respectively. All beams were stripped once compressive strength of concrete reached 24.1 MPa (allowable compressive strength at

prestress transfer) and were stored for 28 days at the casting yard. Then beams were shipped to Michigan State University Civil Infrastructural Laboratory where they were stored at 25^{o}C average temperature and 40% relative humidity till fire tests were conducted (503 days for beams N1 and N1R, and 550 days for beams H1 and H1R). More details on the testing of beams and a summary of fire resistance results are provided in Table 3.1, and details on NSC and HSC concrete mix are provided in Table 3.2.

3.4 Test equipment

The fire resistance tests on PC beams were conducted using structural fire testing furnace at Michigan State University Civil Infrastructural Laboratory (shown in Figure 3.3). This furnace is capable of applying similar fire and loading conditions that are present in real buildings and have been successfully used for several fire tests [96]. Furnace consists of a load bearing steel framework, heating chamber of 2.44 x 3.05 x 1.68 m (width x length x height), six natural gas burners, six thermocouples in heating chamber, exhaust for gases, six hydraulic jacks (three per beam) for applying vertical gravity loads, one small hydraulic jack to apply variable axial restraint, two view ports, and a data acquisition unit to collect and store data electronically. Heating chamber has multiple cutouts specifically designed to accommodate testing of two beams at once inside furnace under four point or three point loading schemes. One of these beams can be tested under simply supported conditions and other can be tested under restrained conditions. This furnace can produce a maximum heat power of 2.5 MW and can apply a maximum gravity load of 244 kN under four point loading scheme and 2668 kN under three point loading scheme.

3.5 Test conditions and procedure

As discussed previously, a total of two fire tests were conducted in this study and they are designated as Test 1 (on NSC beams N1 and N1R) and Test 2 (on HSC beams H1 and H1R). In

both fire tests, realistic fire exposures were selected which are illustrated in Figure 3.4. Fire exposure DF1 is designed to follow slightly higher temperatures than ASTM E119 standard fire curve in the first 60 minutes, and then have a consistent decay after 60 minutes of fire exposure till the failure of beams. This is to represent a realistic building fire with a decay phase, and it was selected for Test 1 NSC PC beams to understand the behavior of PC beams during cooling phase. On the other hand, fire exposure DF2 was designed to follow temperatures higher than ASTM E119 fire exposure for first 120 minutes of fire exposure or failure of beams, and then followed by a sharp decay phase. The 120 minute limit was based on preliminary studies which indicated that HSC PC beams may fail around 120 minutes of fire exposure. During Test 2, HSC beams failed at 62 (beam H1) and 67 (beam H1R) minutes, therefore, cooling phase of DF2 was started at 67 minutes. Also, this fire exposure was selected for Test 2 HSC PC beams to understand the extent of spalling in PC beams, as HSC is more likely to spall than NSC beams.

In Test 1, beam N1 is tested under unrestrained conditions and beam N1R is tested under restrained end conditions. For beam N1, simply supported (unrestrained) end conditions were applied by placing beam ends on half round steel bars. For beam N1R, axial restrained conditions were applied by attaching steel I beam (W16x26) between the center of beam and frame column on one end, and a hydraulic jack on the center of the beam on another end (see Figure 3.3). To make sure there is no local spalling of concrete at beam ends from developed restraint, steel plates of 38.1 mm thickness and same cross section as beams were connected at both ends of restrained N1R beam as shown in Figure 3.3. Also, for safety of the furnace loading frame, maximum developed restraint force is limited to 120 kN. Both beams were loaded using four point loading scheme as shown in Figure 3.1. Also, to measure deflection of beam under applied loads, LVDTs (linear variable displacement transducers) were connected at midspan, and at the center of beam

on left end to measure axial displacement under fire exposure for beam N1. However, for beam N1R, LVDTs were connected to measure deflection under applied loads and at midspan only.

After placing both beams in furnace at desired support conditions and applying loads, all gaps in the furnace lid and cutouts were covered using insulation to minimize heat losses during fire test. Then all instrumentation (thermocouples, strain gauges, and LVDTs) of beams was connected to data acquisition unit to record fire response throughout fire exposure. Both beams N1 and N1R were loaded to 55% load ratio by applying net moment of 131.4 kN-m by two point loads prior to the test, and these loads were maintained throughout the fire test to represent typical loading conditions under fire exposure in buildings. Beams N1 and N1R were exposed to fire exposure DF1, and to ensure desired rapid increase in fire temperature in the initial stages of DF1, furnace was preheated to 200^{o}C prior to starting the fire test. Once the fire test was started, pictures of fire exposed beam surfaces were taken at every 5 minutes to monitor the progression of spalling and fire response was recorded through thermocouples, strain gauges, and LVDTs for the entire duration of fire exposure. At 112 minutes of DF1 fire exposure, both beams N1 and N1R had failed due to inability to carry applied loading. Hence, the fire test was stopped at 116 minutes by turning off all burners, reducing applied loading to zero, and allowing temperatures inside furnace to cool naturally.

Similar procedure was followed in Test 2 for beams H1 and H1R as well where beam H1 was tested under simply supported conditions and beam H1R under restrained. The only key difference is the applied moment (which is 154.36 kN-m for beams H1 and H1R to induce a load ratio of 55%), and fire exposure (fire exposure DF2 is used in Test 2). DF2 fire exposure was planned to have slightly higher temperatures than standard ASTM fire with no decay phase until 120 minutes of fire exposure or till the failure of both beams. Both beams H1 and H1R failed at 67 minutes,

and therefore, all burners were turned-off at this point, loading was removed, and furnace temperatures could cool down naturally. Fire response of all tested beams was recorded in terms of sectional temperatures, strains, fire induced restraint forces, and deflections.

3.6 Results and discussion

The response of the beam is traced using sectional temperatures, midspan deflections, and evolution of fire induced restraint forces for entire duration of fire exposure till failure. Also, observations were made throughout during the test to monitor the changes such as spalling. A detailed discussion on the measured fire response of the beam is provided below.

3.6.1 Thermal response

Thermal response of tested beams is measured in terms of sectional temperatures and evolution of sectional temperatures for all beams is illustrated in Figures 3.5 and 3.6, respectively. For brevity, only thermocouple labels are used in Figures 3.5 and 3.6, and their exact location is same in all beams and can be referred to Figure 3.1. It should be noted that some of the thermocouples failed during fire tests (especially near fire exposed surface for HSC beams) and provided spurious results and are therefore not reported herein. It can be observed from Figure 3.5 that for beams N1 and N1R, thermocouple T7 near exposed surface reported highest temperatures throughout fire exposure, and thermocouples reported gradual decrease in temperatures towards insulated face at the same exposure time. This is due to high thermal inertia of concrete which does not allow the sectional temperatures to increase rapidly at more insulated depths. As we progress from fire exposed bottom face towards unexposed insulated top surface, thermal inertia of concrete keeps on increasing due to increase in volume of concrete between exposed face and the depth at which temperatures are measured. This increase in thermal inertia slows the increase in sectional temperatures, and as a result thermocouples reported lower sectional temperatures towards the top

unexposed face. Also, during the fire test, visual observations made through view ports showed only minor spalling in beams and a minimal reduction in section prior to failure of beam. Only during the last 5 minutes of failure, large chunks of concrete spalled off beams N1 and N1R near midspan. This allowed minimal change in thermal inertia of the concrete beams N1 and N1R prior to failure and therefore, spalling had minimal impact on sectional temperatures prior to failure.

Further, the strand temperatures for beams N1 and N1R (reported by thermocouples T1, T2, T8, T13, and T14) show that strand temperatures increased slowly in the first 20 minutes of DF1 fire exposure, then a gradual increase in strand temperatures is observed between 20 to 130 minutes, followed by a decay of temperatures at a lag of 70 minutes from start of decay phase in DF1 fire temperatures. This initial lag in growth of strand temperatures and lag between start of decay phase between fire temperatures and sectional temperatures is primarily due to high thermal inertia of concrete. Also, corner strand temperatures (reported by thermocouples T1 and T13) are higher than inner strands. This is due the fact that corner strands are closer to the exposed side face, and this causes a rapid increase in these strand temperatures. Also, the variation in strand temperatures at the same depth and width can be attributed to the variation of fire temperatures within the furnace. Therefore, it is possible that one face of the beam got exposed to slightly higher temperatures than other face due to local variation in fire temperatures within the furnace. Therefore, to capture the effect of these local fire temperature variations, thermocouples were provided at all strand locations at three different sections throughout the beam length. Also, it is evident from Figure 3.5 that temperature in the quarter mid-section from top are very similar to the unexposed face temperatures and follow similar trends which can be gain attributed to the high thermal inertia of concrete at these depths. Overall, beams N1 and N1R showed similar sectional temperatures, as they have identical geometry, reinforcement, and material properties.

On the other hand, it can be observed from Figure 3.6 that sectional temperatures in HSC beams H1 and H1R increased at a much faster rate than NSC beams. This is primarily due to relatively higher degree of spalling in HSC beams which caused a reduction in the cross-section (thermal mass) of beams. This reduction in section caused a decrease in the thermal inertia of the beam which allowed a faster progression of sectional temperatures. The corner strand's peak temperature for beam H1R reached as high as 600^{o}C, whereas peak strand temperatures for all other NSC beams are well below 520^{o}C. This high increase in corner strand is attributed to spalling in HSC beam H1R which significantly decreased concrete cover to corner strand. Due to decrease in concrete cover, corner strand temperatures for beam H1R had less thermal inertia to impede the progression of temperatures, and for this reason temperatures increased to as high as 600^{o}C. Also, as compared to NSC beams N1 and N1R, there was relatively less time lag between start of decay phase between corner strand temperatures and fire temperatures due to higher degree of spalling in HSC beams. Further, spalling caused most of the near surface mounted thermocouples to fall off or malfunction, and therefore, those results are not shown in Figure 3.6. A summary of thermal results is provided in Table 3.3.

3.6.2 Structural response

Structural response of tested beams was measured in terms of midspan deflection, axial displacement, and evolution of fire-induced restraint forces and it is shown in Figures 3.7 to 3.8. It can be observed from Figure 3.7 that all beams deflect slightly at the onset of initial loading, which was applied and maintained at 55% of beams capacity about 20 minutes prior to fire exposure. This deflection is at room temperatures, and this is done to represents typical beams in buildings with deflection under service loads. At the start of fire exposure, both beams N1 and N1R show a sudden increase in the deflections in the first 20 minutes of fire exposure. This can be

attributed to the sudden loss of prestress in strands due to rising thermal strains in strands from increase in sectional temperatures. However, the sectional temperatures for concrete are very low in the first 20 minutes of fire exposure (see Figure 3.5) and therefore, cause only minimal material degradation. Then between 20 minutes to 80 minutes of Df1 fire exposure, beams N1 and N1R undergo moderate increase in deflections. This is since strand temperatures are below 400^{o}C and sectional temperatures are below 250^{o}C. While these temperatures can cause material degradation, it is not significant enough to cause rapid increase in deflection of the beams N1 and N1R.

However, after 80 minutes of fire exposure, strand temperatures increase above 400^{o}C, and they undergo significant material degradation as shown in Figure 1.1. Therefore, beam N1 and N1R deflections start to increase rapidly after 80 minutes of fire exposure. However, it can be observed from Figure 3.7 that deflections for beam N1R are significantly less than beam N1 after 80 minutes of fire exposure. This can be attributed to the presence of fire included restraint forces which mitigate the applied moment on the beam and therefore, decrease the rate of deflection in beam N1R. At 102 minutes of DF1 fire exposure, beam N1 deflections started to increase rapidly, and it could no longer maintain the applied loads, thus, causing it to fail. Whereas, due to the mitigation of applied loading by fire induced restraint forces in beam N1R, it failed slightly later at 112 minutes. Thus, fire induced restraint forces increased fire resistance of NSC PC beam N1R by 9.8% as compared to its unrestrained counterpart beam N1. After the failure, loads were removed, and furnace burners were turned off and the furnace was allowed to cool naturally. It should be noted that at the point of failure for beam N1, the displacement transducer hook on the top of beam broke off due to crushing of concrete and therefore a sharp recovery of deflections is observed for the beam N1 only.

On the other hand, HSC beams H1 and H1R failed relatively much faster than NSC beams N1 and N1R. It can be observed from Figure 3.7 that beams H1 and H1R had a similar increase in the deflections in the first 20 minutes of fire exposure due to loss of prestress in strands. However, for both beams H1 and H1R the deflections started to increase rapidly after 40 minutes of fire exposure only as compared to 80 minutes for NSC beams. This is due to the presence of spalling in HSC beams which increases the strand and sectional temperatures much faster in HSC beams than as compared to NSC beams. This can be confirmed by observing Figures 3.5 and 3.6 that sectional temperatures increased much rapidly for HSC beams than for NSC beam. This causes a much faster degradation in the material properties of strands and concrete in HSC beams, and the loss of cross-section from spalling further exacerbates the load capacity of the beam. Therefore, spalling, and rapid rise in sectional temperatures caused an earlier failure in HSC beam H1 at 62 minutes. However, similar to NSC beams, fire induced restraint forces mitigated the applied loading for beam H1R and delayed the failure slightly to 67 minutes. Hence, fire induced restraint forces increased the fire resistance of HSC PC beam H1R by 8% than as compared to unrestrained counterpart beam H1.

Further, to understand the unrestrained thermal expansion of beams, measured thermal expansion for beams N1 and H1 is provided in Figure 3.8. It can be observed from Figure 3.8 that thermal expansion of the beam increases gradually for about 30 minutes for HSC beams H1 and for about 40 minutes for NSC beam N1. Then the thermal expansion of the beam increased consistently with rising sectional temperatures. Then some noise is captured at the end of fire exposure during the failure of the beam as deflection increases suddenly. It should be noted that thermal expansion of HSC beams is slightly faster than the NSC beams due to higher sectional temperatures. However, both NSC beams N1 and HSC beam H1 undergo almost similar peak thermal expansion prior to

the failure. This can be attributed to the identical sections and thermal expansion properties for NSC and HSC concrete.

3.6.3 Evolution of fire induced restraint forces

Evolution of fire induced restraint forces for tested PC beams is shown in Figure 3.9. For PC beam N1R, restraint force is minimal in the first 16 minutes of fire exposure, and then a sudden increase in restraint force occurs at about 20 minutes to 35 kN. Restraint force then undergoes small variation till 60 minutes of fire exposure and then a consistent increase is observed to 60 kN till 90 minutes. After that restraint force fluctuates around 60 kN till failure. Based on these observations from beam N1R, it is inferred that reason for minimal restraint force in the first 16 minutes of fire exposure can be prestressing in the beam which mitigates thermal expansion of beam, thus, reducing the magnitude of restraint force. Sudden increase in restraint force at 20 minutes to 35 kN can be attributed to an increase in thermal expansion of beam due to increasing loss of prestress due to rising temperatures. Small variation in restraint force till 60 minutes can be due to increasing deflection of the beam which keeps pulling beam inwards and reducing thermal expansion, thus, allowing restraint force to constrain thermal expansion of beam for similar magnitude even though temperatures are rising. However, once thermal expansion caused by rising sectional temperatures overcome the effect of deflections and prestress, a consistent increase in thermal expansion occurs which causes a consistent increase in restraint force to 60 kN till 90 minutes. At this stage reduction in strength of strands seems to become more dominant which mitigates thermal expansion of beam by increasing deflections and allows a similar level of restraint force to constrain thermal expansion of beam till failure.

On the other hand, for beam H1R, restraint force suddenly increased to 27 kN at 12 minutes of fire exposure and then fluctuated around that till failure. Relative to beam N1R, a smaller magnitude

of restraint force in beam H1R can be attributed to spalling of concrete which causes a relatively faster increase in deflection, and thus, mitigating thermal expansion of beam. Also, unlike beam N1R, restraint force does not increase again after 60 minutes of fire exposure when thermal expansion from rising sectional temperatures overcomes the effect of deflections and prestress. This can be attributed to the early failure of beam H1R at 67 minutes which does not allow ample time for beam to expand and overcome deflection and prestress effects.

Further, fire induced restraint forces in beams N1R and H1R (see Figure 3.9) follow similar trends as compared to the thermal expansion of unrestrained counterparts beam N1 and H1 in Figure 3.8. This is since fire induced restraint forces are directly proportional to the constrained thermal expansion. Hence, as the magnitude of constrained thermal expansion increases, it also increases the magnitude of fire induced restraint force required to constrain it. A summary of structural results is provided in Table 3.4.

3.6.4 Spalling

Spalling was measured by weighing the beams and onset of spalling was recorded using visual observations through viewing ports of furnace. In case of NSC beams N1 and N1R minor spalling occurred throughout fire exposure and only during failure of beam large chunks of concrete spalled at mid span of the beams. Also, water leaked out of the screw drilled at beam center to measure the axial displacement at beam ends during fire exposure which indicated that pore pressure buildup under fire exposure was mitigated in NSC beams as moisture was able to escape through the NSC beams during fire exposure. This is due to high permeability of the normal strength concrete which allows the moisture migration at elevated temperatures. Therefore, both NSC beams experienced minor spalling during fire exposure prior to failure. However, during failure of the beams N1 and N1R, concrete crushed at the top and spalled at the bottom at the midspan of the

beams. This can be attributed to the increase in compressive and tensile strains at top and bottom during yielding at the midspan which caused concrete crushing at the top and spalling at the bottom.

Unlike normal strength concrete, high strength concrete has a relatively dense microstructure and low permeability. Therefore, during fire exposure, pore pressure buildup cannot be mitigated as there is relatively less moisture movement in HSC beams. Also, no water leaked from beam ends for HSC beams which further indicates significant pore pressure buildup inside the HSC beams at elevated temperatures during fire exposure. This pore pressure buildup along with degradation of tensile strength of HSC at elevated temperatures caused significant spalling throughout fire exposure. Spalling seemed to occur throughout the fire exposed length of the beam, and it increased gradually with increase in temperatures.

To illustrate the differences in the spalling for NSC beams and HSC beams, a comparison of beam surfaces in the furnace prior to failure is shown in Figure 3.10 and beams after failure are shown in Figure 3.11. It can be clearly observed from Figures 3.10 and 3.11 that there is minimal spalling in NSC beams N1 and N1R prior to failure and after failure concrete crushing and spalling occurred at top and bottom of the beams near midspan. On the other hand, HSC beams spalled most of the clear cover concrete below shear reinforcement prior to failure and underwent large crushing at the top near midspan during failure. Moreover, to gauge the extent of spalling, beams were weighed prior to fire exposure and after fire exposure. The spalled concrete weight was measured at 123.3 kg (10.5% of beam H1 original weight) for beam H1, and 73.5 kg (6.3% of beam H1R original weight). Therefore, beam H1 spalled more than beam H1R. This can be attributed to the presence of fire induced restraint forces in beam H1R which mitigate the tensile stresses at the

beam bottom, thus, causing slightly less spalling. A summary of measured spalling and fire resistance is given in Table 3.5.

3.6.5 Fire resistance

Detailed fire resistance of the tested beams is provided in Table 3.5. NSC beams N1 and N1R failed at 102 minutes and 112 minutes, whereas HSC beams H1 and H1R failed at 62 minutes and 67 minutes, respectively. Therefore, restraint forces increased the fire resistance of NSC beams by 10% and by 8% for HSC beams. For beam N1, failure occurred from yielding of strands at the mid-span section when the applied moment significantly exceeded moment capacity at 102 minutes. For the restrained beam N1R, a significant chunk of concrete fell off at the mid-span zone before failure which exposed strands directly to fire. This accelerated the failure of this beam at 112 minutes. It should be noted that minimal spalling occurred in both beams N1 and N1R throughout fire exposure, and only in the last 5 minutes of failure significant spalling occurred by breaking large chunks of concrete at the mid-span zone.

In contrast with NSC beams, HSC beams H1 and H1R experienced spalling throughout fire exposure. This led to an increase in sectional temperatures and a relatively faster degradation in load-carrying capacity. For beam H1, failure occurred through yielding of strands at mid-span once the applied moment surpassed capacity at 62 minutes. In the case of beam H1R, restraint applied additional resisting moment to beam which mitigated the effect of spalling and material degradation to some extent and ultimately failed at 67 minutes. The failure patterns of the four PC beams, as observed in tests, are shown in Figure 3.11.Further, it can be observed from the images of failed beams in Figure 3.11 that restrained beams had relatively less crushing at critical section of midspan than as compared to unrestrained counterparts. Moreover, it should be noted that based on beam width and concrete cover, all these beams are predicted to have a fire resistance of 240

minutes under restrained or unrestrained conditions as per the PCI manual (see Table 1.1). Therefore, prescriptive approach may not yield accurate fire resistance assessment as it doesn't account for all factors governing fire response of PC beams.

3.7 Summary

Two fire tests are conducted on four PC beams under restrained and unrestrained conditions to quantify the effect of fire induced restraint force on the fire resistance of PC beams. In fire test 1, NSC PC beams N1 and N1R are simultaneously tested under DF1 fire exposure in unrestrained and restrained conditions simultaneously. In fire Test 2, HSC PC beams H1 and H1R are simultaneously tested under fire exposure DF2 in unrestrained and restrained end conditions, respectively. All beams were tested under a four point loading setup with a load ratio of 55%. Fire response of tested beams was recorded throughout fire exposure in terms of sectional temperatures, midspan deflections, axial displacements, and fire induced restraint forces. Based on the results of the fire tests it was observed that restraint forces could only increase the fire resistance by 8% to 10% for PC beams, and the beams did not reach their predicted fire resistance of 4 hours as per PCI manual. HSC beams experienced relatively more spalling due to the dense microstructure and consequently had higher section temperatures. This also caused the HSC PC beams to fail much sooner than their NSC counterparts which shows the significant effect of concrete type on fire resistance of PC beams.

Table 3.1 Summary of test parameters used in fire tests

Beam	Fire	Calcareous Concrete Strength, fc' (MPa)	Concrete Mix	Support Type	Load (kN)	Moment Capacity (kN-m)	Applied Moment (kN-m) [Load Ratio %]
N1	DF1	28.1	NSC Mix 1	SS	93.9	238.9	131.4 [55%]
N1R	DF1	28.1	NSC Mix 1	AR	93.9	238.9	131.4 [55%]
H1	DF2	78.4	HSC Mix	SS	110.4	280.7	154.4 [55%]
H1R	DF2	78.4	HSC Mix	AR	110.4	280.7	154.4 [55%]
R1 [9] [+]	SF	58.2	NSC Mix 2	AR	50	127.1	69.9 [55%]

[+]Restrained reinforced concrete beam selected for validation from literature [9]
Note: Strands were prestressed to 70% (1302 MPa) of their ultimate tensile strength in PC beams N1, N1R, H1, and H1R.
SS = Simply supported, AR = Axially restrained, NSC = Normal strength concrete, HSC = High strength concrete, DF1 and 2 = Design Fire 1 and 2, SF = Severe Fire

Table 3.2 Details of NSC and HSC concrete batch mix used in casting of beams

Description	**NSC Mix 1**	**HSC Mix**	**NSC Mix 2** [9]
Beams casted	N1, N1R	H1, H1R	R1
Cement (kg/m^3)	267	415	390
Fire aggregate (kg/m^3)	908	891	830
Coarse aggregate (kg/m^3)	771	1038	1037
Slag (kg/m^3)	77	-	-
Admixture (kg/m^3)	-	2.3	-
Water (kg/m^3)	153	110	156
Air entrainment volume (%)	1.5	0	-
Concrete 28 day compressive strength (MPa)	28	56	52.2
Age of cylinders on day of fire test (days)	503	550	480
Concrete test day compressive strength (MPa)	28.1	78.4	58.2

Table 3.3 Summary of measured thermal response

Beam	Fire Exposure	Strand Peak Temperatures at Failure (ºC)	Unexposed Face Peak Temperatures at Failure (ºC)	Measured Fire Resistance (min)
N1	DF1	470	75	102
N1R	DF1	472	190	112
H1	DF2	381	145	62
H1R	DF2	600	159	67

Table 3.4 Summary of measured structural response

Beam	Fire Exposure	Peak Deflection at Failure (mm)	Peak Axial Displacement at Failure (mm)	Peak Restraint Force (kN)	Failure Times (min)	Failure Modes
N1	DF1	107	8.3	-	102	Flexure-Ductile
N1R	DF1	102	-	65.3	112	Flexure-Brittle
H1	DF2	80	8.1	-	62	Flexure-Ductile
H1R	DF2	84	-	27.8	67	Flexure-Brittle

Table 3.5 Summary of measured spalling and fire resistance

Beam	Fire Exposure	Measured Fire Resistance (min)	Extent of Spalling	Moisture Migration Observation	Spalling Zones
N1	DF1	102	Minor (0.1% by original weight)	Yes, moisture consolidation observed at ends	Limited to Midspan
N1R	DF1	112 *	Major (10.5% by original weight)	Yes, moisture consolidation observed at ends	Limited to Midspan
H1	DF2	62	Minor (0.1% by original weight)	No moisture consolidation observed at ends	Most of the fire exposed length
H1R	DF2	67 *	Major (6.3% by original weight)	No moisture consolidation observed at ends	Most of the fire exposed length
* Restraint caused a 10 minute (9.8%) gain in fire resistance for NSC PC beams, and a 5 minute (8.1%) gain in fire resistance for HSC beams					

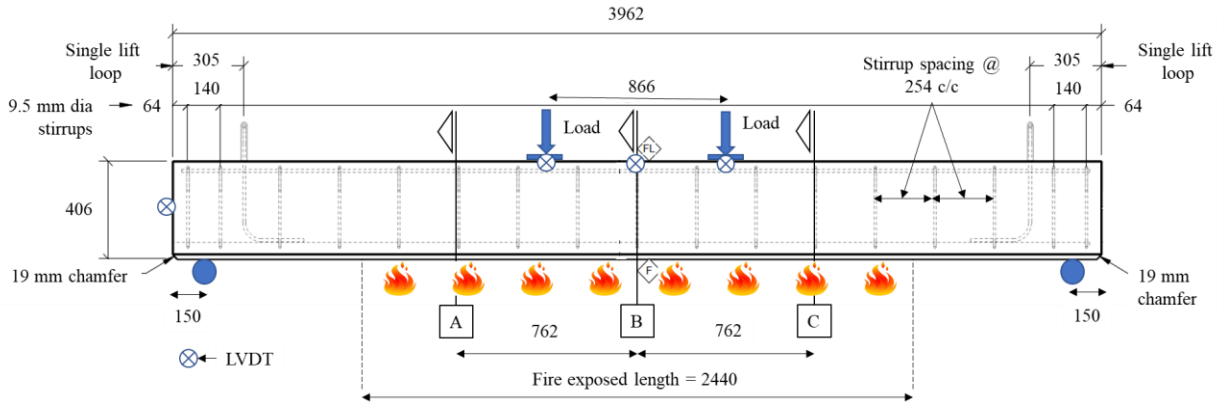

(a)

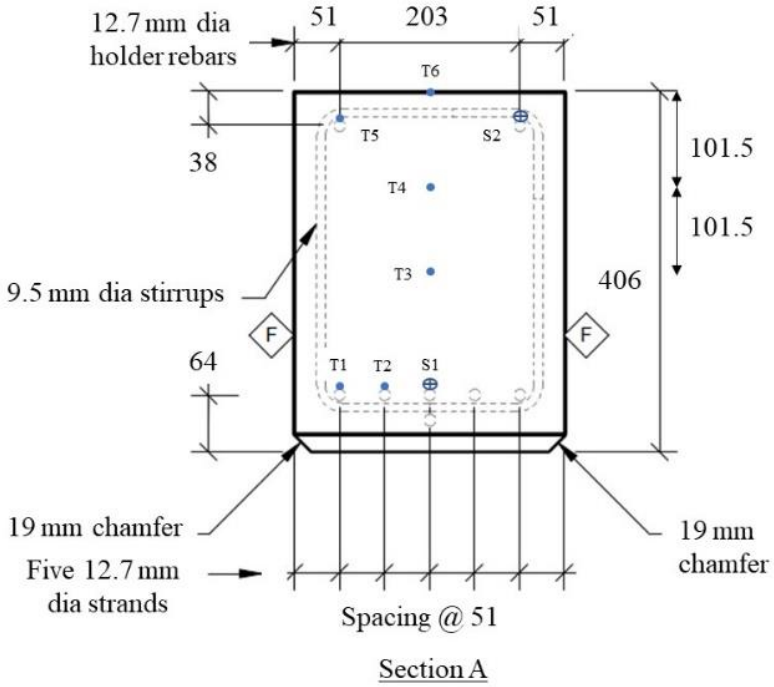

(b)

Figure 3.1 Reinforcement and instrumentation detailing of tested PC beams (a) side view, (b) Section A view, (c) Section B view, (d) Section C view; (all dimensions are in mm)

Figure 3.1 (cont'd)

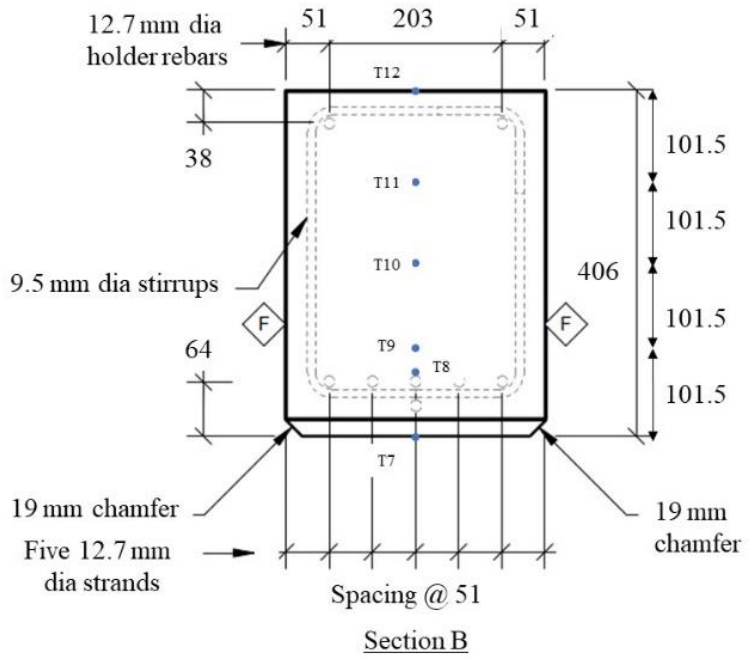

(c)

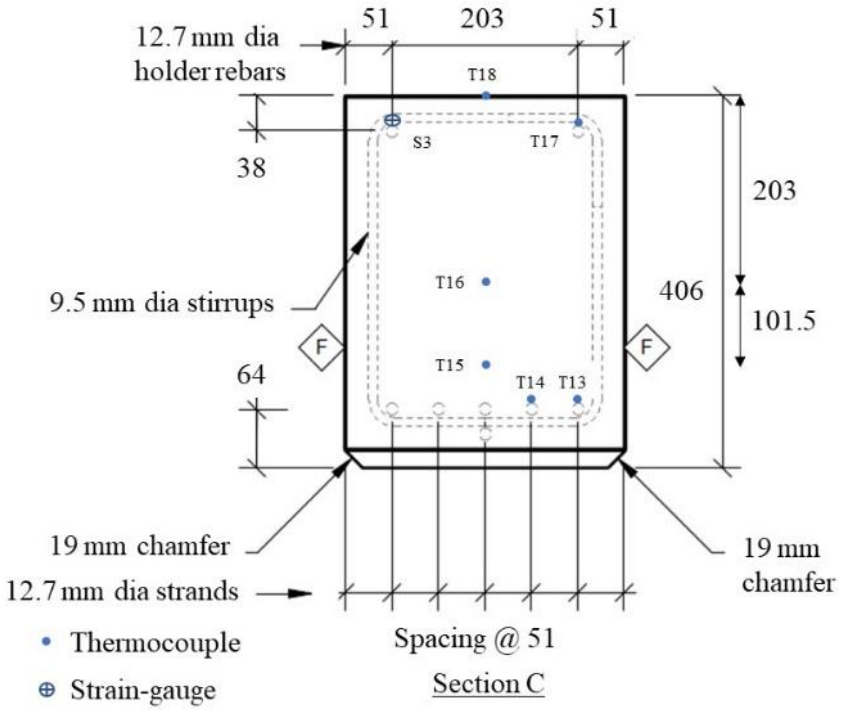

(d)

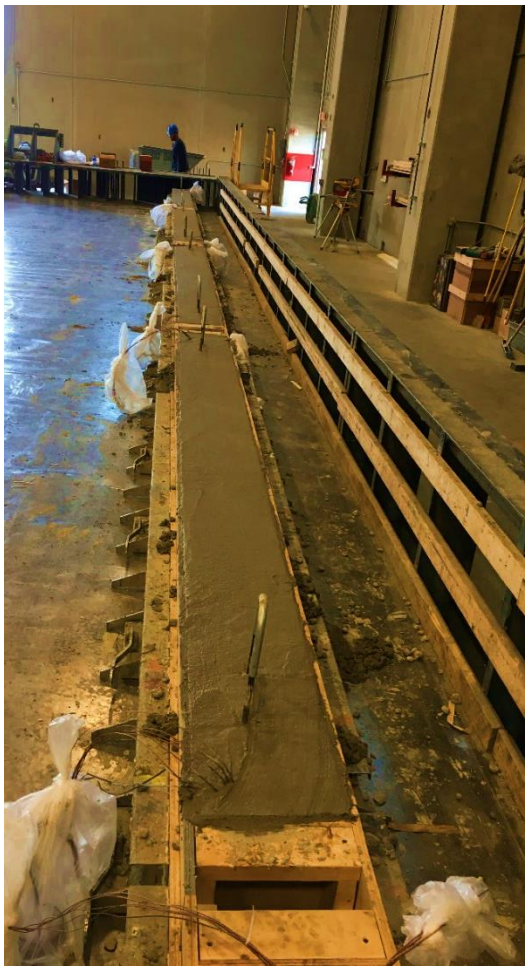

(a) (b)

Figure 3.2 Casting bed with shared continuous strands used for fabrication of PC beams in a continuous formwork (a) prestressing of strands, and (b) after pouring

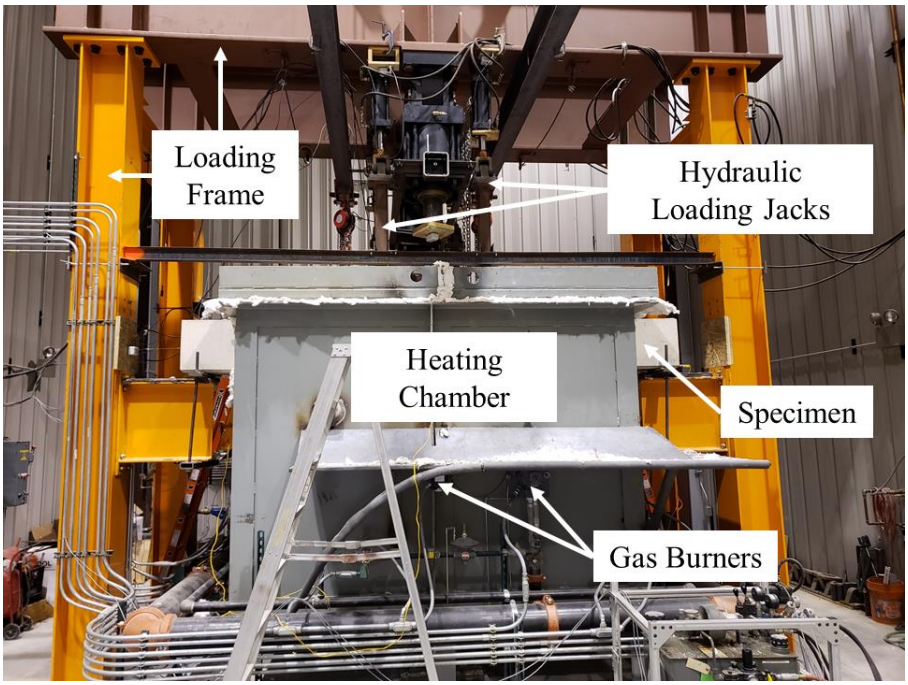

(a)

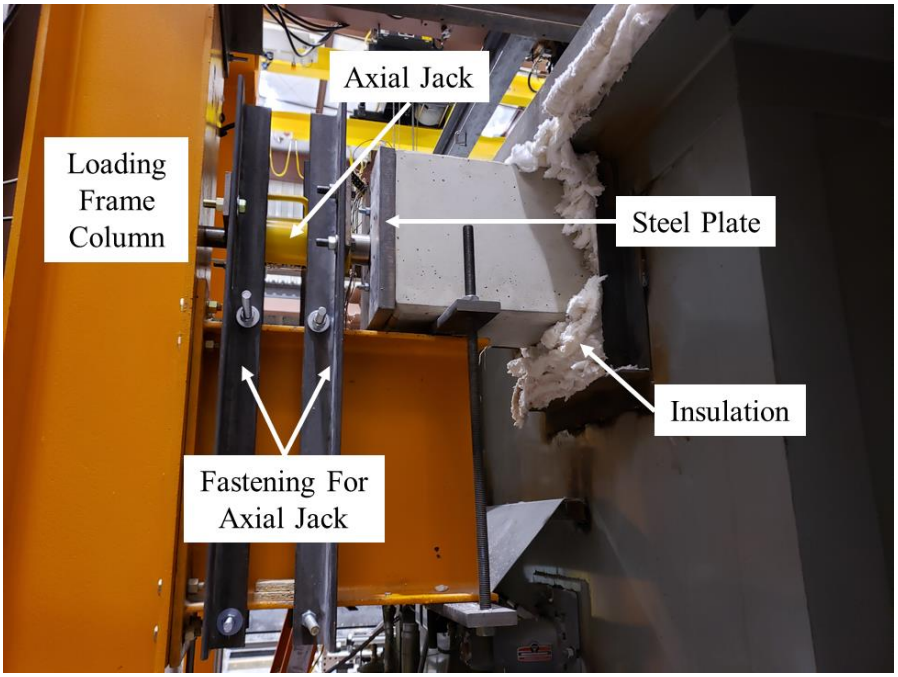

(b)

Figure 3.3 Experimental setup at MSU's fire test furnace (a) front view of fire test setup, (b) restrained end with hydraulic jack to measure developed restraint, (c) fully restrained end with I beam, (d) front view of I beam, (e) side view of I beam (beam and stiffeners have ultimate tensile strength of 415 MPa and all dimensions are in mm

Figure 3.3 (cont'd)

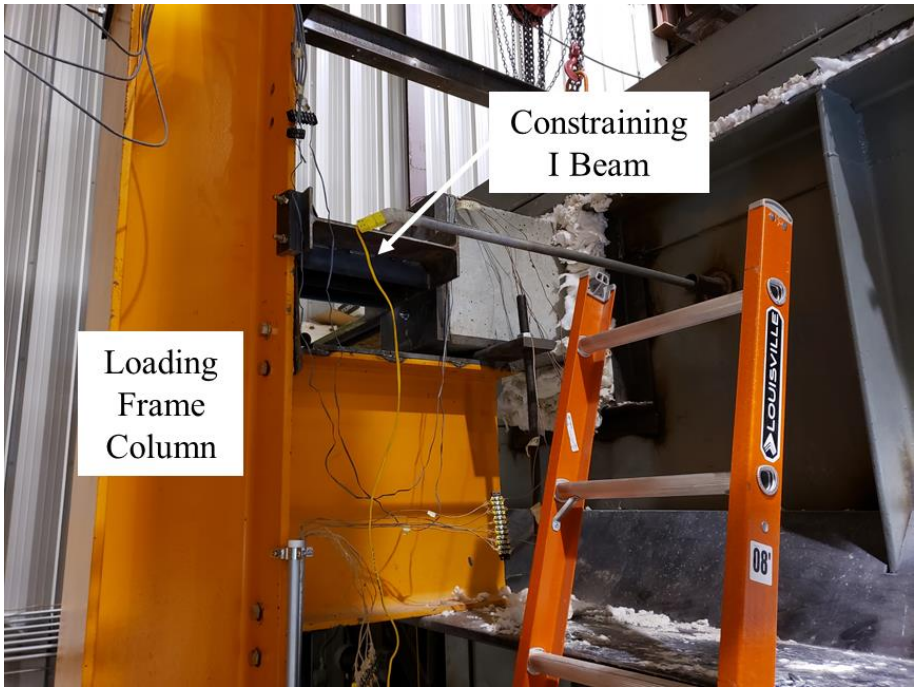

(c)

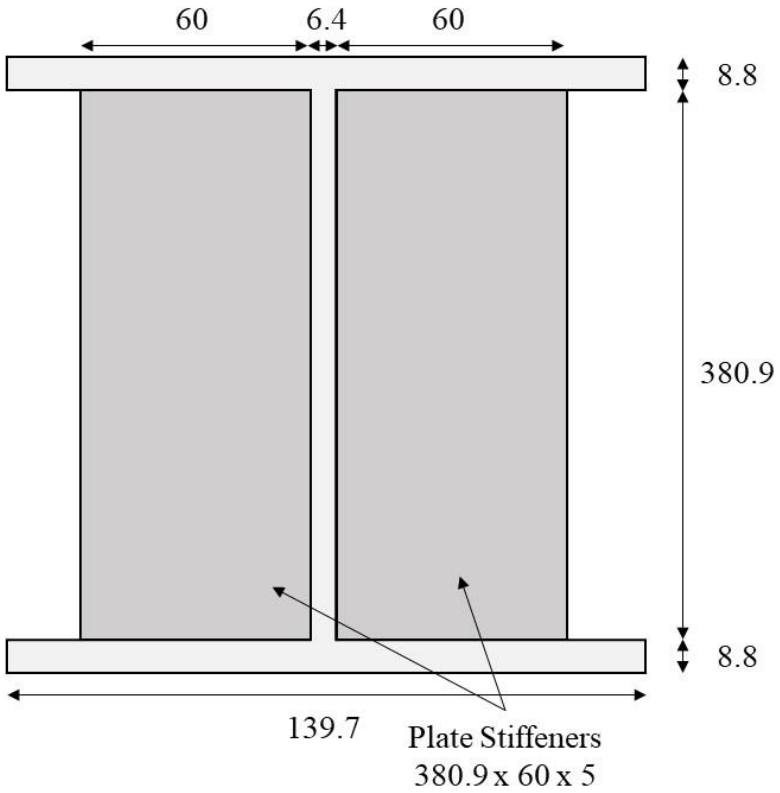

(d)

Figure 3.3 (cont'd)

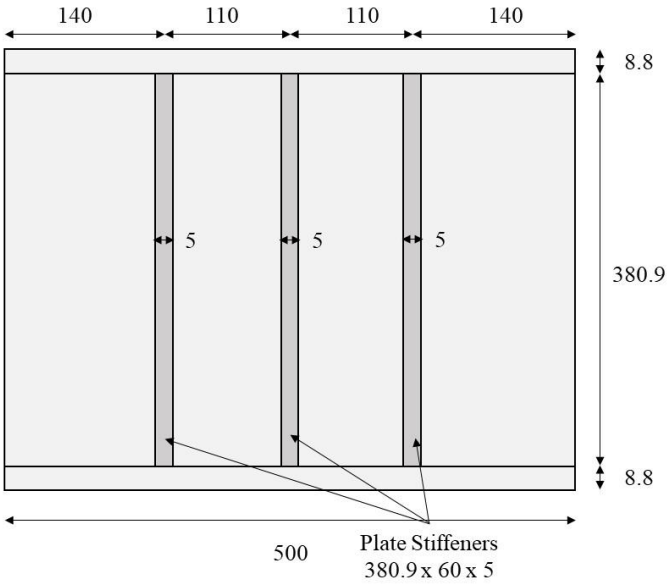

(e)

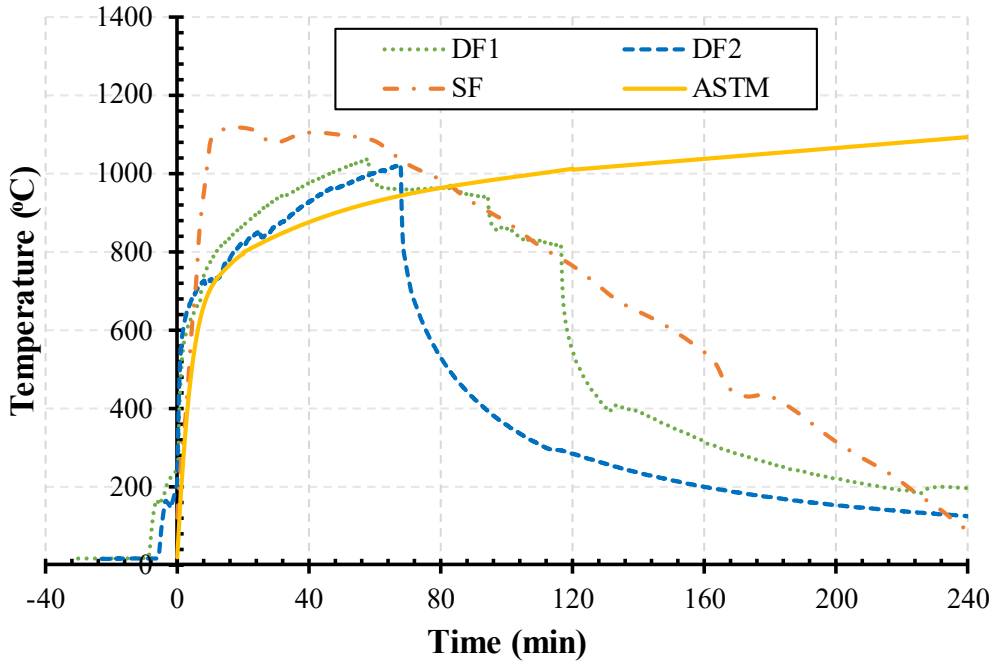

Figure 3.4 Time temperature curves for fire exposure used in the fire tests (DF1 = Design Fire 1, DF2 = Design Fire 2, SF = Sever Fire, ASTM = standard ASTM E119 fire curve)

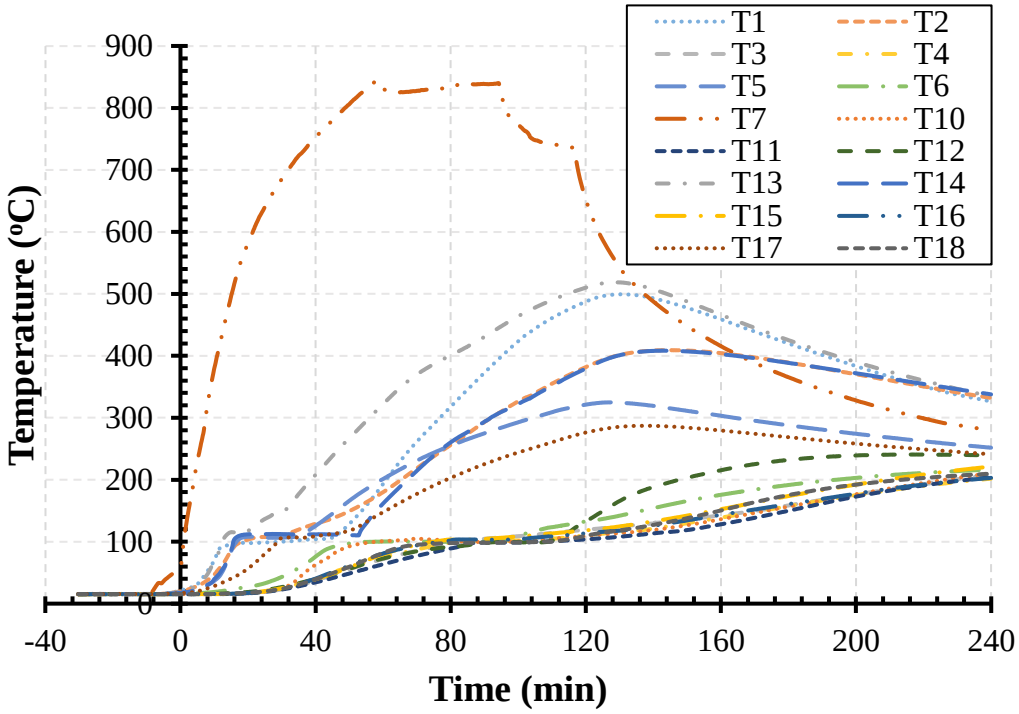

(a)

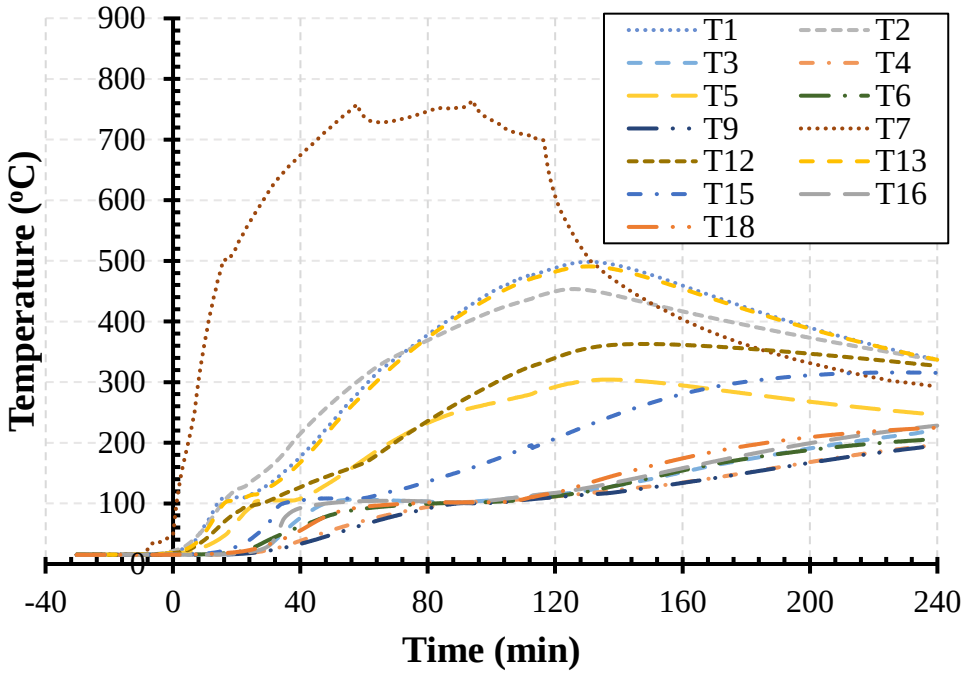

(b)

Figure 3.5 Progression of sectional temperatures in Test 1 under DF1 fire exposure (a) beam N1, (b) beam N1R

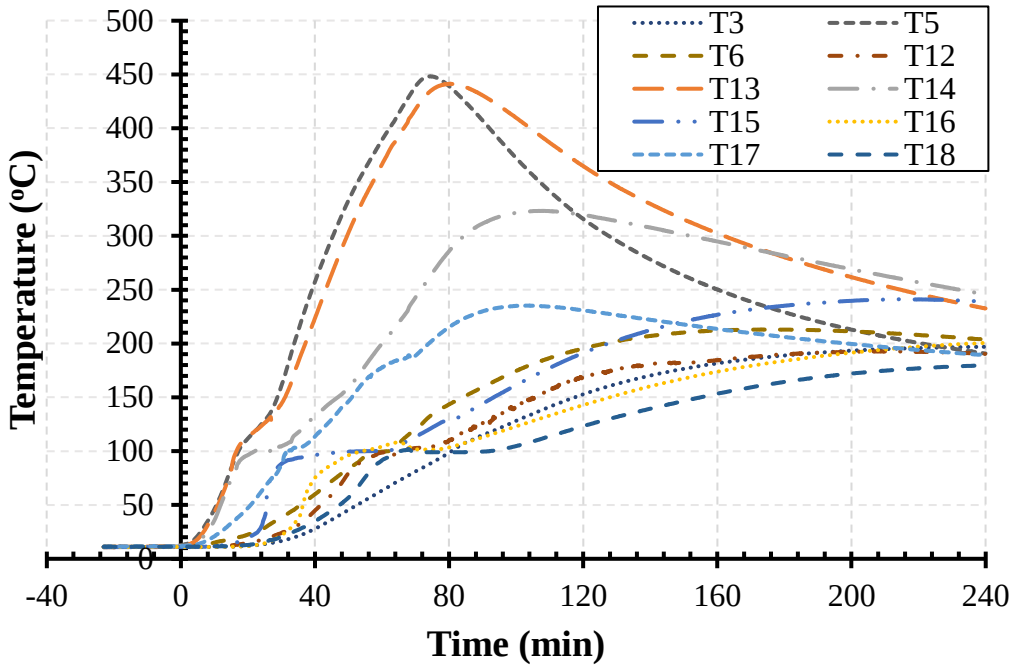

(a)

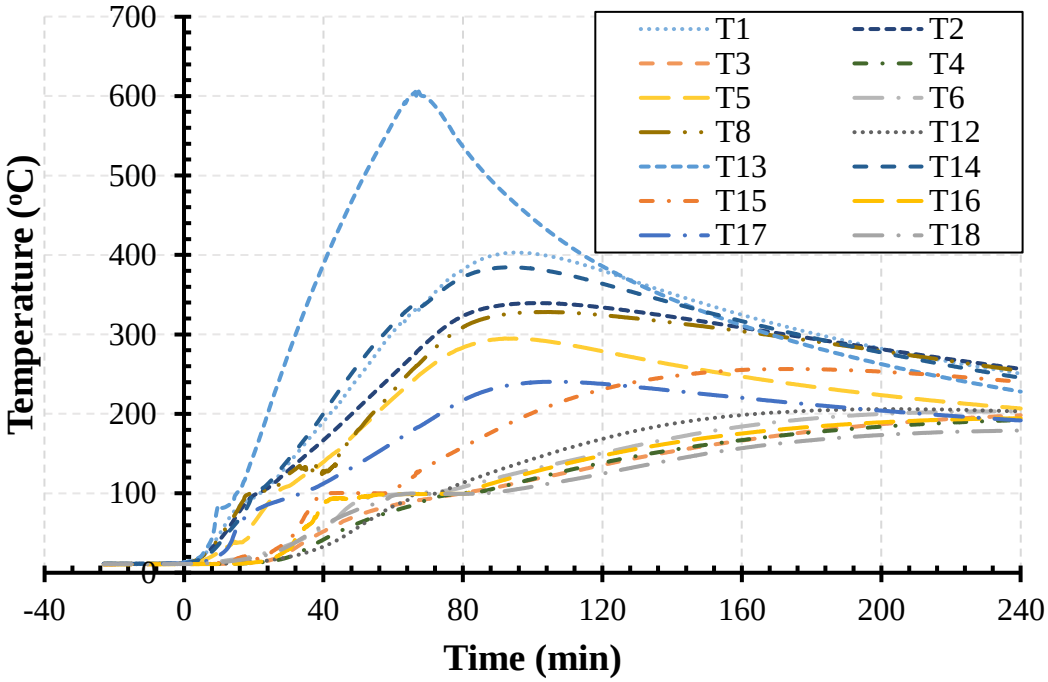

(b)

Figure 3.6 Progression of sectional temperatures in Test 2 under DF2 fire exposure (a) beam H1, (b) beam H1R

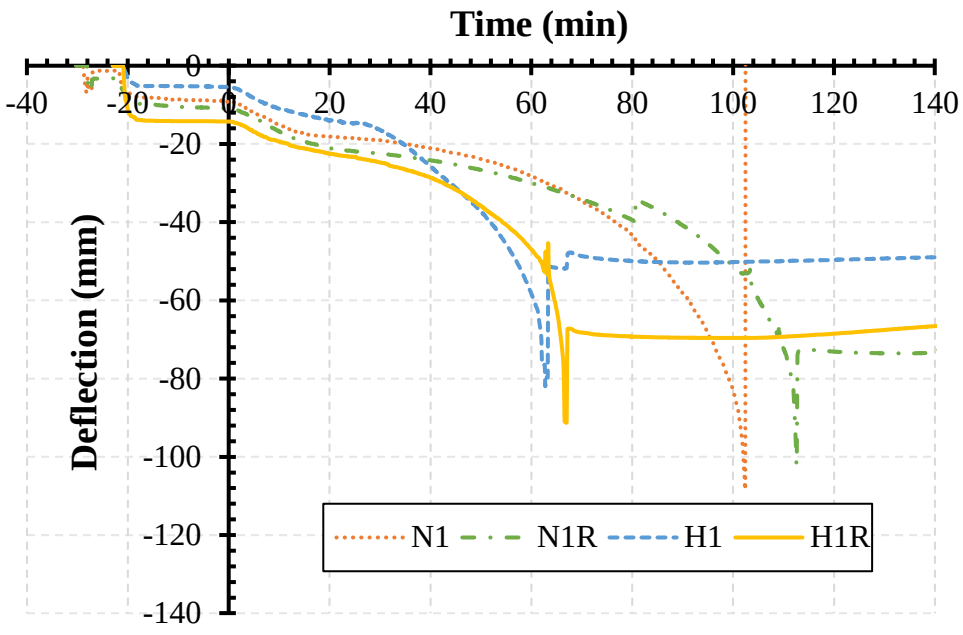

Figure 3.7 Progression of measured midspan deflections for all tested PC beams

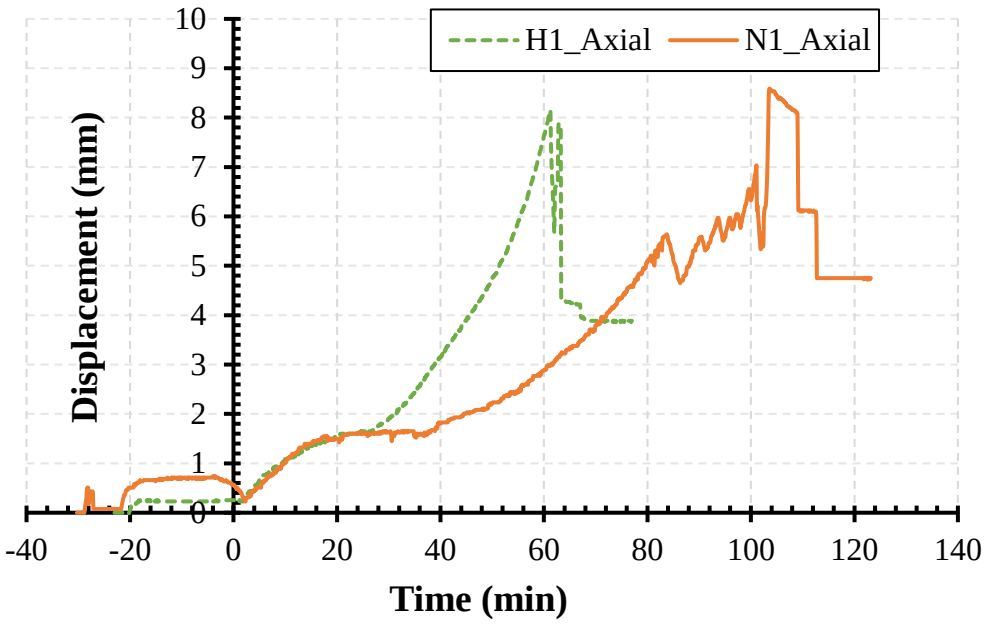

Figure 3.8 Progression of axial displacements for unrestrained PC beams N1 and H1

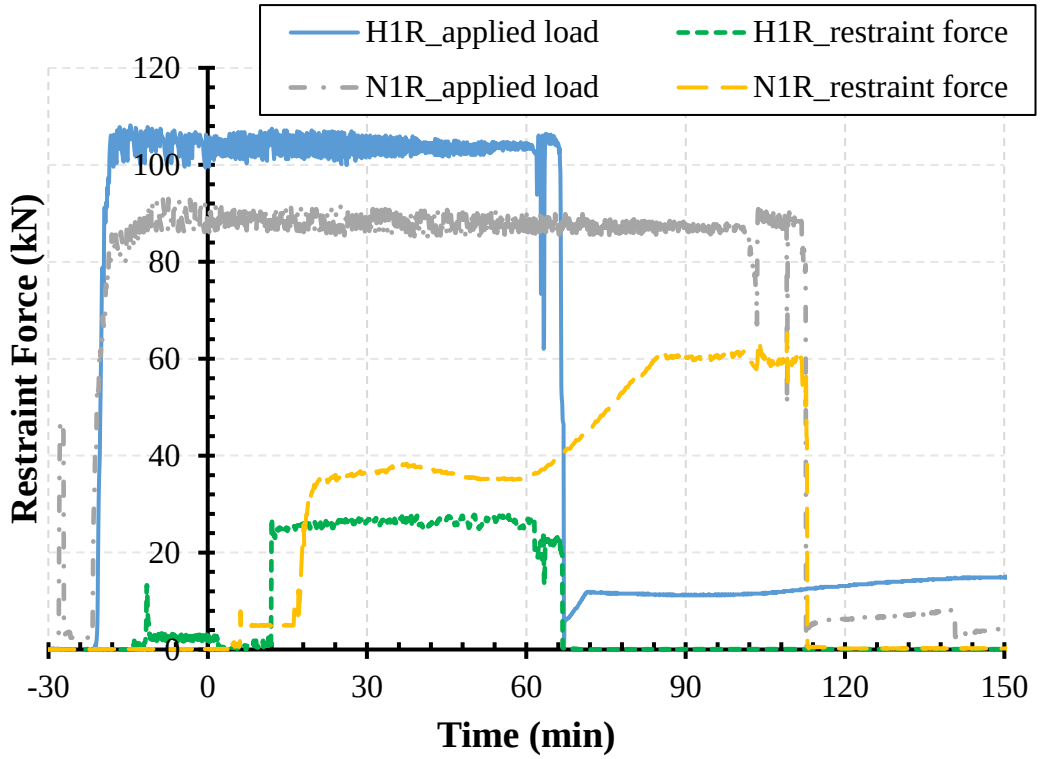

Figure 3.9 Applied loading and evolution of fire induced restraint forces with fire exposure time in NSC and HSC PC beams

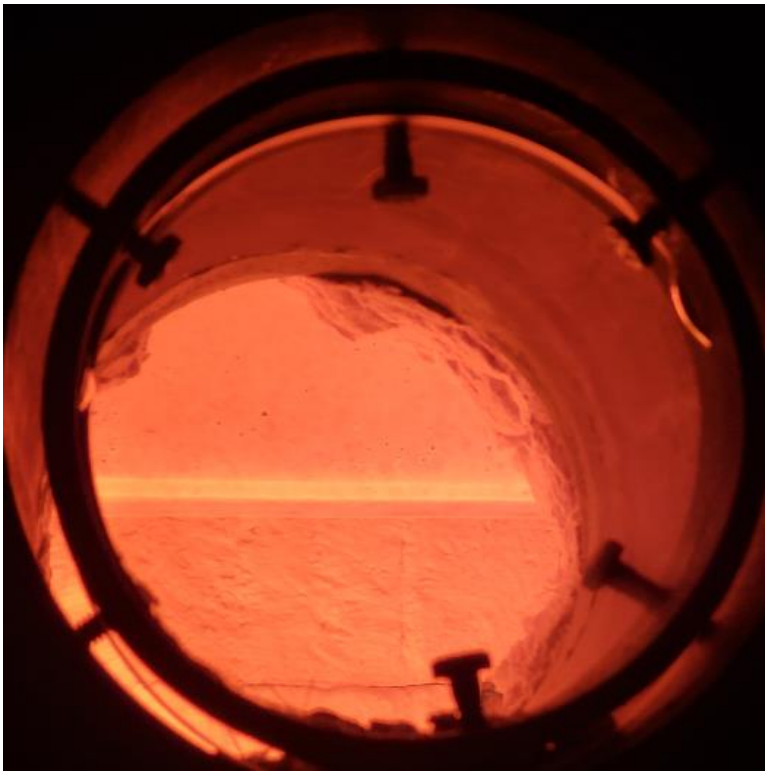

(a) N1

(b) N1R

Figure 3.10 Beam surface images during fire tests (prior to failure) (a) N1, (b) N1R, (c) H1, and (d) H1R

Figure 3.10 (cont'd)

(c) H1

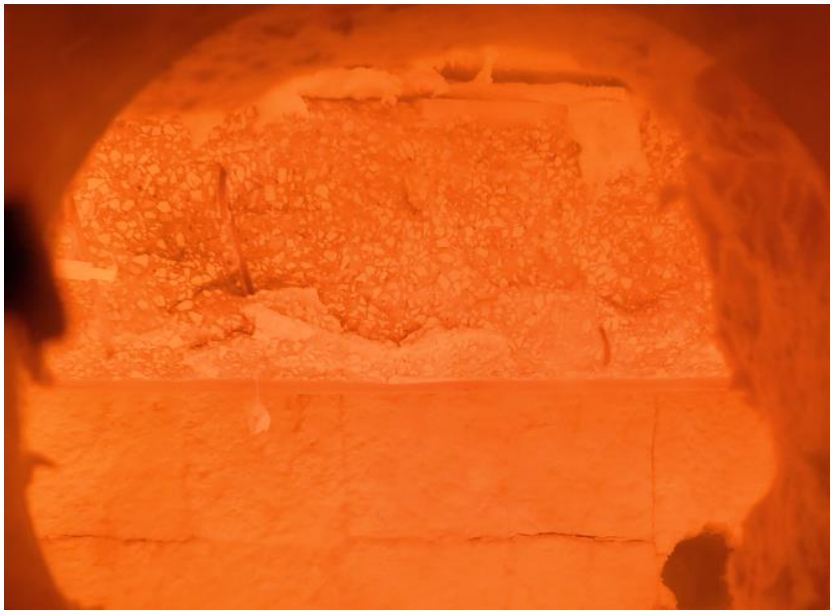

(d) H1R

(a) N1

(b) N1R

(c) H1

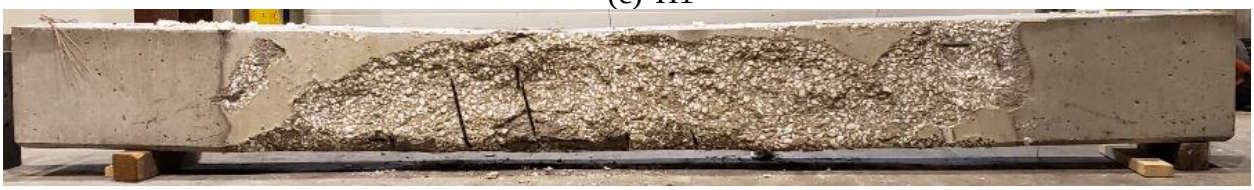

(d) H1R

Figure 3.11 View of tested NSC and HSC beams after failure under fire exposure

CHAPTER 4

4 Numerical Model

4.1 General

As discussed in Chapter 2, there is a need for a numerical model to trace the fire response of restrained PC beams from initial loading to failure stage while accounting for critical governing factors. To address this, a generic three-dimensional (3D) numerical model is developed in this study. The model accounts for all critical factors including effect of fire induced restraint force, capturing failure modes occurring through cracking and crushing of concrete at elevated temperatures, spalling of concrete, material and geometric non-linearity, and temperature induced material degradation [94]. Special emphasis is given to idealizing typical connections used in PC construction to accurately simulate restrained and unrestrained conditions, as it is instrumental in tracing the realistic fire behavior. A new adaptive 3D failure envelope for concrete is implemented at elevated temperatures to capture failure modes occurring through cracking and crushing of concrete under fire conditions. Also, a simplified framework is applied to capture fire induced spalling in concrete. These results have been published by author and can be found in the literature

[94], however, a more detailed discussion on the same is provided below. Full details on the development of finite element model including analysis procedure, numerical model, failure limits states, and numerical instabilities are described below.

4.2 Formulation of finite element analysis

A generic three-dimensional (3D) finite element (FE) based numerical model is developed in ANSYS [97] to trace the response of PC and RC beams in both thermal and structural domains [98]. While thermal model captures the heat transfer between fire and beam and within beam itself, structural model generates corresponding structural response under combined effects of thermal and structural loading.

4.2.1 Formulation for thermal analysis

The heat transfer from fire zone to the exposed surfaces of beam occur through thermal radiation and convection, whereas heat transfer from the surface to the interior of beam occurs through thermal conduction. This heat transfer can be modeled in a 3D physical domain Ω enclosed by boundary Γ in stationary coordinate system of X, Y, Z as shown in Figure 4.1. The domain is subjected to internal heat generation, Q, heat flux, h, and fixed temperature, $\overline{\theta}$, boundary conditions. The governing energy balance equation for heat transfer within domain is given as

$$\rho c \frac{\partial \theta}{\partial t} = \nabla \cdot (\boldsymbol{\lambda} \nabla \theta) + Q, \tag{4.1}$$

where, ρ is density, c is specific heat, θ is temperature, t is time, and $\boldsymbol{\lambda}$ is thermal conductivity tensor. The convection and radiation heat flux are applied in the form of surface thermal loads as

$$h_c = \alpha_c(\theta_g - \theta_s), \tag{4.2}$$

$$h_r = \phi \epsilon_m \epsilon_f \sigma_{sb} [(\theta_g + 273)^4 - (\theta_s + 273)^4], \tag{4.3}$$

where, h_c and h_r are net heat flux from convection and radiation, α_c is coefficient of convection heat transfer, θ_g is the temperature of fire gases, θ_s is the exposed surface temperature, ϕ is configuration factor, ϵ_m is the surface emissivity, ϵ_f is emissivity of fire, and σ_{sb} is Stefan-Boltzman constant. The finite element discretization of temperature field within elements is given as

$$\boldsymbol{\theta}^{(m)}(x, y, z, t) = \mathbf{N}^{(m)}(x, y, z)\, \widehat{\boldsymbol{\theta}}(t), \tag{4.4}$$

where, $\boldsymbol{\theta}^{(m)}(x, y, z, t)$ is continuous temperature field within element, $\mathbf{N}^{(m)}(x, y, z)$ is the interpolation matrix, $\widehat{\boldsymbol{\theta}}(t)$ is nodal temperature vector, and superscript m represents that these properties are for element m. Equation (4.1) can be solved using the Galerkin formulation to get a system of nonlinear equations in time for heat transfer formulation, represented in matrix form as

$$\mathbf{C}\frac{\partial \widehat{\boldsymbol{\theta}}}{\partial t} + \mathbf{K_c}\widehat{\boldsymbol{\theta}} = \mathbf{R_q} + \mathbf{R_Q} \tag{4.5}$$

where, $\mathbf{C}$ represents global capacitance matrix, $\mathbf{K_c}$ is global conductance matrix, $\mathbf{R_q}$ is global nodal vector of heat flow, and $\mathbf{R_Q}$ is global nodal vector of internal heat source. The different matrices of (4.5) are computed using the finite element discretization of (4.4) as

$$\mathbf{C} = \sum_{m=1:M} \int_{\Omega^{(m)}} (\mathbf{N}^{\mathrm{T}} \rho c\, \mathbf{N}) d\Omega^{(m)}, \tag{4.6}$$

$$\mathbf{K_c} = \sum_{m=1:M} \int_{\Omega^{(m)}} (\nabla \mathbf{N}^{\mathrm{T}} \boldsymbol{\lambda}\, \nabla \mathbf{N}) d\Omega^{(m)}, \tag{4.7}$$

$$\mathbf{R_q} = \sum_{m=1:M} \int_{\Gamma_N^{(m)}} \mathbf{N}^{\mathrm{T}} (\boldsymbol{\lambda} \nabla \mathbf{N} \widehat{\boldsymbol{\theta}} \cdot\, \widehat{\mathbf{n}}) d\Gamma^{(m)}, \tag{4.8}$$

$$\mathbf{R_Q} = \sum_{m=1:M} \int_{\Omega^{(m)}} (\mathbf{N}^{\mathrm{T}} Q)\, d\Omega^{(m)}, \tag{4.9}$$

where, M is total number of elements, $\hat{\mathbf{n}}$ is the unit vector normal to surface, $\mathbf{N}^{\mathrm{T}}$ is transpose of interpolation matrix, $\nabla\mathbf{N}$ is partial derivative of $\mathbf{N}$, and $\boldsymbol{\lambda}$ is thermal conductivity tensor. This FE formulation for thermal analysis is implemented in ANSYS [97] using SOLID70, LINK33, SURF152, and COMBIN39 elements.

4.2.2 Formulation for mechanical analysis

The resulting temperatures from thermal analysis are provided as input to the structural model to compute the corresponding thermo-mechanical response. To idealize mechanical behavior, a similar physical domain in Figure 4.1 is considered. The only difference in case of mechanical model is that internal heat is replaced by body forces, $\mathbf{f^B}$, heat flux by surface traction, $\mathbf{f^{S_f}}$, and fixed temperatures with prescribed displacements, $\mathbf{S_u}$. The governing equations for this physical domain can be written as

$$\nabla \cdot \boldsymbol{\sigma} + \mathbf{f^B} = 0 \text{ on } \Omega;\ \boldsymbol{\sigma} \cdot \hat{\boldsymbol{n}} = \mathbf{f^{S_f}}\ on\ \Gamma_N; \mathbf{U} = \mathbf{S_u} \text{ on } \Gamma_D, \tag{4.10}$$

where, $\boldsymbol{\sigma}$ denotes the stress tensor, $\hat{\boldsymbol{n}}$ denotes the unit normal vector to the surface, and $\mathbf{U}$ denotes displacement field. The constitutive relationship is given by

$$\boldsymbol{\sigma} = \mathbf{D}(\boldsymbol{\epsilon}_t - \boldsymbol{\epsilon}_{th}) + \boldsymbol{\sigma}', \tag{4.11}$$

where, $\mathbf{D}$ is the temperature-dependent constitutive matrix, $\boldsymbol{\epsilon}_t$ denotes total strain, $\boldsymbol{\epsilon}_{th}$ denotes thermal strain, and $\boldsymbol{\sigma}'$ denotes initial stress state (if any). To develop the displacement based FE equations, displacement and strain field within each finite element is discretized as a function of its nodal displacements as

$$\mathbf{u}^{(\mathrm{m})}(x,y,z) = \bar{\mathbf{u}}^{(m)}(x,y,z) = \mathbf{H}^{(m)}(x,y,z)\hat{\mathbf{U}}, \tag{4.12}$$

$$\boldsymbol{\epsilon}_t^{(m)}(x,y,z) = \bar{\boldsymbol{\epsilon}}_t^{\,m}(x,y,z) = \mathbf{B}^{(m)}(x,y,z)\hat{\mathbf{U}}, \tag{4.13}$$

where, $\mathbf{u}^{(\mathrm{m})}$ represents continuous displacement field within element, $\mathbf{H}^{(m)}$ is the displacement interpolation matrix, $\hat{\mathbf{U}}$ is the nodal displacement vector in global coordinates, $\boldsymbol{\epsilon}_t^{(m)}$ represent strain

field within element, and $\mathbf{B}^{(m)}$ is known as strain-displacement matrix which is obtained by combining appropriate derivatives of the rows of $\mathbf{H}^{(m)}$ matrix. Virtual components of displacement and strain fields are represented by $\bar{\mathbf{u}}^{(m)}(x, y, z)$ and $\bar{\epsilon}_t^{\,m}(x, y, z)$, and superscript m denotes element m in x, y, z local coordinates. By using Galerkin formulation, the final displacement based FE formulation is given as

$$\mathbf{K}\hat{\mathbf{U}} = \mathbf{R_B} + \mathbf{R_S} - \mathbf{R_I} + \mathbf{R_{th}}, \tag{4.14}$$

where, $\mathbf{K}$ represents global stiffness matrix; and $\mathbf{R_B}, \mathbf{R_S}, \mathbf{R_I}, \mathbf{R_{th}}$ are global load vectors due to body force, surface traction, initial stresses, and thermal exposure, respectively. The matrices of (4.14) are computed as

$$\mathbf{K} = \sum_{m=1:M} \int_{\Omega^{(m)}} \mathbf{B}^{\mathrm{T}(m)} \mathbf{D}^{(m)}\, \mathbf{B}^{(m)} d\Omega^{(m)}, \tag{4.15}$$

$$\mathbf{R_B} = \sum_{m=1:M} \int_{\Omega^{(m)}} \mathbf{H}^{\mathrm{T}(m)} \mathbf{f}^{\mathbf{B}(m)}\, d\Omega^{(m)}, \tag{4.16}$$

$$\mathbf{R_S} = \sum_{m=1:M} \int_{\Gamma_N^{(m)}} \mathbf{H}_{\mathrm{S}}^{\mathrm{T}(m)}\ \mathbf{f}^{\mathbf{S_f}(m)} d\Gamma^{(m)}, \tag{4.17}$$

$$\mathbf{R_I} = \sum_{m=1:M} \int_{\Omega^{(m)}} \mathbf{B}^{\mathrm{T}(m)} \boldsymbol{\sigma}'^{(m)}\, d\Omega^{(m)}, \tag{4.18}$$

$$\mathbf{R_{th}} = \sum_{m=1:M} \int_{\Omega^{(m)}} \mathbf{B}^{\mathrm{T}(m)} \mathbf{D}^{(m)} \boldsymbol{\epsilon}_{th}^{(m)}\, d\Omega^{(m)}, \tag{4.19}$$

$\mathbf{H}_{\mathrm{S}}^{(m)}$ is surface interpolation matrix which is obtained by substitution of element surface coordinates in $\mathbf{H}^{(m)}$. The above finite element formulation for structural analysis is implemented in ANSYS [97] program using SOLID65, LINK180, SURF154, and COMBIN39 elements.

4.3 Analysis procedure

The above discretized numerical procedure forms the basis for finite element formulation using ANSYS [97] for fire resistance evaluation of PC and RC beams. Development of numerical model in ANSYS [97] involves idealization of connection for restraint, discretization of beam and defining temperature dependent material properties, defining an appropriate fire exposure, and the performing a coupled thermal-structural analysis, and applying relevant failure limit states. The step by step procedure adopted for analysis is illustrated in a flow chart in Figure 4.2. The first step in the analysis is to idealize connection between beam under consideration and connecting structural members (columns, beams etc.) into an equivalent system using springs which imparts similar restraint as from actual connection (see Section 4.3 for details). This idealization significantly reduces the number of elements required to develop FE model which leads to faster simulation and provides a generic procedure to idealize typical connections. After this step, geometry of PC beam, along with connection idealizations, is defined in ANSYS. This can be achieved by either creating it in ANSYS itself or importing it though a compatible CAD (computer aided design) based software. This geometry (beam) is then discretized using two sets of finite elements to facilitate thermal and structural analysis which are assigned corresponding material properties. As the temperatures from thermal analysis form input for structural analysis, thermal analysis is carried first, followed by structural analysis.

At this stage, relevant fire exposure is input as time temperature relations on the external fire exposed surfaces of the beam along with other thermal boundary conditions. Based on selected fire exposure and applied thermal boundary conditions, heat transfer analysis is carried out to evaluate cross-sectional temperature evolution within the section of the beam in incremental time steps for entire duration of fire exposure. During heat transfer analysis, at every incremental time

step, convergence of finite element solution is checked and in case the solver iterations do not converge to a solution, the corresponding time step duration is refined to smaller time increment to achieve convergence. At the end of thermal analysis, thermal elements are switched to structural elements and resulting nodal temperatures from thermal analysis are supplied to structural analysis. Appropriate structural boundary conditions are specified to simulate loading and support conditions. Then coupled thermal-structural response is simulated at each incremental time step. At each incremental time step, corresponding temperature dependent mechanical properties are determined for every element, and structural response of the beam is computed in terms of deflections and stresses. This temperature dependent structural analysis is carried out until failure of the beam or end of fire exposure duration if no failure is observed. The output parameters from thermal and structural analysis are utilized to evaluate failure at the end of each time step, and time to reach any of the specified failure limit states is taken as the fire resistance of beam. It should be noted that FE model only gives deflections as primary output, and to calculate internal stresses, internal mechanical equations are used for every element to get the resulting stresses for the corresponding resulting deflections. Further, there is no direct procedure to get the moment capacity from FE analysis, so temperatures from FE analysis are used in temperature dependent moment capacity equations (from rational design approaches [6]) to manually calculate temperature dependent moment capacity.

4.4 Idealization of typical connections

The main purpose of idealizing a connection is to develop a generic procedure that allows to account for typical connections with ease and achieve same level of axial and rotational restraint (as in real connection) using minimal number of elements for higher computational efficiency. Therefore, a generic approach to idealize connections using nonlinear spring elements is proposed

herein. In this approach, combined stiffness of a structural connection is derived by adding individual stiffness contribution from every connecting structural member (i.e., beam and column) using direct stiffness method. Since most of the connections used in buildings with PC beams are simply supported (as it facilitates speedy construction and is easy for fabrication), therefore, such idealizations for simply supported connections are developed in this study.

To generalize idealization in a typical moment frame of building, connections are classified based on number of members involved as corner, side, and interior as shown in Figure 4.3. Fire behavior of all these connections is discussed below to set the context and then corresponding idealizations are made. A typical simply supported interior connection in a building with PC beams is illustrated in Figure 4.4(a) and force-displacement behavior for its corresponding individual non-linear spring idealization is given in Figure 4.4(b). In this connection, Beam 1 is of concern and remaining structural elements at the connection are to be idealized using non-linear springs instead of discretizing entire connection using finite elements.

Under fire exposure, Beam 1 will undergo free thermal expansion which will not be restrained until that thermal expansion exceeds initial gap (G_1) between Beam 1 and Columns 1 and 2. It should be noted that PC beams are often connected with columns using single steel angle sections at top, but these joints usually have low structural strength as their only function is to ensure PC beam's stability during construction. Therefore, these connections are assumed to fail under fire conditions and their corresponding restraint to thermal expansion is not considered in idealization. Also, frictional resistance between connecting members, and between beams and slabs is ignored for simplicity. Hence, idealizing spring is assigned zero force until gap G_1 is overcome, as shown in Figure 4.4 (b).

Once initial gap (G_1) is overcome by thermal expansion of Beam 1, axial restraint is applied by combined stiffness of Column 1 and 2 which can be gauged by slope K_1 in the force deflection relation for idealized spring in Figure 4.4(b). Note that no stiffness is transferred from Beam 3 and Beam 4 to Beam 1 as they are simply supported on the column and do not transfer any forces to Beam 1 or 2. Also, only axial restraint to thermal expansion of Beam 1 is provided from other structural members as it is a simply supported connection. If the beam continues to expand thermally and overcome gap (G_2) between columns and Beam 2, then axial restraint is applied by combined stiffness of Column 1 and 2 and Beam 2 which is illustrated by slope K_2 in Figure 4.4(b). This allows to idealize for total stiffness of connection which significantly governs magnitude of developed restraint.

However, as discussed in Chapter 1, it is important to properly account for both magnitude and location of restraint which keeps shifting with fire exposure time. To idealize location of restraint from connection to Beam 1, it is important to identify individual points of contact between Beam 1 and columns. To do so, entire face of restrained Beam 1 end is discretized with non-linear springs (each assigned force-deflection relation as in Figure 4.4(b)) which simulates realistic contact between Beam 1 and columns. It is due to this reason that K_1 and K_2 are divided by total number of springs (n). Also, to limit the maximum force exerted by connection, failure at critical load of connection (F_{cr}) is inbuilt to the springs which sets stiffness of all springs to zero once summation of force exerted by individual springs ($\sum_{i=1}^{n} F_i$) exceed F_{cr}. This allows the users to either reverse engineer maximum desired F_{cr} to achieve certain fire resistance for a restrained beam or evaluate fire resistance of restrained PC beam for a given F_{cr}. All stiffness parameters then can be evaluated using direct stiffness method as:

$$K_1 = (K_{C1} + K_{C2})/n \tag{4.20}$$

$$K_2 = (K_{B2} + K_{C1} + K_{C2})/n \tag{4.21}$$

$$K_{C1} = \left(\frac{12EI_z}{L^3}\right)_{Column\ 1} \tag{4.22}$$

$$K_{C2} = \left(\frac{12EI_z}{L^3}\right)_{Column\ 2} \tag{4.23}$$

$$K_{B2} = \left(\frac{AE}{L}\right)_{Beam\ 2} \tag{4.24}$$

where, K_{C1}, K_{C2}, and K_{B2} are stiffness contribution from Column 1, Column 2, and Beam 2; respectively. A is area of cross-section, E is modulus of elasticity, L is length, I_z is moment of inertia about z-axis (cartesian axis are marked in Figure 4.4(a)); and suffix Beam 2, Column 1, and Column 2 represent that stiffness parameters (A, E, L or I_z) are evaluated for that beam or column. Since, Beam 3 and Beam 4 do not have any contribution to the stiffness of connection, this idealization for interior connections becomes applicable to side and corner connections as well. Therefore, Eqs. (4.20) to (4.24) are applicable for side and corner connections as well. As there is no Beam 2 inside and corner connections to provide axial restraint, total stiffness of connection is governed by Column 1 and Column 2 only which can be evaluated using Eqs. (4.20), (4.22) and (4.23). Also, for clarity, force-deflection relation for springs idealizing side and corner connections is illustrated in Figure 4.5 where stiffness contribution from only columns can be clearly observed. To evaluate fire resistance of PC beam, it is discretized into structural and thermal elements in ANSYS [97], and temperature dependent material properties of concrete and reinforcement are assigned to corresponding elements based on Eurocode 2 [4] recommendations. For thermal analysis, PC beam is discretized using SOLID70, LINK33, SURF152, and COMBIN39 elements; and they are assigned corresponding temperature dependent thermal properties. SOLID70 is an eight node element capable of simulating conduction and is used to discretize concrete in PC beam. LINK33 is a linear two node element capable of simulating conduction and is used to discretize

prestressing strands and steel reinforcement. SURF152 is a four node surface element capable of simulating heat transfer via conduction, convection, and radiation; and is overlaid on fire exposed and non-insulated surface of PC beam.

This discretized beam is subjected to fire exposure on relevant surfaces (usually bottom and side faces) and other initial temperature conditions are defined using thermal boundary conditions. The evolution of sectional temperatures is then traced in incremental time steps till the complete duration of fire exposure. At this stage, thermal elements are switched to corresponding structural elements and they are assigned corresponding temperature dependent mechanical properties. SOLID70 is switched to SOLID65, LINK33 is switched to LINK180, SURF152 is switched to SURF154, and COMBIN39 is kept same as it works in structural analysis. SOLID65 is an eight node element utilized to simulate cracking and crushing effects in concrete, LINK180 is a two node element used to simulate prestressing effects in strands and tension and compression in reinforcement. SURF154 is used to apply surface loads on beam, and COMBIN39 is used to simulate beams connection using a 3D non-linear spring. The force-displacement relationship of connection (calculated in Section 4.2) is provided as input to ANSYS as force-displacement relation of COBIN39 element. Also, to ensure that there is no crushing or stress concentration at the beam ends, rigid steel plates of 25 mm thickness are used at beam ends. A typical PC beam discretized into several elements is shown in Figure 4.6.

4.5 High temperature property relations for concrete and reinforcement

Concrete and steel reinforcement experience significant degradation in thermal and mechanical properties at elevated temperatures. Therefore, to capture the property degradation effect on thermo-mechanical response of PC beams, temperature dependent thermal and mechanical properties are to be provided as input to ANSYS [97]. The thermal properties include specific heat,

thermal conductivity, and density, whereas mechanical properties include elastic modulus, stress-strain relations, and coefficient of thermal expansion. These temperature dependent properties of concrete and steel rebars are incorporated as per recommendations of Eurocode 2 [17]. It should be noted that nodal temperatures are main output parameters from the thermal analysis, therefore, one element (consisting of 2 or more nodes) may have different nodal temperatures. As every individual element can account for variation in material properties at only one temperature state at a time, therefore, the temperature dependent material properties are evaluated at the average nodal temperature of the element in both thermal and structural analysis. Also, temperature dependent creep effects are not accounted explicitly for concrete Eurocode 2 material properties, and therefore, these properties for concrete are only applicable for heating rates between 2 to 50 K/min [17]. Whereas bond effects as well as explicit creep between reinforcement and concrete are not specifically considered.

4.5.1 Cracking and crushing of concrete

Material degradation resulting from elevated temperatures can cause significant levels of cracking and crushing of concrete which can ultimately lead to early failure. Therefore, it is important to account for cracking and crushing of concrete at elevated temperatures. Hence, to accurately capture this intricate thermo-mechanical response, cracking and crushing of SOLID65 concrete elements is simulated using extended Willam Warnke failure envelope [97]. This failure envelope is originally proposed for multiaxial stress state in concrete at room temperature and has been successfully applied to other concrete members under fire exposure by researchers [99–101]. However, with significant material degradation failure envelope for concrete keeps evolving as sectional temperatures increase. Therefore, Willam Warnke failure envelope [97] is extended to an adaptive temperature dependent failure envelope in this study. For a given multiaxial stress

state of concrete element the adaptive failure envelope is illustrated in Figure 4.7, and this failure envelope is implemented in the developed model as:

$$\frac{F}{f_{c\theta_e}} - S \geq 0 \tag{4.25}$$

where, F is a function of principal stress state ($\sigma_1, \sigma_2, \sigma_3$), S is a continuous failure surface, and $f_{c\theta_e}$ is compressive strength of concrete at average element nodal temperature θ_e. Both F and S are defined for four domains of principal stress state in concrete elements. For compression dominated principal stress state ($0 \geq \sigma_1 \geq \sigma_2 \geq \sigma_3$), domain 1, F_1 and S_1 are defined as:

$$F = F_1 = \frac{1}{\sqrt{15}} \left[(\sigma_1 - \sigma_2)^2 + (\sigma_2 - \sigma_3)^2 + (\sigma_3 - \sigma_1)^2 \right]^{0.5} \tag{4.26}$$

$$S = S_1 = \frac{2r_2(r_2^2 - r_1^2)\cos(\eta) + r_2(2r_1 - r_2)[4(r_2^2 - r_1^2)\cos^2(\eta) + 5r_1^2 - 4r_1r_2]^{0.5}}{4(r_2^2 - r_1^2)\cos^2(\eta) + (r_2 - 2r_1)^2} \tag{4.27}$$

where,

$$\cos(\eta) = \frac{2\sigma_1 - \sigma_2 - \sigma_3}{\sqrt{2}\left[(\sigma_1 - \sigma_2)^2 + (\sigma_2 - \sigma_3)^2 + (\sigma_3 - \sigma_1)^2 \right]^{0.5}} \tag{4.28}$$

$$r_1 = a_0 + a_1\xi + a_2\xi^2 \tag{4.29}$$

$$r_2 = b_0 + b_1\xi + b_2\xi^2 \tag{4.30}$$

$$\xi = \frac{\sigma_h}{f_{c\theta_e}} \tag{4.31}$$

where, σ_h is hydrostatic stress; and coefficints a_0, a_1, and a_2 in Eq. (4.31) are determined from the simultaneous equations given below:

$$\begin{Bmatrix} \frac{F_1}{f_{c\theta_e}}(\sigma_1 = f_{t\theta_e}, \sigma_2 = \sigma_3 = 0) \\ \frac{F_1}{f_{c\theta_e}}(\sigma_1 = 0, \sigma_2 = \sigma_3 = -f_{cb}) \\ \frac{F_1}{f_{c\theta_e}}(\sigma_1 = -\sigma_h^a, \sigma_2 = \sigma_3 = -\sigma_h^a - f_1) \end{Bmatrix} = \begin{bmatrix} 1 & \xi_t & \xi_t^2 \\ 1 & \xi_{cb} & \xi_{cb}^2 \\ 1 & \xi_1 & \xi_1^2 \end{bmatrix} \begin{Bmatrix} a_0 \\ a_1 \\ a_2 \end{Bmatrix} \tag{4.32}$$

where, $f_{t\theta_e}$ is tensile strength of concrete at θ_e, f_{cb} is biaxial compressive strength of concrete, and f_1 is ultimate compresive strength for biaxial compression superimposed on ambient hydrostratic stress state (σ_h^a). The default value of f_{cb} and f_1 is taken as $1.2f_{c\theta_e}$ and $1.45f_{c\theta_e}$, respectively [97]. Other unknowns in Eq. (4.32) are given as:

$$\xi_t = \frac{f_{t\theta_e}}{3f_{c\theta_e}}, \xi_{cb} = -\frac{2f_{cb}}{3f_{c\theta_e}}, \xi_1 = -\frac{\sigma_h^a}{f_{c\theta_e}} - \frac{2f_1}{3f_{c\theta_e}} \tag{4.33}$$

Coefficints b_0, b_1, and b_2 in Eq. (4.30) are determined from the simultaneous equations given below:

$$\begin{Bmatrix} \frac{F_1}{f_{c\theta_e}}(\sigma_1 = \sigma_2 = 0, \sigma_3 = -f_{c\theta_e}) \\ \frac{F_1}{f_{c\theta_e}}(\sigma_1 = \sigma_2 = -\sigma_h^a, \sigma_3 = -\sigma_h^a - f_2) \\ \frac{F_1}{f_{c\theta_e}}(0) \end{Bmatrix} = \begin{bmatrix} 1 & -\frac{1}{3} & \frac{1}{9} \\ 1 & \xi_2 & \xi_2^2 \\ 1 & \xi_0 & \xi_0^2 \end{bmatrix} \begin{Bmatrix} b_0 \\ b_1 \\ b_2 \end{Bmatrix} \tag{4.34}$$

where, f_2 is ultimate compresive strength for uniaxial compression superimposed on ambient hydrostratic stress state, and has a default value of $1.725f_{c\theta_e}$. Other variables in Eq. (4.34) are given as:

$$\xi_2 = -\frac{\sigma_h^a}{f_{c\theta_e}} - \frac{f_2}{3f_{c\theta_e}} \tag{4.35}$$

$$r_2(\xi_0) = a_0 + a_1\xi_0 + a_2\xi_0^2 = 0 \tag{4.36}$$

For tension-compression-compression principal stress state ($\sigma_1 \geq 0 \geq \sigma_2 \geq \sigma_3$), domain 2, F_2 and S_2 are defined as:

$$F = F_2 = \frac{1}{\sqrt{15}} [\,(\sigma_2 - \sigma_3)^2 + \sigma_2^2 + \sigma_3^2]^{0.5} \tag{4.37}$$

$$S = S_2$$

$$= \left(1 - \frac{\sigma_1}{f_{t\theta_e}}\right) \frac{2p_2(p_2^2 - p_1^2)\cos(\eta) + p_2(2p_1 - p_2)[4(p_2^2 - p_1^2)\cos^2(\eta) + 5p_1^2 - 4p_1p_2]^{0.5}}{4(p_2^2 - p_1^2)\cos^2(\eta) + (p_2 - 2p_1)^2} \tag{4.38}$$

where,

$$p_1 = a_0 + a_1\chi + a_2\chi^2 \tag{4.39}$$

$$p_2 = b_0 + b_1\chi + b_2\chi^2 \tag{4.40}$$

$$\chi = \frac{\sigma_2 + \sigma_3}{3f_{c\theta_e}} \tag{4.41}$$

Coefficints $a_0, a_1, a_2, b_0, b_1,$ and b_2 in Eq. (4.39) and (4.40) are evaluated using Eq. (4.32) and (4.34) only. For tension-tension-compression principal stress state ($\sigma_1 \geq \sigma_2 \geq 0 \geq \sigma_3$), domain 3, F_3 and S_3 are defined as:

$$F = F_3 = \sigma_i; i = 1,2 \tag{4.42}$$

$$S = S_3 = \frac{f_{t\theta_e}}{f_{c\theta_e}}\left(1 + \frac{\sigma_3}{f_{c\theta_e}}\right) \tag{4.43}$$

For domain 4, tenson-tension-tension principal stress state ($\sigma_1 \geq \sigma_2 \geq \sigma_3 \geq 0$), F_4 and S_4 are defined as:

$$F = F_4 = \sigma_i; i = 1,2,3 \tag{4.44}$$

$$S = S_4 = \frac{f_{t\theta_e}}{f_{c\theta_e}} \tag{4.45}$$

Using these four domains, a new failure enevelope is generated for every SOLID65 element at its current temperature θ_e as illustrated in Figure 4.7. Therefore, for every element, failure envelope is defined by its current temperature dependent compressive ($f_{c\theta_e}$) and tensile strength ($f_{t\theta_e}$). Once the requirements for crushing failure are met, crushing of an element is simulated by reducing

its stiffness to a negligible value. Whereas, to simulate cracking, a plane of weakness is introduced in element where stiffness along cracking plane is controlled by open and closed crack coefficients. Value of these coefficients vary between 0 to 1 with 0 representing complete loss of shear transfer (smooth crack) and 1 representing no loss of shear transfer (rough crack). This adaptability of failure envelope to temperature induced material degradation allows proposed model to account for effect of temperature on cracking and crushing of concrete and accurately capture failure modes arising from cracking and crushing in restrained and unrestrained beams. It should be noted that ANSYS checks the cracking within every SOLID65 elements at the integration points only. Therefore, to improve cracking check at elemental level, SOLID65 elements with cubic shape are utilized for discretization -as cubic elements have the highest number of integration points.

4.5.2 Spalling of concrete

Fire induced spalling can occur in higher strength concrete, due to buildup of pore pressure within the concrete having lower permeability [102]. Simulating spalling requires a coupled hygro-thermal-mechanical analysis which can trace pore pressure buildup at elevated temperatures and capture corresponding spalling at fire exposed surface of beam when pore pressure exceeds tensile strength of elements [103]. However, such hygro-thermal-mechanical analysis is highly complex and requires large set of input parameters. Based on a detailed literature review [102,104,105], a new simplified framework is proposed in this study where spalling is accounted for using following broad guidelines:

1. Check the following conditions of spalling for the beam under consideration prior to the finite element analysis:
    a. Spalling is assumed to occur in beams when the compressive strength of concrete is greater than 70 MPa or if the water permeability of the concrete is less than 10^{-16} m^2.

This assumption is based on the hypothesis that concretes with strengths higher than 70 MPa or permeability lower than 10^{-16} m^2 generally have dense microstructure which leads to spalling due to pore pressure buildup.

b. No spalling occurs if concrete has polypropylene fibers (0.1 – 0.2 % by volume). This is because based on literature polypropylene fibers (0.1 – 0.2 % by volume) often melt at elevated temperatures and create micro conduits for pore pressure dissipation. Therefore, concretes with polypropylene fibers (0.1 – 0.2 % by volume) may not undergo spalling.

2. If the beam is susceptible to spalling, then spalling is assumed to occur in concrete elements when tensile strength of concrete element decreases to 0 at a given temperature. Eurocode 2 [16] recommendation that tensile strength becomes 0 at a temperature of 600 ◦C is adopted herein, however, other user specified temperatures can be used as well. This spalling criterion is implemented in ANSYS analysis using following steps:

   a. Spalling in thermal analysis is implemented by identifying spalled elements (elements with average nodal temperatures ≥600 ◦C) at every time step and then increasing thermal conductivity of spalled elements by 1000 times and reducing their thermal specific heat capacity by 1000 times. This transmits surface fire temperatures to internal non-spalled elements and allows propagation of spalling.

   b. Then to implement spalling in ANSYS structural analysis, spalling history is imported from thermal analysis to structural analysis to identify spalled concrete elements at every time step. Then at every time step, the stiffness of corresponding spalled elements is decreased to 0.001% of its room temperature stiffness for the rest of

structural analysis. Note that stiffness of spalled elements is not reduced to 0 to ensure numerical stability.

It should be noted that this simplified framework can yield an approximate estimate of spalling only, and for that reason relatively conservative guidelines were adopted where elements spall only after they have completely lost their tensile strength. In reality, spalling starts much earlier as the increase in pore pressure can dominate the remaining tensile strength of concrete elements on the fire exposed surface of the beam before complete loss of tensile strength and cause spalling. However, due to the significant complexity involved, a 3D hygro-thermal-**m**echanical analysis was not performed.

4.6 Failure limit states

Failure under fire exposure occurs when a structural member is not able to carry applied loading, and this failure is classified as strength failure in codes and standards. Under prescriptive approach, strength failure is assessed through a simplistic approach wherein strength failure occurs when temperature in strands surpasses critical temperature of 427^{o}C (temperature at which strands lose 50% of its room temperature strength) [5]. It is based on the hypothesis that strands are main contributors to the load carrying capacity, and typical load ratio in buildings is 50% under fire conditions. Therefore, when the strength of strands falls below 50%, load carrying capacity falls below 50% (which is less than applied loading as per 50% load ratio) and it causes strength failure. This is not realistic representation of actual failure state occurring through intricate thermo-mechanical response of a structural member and thus may not yield actual fire resistance of a beam. Therefore, for evaluating realistic fire resistance, strength failure criterion is applied by considering limiting deflection values and degradation in moment capacity in this study. For deflection failure limit state, failure is said to occur when the maximum deflection in the beam

exceeds span/20 (mm) at any fire exposure time, or the rate of deflection between two time increments exceeds the limit by span^2/9000d (mm/min), after attaining a maximum deflection of span/30 (mm) [106]. Also, since design of most PC beams is controlled by flexure due to their long spans, shear capacity isn't considered herein. However, same procedure can be extended to shear capacity as well.

For moment capacity limit state, failure is said to occur when applied moment exceeds beam's current moment capacity. The reduced moment capacity at time t under fire exposure (M_{nt}) is evaluated by coupling temperatures from FE analysis with moment capacity equations proposed by PCI [6] as:

$$M_{nt} = A_{ps} f_{ps\theta_s t} \left(d - \frac{a_t}{2}\right), \tag{4.46}$$

$$f_{ps\theta_s t} = f_{pu\theta_s t} \left(1 - \frac{0.5\, A_{ps}\, f_{pu\theta_s t}}{b d\, f_{c\theta_c t}}\right), \tag{4.47}$$

$$a_t = \frac{A_{ps} f_{ps\theta_s t}}{0.85\, f_{c\theta_c t}\, b}, \tag{4.48}$$

where, A_{ps} is area of prestressing steel, *b* is width of beam, *d* is effective depth of beam, $f_{ps\theta_s t}$ and $f_{pu\theta_s t}$ are actual and ultimate stresses in prestressing strands at average strand temperature θ_s corresponding to time *t*, a_t is depth of equivalent rectangular stress block at time t, and $f_{c\theta_c t}$ is compressive strength of concrete evaluated at average temperature in zone of rectangular stress block (θ_c) at time *t*, respectively. Failure is checked against these limit states at the end of each time step, and the least time to reach a specific failure limit state is taken as the fire resistance of the beam.

4.7 Numerical instabilities

One of the main challenges in finite element analysis of structural members under fire exposure comes from numerical convergence hurdles which arise from temperature induced material

softening and associated non-linearities, geometric non-linearities, and cracking and crushing phenomenon in concrete. This causes reduction in stiffness of global stiffness matrix which can make it ill-conditioned (non-invertible) and lead to convergence hurdles at any time step. To overcome these convergence hurdles, Newmark algorithm is utilized in capturing transient thermal response at each time step, and an iterative Newton-Raphson solver is utilized to capture corresponding structural response. In case, analysis fails to converge after a prescribed number of iterations; due to combination of geometric non-linearity, cracking and crushing, and material softening at elevated temperatures; the time step is refined with relatively smaller time increments to reduce loading increments. However, assigning smaller time increments can increase the computational effort, therefore, time step increments are resumed to initial default value in subsequent time steps, once convergence hurdle at that time step is overcome.

4.8 Model validation

The developed numerical model is validated to gauge efficacy and accuracy of both thermal and structural response of PC and RC beams under fire exposure. Thermal response is validated by comparing predicted sectional temperatures against measured values, and structural response is validated by comparing predicted deflections and restraint force against measured values. Also, trends in thermal and structural response of tested PC beams are discussed in detail to set the context for validation.

4.8.1 Details of beams selected for validation

All four tested PC beams described in Chapter 3 together with an additional RC beam, R1 (tested by Dwaikat and Kodur [9]) are selected for model validation. Full details of fire test on PC beams are provided in Chapter 3, therefore, only details of fire test on RC beam (R1) are discussed herein. The tested RC beam is 254 x 406 x 3960 mm in size, and it was fabricated with NSC with a

compressive strength of 58 MPa. Main tension reinforcement in this beam constitutes of three 19 mm diameter bars, and two 13 mm diameter bars were provided as compression reinforcement. For shear reinforcement, 6 mm diameter stirrups were provided at a spacing of 150 mm over the length of beam. Yield strength of tension and compression rebars (deformed rebars) was 420 MPa, and yield strength of stirrups (plain rebars) was 280 MPa. This RC beam was tested under four point loading scheme with two point loads of 50 kN each with SF fire exposure (see Figure 3.1). Restraint forces are allowed to increase to the maximum restraint capacity of loading frame (120 kN), and afterwards, a constant restraint to thermal expansion was maintained to keep restraint force below 120 kN. The beam response was measured throughout fire test in terms of sectional temperatures, developed axial restraint force, and midspan deflection. During the fire test this beam experienced minor spalling, but no failure was observed at the end of 4 hours of fire test. More details on cross-sectional dimensions, location of thermocouples, strain gauges, and displacement transducers can be referred to Dwaikat and Kodur [9].

4.8.2 Analysis details

The above selected beams are replicated with identical materials, geometry, loading, fire, and support conditions for finite element analysis. The simulations are conducted in accordance with analysis procedure and details discussed in Sections 4.2 to 4.7. Due to symmetry in loading, geometry, material properties, and boundary conditions only half symmetric model is analyzed to save computational effort in analysis. The symmetric boundary condition is implemented by constraining the perpendicular displacement and out-of-plane rotation degrees of freedom for all nodes located at the plane of symmetry. These simplifications reduced the total number of elements in the numerical model and resulted in lower computational effort and swift analysis.

4.8.3 Comparison of thermal response

Comparison of predicted and measured thermal response for beams N1 and H1R is illustrated in Figures 4.8 and 4.9; and measured thermal response for all tested PC beams is shown in Figures 3.5 and 3.6. It should be noted that NSC beams N1 and N1R and HSC beams H1 and H1R have a very similar thermal response due to identical material properties and same fire exposure. Therefore, for brevity, only thermal response of beams N1 and H1R are compared. It can be observed from Figure 4.8 that for beam N1, model predictions for strand temperatures are in good correlation with measured values. However, model under predicts the sectional temperatures in the initial 40 minutes for ¼ depth and for 80 minutes for ½ depth followed by over predicted temperatures for both depths. This can be attributed to the inability of the model to capture local heat fluxes within the furnace as beams are only exposed to the average furnace temperature. However, beams can be subjected to slightly different local fire temperatures in the furnace during the fire test. Also, the variation in the temperatures can be attributed to the variation in actual material properties versus the Eurocode 2 material properties which are adopted within the model. Overall, model predictions for the NSC PC beam N1 are within reasonable agreement with measured values.

In case of HSC beam H1R, comparison between predicted and measured temperatures is shown in Figure 4.9. It can be observed from Figure 4.9 that model temperatures are within reasonable agreement with measured sectional temperatures till 70 minutes of fire exposure and then model significantly over predicts the sectional temperatures. This is due to the fact that beam underwent significant spalling at failure (67 minutes) which caused significant increase in sectional temperatures. Since, the spalling framework adopted in this numerical model is more conservative (discussed in Section 4.5.2) it predicts higher level of spalling than actual spalling in fire test. This

causes a significant reduction in concrete section, thus, reducing the thermal inertia of concrete significantly which ultimately causes the model to overpredict sectional temperatures after failure of the beam.

In case of RC beam R1 [9] (comparison shown in Figure 4.10), rebar temperatures increase relatively faster as compared to PC beams. This is due to smaller concrete cover for rebars in selected RC beams (37 mm) as compared to PC beams (64 mm). After that rebar temperatures increase to a maximum of 524^{o}C at a time lag of 50 minutes from the start of decay phase in fire temperatures. Like PC beams, sectional temperatures at higher depths from exposed face increase at a slower pace with higher time lag from start of decay phase in fire exposure. As can be observed from Figure 4.10, model predicts these trends with reasonable accuracy for beam R1. Therefore, overall, model predictions are in reasonable agreement with measured values which makes it applicable to trace thermal response of PC and RC beams.

4.8.4 Comparison of structural response

Structural response of tested PC beams and RC beam R1 is compared in terms of mid-span deflections in Figures 4.11 and 4.12. It can be observed from Figure 4.11 that measured and predicted midspan deflections are in reasonable agreement with each other. For all beams, model underpredicts the deflections at the application of load prior to fire exposure. This can be related to the difference in actual and predicted elastic modulus of concrete as deflections are primarily elastic in this stage and are controlled by elastic modulus. However, as the fire exposure starts, model predicts same sudden increase in deflection in the first 20 minutes of fire exposure as observed in fire tests indicating that it can capture sudden loss of prestress (as discussed in Section 3.6.2) in the initial stage of fire exposure. Then model predictions follow a similar trend as measured deflections prior to failure. However, prior to last 10 minutes of fire exposure, model

predicts an early failure than as observed in fire tests by rapid increase in deflections. This can be attributed to the difference in actual and Eurocode 2 material properties as code material properties are more conservative than in real life.

To further demonstrate the effect of actual versus code recommended material properties on fire response of PC beams, beams H1 and H1R are analyzed with actual stress-strain material properties of strands and the comparison is shown in Figures 4.11(b) and (c). Also, to show the effect of spalling on fire response as well, results of model with Eurocode 2 material properties and spalling framework are also shown in Figures 4.11(b) and (c). It can be observed from Figures 4.11(b) and (c) that model deflection predictions for both H1 and H1R beams are very close to observed deflections from the fire test. Also, a significant difference can be observed in the predicted deflections with Eurocode 2 material properties when spalling is accounted and when it is not accounted. For both beams H1 and H1R, no failure is observed when spalling is not considered in the model. Which shows the significance of accounting for spalling in tracing the fire response of HSC PC beams.

In contrast to the behavior of unrestrained beams N1 and H1, restrained beams N1R and H1R have different deflection response after 20 minutes of fire exposure. This variation in response is due to the development of fire-induced restraint forces with a rise in temperatures and this reduces the rate of deflection. The additional moment resulting from fire-induced restraint force controls deflection response till strand temperatures remain below 400^{o}C. Once strand temperatures rise above 400^{o}C, midspan deflection increases rapidly even under restrained conditions as a significant reduction in strength of strands occurs above 400^{o}C. These trends in deflection for restrained beam N1R and H1R are well captured by predicted deflections by the model. However,

the failure of beam N1R and H1R is slightly under-predicted by the model by 8 and 6 minutes, respectively.

Further, the effect of prestress on the fire response of restrained beams can be gauged by comparing the deflection response of restrained PC beams N1R and H1R with a similar restrained RC beam R1. Unlike PC beams N1R and H1R, RC beam R1 experienced a relatively fast increase in deflections in the first 20 minutes of fire exposure as shown in Figure 4.12. This can be attributed to no prestress in beam R1, as in PC beams rate of deflection remained moderate till prestress was overcome by resulting thermal and mechanical stress. Also, due to no prestress in beam R1, it was able to undergo relatively more thermal expansion, and therefore, developed higher restraint forces as compared to PC beams. The resisting moment developed from fire-induced restraint force in beam R1 was able to mitigate the degradation in load-carrying capacity of beam from resulting material degradation and cracking and crushing of concrete for the entire duration of fire exposure. This can be attributed to relatively higher thermal expansion in RC beam R1 as compared to PC beams, and a relatively slower rate of degradation in rebar strength as compared to prestressing strands. Hence, unlike PC beams N1R and H1R, no failure was observed for RC beam R1. Model captured these trends in measured deflection with reasonable accuracy as shown in Figure 4.12. Overall, model predictions are in good correlation with measured deflections for PC and RC beams. Also, model under predicted fire resistance by 1% for beam N1, 7% for beam N1R, 13% for beam H1, and 9% for beam H1R. Therefore, model predictions are on the safe side and within reasonable accuracy, thus, the developed model can be applied to trace the fire response of PC beams with reasonable accuracy.

4.8.5 Comparison of fire induced restraint force

To evaluate the effect of restraint on the fire response of PC and RC beams, the evolution of restraint force in PC and RC beams is compared in Figure 4.13. It can be seen from Figure 4.13 that predicted restraint forces from model are in good agreement with measured values and capture the trends in the evolution of fire induced restraint forces with reasonable accuracy. It can be observed from Figure 4.13 that predicted restraint forces are relatively smaller than measured values in the beginning of fire exposure and then model predictions over predict the restraint forces. This can be attributed to the difference in actual and model Eurocode 2 material properties, and under predicted temperatures by the model in the initial phase of fire exposure. Due to under predicted temperatures model is expanding less than actual beam in fire tests and therefore under predicting the restrain forces. However, as the fire exposure progresses, model over predicts sectional temperatures, and this causes the model to over predict restraint forces as well.

In contrast to PC beams N1R and H1R, RC beam R1, experienced a consistent increase in restraint force to 117 kN till 90 minutes of fire exposure, after that restraint force was manually controlled to stay under 120 kN (due to safety reasons) till failure. This can be attributed to the fact that thermal expansion of the beam R1 is not influenced by prestress (as it does not have any) which allows restraint force to increase consistently with a rise in sectional temperatures. Also, it should be noted that unlike PC beams which failed within 112 minutes, RC beam R1 withstood a much severe fire exposure for 300 minutes without failure as rebars do not lose their strength as rapidly as prestressing strands. Therefore, it can be inferred that RC beams are more likely to undergo higher thermal expansion under fire exposure as they do not fail as rapidly as PC beams. Thus, RC beams are more prone to experience higher restraint forces under fire exposure as compared to

similar PC beams. Overall, a reasonable correlation was observed between measured and predicted restraint force for all beams.

4.9 Summary

A three-dimensional numerical model is developed and validated for PC and RC beams to trace their fire resistance under restrained and unrestrained conditions. Special emphasis is given to tracing the fire induced restraint forces by idealizing connection between beam and framing elements using springs. The model accounts for effect of fire induced restraint force, capturing failure modes occurring through cracking and crushing of concrete at elevated temperatures, spalling of concrete, material and geometric non-linearity, and temperature induced material degradation. The model is validated by comparing the results from model against measured data from fire tests. The model captures overall trends in the fire response of PC and RC beams with reasonable accuracy, and therefore, can be utilized to trace their fire response.

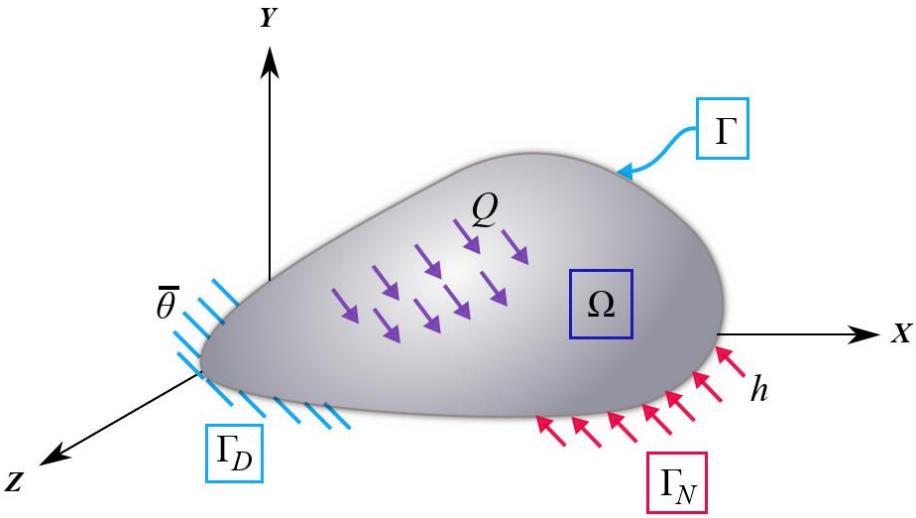

Figure 4.1 General three dimensional body with boundary conditions for finite element model formulation

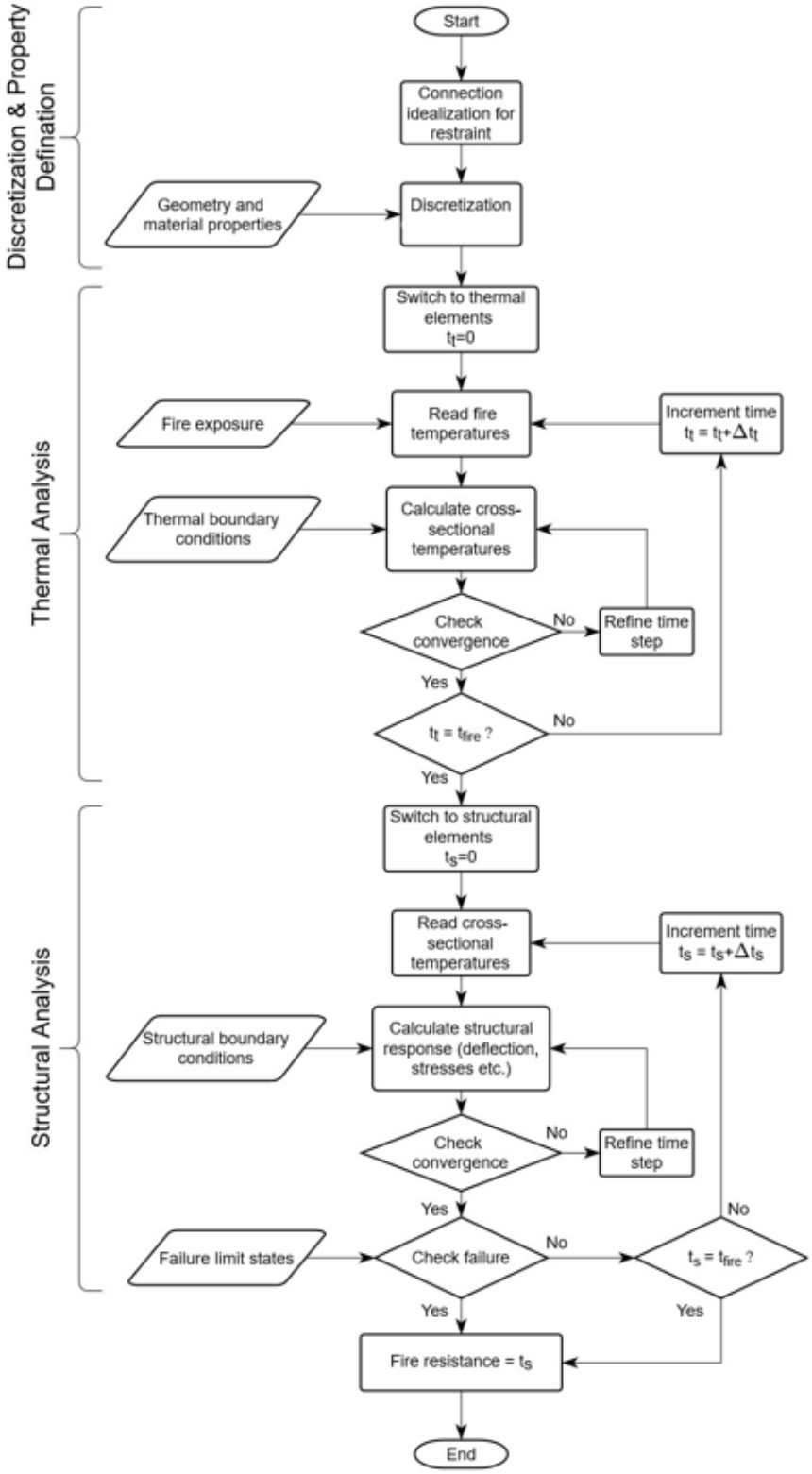

Figure 4.2 Analysis procedure for fire resistance evaluation of PC beams

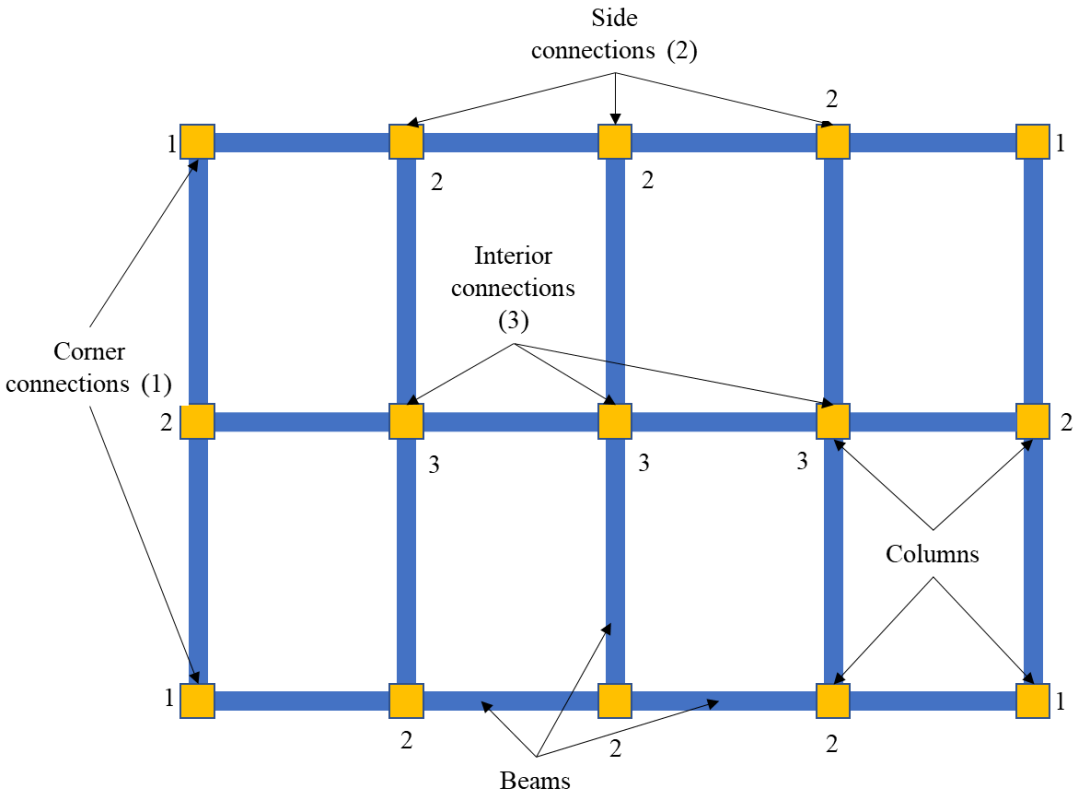

Figure 4.3 Classification of connections in buildings based on number of members (1) corner connection, (2) side connection, (3) interior connection

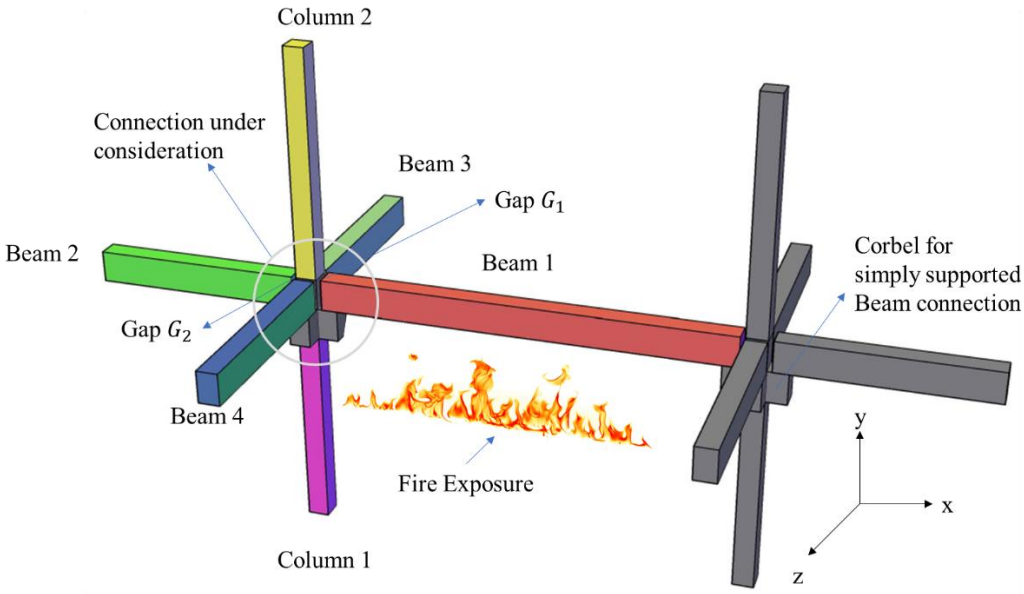

(a)

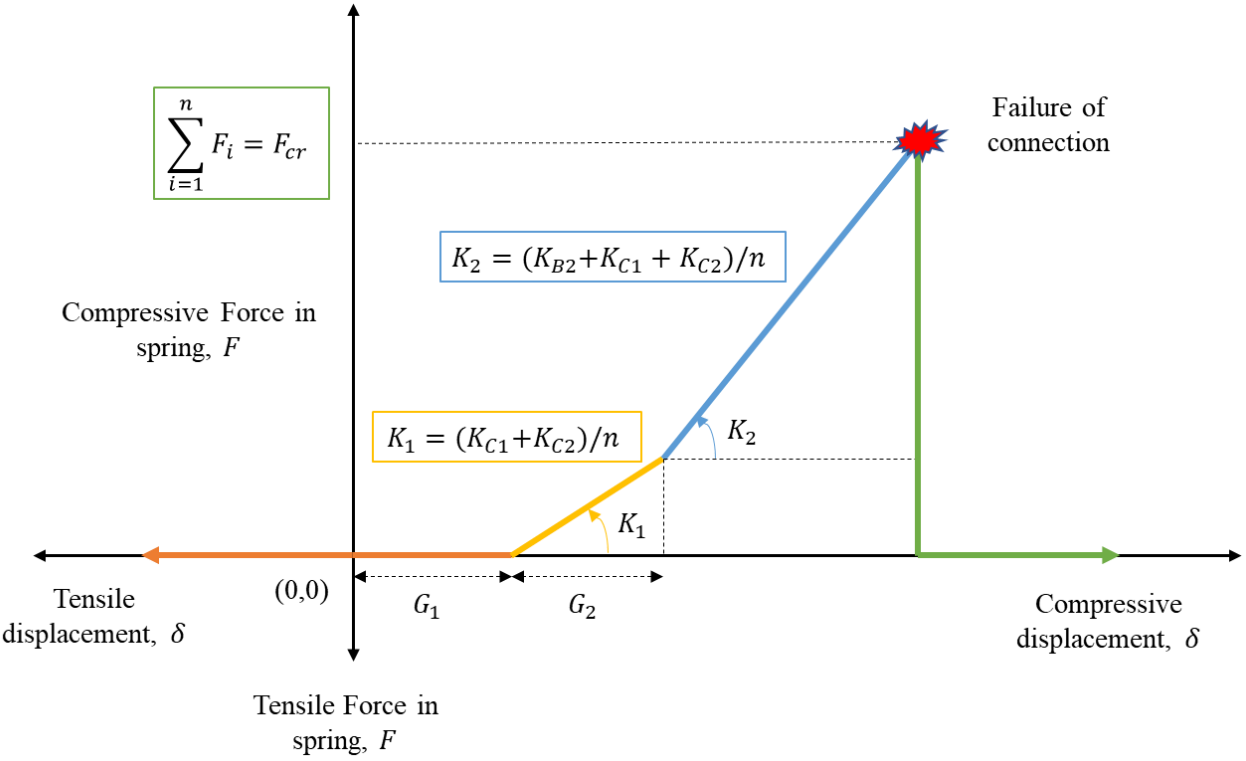

(b)

Figure 4.4 Simply supported interior beam column connection (a) schematic representation, and (b) force-deflection curve of springs for idealization

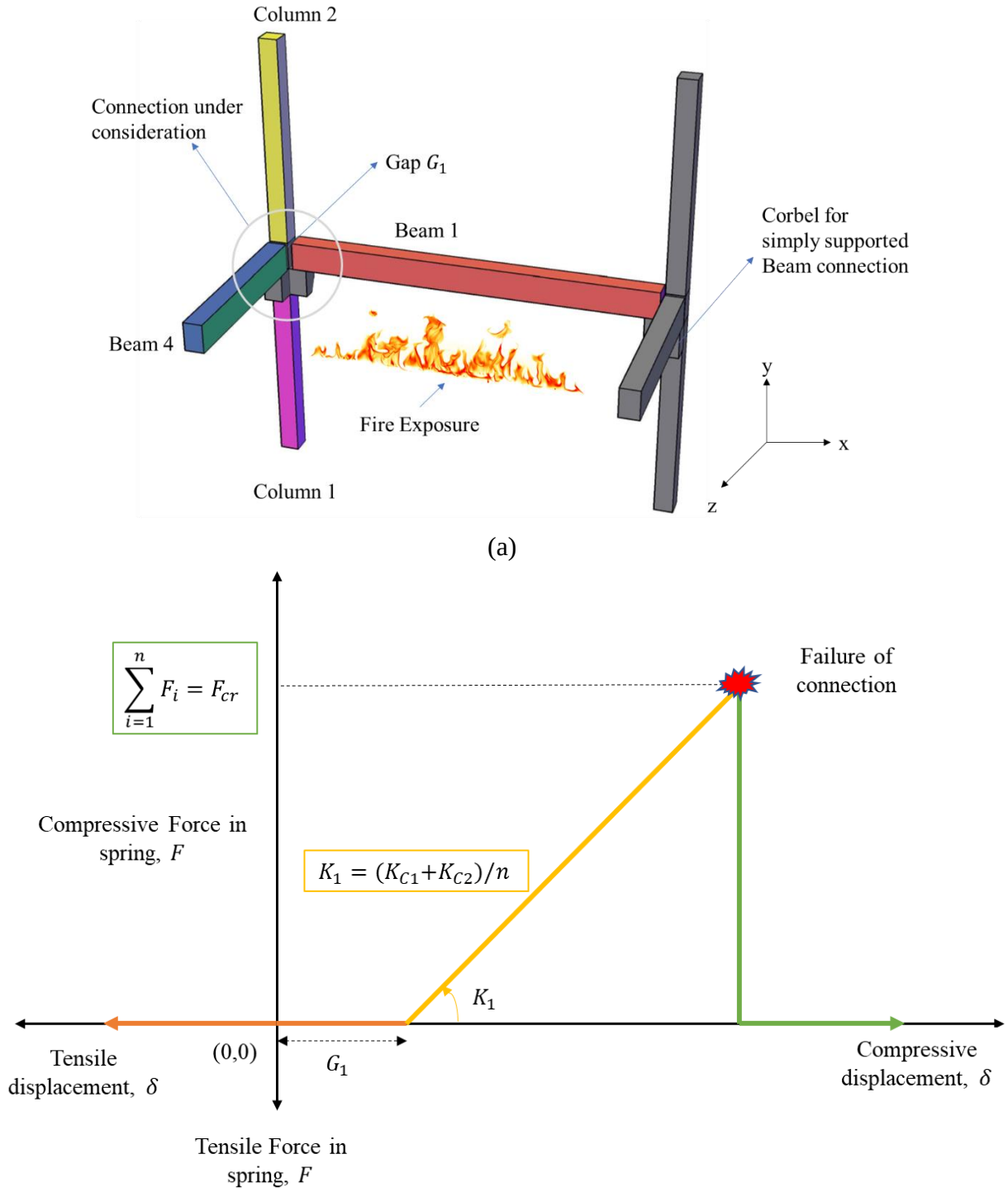

Figure 4.5 Simply supported corner beam column connection (a) schematic representation, and (b) force-deflection curve of springs for idealization of side and corner connections

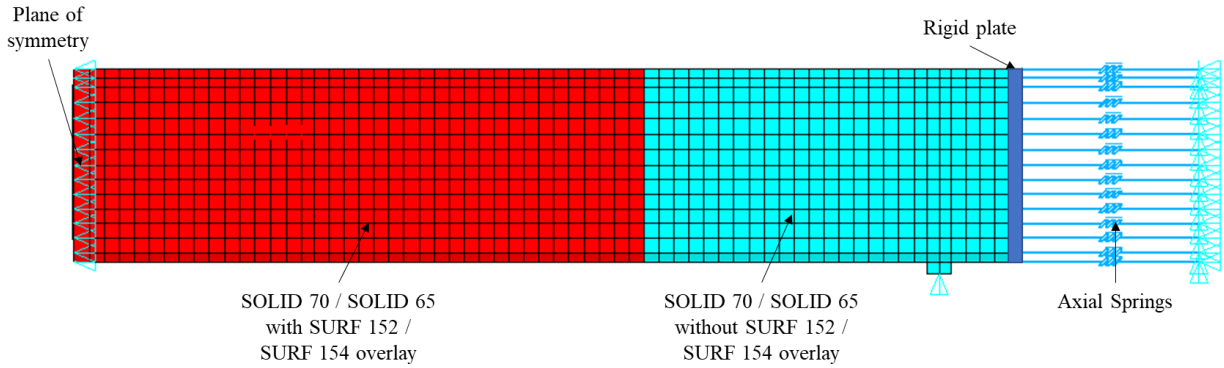

(a)

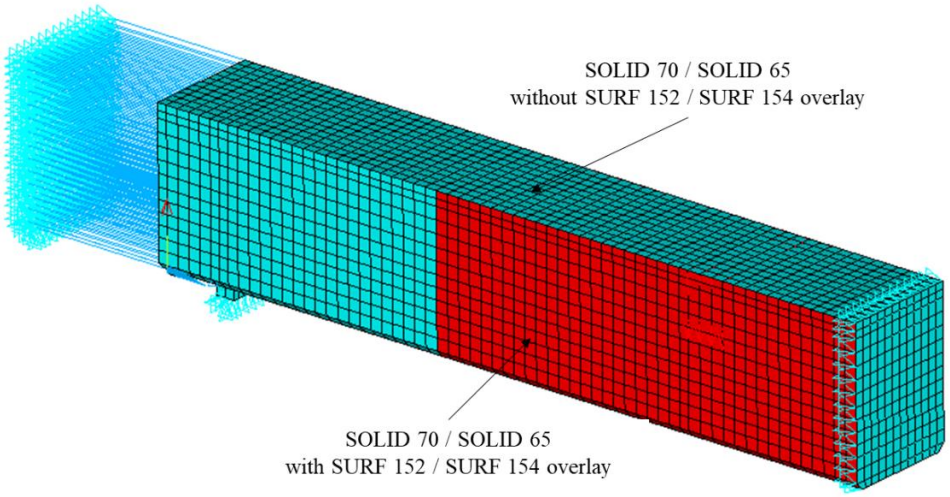

(b)

Figure 4.6 Discretization of PC beam using various elements for a half symmetric FE model (a) side view, (b) perspective view, and (c) inside view

Figure 4.6 (cont'd)

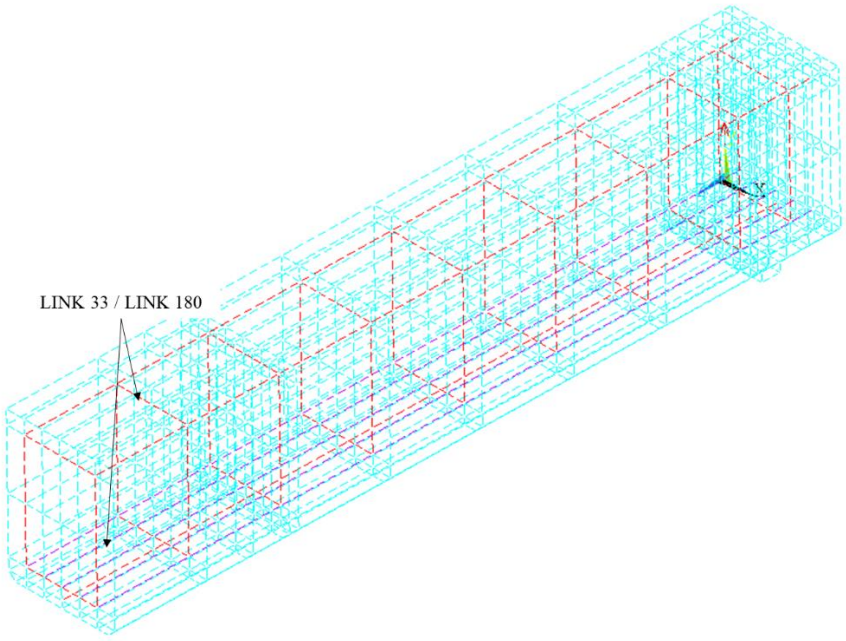

(c)

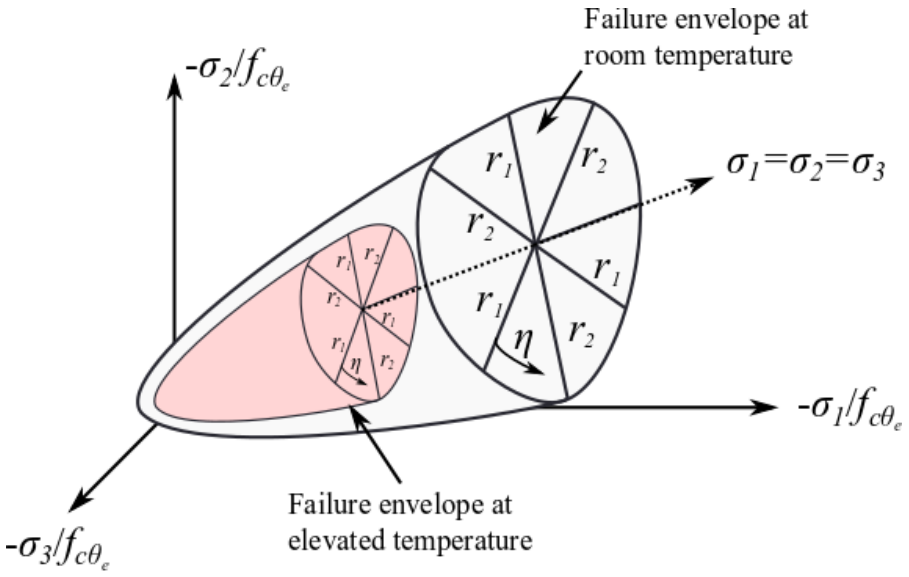

Figure 4.7 Temperature adaptive Willam Warnke failure envelope for concrete in three dimensional principal stress state

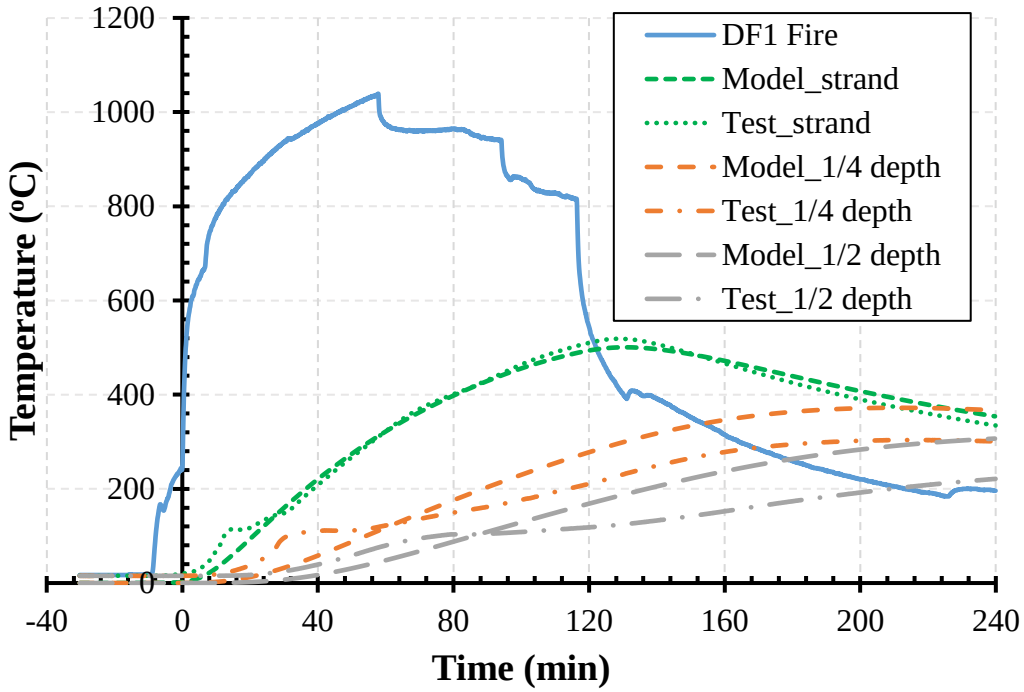

Figure 4.8 Comparison between predicted and measured sectional temperatures for PC beam N1

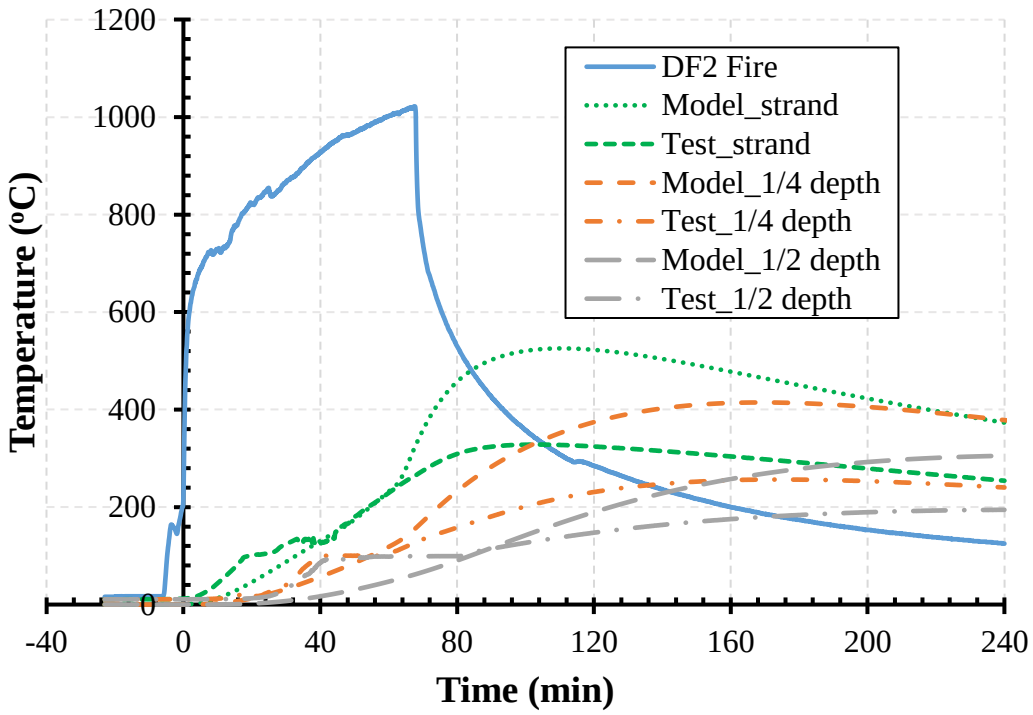

Figure 4.9 Comparison between predicted and measured sectional temperatures for PC beam H1R

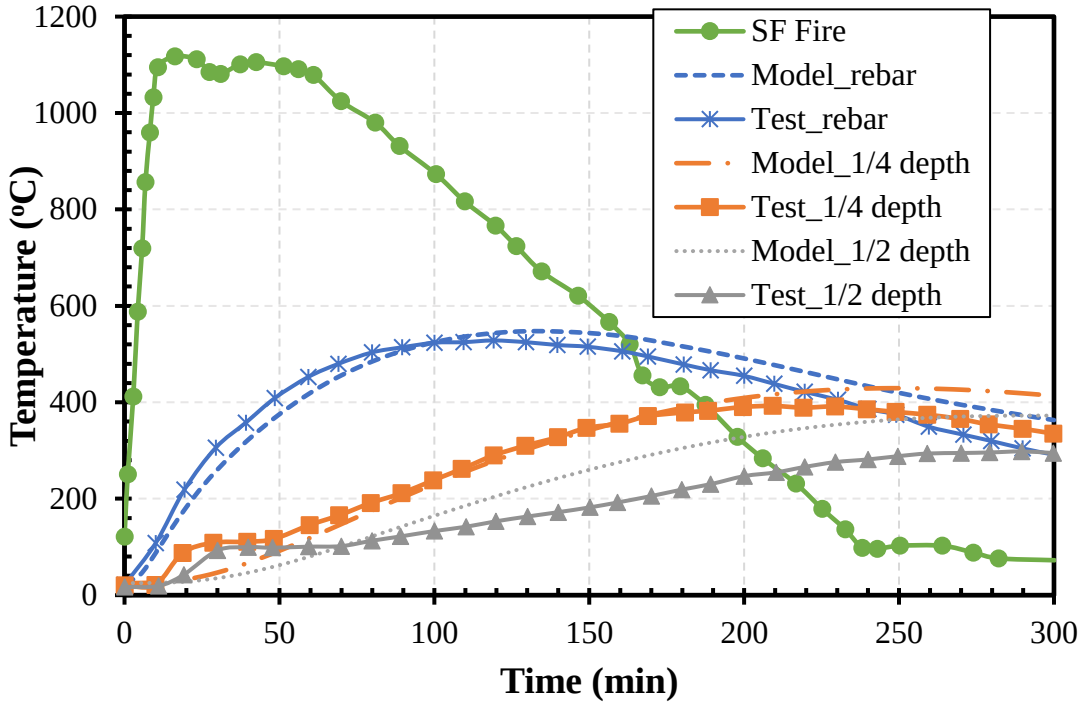

Figure 4.10 Comparison between predicted and measured sectional temperatures for RC beam R1

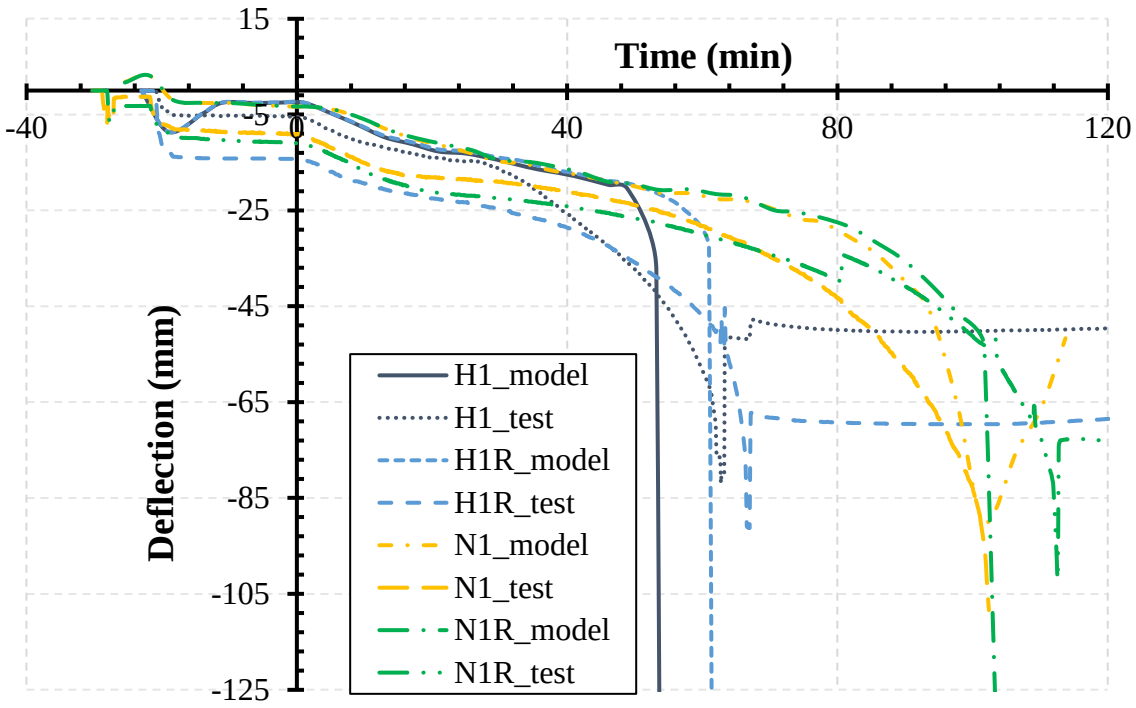

(a)

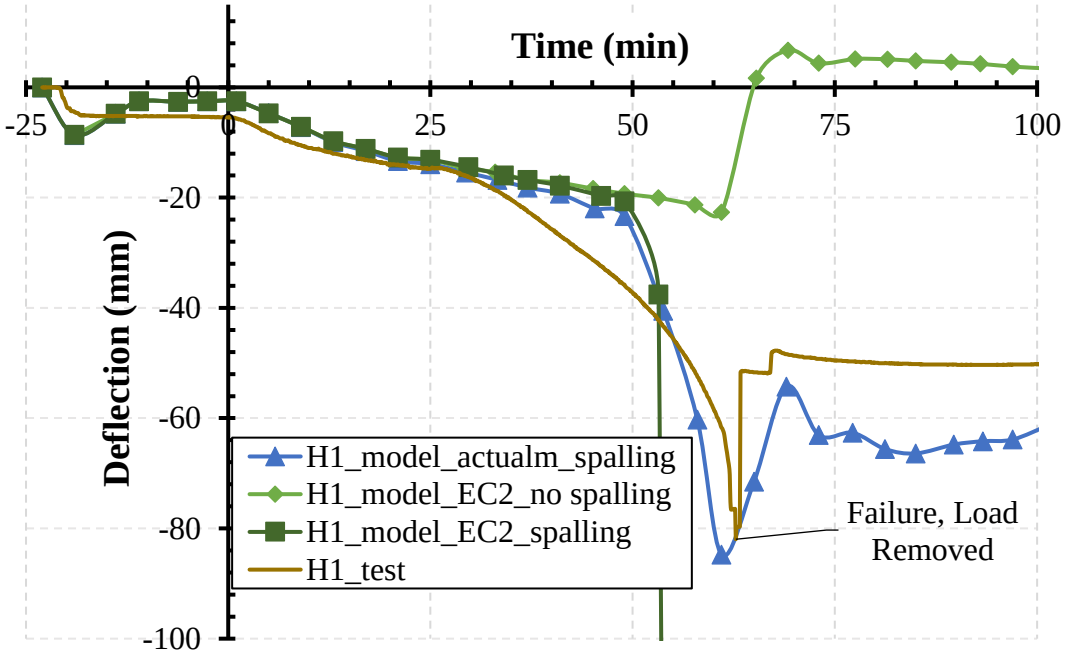

(b)

Figure 4.11 Comparison between predicted and measured midspan deflections for tested PC beams (a) comparison for all beams, (b) effect of spalling and actual strand material properties for beam H1, (c) effect of spalling and actual strand material properties for beam H1R

Figure 4.11 (cont'd)

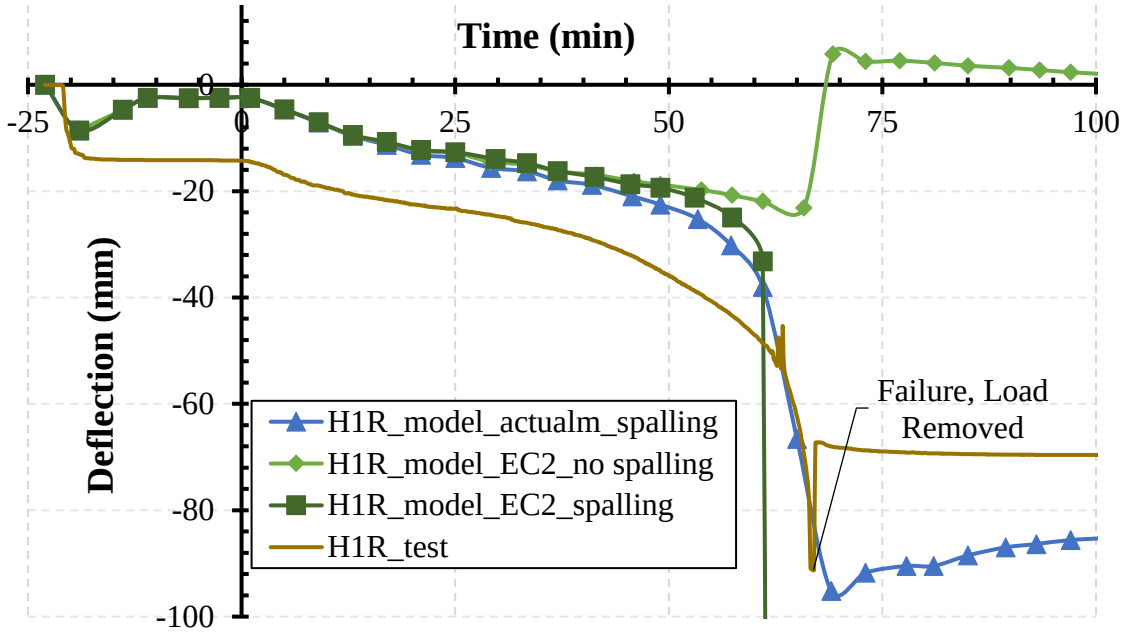

(c)

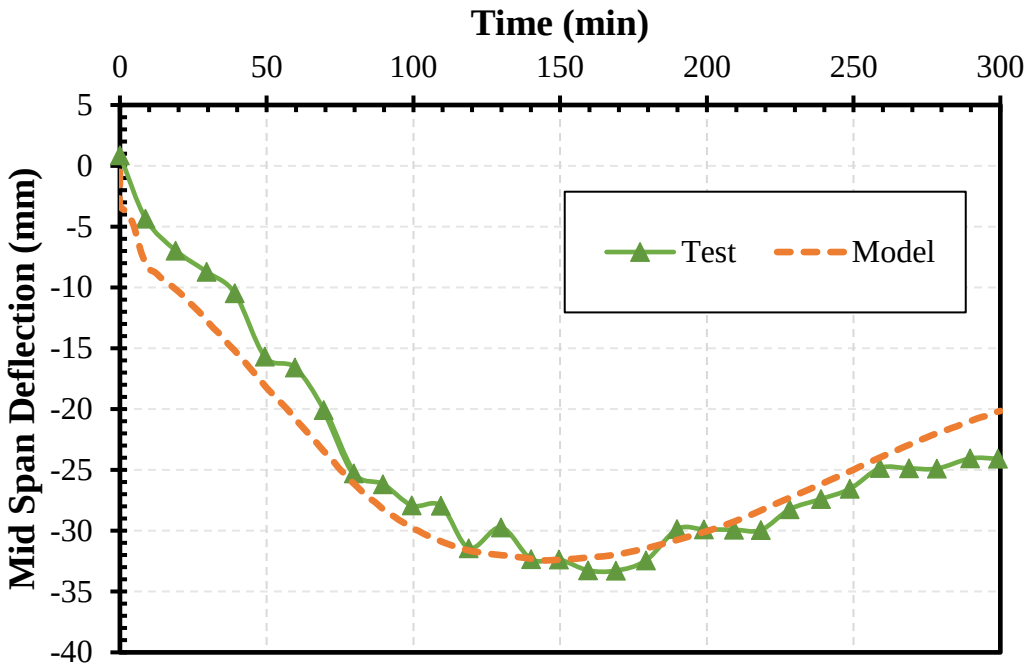

Figure 4.12 Comparison between predicted and measured midspan deflections for RC beam R1

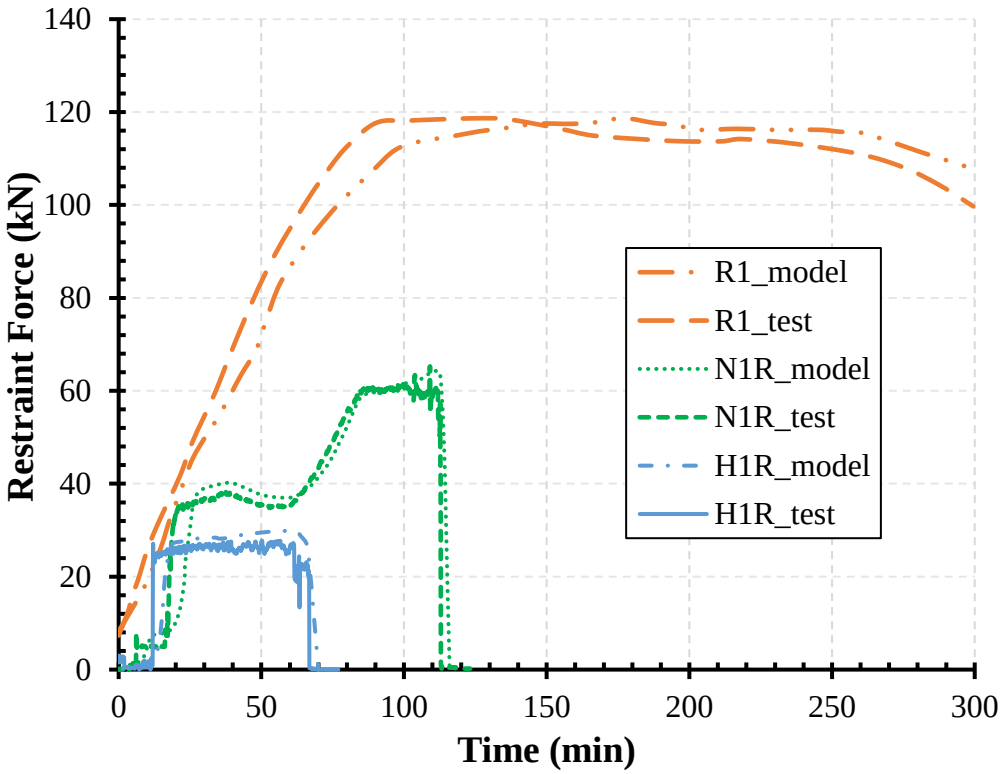

Figure 4.13 Comparison between predicted and measured fire induced restraint force for PC and RC beams

CHAPTER 5

5 Parametric studies

5.1 General

The model developed in Chapter 4 is applied to undertake a series of numerical studies on the effect of fire induced restraint forces on the response of prestressed concrete (PC) beams. Main parameters studied include the effect of cross sectional shape, support conditions, and level of prestress. The effect of restraint on fire response of PC beams is compared with equivalent RC beams to identify key difference in the fire behavior of PC and RC beams. The numerical studies are conducted using a validated three-dimensional finite element based numerical model. The model, discussed in Chapter 4, accounts for critical factors governing fire response of PC beams including fire-induced restraint forces, cracking and crushing of concrete, spalling, and geometry of beam. Specifically, the model accounts for varying fire-induced restraint forces with fire exposure duration. Some of the results from parametric studies have been published by author and can be found in the literature [107], however, complete results of parametric studies along with a more detailed discussion are presented in this Chapter 5.

5.2 Design of beams for parametric studies

A total of 76 numerical simulations were carried out on PC and equivalent RC beams to evaluate the effect of different sectional sizes, varying support conditions, different levels of prestress in strands, and gap in connection. Four sections are selected herein represent the narrow (12RB20) and deep (16RB40) PC beam sections and these sections are selected from the PCI handbook [108] to encompass wide range of sections used in practice. A total of 8 support conditions were selected namely: simply supported, fixed support, interior connection with no gap (IC0), interior connection with 25 mm gap (IC25), interior connection with 50 mm gap (IC50), corner connection with no gap (CC0), corner connection with 25 mm gap (CC25), and corner connection with 50 mm gap (CC50). The simply supported condition is selected to gauge the effect of onset of maximum deflections on the response of the beam in unrestrained conditions, and fixed end condition is selected to gauge the effect of maximum fire induced restraint force developed in beam. However, in real practice, most PC and RC beams have flexible connections depending on the connection of the beam to the framing members. Also, as interior and corner connections provide the highest and the lowest stiffness to the connecting beam under consideration, only these two connection types are studied herein to encompass full range of fire induced restraint force's effect.

Interior and corner connections can be further divided into 3 sub-categories depending on the gap (spacing) between the beam under consideration and connecting column. As the gap in PC beams typically varies between 25 mm to 50 mm, three connection subcategories are selected as connections with 0 mm or no gap, 25 mm gap, and 50 mm gap. A typical interior and corner connection along with the corresponding idealized force deflection curve is illustrated in Figures 4.4 and 4.5. Details on the stiffness calculation and variables used in Figures 4.4 and 4.5 can be referred to Section 4.4. Further to study the effect of prestress in strands, three prestress levels

were considered as 60%, 70%, and 80% under fixed end conditions to gauge the effect of prestress on fire resistance of restrained PC beams. Moreover, to understand the key differences in the fire behavior of PC and RC beams, equivalent RC beams were analyzed by changing the prestressing strand properties to conventional rebar material properties and setting prestress to 0%. It should be noted that all analyzed numerical simulations maintained a load ratio of 50% and are tested under standard ASTM E119 fire exposure. Also, all parametric studies with focus on support ends and effect of prestress are designed with a concrete cover of 76 mm to achieve a fire resistance of 4 hours (even under unrestrained conditions -as recommended by PCI manual [6]), and a few studies are designed with variable cover thickness (38mm to 76 mm cover), as shown in Table 5.1.

For simplification, the beam designation is abbreviated using four main components separated by period as "WW.X.YYY.ZZ_CC". First part of the abbreviation (WW) is to represent a beam as reinforced or prestressed and is given as "PC" or "RC". Second part of the designation (X) is to represent the sectional size used in the analysis; "1" for 12RB20 (305 mm x 508 mm x 5080 mm section), "2" for 12RB36 (305 mm x 914 mm x 9140 mm section), "3" for 16RB24 (406 mm x 610 mm x 6100 mm), "4" for 16RB40 (406 mm x 1016 mm x 10160 mm section), and "5" for 8RB20 (203 mm x 508 mm x 5080 mm section). Third part of the designation (YYY) is to represent the support condition of the beam used in the analysis and is given as "SS" for Simply supported, "FX" for Fixed support, "IC0" for Interior connection with no gap, "IC25" for Interior connection with 25mm gap, "IC50" for Interior connection with 50 mm gap, "CC0" for Corner connection with no gap, "CC25" for Corner connection with 25 mm gap, "CC50" for Corner connection with 50 mm gap. The fourth part of designation (ZZ) represents level of prestress in the strands or main reinforcement as 0%, 60%, 70%, and 80% of prestress corresponding to ultimate strength of strands. The fifth part of designation (CC) represents concrete cover thickness

to strands as 64 mm, 48 mm, or 38 mm. It should be noted that most beams in the parametric study are designed with 76 mm cover thickness, so for brevity, fifth part of designation (CC) is only used if the clear cover is different than 76 mm. Therefore, "PC.1.FX.70_64" indicates a "prestressed concrete" beam with section "12RB20" analyzed under "fixed end" conditions and with "70%" prestress in strands and a concrete cover of "64 mm" to strands. Similarly, all other beams are designated. A detailed list of numerical studies undertaken is given in Table 5.1 and beam reinforcement details are given in Table 5.2. It can be observed from Table 5.1 that for every section a total of 10 simulations are carried out with PC sections and 8 simulations are carried out on equivalent RC beams.

Results from the simulations are analyzed to evaluate effect of key factors influencing fire response of restrained PC beams. Special emphasis is given to monitor the progression of restraint forces and deflections with fire exposure time in PC beams.

5.3 Analysis details

The above designed beams for numerical studies are replicated with identical materials, geometry, loading, fire, and support conditions for finite element analysis as discussed in Section 5.2. The numerical simulations are conducted in accordance with analysis procedure and details discussed in Sections 4.2 to 4.7. All analyzed beams have symmetry in loading, geometry, material properties, and boundary conditions, therefore, only quarter symmetric model is analyzed to save computational effort. To implement the symmetric boundary conditions, the out of plane degrees of freedom are constrained at planes of symmetry. These simplifications significantly reduced the total number of elements required to analyze the beam, and therefore provide swift analysis at lower computational effort. For every numerical analysis thermos-mechanical response of the beam is recorded in terms of sectional temperatures, displacements, and developed fire induced

restraint forces. Then the failure of the beam is determined using failure limit states discussed in Section 4.6. For deflection failure limit state, failure is said to occur when the maximum deflection in the beam exceeds span/20 (mm) at any fire exposure time, or the rate of deflection between two time increments exceeds the limit by $span^2/9000d$ (mm/min), after attaining a maximum deflection of span/30 (mm). On the other hand, for moment failure limit state failure is assumed to occur when the capacity of the beam falls below applied loading.

5.4 Effect of critical factors

To understand the effect of critical factors governing fire response of the PC beams on the evolution of fire induced restraint forces and their effect on fire resistance of PC beams, results from all 76 parametric studies are analyzed herein. Special emphasis is given to identifying trends in evolution of restraint forces, and quantifying fire resistance under restrained conditions.

5.4.1 Evolution of fire induced restraint forces

The development of fire induced restraint forces across width and height of PC and equivalent RC beam with 12RB20 section is illustrated through Figures 5.1 and 5.2, and typical sectional temperatures are shown in Figure 5.3. It should be noted that all beam sections have similar variation in restraint across width and depth and therefore only results for 12RB20 under fixed conditions are discussed in detail herein for brevity. Also, as shown in Figure 5.3, the variation in restraint forces along the width is taken from the beam center (0 mm at beam center) to the right at the bottom face of the beam, and variation in restraint along depth is taken from the bottom (0 mm at bottom) to the top at the right face. These points of observation are selected to study the trends in evolution of restraint forces as they encompass the peak fire induced restraint forces in beams.

It can be observed from Figures 5.1 and 5.2 that there is significant variation in the development of restraint forces throughout fire exposure for both PC and RC beams. For variation in restraint forces across width, there is a lag in the increase of fire induced restraint forces across width for inner layers closer to the beam center. However, there is almost negligible delay in the evolution of restraint forces across depth. This is because section temperatures vary across the width at observed points, and there is almost no variation in sectional temperatures at the observed points across depth, as shown in Figure 5.3. This causes a slow increase in the fire induced restraint forces across widths closer to the beam center as inner widths are more insulated to sectional temperature increase. This is due to high thermal inertia of concrete which causes higher temperatures near fire exposed surfaces and relatively cooler interior as shown in Figure 5.3. Thus, there is relatively higher thermal expansion on the fire exposed surfaces which results in a higher and relatively faster increase in restraint force at these widths. On the other hand, the variation in restraint across the height shows that restraint at bottom is higher than the restraint on the top. This is primarily due to the bending of beam which causes higher axial displacement at the bottom than top which causes higher restraint to thermal expansion at the bottom, thus, resulting in higher restraint forces.

Also, it should be noted that restraint force on top shows negative values (forces away from the face of beam) in the very beginning of fire exposure due to the fixed end conditions. As the beam is exposed to fire, beam undergoes slight increase in deflection as the material properties degrade slightly. This causes the beam to pull inwards at the ends, and hence, a negative restraint value is observed at the top and heights near the top. However, as the thermal expansion of the beam becomes dominant, the restraint forces become positive again (acting towards the beam face). This phenomenon is only observed for the fixed end conditions, and not for flexible end conditions with

idealized springs for interior and corner connections as the springs are designed not to carry any tension to represent realistic boundary conditions.

Further, it should be noted that restraint forces along the depth are relatively higher for equivalent RC beam (RC.1.FX.70) than the PC beam (PC.1.FX.70). This is due to the presence of prestress in the PC beam which carries most of the applied loading for the PC beams. As the temperature increases, thermal expansion of beam causes significant loss of prestress which causes an increase in the mid span deflections. This causes an inward pull at the ends and ultimately mitigates the fire-induced axial displacement of the beam, thus, decreasing the magnitude of restraint force. However, this is not the case for RC beam, and the beam experiences relatively higher fire-induced axial displacement, thus, develops relatively higher restraint force.

Further, it should be noted that type of concrete can have significant effect on the evolution of fire-induced restraint forces as well. For HSC PC beams, the rate of loss in strength is relatively much higher than NSC PC beams due to spalling and higher loss in yield strength at elevated temperatures. Therefore, HSC PC beams are likely to undergo relatively higher midspan deflections under same fire exposure when compared to the equivalent NSC PC beams. This increase in the midspan deflections cause an inward pull at the beam ends which mitigates the thermal expansion of the beam under fire exposure, thus, mitigating the development of restraint forces. On the other hand, NSC beams have relatively slower degradation in material strength and relatively less spalling, which allows them to withstand the fire exposure for relatively longer durations than HSC counterparts, and therefore experience a higher thermal expansion which leads to a higher fire-induced restraint force.

Overall, the evolution of fire-induced restraint forces in PC beams is governed by thermal expansion of the beam and material degradation, and it can be grouped under two main stages as:

growth stage, and decay stage. In the growth stage, the material degradation in the beam is minimal as the sectional temperatures are still considerably low, and the thermal expansion is continuously increasing as the sectional temperature rise. This causes a consistent increase in the restraint forces on the end across width and depth of the beam as can be seen from Figures 5.1 and 5.2. However, as the sectional temperatures become high enough to cause significant material degradation, the mid span deflection increases, and the beam is pulled inwards. This mitigates the fire-induced axial displacement of the beam which causes a decay in the fire-induced restraint forces.

5.4.2 Effect of support conditions

The deflection response for all parametric studies for 8 different end support conditions is illustrated through Figures 5.4 to 5.11. It can be observed from Figures 5.4 to 5.11 that higher deflections are observed for the simply supported end conditions (shown in Figure 5.4). This is because there is no restraint force in simply supported beams to resist the applied external moment, and therefore, these beams experienced highest deflections. Due to large deflections and lack of restraint forces, most simply supported PC and RC beams failed under fire conditions. It can be observed from Figure 5.4 that PC beams failed at least 60 minutes prior to the RC counterparts. Moreover, RC beams with 16RB24 and 16RB40 sections (RC.3.SS.0 and RC.4.SS.0) did not fail even under simply supported conditions as shown in Figure 5.4. This higher fire resistance of RC beams is due to the slower strength degradation in rebars at elevated temperatures as compared to prestressing strands. Also, for the PC and RC beams with 16RB24 and 16RB40 sections, the sectional area is significantly higher than the 12RB20 and 12RB36 sections which provides them with higher thermal inertia due to larger volume which impedes the rise in sectional temperatures. It is due to this reason that PC and RC beams with 16RB24 and 16RB40 sections fail much later than beams with 12RB20 and 12RB36 sections.

On the other hand, no beams undergo failure under fully fixed end conditions as shown in Figure 5.5. This is primarily due to the capability of fixed end conditions to develop high restraint forces at ends as this support condition does not allow any thermal expansion of the beams. The developed restraint forces significantly mitigate the applied moment on the beam which leads to much smaller deflections. Therefore, Figure 5.5 shows that even for PC beams, restraint can help achieve high fire resistance even if there is rapid degradation of strength for strands. A similar trend was observed for the interior flexible connection with no gap which has the highest stiffness among all flexible connections, and the beams seem to behave like that under fixed end conditions, as shown in Figure 5.6. Also, it should be noted that significant restraint forces (as high as 2286 kN) were developed in these FX and IC0 end conditions, and connections are not typically designed to withstand such high restraint forces.

For the same interior connection, as the gap G_1 was increased from 0 mm in IC0 to 25 mm and 50 mm in IC25 and IC50 connections, a significant decrease in the restraint forces was observed and the PC beams did undergo failure under these end conditions, as shown in Figure 5.7 and 5.8. While a small increase in the fire resistance of the PC beams was observed, no beams could achieve PCI manual predicted fire resistance of 4 hours. A similar trend was observed for corner connections as well, where best fire resistance was observed for CC0 connection as compared to CC25 and CC50 as shown in Figures 5.9 to 5.11. Therefore, as the gap increased from 0 mm to 50 mm in flexible connections a significant decrease in the magnitude of restraint forces and fire resistance of PC beams was observed. Hence, it is very important to account for the actual gap between beam and columns in the design process of restrained PC beams which is currently not accounted for by codes and standards.

It can be observed from Figures 5.4 to 5.11 that even though there are similar restraint forces in PC and equivalent RC beams, PC beams still fail much earlier than RC beams. This is primarily due to the rapid degradation in strength of strands which cause the failure of the beam much earlier than the equivalent RC beams. Also, it should be noted that resisting moment developed from fire induced restraint forces is much smaller than the capacity of the PC beam than the capacity of RC beam as the strength of strands is 3 to 4 times that of rebars. Therefore, even if, identical restraint resisting moment is developed in the PC beams as in equivalent RC beams, it cannot prolong the failure as it is relatively smaller percentage of capacity in PC beams than as compared to in RC beams. This is clearly represented by deflection results shown in Figures 5.4 to 5.11 where PC beams fail 1 to 2 hours before equivalent RC beams even though they have similar magnitudes of restraint forces.

5.4.3 Effect of section type

The effect of section type on development of restraint forces is illustrated by Figures 5.12 to 5.16. It can be observed from the Figure 5.12 that the highest restraint forces are developed for fixed (FX) and interior connection with no gap (IC0). This trend is similar for all sections, hence results for only 12RB20 are shown in Figure 5.12 for brevity. This is since thermal expansion of the beam is completely resisted with very high stiffness for these two end conditions and as a result a very high restraint force is developed. Also, it can be observed from Figure 5.12 that restraint force for RC beams (RC.1.FX.0 and RC.1.IC0.0) is higher than PC counterparts (PC.1.FX.0 and PC.1.IC0.0). This is due to the loss of prestress in PC beams during fire exposure which causes increase in deflection which pulls the beams inward, thus, mitigating the thermal expansion. On the other hand, RC beams do not have any prestress, therefore, PC beams experience lower restraint forces than equivalent RC beams. Also, it can be observed from Figure 5.12 that restraint

forces under fixed (FX) and interior connection with no gap (IC0) for section 12RB20 are significantly higher than all other end conditions. However, most buildings have flexible connections with gap ranging between 0 to 50 mm, and therefore, it is important to understand trends in the development of restraint for these conditions in different sections. For this purpose, variation of restraint for all four sections are shown in Figures 5.13 to 5.16 excluding the FX and IC0 end support conditions.

It can be observed from Figures 5.13 that after FX and IC0, the highest restraint forces are developed in CC0 end conditions. This is because after FX and IC0, CC0 end conditions have the highest stiffness, and same trend is observed for all other sections as shown in Figure 5.13 to 5.16. However, the magnitude of restraint forces under CC0 end conditions is significantly less than the FX and IC0 end conditions. This is because the stiffness of CC0 is significantly less than FX and IC0 connections as it does not have the Beam 2 of interior connections (see Figure 4.4). Also, it can be observed from Figure 5.13 that while restraint force for RC beam (RC.1.CC0.0) under CC0 keeps increasing throughout fire exposure, restraint forces for counterpart PC beam (PC.1.CC0.0) increase relatively slowly and drop to 0 as the beam fails under fire exposure. The slow increase in restraint force in PC.1.CC0.0 is due to loss of prestress, as discussed in Section 5.4, and relatively early failure than RC.1.CC0.0 is due to the rapid degradation of strength in strands, as discussed in Section 5.5. On the other hand, the restraint forces are minimal for all other end conditions with gaps in connection for section 12RB20, as shown in Figure 5.13. This can be inferred to the fact that beam thermal expansion could not overcome gap in connection, and therefore, no restraint forces were developed for fire exposure till gap was overcome and some restraint forces are observed towards the end when beam had had ample time to expand. Also, for

PC beams, the beams failed prior to the thermal expansion overcoming gap in connection, and therefore, no restraint forces are observed.

On the other hand, it can be observed from Figure 5.14 that for section 12RB36 the restraint force for PC.2.IC25.70 did increase significantly once the thermal expansion of the beam overcame gap in connection. This is observed for beams with section 12RB36 and not 12RB20 as top and bottom axial displacements at the beam ends are higher for 12RB36 than 12RB20 due to higher depth. Therefore, for same degree of rotation at ends, beams with section 12RB36 will experience higher top and bottom axial displacements at beam ends which helps in overcoming the connection gap, and therefore, results in higher restraint force. A similar trend is observed for beams with sections 16RB24 and 16RB40, as shown in Figures 5.15 and 5.16. Overall, it can be observed from Figures 5.12 to 5.16 that the magnitude of restraint forces is higher for beams with bigger sections under same fire exposure. This is since same degree of rotation at the ends will cause higher axial displacement at the ends of deeper and wider beams due to geometry, and ultimately causes higher restraint forces in these beams. This can be observed from Figure 5.16, where restraint forces are the highest under all end conditions, as compared to smaller beam sections shown in Figures 5.12 to 5.16.

5.4.4 Effect of prestress

To illustrate the effect of prestress on fire response of PC and RC beams, the deflection response for all beams under varying degrees of prestress (0% to 80%) is shown in Figure 5.17. It should be noted that prestress of 0% is defined for equivalent RC beams and they are shown in Figure 5.17 to set the context for difference in the fire response of PC and equivalent RC beams. For PC beams, the prestress was varied from 60% to 80% and as can be seen from Figure 5.17, variation in prestress only had a minor effect on the fire response of the PC beams. This is due to the fact

that under fire conditions, majority of prestress is lost in the early stages of fire exposure only and therefore does not play a key role in the fire response of the PC beams. Further, it can be observed form Figure 5.17 that without the presence of prestress (0% prestress case), RC beams had minimal deflections. However, all PC beams with 60% to 80% of prestress experienced relatively higher deflections. This is due to increase in deflections from loss of prestress in PC beams under fire exposure, and relatively rapid degradation in strength and stiffness of strands than rebars.

Moreover, for PC beams, there is minute difference between the deflected response for 60% to 80% of prestress. Beams with prestress of 80% are observed to deflect slightly more in the beginning as compared to beams with 60%. This can be attributed to relatively higher decrease in the prestress for beams with 80% prestress at the start of fire exposure, as compared to beams with 60% prestress. This causes a relatively higher degradation of strength for PC beams with 80% of prestress than as compared to the PC beams with 60% prestress. Thus, causing slightly more deflections for beams with 80% prestress. However, the difference in the deflections for all beam sections is minimal for prestress of 60% to 80%.

5.4.5 Peak fire induced restraint forces

To explain the difference in the evolution of peak restraint in PC vs RC beams, the development of maximum restraint in all beams is illustrated by further analyzing restraint forces for beams with fixed end conditions. The resulting evolution in the maximum restraint forces is plotted for PC and equivalent RC beams in Figure 5.18. It can be observed from the Figure 5.18 that the evolution of maximum restraint force is similar for PC and equivalent RC beams as they share identical geometry and material properties. However, the magnitude of restraint force is slightly higher for RC beams than as compared for the PC beams. This is due to the loss of prestress in the beginning of fire exposure in PC beams which causes an increase in the mid span deflection and

causes an inward pull at ends, thus, inhibiting fire-induced thermal expansion of the beam. This lag in increase in initial thermal expansion of PC beams is what causes the slightly lower restraint forces for PC beams than as compared to the equivalent RC beams.

Other factor contributing to the relatively lower peak restraint forces in PC beams is the inability of the PC beams to withstand fire exposure for long durations as compared to equivalent RC beams. This is due to relatively faster strength degradation of strands in PC beams than as compared to rebars in RC beams, thus, causing an earlier failure. This earlier failure does not allow ample time for PC beams to expand as much as equivalent RC beams. Therefore, relatively lower fire induced restraint forces are developed in PC beams. However, it can be observed from Figure 5.18 that significant restraint forces are developed for both PC and RC beams.

Also, it can be observed from Figure 5.18 that beams with section 1 experience lowest restraint forces, whereas beams with section 4 experienced highest restraint forces. This can be attributed to the beam size. As section 1 has the lowest sectional area, thermal expansion is lowest in this beam due to smaller heated volume of the concrete. On the other hand, section 4 represents widest and deepest section. Therefore, relatively higher restraint forces are observed in section 4 as compared to section 1. However, it should be noted that for all sections similar trends in restraint forces are observed. This is due to similar fire exposure used in all numerical studies which causes similar thermal expansion of the beams.

5.4.6 Effect of gap in connections

Gap in connections is vital for the development of fire induced restraint forces, as restraint forces cannot develop until thermal expansion of the beam overcomes gap in connection. To understand the effect of gap in connections on the fire resistance, a summary of variation in fire resistance from all parametric studies is shown in Figure 5.19. It can be observed form Figure 5.19 that lowest

fire resistance is for numerical studies with highest gap and lowest connection stiffness. Whereas, for most cases with no gap in connections, significant restraint forces were developed at ends and no failure of the beam was observed. It should be noted that all PC and RC beams studied in the parametric studies were predicted to have a fire resistance of 4 hours as per PCI Manual 126 [6]. However, most of the PC beams failed before 2 hours of fire exposure. Therefore, it can be inferred from these results that fire resistance predictions from codes and standards may not be accurate, especially under restrained conditions.

To further understand the effect of gap in connections on the fire resistance of PC beams, variation in peak fire induced restraint forces is shown for all sections as a function of gap thickness in Figure 5.20. It can be observed from Figure 5.20 that significant restraint forces developed for all sections at 0 mm gap. However, peak fire induced restraint forces experienced an exponential decay with increase in gap thickness from 0 mm to 25 mm and reduced to almost negligible values at a gap of 50 mm. Also, it can be observed from Figure 5.20 that for interior connection with 25 mm gap thickness (IC25) was the connection with highest restraint force at 25 mm. Also, as discussed in previous section, restraint forces for RC counterparts were highest at 0 mm gap thickness than PC beams. However, all beams and connection types experienced an exponential decay in magnitude of peak restraint force as gap increased from 0 mm to 25mm. Therefore, it is important to account for the gap thickness in evaluating the fire response of PC beams under restrained conditions.

5.4.7 Effect of cover thickness and beam width

In current prescriptive design practice, cover thickness and beam width are the main parameters that are considered for determining the fire resistance of PC beams. To analyze the effect of concrete cover thickness to strands and beam width on the development of fire induced restraint

forces and fire response of beam, 12RB20 beam section is analyzed under different concrete cover and width recommendations as per PCI manual [6]. Results from corresponding parametric studies are shown in Figures 5.21 to 5.23. It can be observed from Figure 5.21 that beam with highest cover thickness undergo least mid-span deflection and the beam deflections increase with decreasing cover thickness. This is because reduction in cover thickness leads to reduction in thermal mass between the fire exposed beam face and the prestressing strands. This leads to a reduction in thermal inertia of concrete protecting the strands, and it leads to faster increase in strand temperatures causing relatively faster degradation in strength and stiffness of strands. Therefore, beams with lower cover thickness undergo higher mid span deflections.

Also, it can be observed from Figure 5.22 that the beam deflection increased significantly faster for 8RB20 than as compared to 12RB20. It should be noted that both beams are analyzed under fixed end conditions to allow development of maximum fire induced restraint forces for the section. Therefore, even when PC beam 8RB20 is allowed to develop peak fire induced restraint forces under fixed end conditions, still deflections increase more rapidly for 8RB20 than 12RB20. This can be attributed to reduced thermal mass of the beam due to relatively less volume which results in lower thermal inertia and higher sectional temperatures. This causes faster degradation in strand strength and stiffness in 8Rb20 than 12RB20 which leads to relatively faster increase in deflection in 8RB20.

Further, it can be noted from Figure 5.23 that decrease in cover slightly increases the fire induced restraint force for 12RB20 beams, and the fire induced force in 8RB20 is lower than 12RB20. This is because while decrease in cover thickness increases strand temperatures, thermal inertia of the entire beam is still the same and therefore, only slight increase in restraint forces is observed which is to compensate for the rapid strength reduction in strands with lower concrete cover. On the other

hand, lower fire induced restraint forces in beam 8RB20 can be attributed to lower axial stiffness of 8RB20 than as compared to 12RB20. Therefore, lower force is required to prevent thermal expansion in beam 8RB20 than as compared to 12RB20, and this causes lower fire induced restraint forces in 8RB20.

5.5 Summary

A total of 76 numerical studies are conducted to quantify the effect of restraint on fire resistance of PC and equivalent RC beams. Main parameters of investigation include support conditions, section type, gap, prestress, cover thickness, and beam width. To identify the effect of these parameters, evolution of fire induced restraint forces and deflection response is analyzed in detail. Also, to study the effect of gap on fire resistance of PC beams, a variation in the peak fire induced restraint forces is studied for all sections at varying gap thickness. Special emphasis is given to the evolution of restraint forces and their effect on PC and equivalent RC beams. It can be observed from the results of the parametric studies that support conditions, section type and gap are key factors governing fire response of restrained PC beams. Also, it can be inferred that current prescriptive based fire codes and standards can over predict fire resistance of PC beams by as high as 50% under restrained conditions. Moreover, minimal fire induced restraint forces are observed for all beams with gap of 50 mm at connection.

Table 5.1 Details of varying parameters in parametric studies for studying the effect of fire-induced restraint forces

Parameters*	Beam designation +	Connection type	Prestress level (%)	Gap in connection (mm)	Cover (mm)	Failure time (Fire resistance, min)
Effect of support conditions and prestress on 12RB20 PC beams	PC.1.SS.70	SS	70	-	76	124
	PC.1.FX.70	FX	70	0	76	No failure
	PC.1.IC0.70	IC0	70	0	76	No failure
	PC.1.IC25.70	IC25	70	25	76	128
	PC.1.IC50.70	IC50	70	50	76	124
	PC.1.CC0.70	CC0	70	0	76	136
	PC.1.CC25.70	CC25	70	25	76	128
	PC.1.CC50.70	CC50	70	50	76	124
	PC.1.FX.60	FX	60	0	76	No failure
	PC.1.FX.80	FX	80	0	76	No failure
Effect of support conditions and prestress on 12RB20 equivalent RC beams	RC.1.SS.0	SS	0	-	76	220
	RC.1.FX.0	FX	0	0	76	No failure
	RC.1.IC0.0	IC0	0	0	76	No failure
	RC.1.IC25.0	IC25	0	25	76	No failure
	RC.1.IC50.0	IC50	0	50	76	224
	RC.1.CC0.0	CC0	0	0	76	No failure
	RC.1.CC25.0	CC25	0	25	76	No failure
	RC.1.CC50.0	CC50	0	50	76	224
Effect of support conditions and prestress on 12RB36 PC beams	PC.2.SS.70	SS	70	-	76	112
	PC.2.FX.70	FX	70	0	76	No failure
	PC.2.IC0.70	IC0	70	0	76	No failure
	PC.2.IC25.70	IC25	70	25	76	120
	PC.2.IC50.70	IC50	70	50	76	112
	PC.2.CC0.70	CC0	70	0	76	132
	PC.2.CC25.70	CC25	70	25	76	120

Table 5.1 (cont'd)

	PC.2.CC50.70	CC50	70	50	76	112
	PC.2.FX.60	FX	60	0	76	No failure
	PC.2.FX.80	FX	80	0	76	No failure
Effect of support conditions and prestress on 12RB36 equivalent RC beams	RC.2.SS.0	SS	0	-	76	212
	RC.2.FX.0	FX	0	0	76	No failure
	RC.2.IC0.0	IC0	0	0	76	No failure
	RC.2.IC25.0	IC25	0	25	76	No failure
	RC.2.IC50.0	IC50	0	50	76	No failure
	RC.2.CC0.0	CC0	0	0	76	No failure
	RC.2.CC25.0	CC25	0	25	76	No failure
	RC.2.CC50.0	CC50	0	50	76	No failure
Effect of support conditions and prestress on 16RB24 PC beams	PC.3.SS.70	SS	70	-	76	140
	PC.3.FX.70	FX	70	0	76	No failure
	PC.3.IC0.70	IC0	70	0	76	No failure
	PC.3.IC25.70	IC25	70	25	76	152
	PC.3.IC50.70	IC50	70	50	76	140
	PC.3.CC0.70	CC0	70	0	76	196
	PC.3.CC25.70	CC25	70	25	76	152
	PC.3.CC50.70	CC50	70	50	76	140
	PC.3.FX.60	FX	60	0	76	No failure
	PC.3.FX.80	FX	80	0	76	No failure
Effect of support conditions and prestress on 16RB24 equivalent RC beams	RC.3.SS.0	SS	0	-	76	No failure
	RC.3.FX.0	FX	0	0	76	No failure
	RC.3.IC0.0	IC0	0	0	76	No failure
	RC.3.IC25.0	IC25	0	25	76	No failure
	RC.3.IC50.0	IC50	0	50	76	No failure
	RC.3.CC0.0	CC0	0	0	76	No failure
	RC.3.CC25.0	CC25	0	25	76	No failure

Table 5.1 (cont'd)

	RC.3.CC50.0	CC50	0	50	76	No failure
Effect of support conditions and prestress on 16RB40 PC beams	PC.4.SS.70	SS	70	-	76	132
	PC.4.FX.70	FX	70	0	76	No failure
	PC.4.IC0.70	IC0	70	0	76	No failure
	PC.4.IC25.70	IC25	70	25	76	156
	PC.4.IC50.70	IC50	70	50	76	156
	PC.4.CC0.70	CC0	70	0	76	204
	PC.4.CC25.70	CC25	70	25	76	156
	PC.4.CC50.70	CC50	70	50	76	132
	PC.4.FX.60	FX	60	0	76	No failure
	PC.4.FX.80	FX	80	0	76	No failure
Effect of support conditions and prestress on 16RB40 equivalent RC beams	RC.4.SS.0	SS	0	-	76	No failure
	RC.4.FX.0	FX	0	0	76	No failure
	RC.4.IC0.0	IC0	0	0	76	No failure
	RC.4.IC25.0	IC25	0	25	76	No failure
	RC.4.IC50.0	IC50	0	50	76	No failure
	RC.4.CC0.0	CC0	0	0	76	No failure
	RC.4.CC25.0	CC25	0	25	76	No failure
	RC.4.CC50.0	CC50	0	50	76	No failure
Effect of cover thickness on 12RB20 PC beams	PC.1.FX.70_64	FX	70	0	64	No failure
	PC.1.FX.70_48	FX	70	0	48	No failure
	PC.1.FX.70_38	FX	70	0	38	No failure
Effect of beam Width on 12RB20 PC beams	PC.1.FX.70	FX	70	0	76	No failure
	PC.5.FX.70	FX	70	0	76	No failure

Table 5.1 (cont'd)

Note: *All beams constitute calcareous aggregate based concrete with a characteristic compression strength of 50 MPa, all PC beams have low relaxation prestressing strands with a tensile strength of 1861 MPa, and all RC beams have rebars with a tensile strength of 415 MPa

[+] Beam legends are abbreviated for brevity (see Section 5.2) using following: PC = Prestressed concrete, RC = Reinforced concrete, 1 = Section 12RB20, 2 = Section 12RB36, 3 = 16RB24, 4 = 16RB40, 5 = 8RB20, SS = Simply supported, FX = Fixed support, IC0 = Interior connection with no gap, IC25 = Interior connection with 25mm gap, IC50 = Interior connection with 50 mm gap, CC0 = Corner connection with no gap, CC25 = Corner connection with 25 mm gap, CC50 = Corner connection with 50 mm gap. Also, the prestress in reinforcement is represented at end of label as 0%, 60%, 70% and 80% of tensile strength

Table 5.2 Reinforcement and concrete strength details for parametric studies

<table>
<tr><th>Beam Type</th><th>Beam Section+</th><th>Steel Reinforcement*</th><th>Concrete Strength (MPa)</th><th>Concrete cover (mm)</th></tr>
<tr><td rowspan="6">PC</td><td>12RB20</td><td rowspan="2">5 Φ12.7 mm strands with 2 Φ12.7 mm holder rebars</td><td rowspan="10">Calcareous aggregate based concrete with a characteristic compression strength of 50 MPa</td><td rowspan="10">Main flexural reinforcement is kept at a concrete cover of 76 mm from bottom, and holder rebars are kept at a concrete cover of 51 mm from top</td></tr>
<tr><td>12RB36</td></tr>
<tr><td>16RB24</td><td rowspan="2">7 Φ12.7 mm strands with 2 Φ12.7 mm holder rebars</td></tr>
<tr><td>16RB40</td></tr>
<tr><td>8RB20</td><td>3 Φ12.7 mm strands with 2 Φ12.7 mm holder rebars</td></tr>
<tr><td rowspan="4">RC</td><td>12RB20</td><td rowspan="2">5 Φ12.7 mm rebars with 2 Φ12.7 mm holder rebars</td></tr>
<tr><td>12RB36</td></tr>
<tr><td>16RB24</td><td rowspan="2">7 Φ12.7 mm rebars with 2 Φ12.7 mm holder rebars</td></tr>
<tr><td>16RB40</td></tr>
<tr><td colspan="5">*All beams constitute low relaxation prestressing strands with a tensile strength of 1861 MPa, all rebars have a tensile strength of 415 MPa
+All temperature dependent material properties are assigned as per Eurocode 2 recommendations</td></tr>
</table>

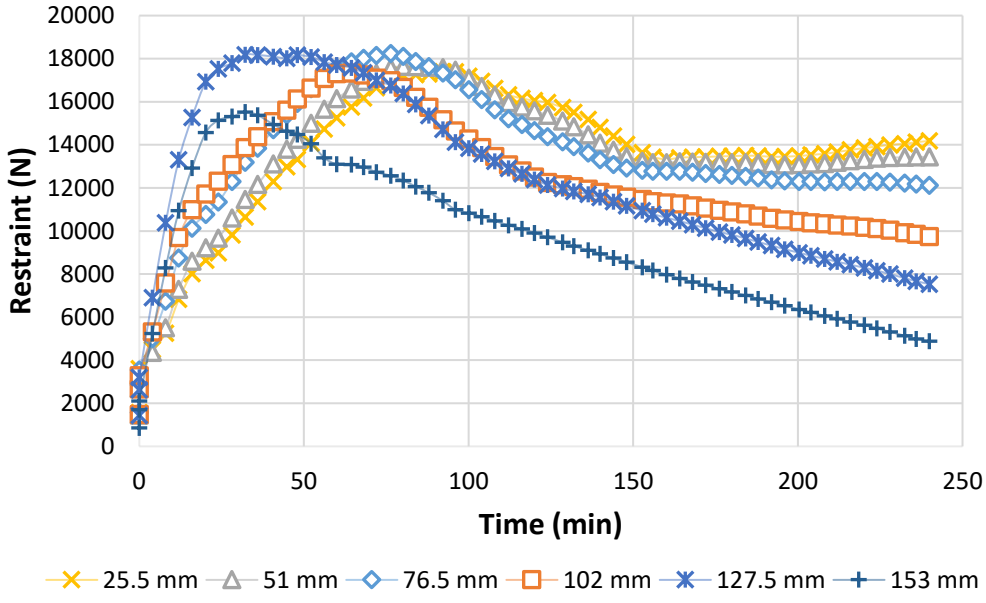

(a)

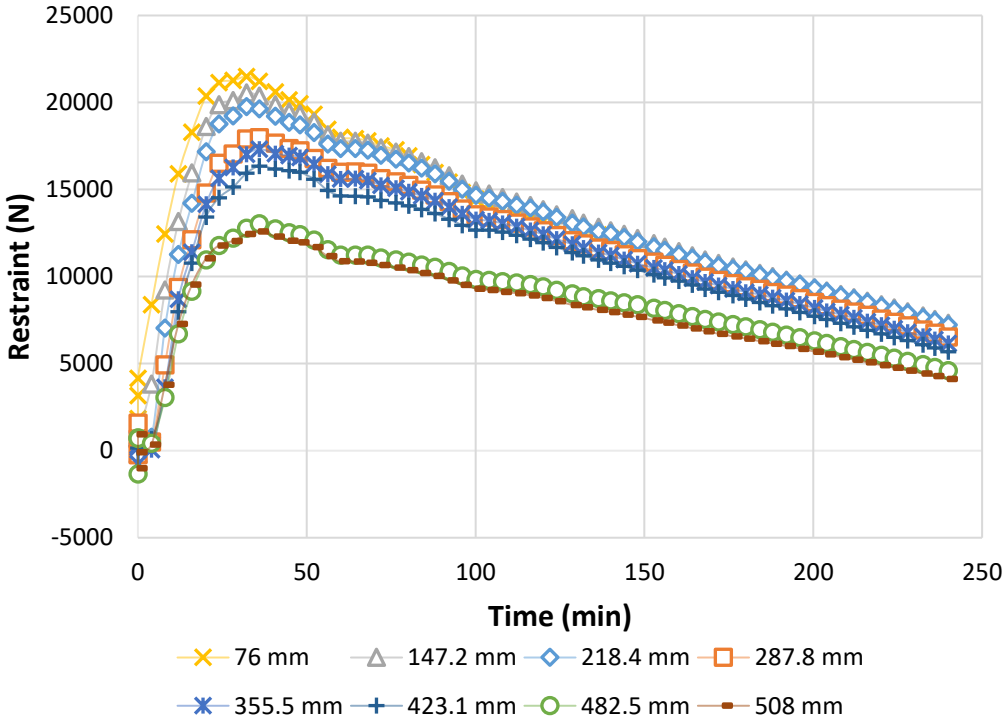

(b)

Figure 5.1 Variation in fire induced restraint force across (a) width (measured from beam center) and (b) height (measured from bottom at corner) in beam PC.1.FX.70 (PC beam with 12RB20 section, fixed end, and 70% prestress)

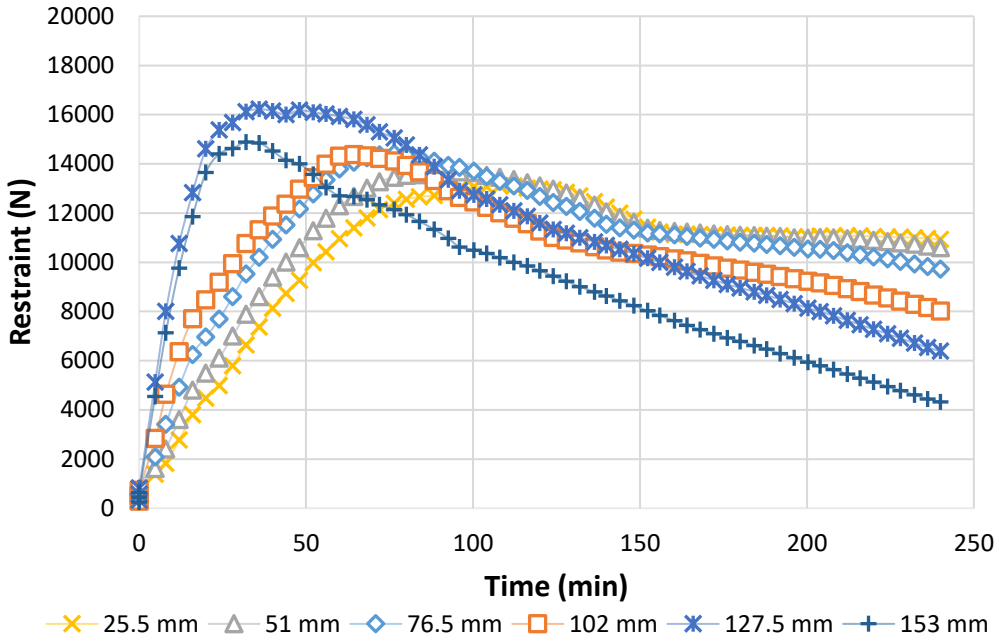

(a)

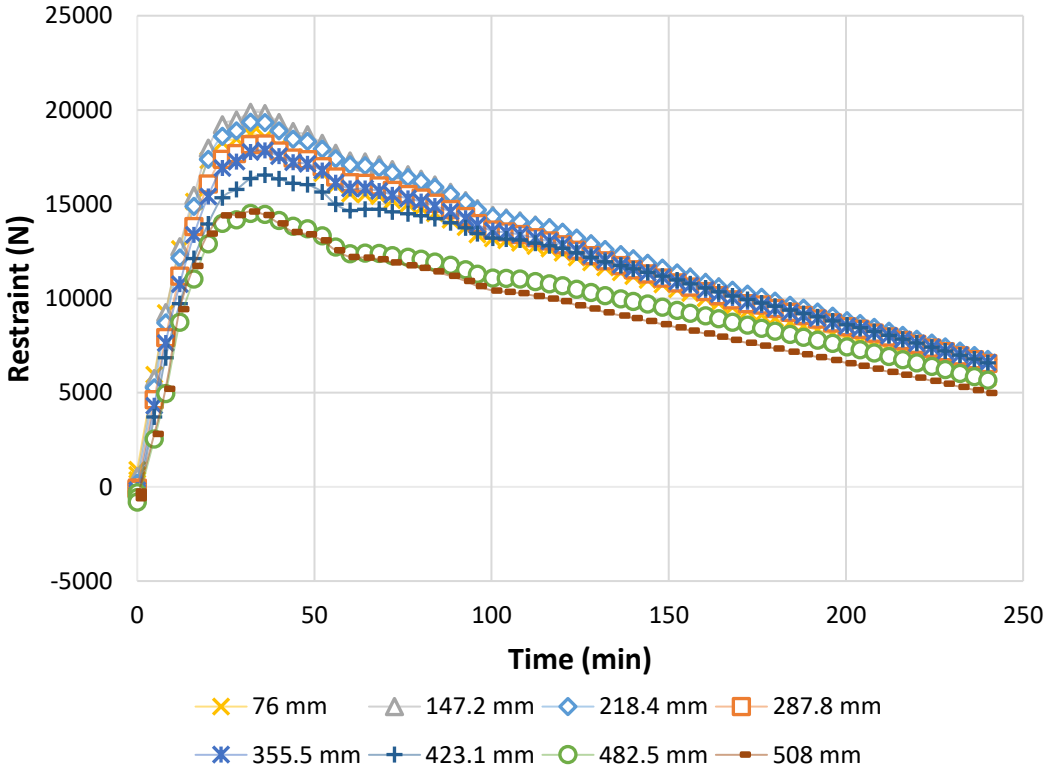

(b)

Figure 5.2 Variation in fire induced restraint force (a) width (measured from beam center) and (b) height (measured from bottom at corner) in beam RC.1.FX.70 (RC beam with 12RB20 section, fixed end, and 70% prestress)

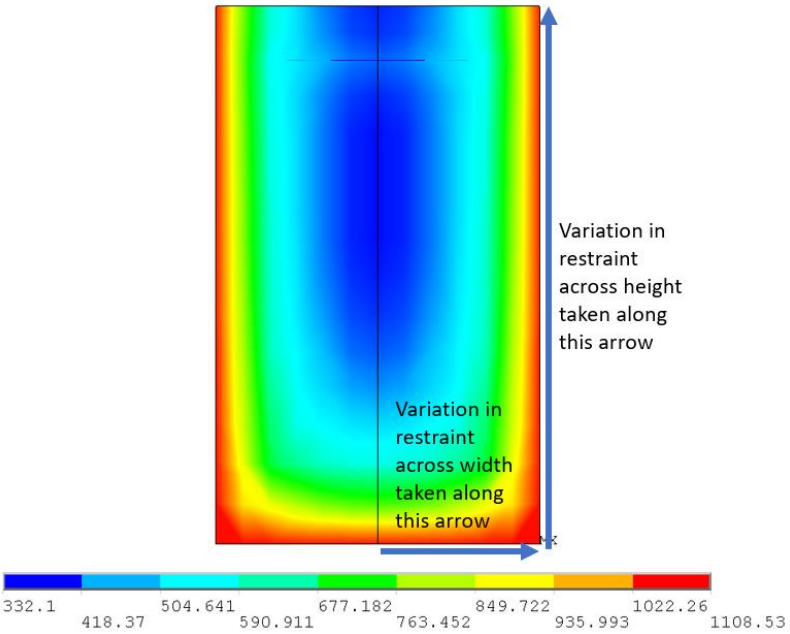

Figure 5.3 Sectional temperatures for 12RB20 section at 4 hours of fire exposure and location of restraint variations across width and height

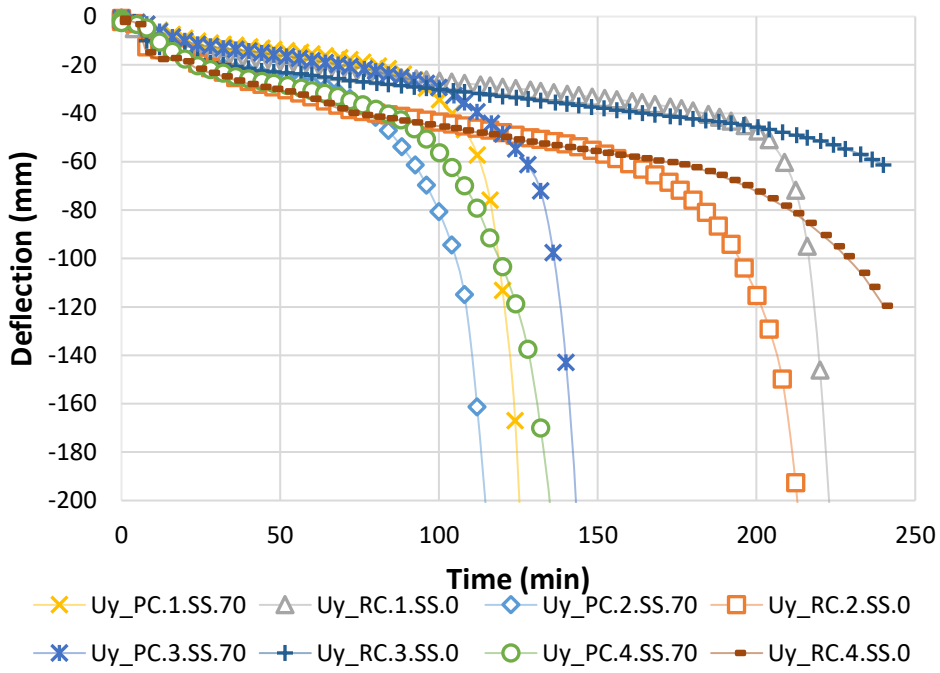

Figure 5.4 Comparison of deflection for all simply supported end condition (SS) beams

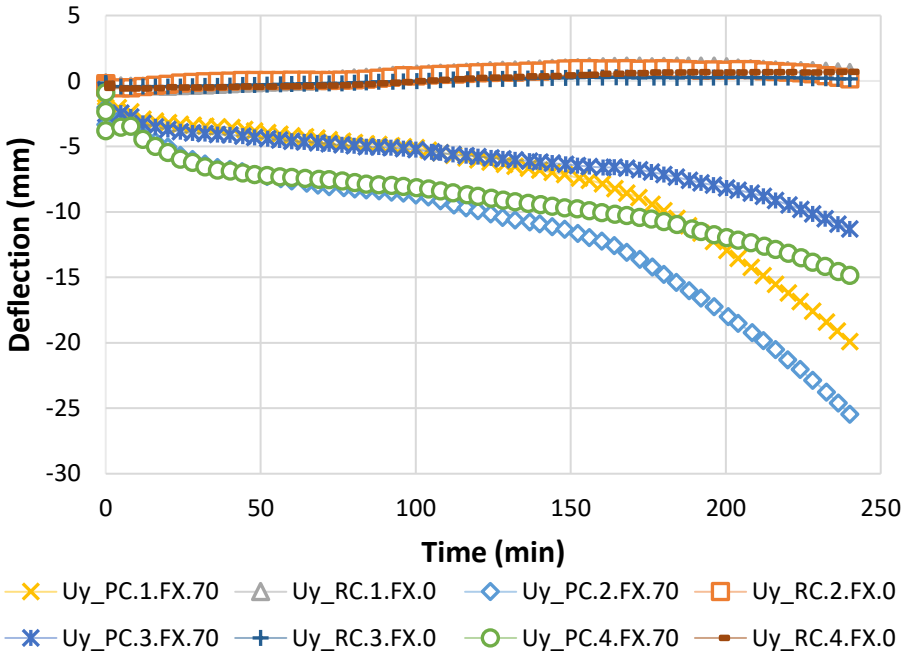

Figure 5.5 Comparison of deflection for all fixed end condition (FX) beams

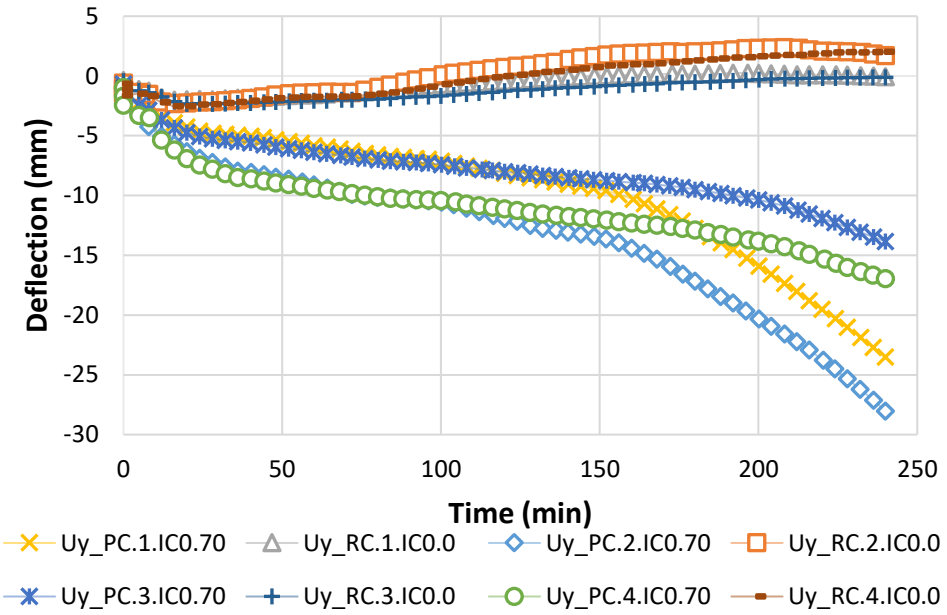

Figure 5.6 Comparison of deflection for all interior connection with 0 mm gap end condition (IC0) beams

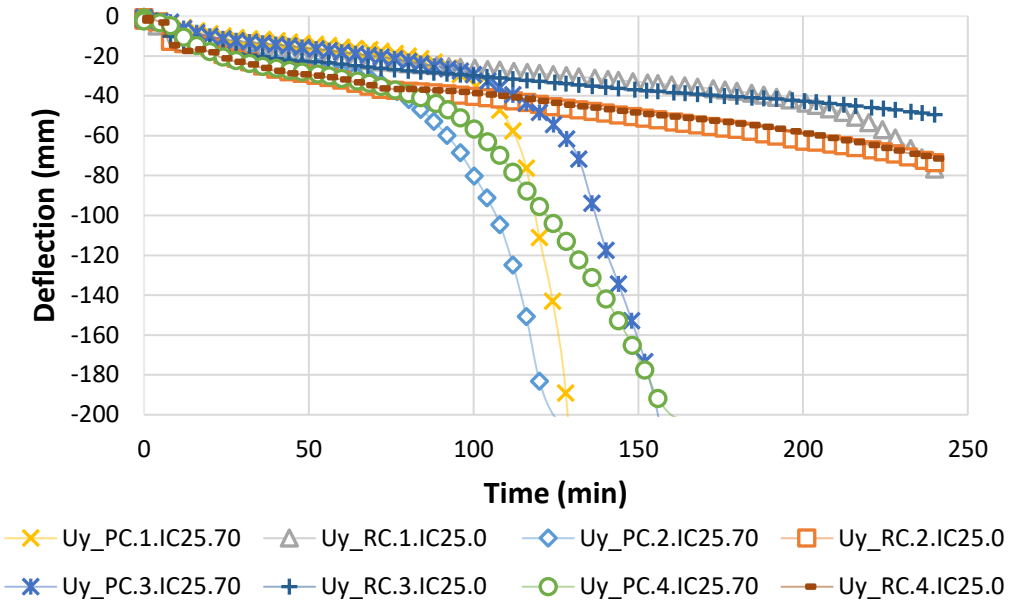

Figure 5.7 Comparison of deflection for all interior connection with 25 mm gap end condition (IC25) beams

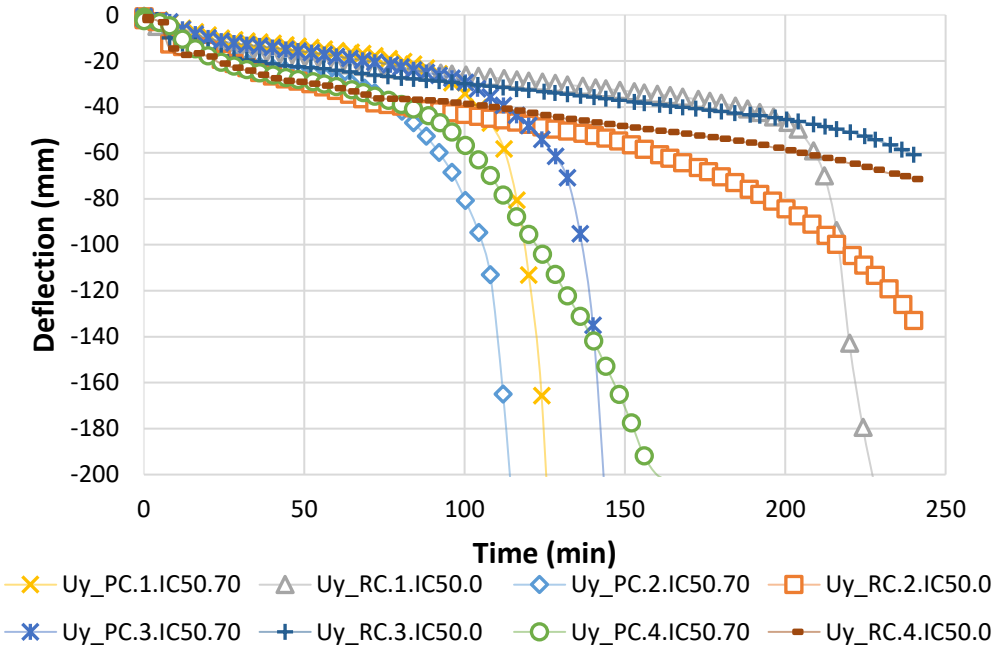

Figure 5.8 Comparison of deflection for all interior connection with 50 mm gap end condition (IC50) beams

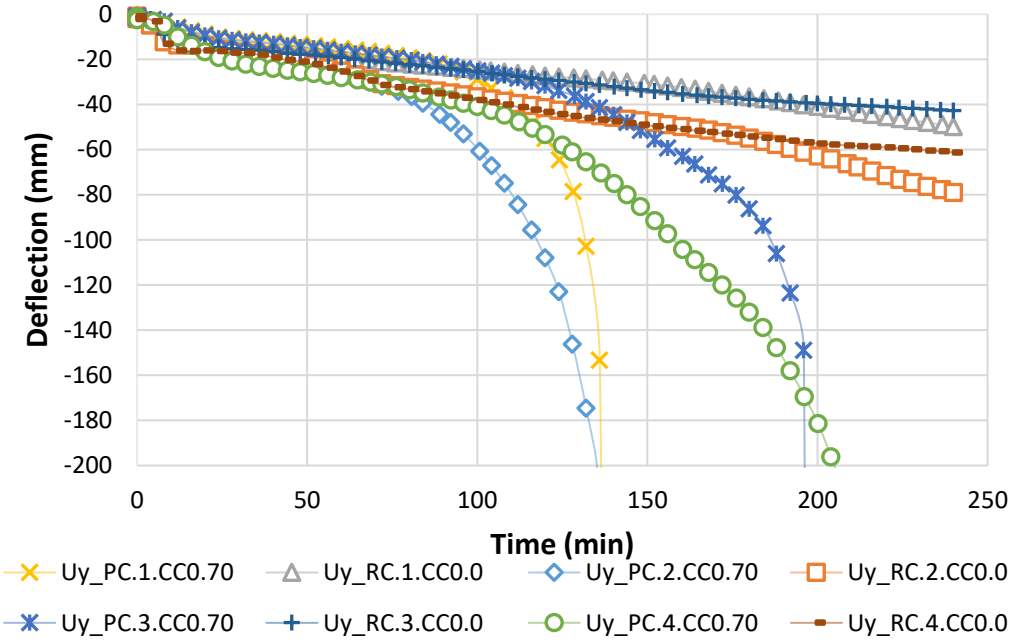

Figure 5.9 Comparison of deflection for all corner connection with 0 mm gap end condition (CC0) beams

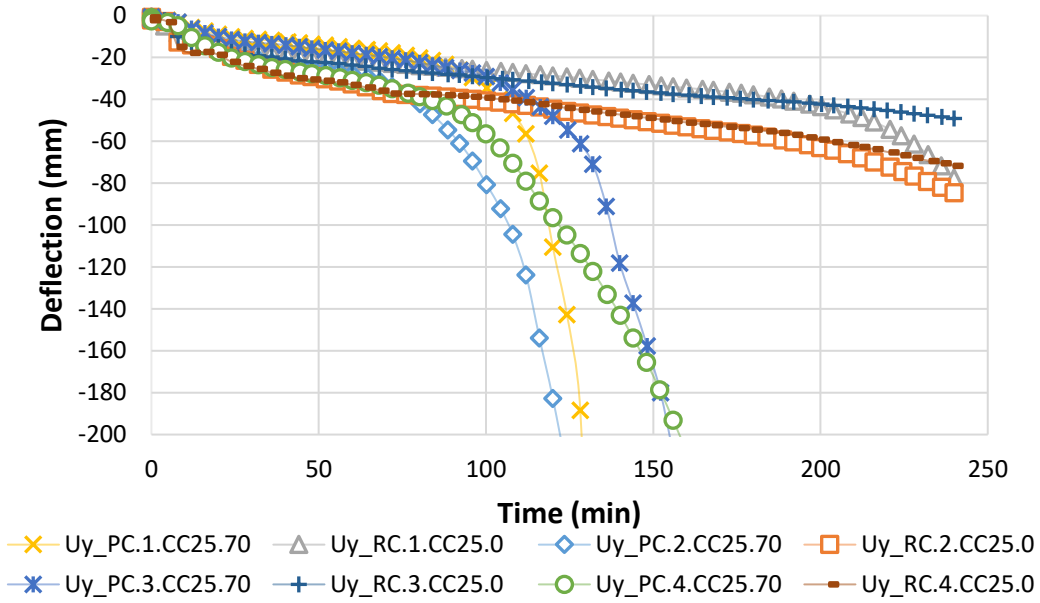

Figure 5.10 Comparison of deflection for all corner connection with 25 mm gap end condition (CC25) beams

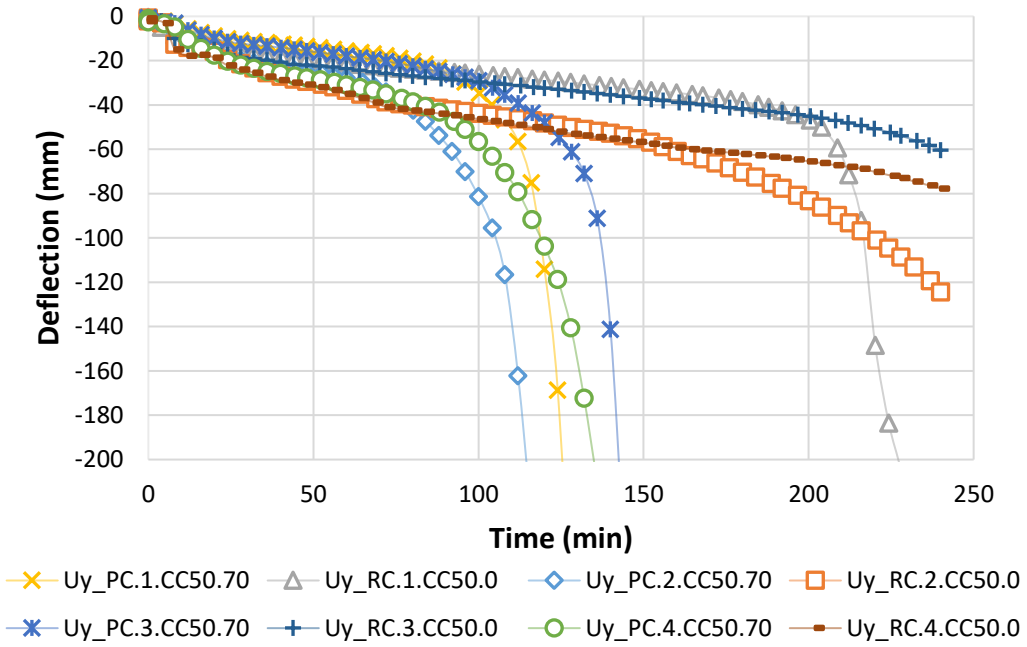

Figure 5.11 Comparison of deflection for all corner connection with 50 mm gap end condition (CC50) beams

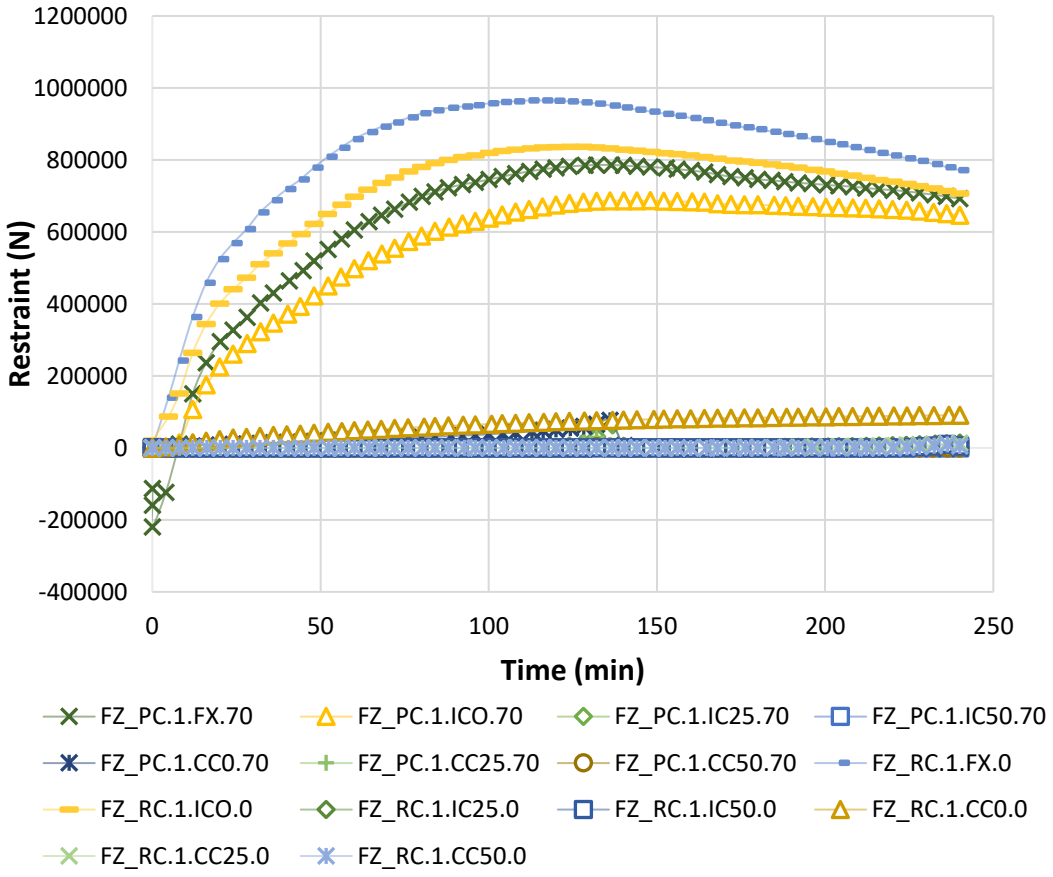

Figure 5.12 Comparison of restraint force for section 12RB20 under different end conditions

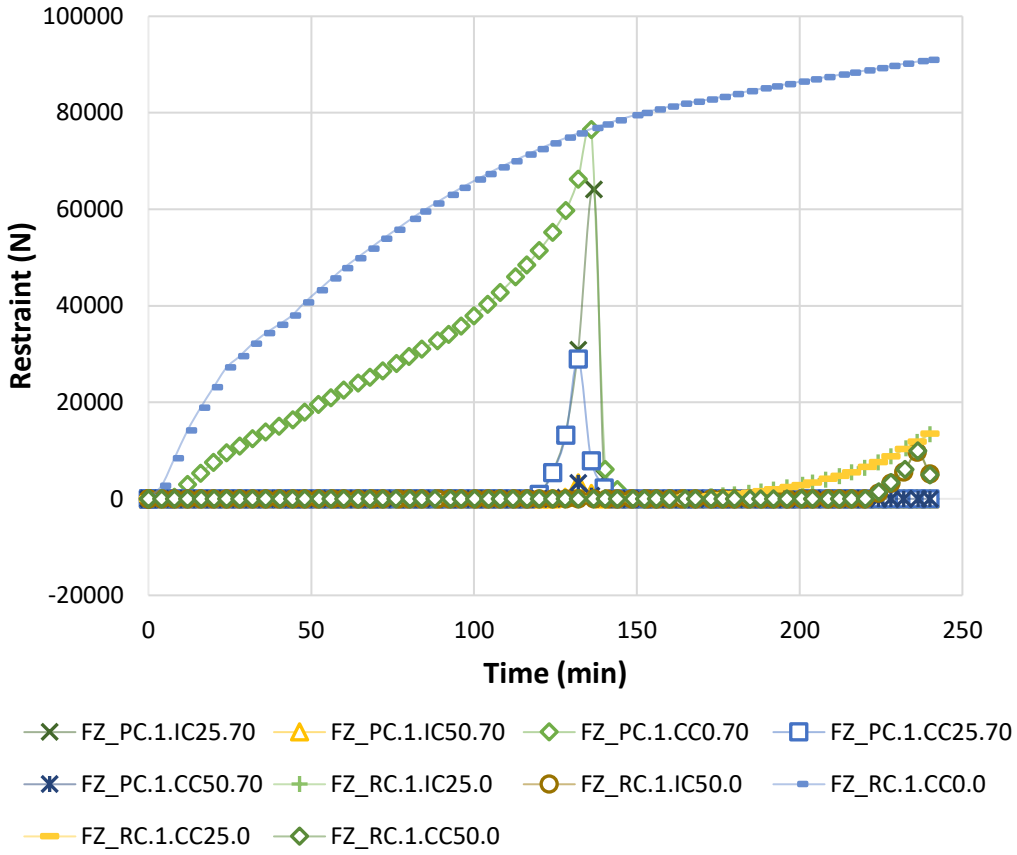

Figure 5.13 Comparison of restraint force for section 12RB20 under different end conditions (excluding FX and IC0 end conditions)

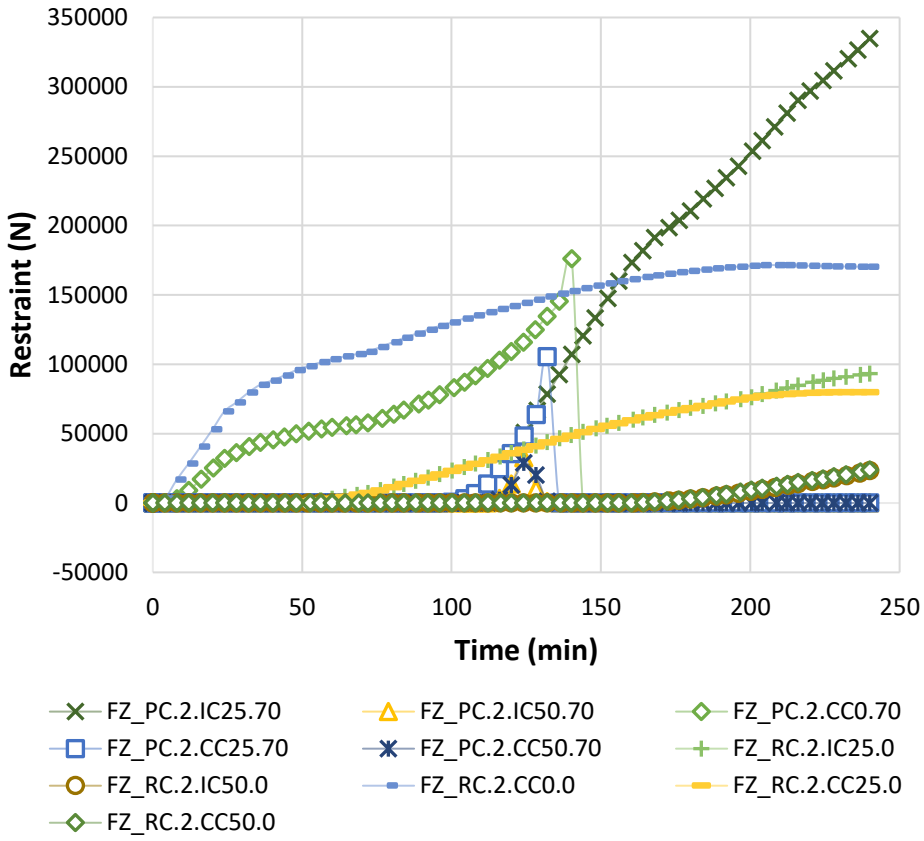

Figure 5.14 Comparison of restraint force for section 12RB36 under different end conditions (excluding FX and IC0 end conditions)

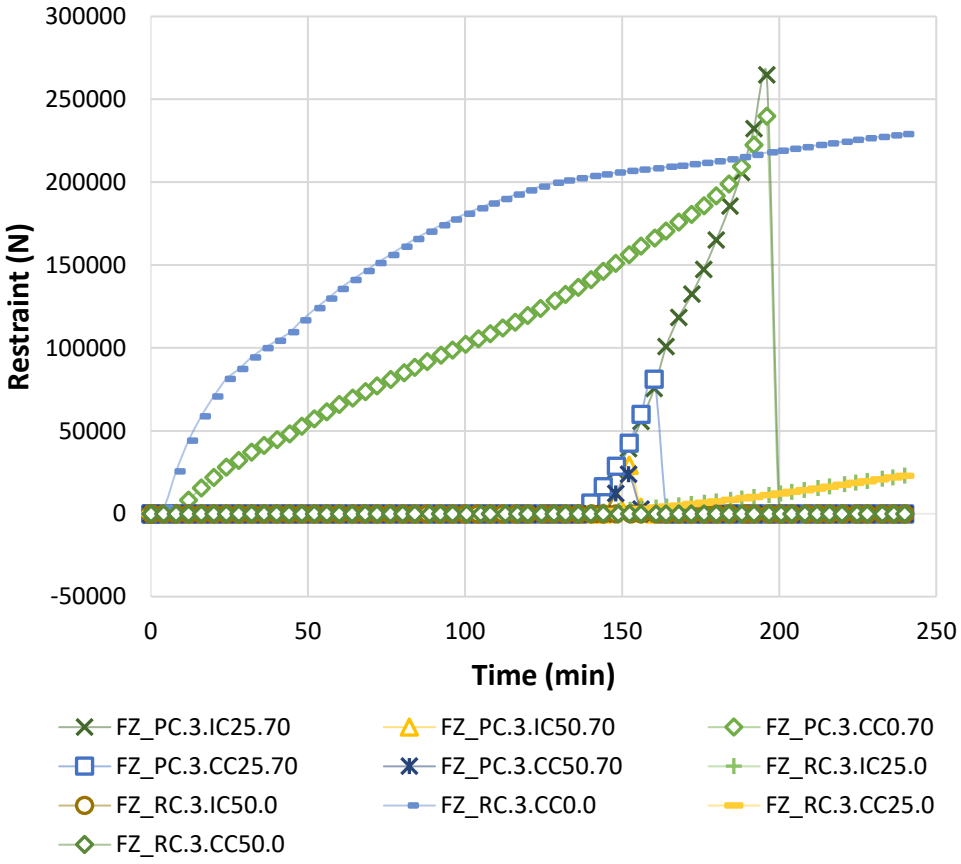

Figure 5.15 Comparison of restraint force for section 16RB24 under different end conditions (excluding FX and IC0 end conditions)

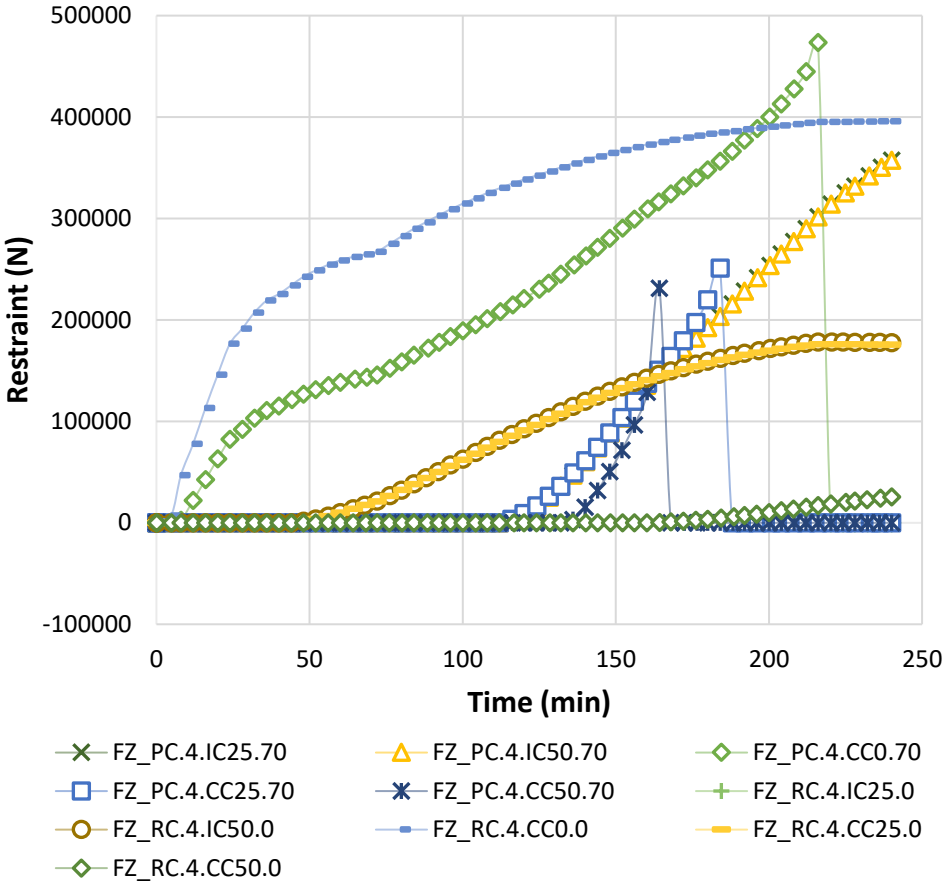

Figure 5.16 Comparison of restraint force for section 16RB40 under different end conditions (excluding FX and IC0 end conditions)

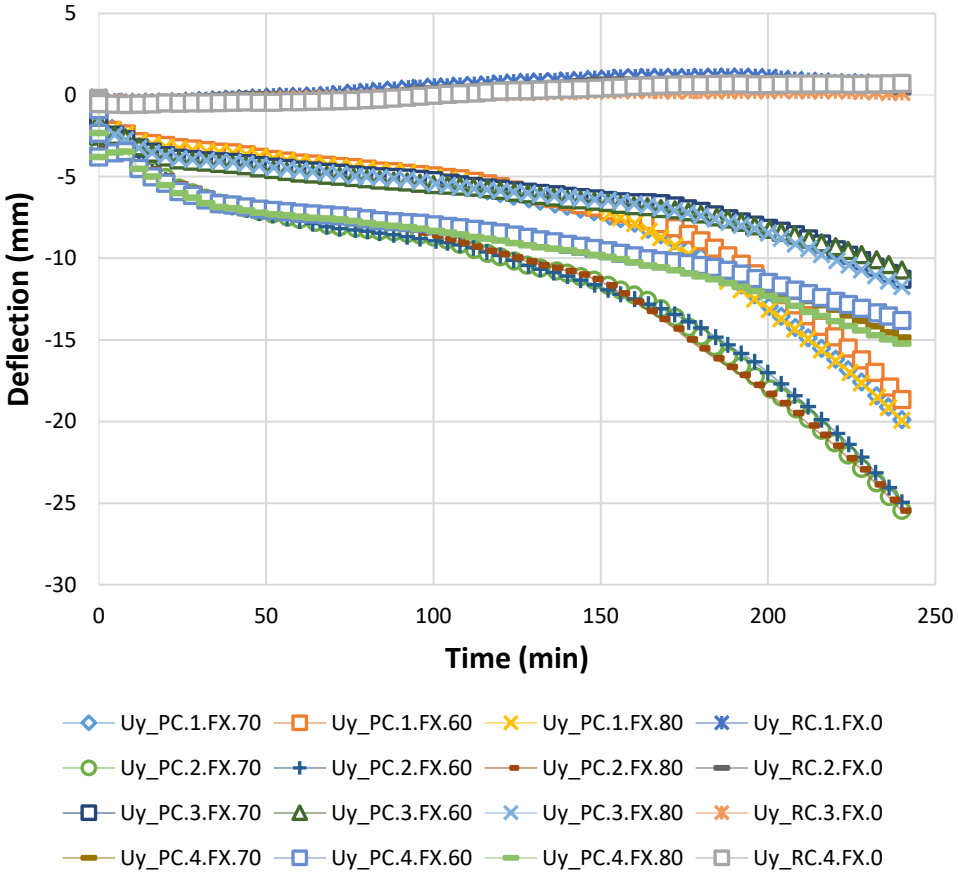

Figure 5.17 Comparison of deflection response for varying prestress in all beams

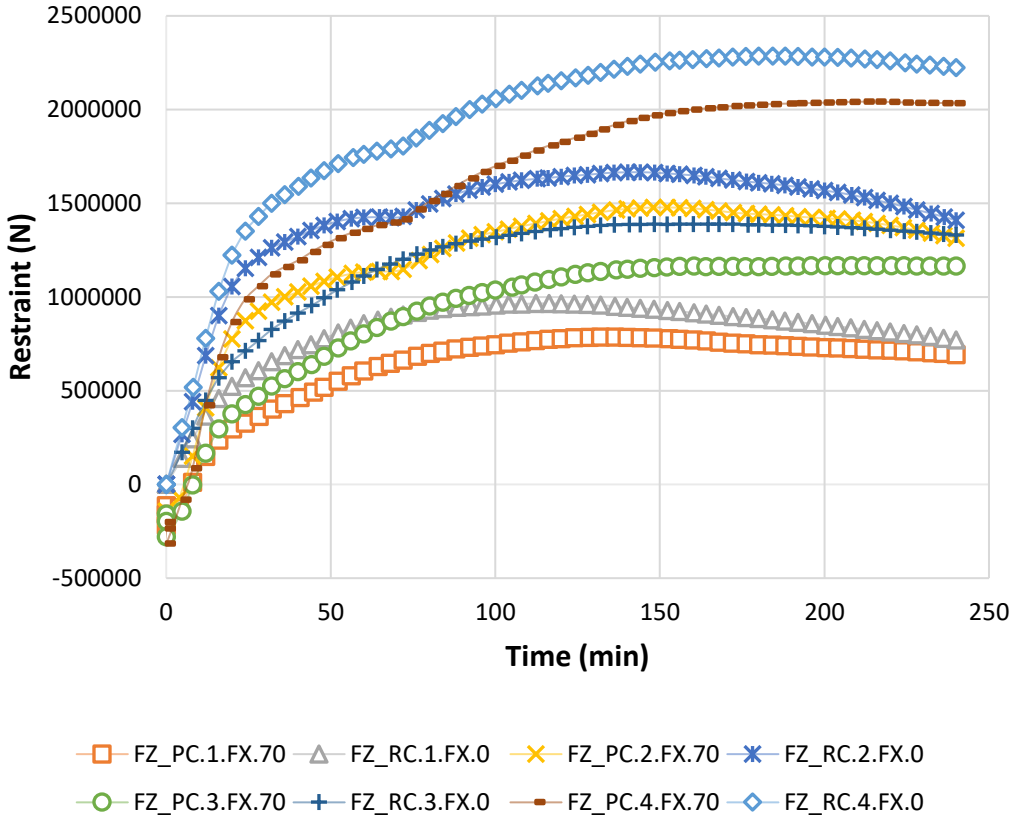

Figure 5.18 Comparison of maximum fire induced restraint in PC and RC beams

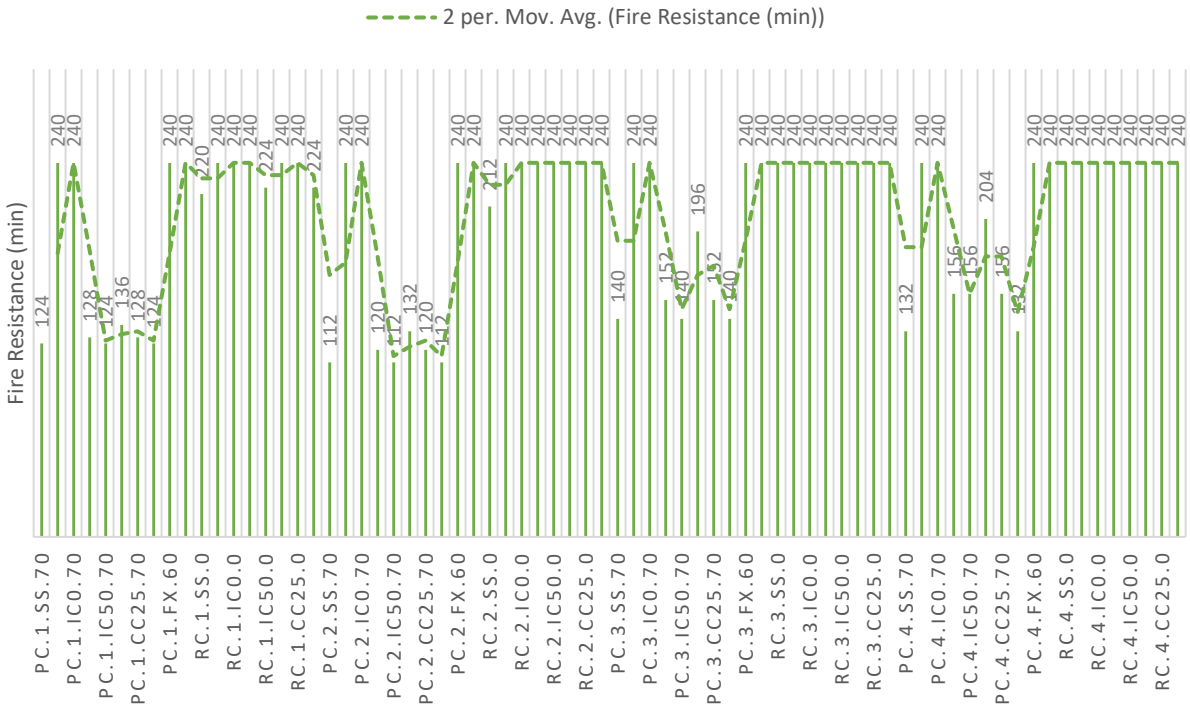

Figure 5.19 Summary of variation in fire resistance for parametric studies

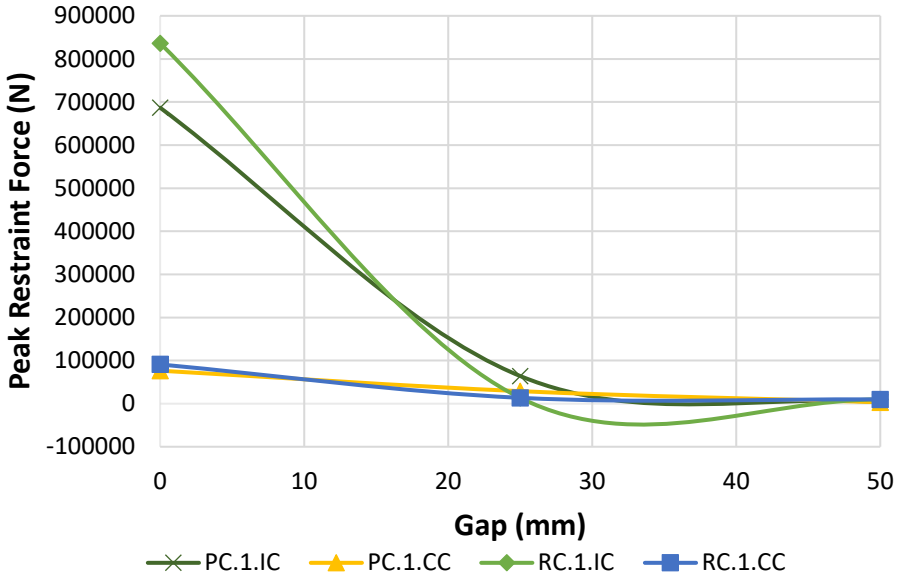

(a)

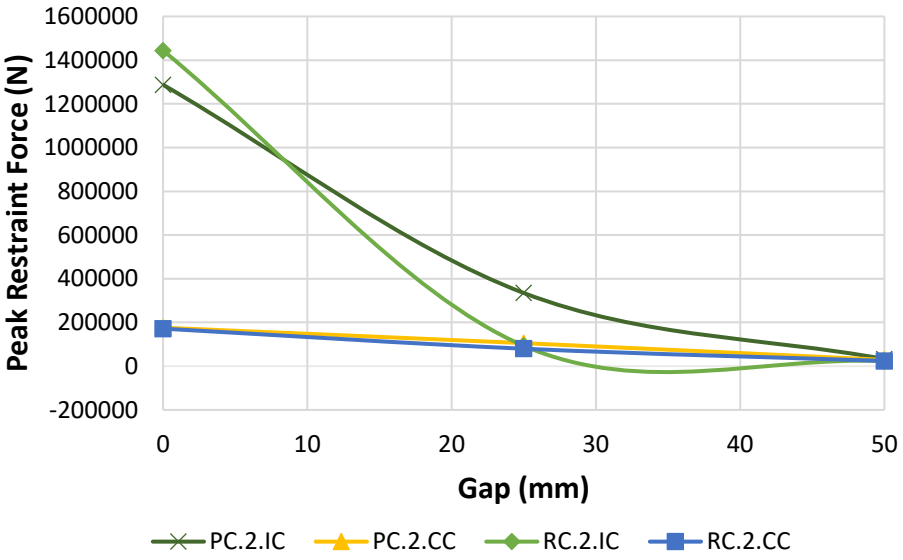

(b)

Figure 5.20 Effect of gap in connection on peak fire induced restraint forces for sections (a) 12RB20, (b) 12RB36, (c) 16RB24, and (d) 16RB40

Figure 5.20 (cont'd)

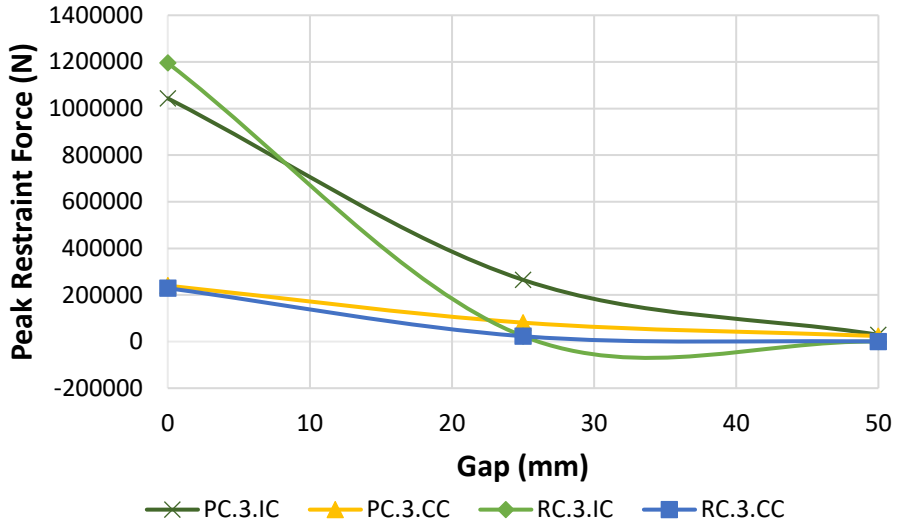

(c)

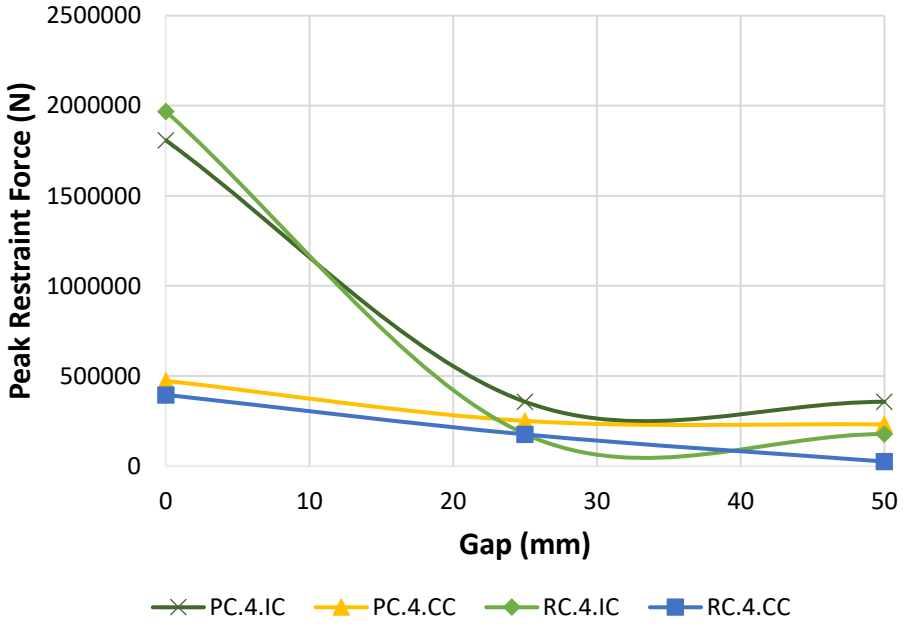

(d)

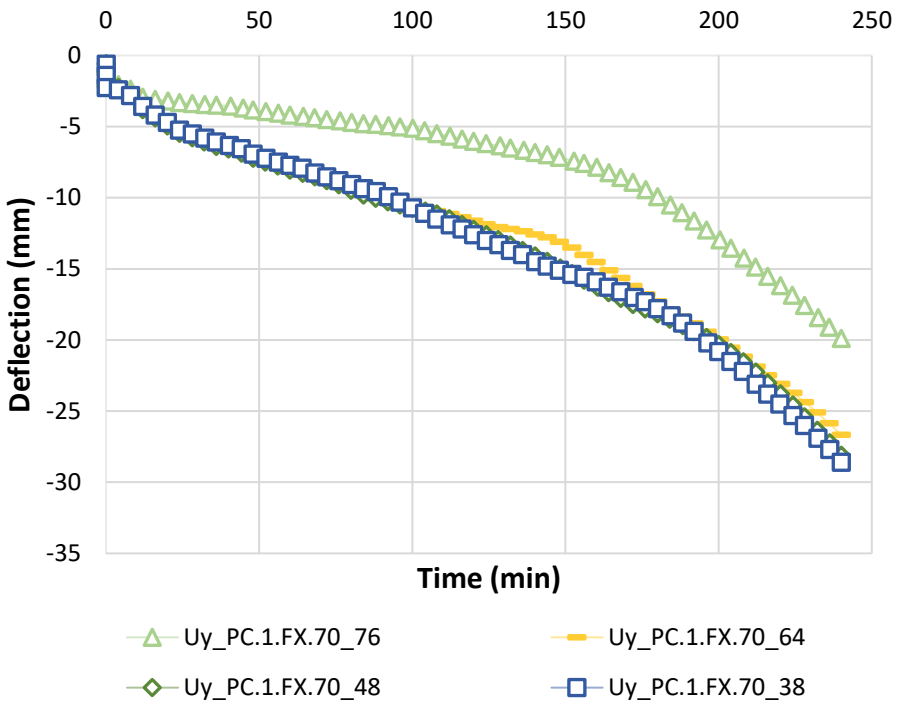

Figure 5.21 Effect of cover thickness on deflections under fire exposure

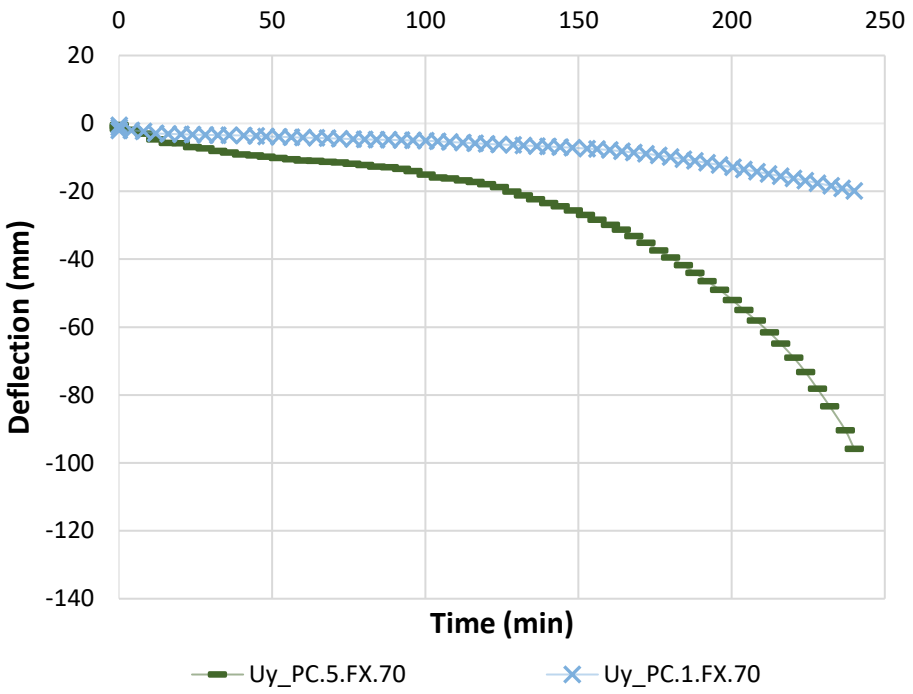

Figure 5.22 Effect of member width on deflections under fire exposure

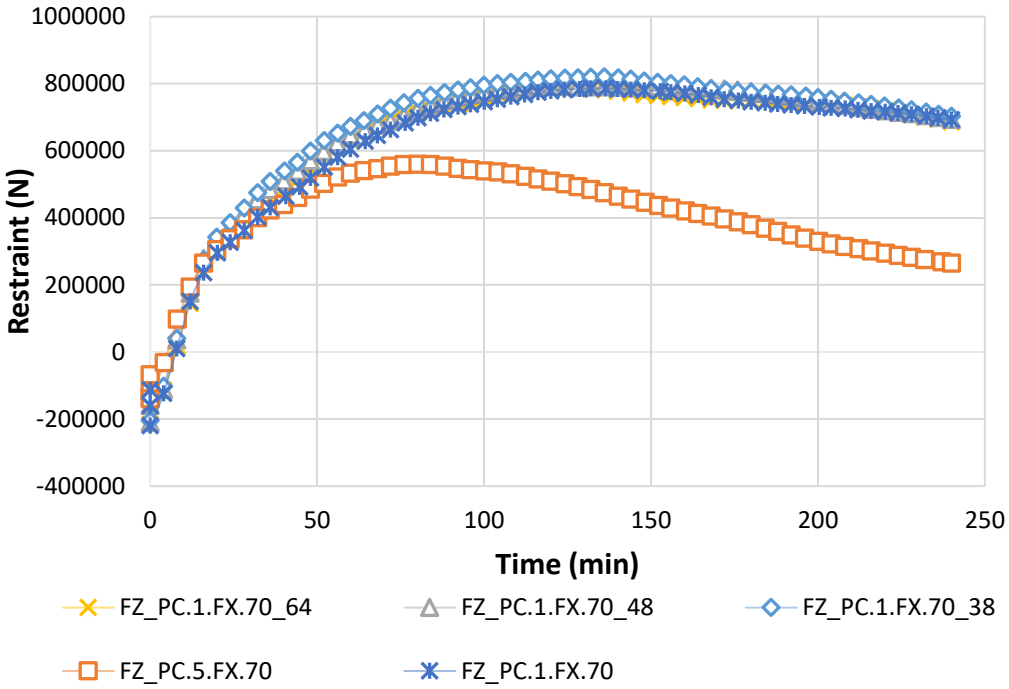

Figure 5.23 Effect of cover thickness and member width on evolution of fire induced restraint forces

CHAPTER 6

6 Design recommendations

6.1 General

Prestressed concrete beams are designed to outperform conventional reinforced concrete beams to achieve better performance. While these beams exhibit good structural performance at ambient temperature, studies clearly indicate that they have lower fire resistance as compared to their RC counterparts. This is primarily due to the faster degradation in mechanical properties of prestressing strands at elevated temperatures than that in RC beams with conventional rebars. Further, high strength concrete (HSC) PC beams are prone to fire induced spalling which can lead to reduction in the cross-section of the beam, and thus, relatively faster rise in temperatures of strands. Moreover, under restrained conditions at supports, PC beams can develop significant fire induced restraint forces which can be beneficial or detrimental to the resulting fire resistance depending on several governing factors. Magnitude and location of such fire induced restraint forces vary with fire exposure time, and this makes fire response of restrained PC beams even more intricate. Due to limited studies on fire response of restrained PC beams, there are minimal

guidelines on the rational treatment of fire induced restraint forces in evaluating the fire resistance of PC beams.

The current provisions in codes and standards provide prescriptive fire resistance ratings, and there are no specific guidelines in codes and standards to evaluate the magnitude of fire induced restraint forces at a given fire exposure duration. Likewise, there are no simplified design methodologies or expressions for evaluating the fire resistance of PC beams, incorporating realistic restraint conditions. Nonetheless, based on the results from research undertaken herein, preliminary guidelines are proposed in this study for evaluating fire resistance of restrained PC beams.

6.2 Current codal provisions for fire design of PC beams

Current provisions for fire design of PC beams and their limitations are discussed in detail in Section 2.4. Therefore, only a brief discussion is provided herein to set the context on current state-of-the-art. Currently, code and standards utilize prescriptive approaches to evaluate fire resistance of PC beams. Beams are first identified as restrained or unrestrained based on qualitative guidelines, and then minimum beam width and concrete cover to rebars or strands are recommended to achieve desired fire resistance rating. Also, there are some simplified rational design approaches as well in some codes and standards. PCI Manual 124 [6] provides a rational design approach in which moment capacity of the PC beam is evaluated at a given time by applying the room temperature moment capacity equation with adjustment to account for temperature dependent strength reduction factors for concrete and strands . The strength reduction factors are to be evaluated based on sectional temperatures at a specified fire exposure the time. ACI 216.1 [7] provides a similar approach for moment capacity calculation with temperature dependent strength reduction Factors. On the other hand, Eurocode 2 [4], provides two simplified design approaches; namely 500^{o}C isotherm, and zone method. In 500^{o}C isotherm method sectional

temperatures are calculated at required time and the concrete layers above 500^{o}C are assumed to contribute zero strength to the sectional capacity. In zone method, section is divided into zones (rectangular areas) and the strength contribution from each zone to moment capacity is calculated based on the concrete strength at the average temperature of the zone. However, there are no tools in the codes and standards to calculate the magnitude of fire induced restraint forces or trace the effect of variation in their location with fire exposure time on fire resistance of PC beams.

6.3 Critical factors governing fire performance of PC beams

Data from the fire tests and numerical studies clearly show that the fire response of PC beams, especially under restrained end conditions, is governed by several interdependent factors. Results generated from experimental and numerical studies presented in presented in Chapters 3, 4, and 5 show that the key governing factors are support conditions, gap in connections, section type, temperature induced property degradation in concrete and reinforcement, cover thickness, and spalling. The extent of influence of these governing factors on the fire resistance of PC beams is summarized herein, and then preliminary design guidelines are laid out.

6.3.1 Support conditions

Extent of fire induced restraint forces at the supports can vary from simply supported end conditions to fixed end conditions. There is a range of flexible interior, corner, and edge connections that are possible in a PC beam, as shown in Figures 4.3 to 4.5. In case of simply supported connections, PC beams experience highest degree of deflection (see Figure 5.4) as there is no fire induced restraint forces at ends to counter act the applied loading, as discussed in Section 5.5. Whereas, in case of fixed and interior connections without gaps, PC beams undergo minimal deflection (see Figures 5.5 and 5.6) as minimal beam displacement is allowed at ends which leads to development of highest magnitude of restraint forces (see Figure 5.12). Moreover, for interior

connections with gap, and side or corner connections with or without gap, minimal restraint forces developed at ends, as discussed in Section 5.4. Therefore, only PC beams with interior flexible connections, without any gaps and fixed end conditions, are classified currently as restrained for specifying the prescriptive fire ratings. On the other hand, PC beams with other flexible connection types (interior connections with gap, and side or corner connections with or without gap) are classified as unrestrained for prescriptive fire resistance rating evaluation, unless proven otherwise with advanced analysis procedures.

6.3.2 Gap at connection

Gap (spacing between beam end and connecting framing elements, as shown in Figure 4.4) in connection influences the magnitude and location of fire induced restraint forces. This is due to the fact that the restraint forces cannot develop until the gap is overcome by the thermal expansion of the beam, as discussed in Section 5.4.6. As shown in Figure 5.20, increase in gap in connections can lead to lowering the fire induced restraint forces and at a gap of 50 mm only minimal restraint forces develop. Also, in most PC constructions often a gap is left between the beam and connecting structural members at a connection due to member size tolerance limitations. These tolerance limits are important for erection purposes, as they account for accidental errors in member dimensions during prefabrication process which can cause issues in installation of precast beams in between connecting framing elements. Therefore, to account for realistic fire induced restraint forces and their effect on fire resistance of PC beam, it is important to account for actual gap in connection. Also, since minimal restraint forces were observed for all connection types with gaps of 50 mm (shown in Figure 5.20), therefore, these connections are to be designed unrestrained classification for determining prescriptive fire resistance ratings.

6.3.3 Section type

Type of beam section, as discussed in Section 5.4.3, controls the thermal inertia of the beam which in turn influences the progression of sectional temperatures within beam, and therefore, has significant effect on the response of PC beams under fire exposure. Therefore, fire resistance of PC beams for different sectional types under varying end conditions can be taken from results in Table 5.1, and linear interpolation can be done for section sizes in between. Also, it can be observed from Figures 5.12 to 5.16 that under restrained conditions, deeper concrete beams experience higher fire induced restraint forces than shallower counterparts. This is because for same angle of rotation at the ends, more axial displacement occurs at beam ends at the top and bottom for deeper beams than for shallower beams, thus, causing higher restraint forces (as shown in Figures 5.12 to 5.16). This axial displacement due to bending of the beam at ends adds to the thermal expansion of the beam, and therefore, higher restraint forces are developed in deep beams as compared to their shallow counterparts.

6.3.4 Temperature induced property degradation

The most critical factor that influences the fire resistance of PC beams is temperature induced degradation in strength and stiffness of concrete and reinforcing (or prestressing) steel. As discussed in Chapter 3, there can be significant variation in the material properties of concrete and steel at elevated temperature which control the thermo-mechanical response of PC beams under fire exposure. It can be observed from Figure 3.7 that even though beams in fire tests were designed to have a fire resistance of 4 hours (as per prescriptive provisions [6]), NSC PC beams failed within 2 hours of fire exposure, and HSC PC beams failed within 1 hour of fire exposure. This is primarily due to the rapid temperature induced strength and stiffness loss in prestressing strands and relatively faster loss of strength in NSC than as compared to HSC.

To increase the fire resistance of PC beams, the cover to the strands can be increased to mitigate increase in strand temperatures and additional rebars can be provided below strands to carry the applied load. The provision of rebars in prestressing beams is a good option to increase the fire resistance of PC beams, as providing rebars allows to increase the cover to the strands and rebars have relatively slower degradation in strength than as compared to prestressing strands (see Figure 1.1). Further, as discussed in Chapters 3 and 5, most PC beams could not achieve fire resistance over 120 minutes for NSC PC beams, and 60 minutes for HSC PC beams. Therefore, PC beams should be designed with rebars in addition to strands to achieve higher fire ratings. Hence, for NSC PC beams, rebars should be used below prestressing strands to achieve fire ratings over 2 hours, and for HSC beams, rebars should be used to achieve fire ratings over 1 hours.

6.3.5 Spalling

While both NSC and HSC beams experience spalling under fire exposure, spalling is more prominent in HSC PC beams. As discussed in Chapter 3 and 5, spalling of concrete can increase sectional temperatures due to loss of thermal inertia, and cause relatively faster failure. It can be observed from the PC beam fire resistance test results shown in Figures 3.10 and 3.11 that HSC beams are prone to more spalling under fire exposure than NSC counterparts. This is primarily due to relatively dense microstructure of concrete in HSC, which does not allow moisture propagation under fire exposure. This causes pore pressure buildup under fire exposure which ultimately leads to spalling of concrete near exposed faces. On the other hand, NSC has relatively coarse microstructure which mitigates the pore pressure buildup, and therefore, undergo relatively less spalling. Therefore, when higher fire resistance is required in PC beam designs, it is recommended to use NSC over HSC as it is significantly less prone to spalling.

6.3.6 Cover thickness

As discussed in Section 5.4.7, sufficient concrete cover to the prestressing strands is crucial in slowing the increase in the strand temperatures, thus, increasing fire resistance. Also, as shown in prescriptive based Table 1.2, only 38 mm of cover is required to achieve a fire resistance of up to 3 hours for restrained PC beams with widths more than 203 mm, and 48 mm for fire rating of 4 hours. Note that all 4 beams tested in fire tests and 76 beams in parametric studies had a clear cover of 76 mm, which as per Table 1.2 should provide a fire rating of 4 hours for PC beams under restrained or unrestrained conditions. However, it can be observed from Table 3.4 and Table 5.1 that most of the PC beams failed within 2 hours. These observations infer that the prescriptive guidelines for cover thickness do not provide accurate fire resistance evaluations, as prescriptive fire resistance approach over predicted fire resistance by 100% for most PC beams. Therefore, based on these observations, it is proposed that all NSC PC beams (restrained or unrestrained) requiring more than 2 hour fire rating should be provided with minimum cover of 76 mm, and all HSC PC beams (restrained or unrestrained) requiring more than 1 hour fire resistance should be provided with minimum cover of 76 mm.

6.4 Preliminary design recommendations for PC beams

Based on the experimental and numerical results presented in this thesis, following preliminary design recommendations are proposed for PC beams:

- PC beams with fixed end (FX) and with interior connections without gap (IC0) end conditions are assigned prescriptive fire rating based on restrained classification.
- PC beams with interior connections with gap (IC25, IC50), and all corner connections (CC0, CC25, CC50) are assigned unrestrained classification.

- Table 6.1 gives fire resistance for PC and RC beams with different sections under different end conditions, and linear interpolation is permitted for section sizes in between.
- In NSC PC beams, rebars should be used below prestressing strands to carry at least 50% of the applied service load at required design fire resistance time to achieve fire ratings over 2 hours.
- In HSC PC beams, rebars should be used below prestressing strands to carry at least 50% of the applied service load at required design fire resistance time to achieve fire ratings over 1 hour.
- NSC PC beams (restrained or unrestrained) requiring more than 2 hour fire rating should be provided with minimum cover of 76 mm.
- HSC PC beams (restrained or unrestrained) requiring more than 1 hour fire resistance should be provided with minimum cover of 76 mm.
- Advanced finite element analysis is needed if the PC beams are not to be designed under 50% load ratio and ASTM E-119 fire exposure.

6.4.1 Guidance for enhancing fire resistance under restrained conditions

As discussed in Chapter 1, fire induced restraint forces can have beneficial or detrimental effect on fire resistance of PC beams. However, by incorporating proper connection configuration, fire induced restraint forces can be utilized to enhance the fire resistance of PC beams, and therefore, guidelines are given below to optimize the beneficial effect of fire induced restraint forces on PC beams as:

- PC beams should be designed with dapped end conditions (shown in Figure 6.1) or similar connections which ensures the location of fire induced restraint forces to remain below centroidal axis of the beam throughout fire exposure.
- On the other hand, if it is not possible to design a connection type which ensures restraint forces location, then it is recommended to use NSC carbonate concrete for PC beam and to design it with multiple rebars as part of main reinforcement to carry at least 50% of the applied loading to ensure ductile failure.
- When the connection is on the top of the beam, the gap between the beam and connected structural members should be increased to at least 50 mm to ensure no fire induced restraint forces are developed.
- Also, for getting higher restraint forces in connections like dap connections (see Figure 6.1), deeper beam sections should be used with at least cover of 76 mm to prestressing strands.

6.4.2 Limitations

Although the proposed recommendations in this section above can be applied to evaluate the fire resistance of PC beams, the limitations of this approach are identified as following:

- Preliminary recommendations provided in Section 6.4 are based on the results from parametric studies on PC beams under dominant flexural loading and may not be fully applicable for shear dominant loading.
- The proposed recommendations are validated only for the rectangular PC beams and for the use of other beam shapes, advanced finite element analysis is needed.

- The guidelines are only applicable for 1 to 4 hours of ASTM E119 fire exposure and 50% load ratio at room temperature, and any other fire or loading scenario may need to be analyzed using advanced numerical model.

6.5 Guidance for undertaking advanced fire resistance analysis

Advanced fire resistance analysis procedure is discussed in detail in Chapter 4, and only highlights of the same are provided herein along with an example to provide guidance to the structural engineers to implement this procedure with ease. The design recommendations in Section 6.4 are given based on results from numerical studies on PC beams analyzed under 50% load ratio and ASTM E-119 fire exposure. Therefore, if the fire exposure or loading ratio is significantly different from these adopted parameters, then it is recommended to undertake an advanced finite element analysis. For advanced analysis, the numerical model developed in Chapter 4 can be implemented in ANSYS or other commercial finite element programs. For clarity a step-by-step approach is listed below for evaluating fire resistance of PC beam using advanced analysis. The selected PC beam for this example has a section of 305 mm x 508 mm x 5080 mm, 50 MPa calcareous concrete, 5 low relaxation strands with an ultimate strength of 1861 MPa at a cover of 76 mm, 2 holder rebars at top with an ultimate strength of 415 MPa, under restrained end conditions, load ratio of 50%, and exposed to realistic design fire exposure DF1.

6.5.1 Step 1: Discretization of the beam

The PC beam is discretized using thermal and structural elements to capture the thermo-mechanical response. The discretized beam is shown in Figure 6.2. Note that in this example ANSYS is used for discretization, and therefore, finite elements names are given as per ANSYS in Figure 6.2. The element names may vary from one commercial software to other and should be picked as per the discussion of Chapter 4. Also, it is important to ensure that the elements have

good aspect ratios as per software recommendations, and an optimal mesh size (25 mm is used herein) is used. This can be achieved by dividing the geometry lines in element sizes before meshing in ANSYS, and similar options can be explored in other software as well. Also, to ensure that there is no crushing or solid element stress concentration at the loaded ends from restraint forces, rigid steel plates of 25 mm thickness are recommended at beam ends. Further, all elements should be assigned temperature dependent material properties, and variation in thermal and structural material properties with respect to temperature is taken as per Eurocode 2 recommendations herein.

6.5.2 Step 2: Evaluation of fire temperatures

The thermal analysis is to be carried out in a series of time steps. At each step in the thermal analysis, fire temperatures are established as per the realistic DF1 fire exposure (shown in Figure 6.3). For this design example, realistic DF1 fire exposure is input as an excel sheet in ANSYS and the time-temperature relationship for realistic DF1 fire exposure is shown in Figure 6.3. However, other fire curves (design or standard fire curves) can be input as well, and most commercial FE software allow the fire curve to be input as a function or as excel sheet.

6.5.3 Step 3: Evaluation of sectional temperatures

PC beam is exposed to DF1 fire temperatures on three sides (bottom, left, and right). The top face of the beam is not exposed to fire exposure to simulate the thermal boundary conditions from a slab resting above the beam. The progression of sectional temperatures is calculated using incremental thermal analysis discussed in Chapter 4. The resulting sectional temperatures for the PC beam (output from ANSYS) under realistic DF1 fire exposure are shown in Figure 6.4.

6.5.4 Step 4: Evaluation of fire induced restraint force

After thermal analysis is complete, thermo-mechanical analysis of the PC beams is to be undertaken at each time step as per discussion in Chapter 4. Then fire induced restraint force is calculated at the end of each time step, and the resulting fire induced restraint forces for PC beam are shown in Figure 6.5. ANSYS allows a nodal sum command at the selected nods to get the sum of all nodal forces, and it can be looped to get the results for fire induced restraint forces for the entire fire exposure duration. Similar commands can be implemented in other commercial FE software as well. During this process, special attention should be given to the sign convention for nodal forces, as nodal forces are in the opposite direction of reaction forces.

6.5.5 Step 5: Evaluation of fire resistance

To calculate the fire resistance, strength limit state is implemented by checking deflection and moment limit states as per Section 4.6. The resulting mid span deflections for the PC beam under consideration are shown in Figure 6.6. For deflection failure limit state, failure is said to occur when the maximum deflection in the beam exceeds span/20 (mm) at any fire exposure time, or the rate of deflection between two time increments exceeds the limit by span^2/9000d (mm/min), after attaining a maximum deflection of span/30 (mm) [106]. For the beam under consideration, failure occurred at 104 minutes. For moment limit state, the reduced moment capacity at time t under fire exposure (M_{nt}) is evaluated by coupling temperatures from FE analysis with moment capacity equations proposed by PCI [6] as:

$$M_{nt} = A_{ps} f_{ps\theta_s t} \left(d - \frac{a_t}{2}\right), \tag{6.1}$$

$$f_{ps\theta_s t} = f_{pu\theta_s t} \left(1 - \frac{0.5\, A_{ps}\, f_{pu\theta_s t}}{b d\, f_{c\theta_c t}}\right), \tag{6.2}$$

$$a_t = \frac{A_{ps} f_{ps\theta_s t}}{0.85\, f_{c\theta_c t}\, b}, \tag{6.3}$$

where, A_{ps} is area of prestressing steel, *b* is width of beam, *d* is effective depth of beam, $f_{ps\theta_s t}$ and $f_{pu\theta_s t}$ are actual and ultimate stresses in prestressing strands at average strand temperature θ_s corresponding to time *t*, a_t is depth of equivalent rectangular stress block at time t, and $f_{c\theta_c t}$ is compressive strength of concrete evaluated at average temperature in zone of rectangular stress block (θ_c) at time *t*, respectively.

6.6 Summary

This chapter provides preliminary design recommendations for evaluating fire resistance of PC beams under restrained and unrestrained conditions. First, critical factors influencing fire resistance of PC beams are identified based on results from parametric studies and then their effect on fire resistance of PC beams is briefly summarized to set the context. The most critical factors that govern fire resistance of PC beams are support conditions, gap at connection, spalling, section type, and temperature dependent material degradation. Then preliminary recommendations are provided for design of restrained and unrestrained PC beams, with special emphasis on identifying key critical cases which may need to be analyzed by advanced numerical analysis. Also, recommendations are provided on optimizing the effect of fire induced restraint forces by selecting a connection to either keep the fire induced restraint forces below centroidal axis or add ample gap to mitigate the negative effect of restraint forces in beams with connections on top. Also, guidance is provided for undertaking advanced analysis, and the limitations of the design recommendations are listed.

Table 6.1 Fire resistance of PC and RC beams

Beam designation [+]	Connection type	Prestress level (%)	Gap in connection (mm)	Cover (mm)	Fire resistance (min)
PC.1.SS.70	SS	70	-	76	124
PC.1.FX.70	FX	70	0	76	240
PC.1.IC0.70	IC0	70	0	76	240
PC.1.IC25.70	IC25	70	25	76	128
PC.1.IC50.70	IC50	70	50	76	124
PC.1.CC0.70	CC0	70	0	76	136
PC.1.CC25.70	CC25	70	25	76	128
PC.1.CC50.70	CC50	70	50	76	124
PC.1.FX.60	FX	60	0	76	240
PC.1.FX.80	FX	80	0	76	240
RC.1.SS.0	SS	0	-	76	220
RC.1.FX.0	FX	0	0	76	240
RC.1.IC0.0	IC0	0	0	76	240
RC.1.IC25.0	IC25	0	25	76	240
RC.1.IC50.0	IC50	0	50	76	224
RC.1.CC0.0	CC0	0	0	76	240
RC.1.CC25.0	CC25	0	25	76	240
RC.1.CC50.0	CC50	0	50	76	224
PC.2.SS.70	SS	70	-	76	112
PC.2.FX.70	FX	70	0	76	240
PC.2.IC0.70	IC0	70	0	76	240
PC.2.IC25.70	IC25	70	25	76	120
PC.2.IC50.70	IC50	70	50	76	112
PC.2.CC0.70	CC0	70	0	76	132
PC.2.CC25.70	CC25	70	25	76	120
PC.2.CC50.70	CC50	70	50	76	112
PC.2.FX.60	FX	60	0	76	240

Table 6.1 (cont'd)

PC.2.FX.80	FX	80	0	76	240
RC.2.SS.0	SS	0	-	76	212
RC.2.FX.0	FX	0	0	76	240
RC.2.IC0.0	IC0	0	0	76	240
RC.2.IC25.0	IC25	0	25	76	240
RC.2.IC50.0	IC50	0	50	76	240
RC.2.CC0.0	CC0	0	0	76	240
RC.2.CC25.0	CC25	0	25	76	240
RC.2.CC50.0	CC50	0	50	76	240
PC.3.SS.70	SS	70	-	76	140
PC.3.FX.70	FX	70	0	76	240
PC.3.IC0.70	IC0	70	0	76	240
PC.3.IC25.70	IC25	70	25	76	152
PC.3.IC50.70	IC50	70	50	76	140
PC.3.CC0.70	CC0	70	0	76	196
PC.3.CC25.70	CC25	70	25	76	152
PC.3.CC50.70	CC50	70	50	76	140
PC.3.FX.60	FX	60	0	76	240
PC.3.FX.80	FX	80	0	76	240
RC.3.SS.0	SS	0	-	76	240
RC.3.FX.0	FX	0	0	76	240
RC.3.IC0.0	IC0	0	0	76	240
RC.3.IC25.0	IC25	0	25	76	240
RC.3.IC50.0	IC50	0	50	76	240
RC.3.CC0.0	CC0	0	0	76	240
RC.3.CC25.0	CC25	0	25	76	240
RC.3.CC50.0	CC50	0	50	76	240
PC.4.SS.70	SS	70	-	76	132
PC.4.FX.70	FX	70	0	76	240

Table 6.1 (cont'd)

PC.4.IC0.70	IC0	70	0	76	240
PC.4.IC25.70	IC25	70	25	76	156
PC.4.IC50.70	IC50	70	50	76	156
PC.4.CC0.70	CC0	70	0	76	204
PC.4.CC25.70	CC25	70	25	76	156
PC.4.CC50.70	CC50	70	50	76	132
PC.4.FX.60	FX	60	0	76	240
PC.4.FX.80	FX	80	0	76	240
RC.4.SS.0	SS	0	-	76	240
RC.4.FX.0	FX	0	0	76	240
RC.4.IC0.0	IC0	0	0	76	240
RC.4.IC25.0	IC25	0	25	76	240
RC.4.IC50.0	IC50	0	50	76	240
RC.4.CC0.0	CC0	0	0	76	240
RC.4.CC25.0	CC25	0	25	76	240
RC.4.CC50.0	CC50	0	50	76	240

Note: *All beams constitute calcareous aggregate based concrete with a characteristic compression strength of 50 MPa, load ratio of 50%, all PC beams have low relaxation prestressing strands with a tensile strength of 1861 MPa, and all RC beams have rebars with a tensile strength of 415 MPa

[+] Beam legends are abbreviated for brevity (see Section 5.2) using following: PC = Prestressed concrete, RC = Reinforced concrete, 1 = Section 12RB20, 2 = Section 12RB36, 3 = 16RB24, 4 = 16RB40, SS = Simply supported, FX = Fixed support, IC0 = Interior connection with no gap, IC25 = Interior connection with 25mm gap, IC50 = Interior connection with 50 mm gap, CC0 = Corner connection with no gap, CC25 = Corner connection with 25 mm gap, CC50 = Corner connection with 50 mm gap. Also, the prestress in reinforcement is represented at end of label as 0%, 60%, 70% and 80% of tensile strength

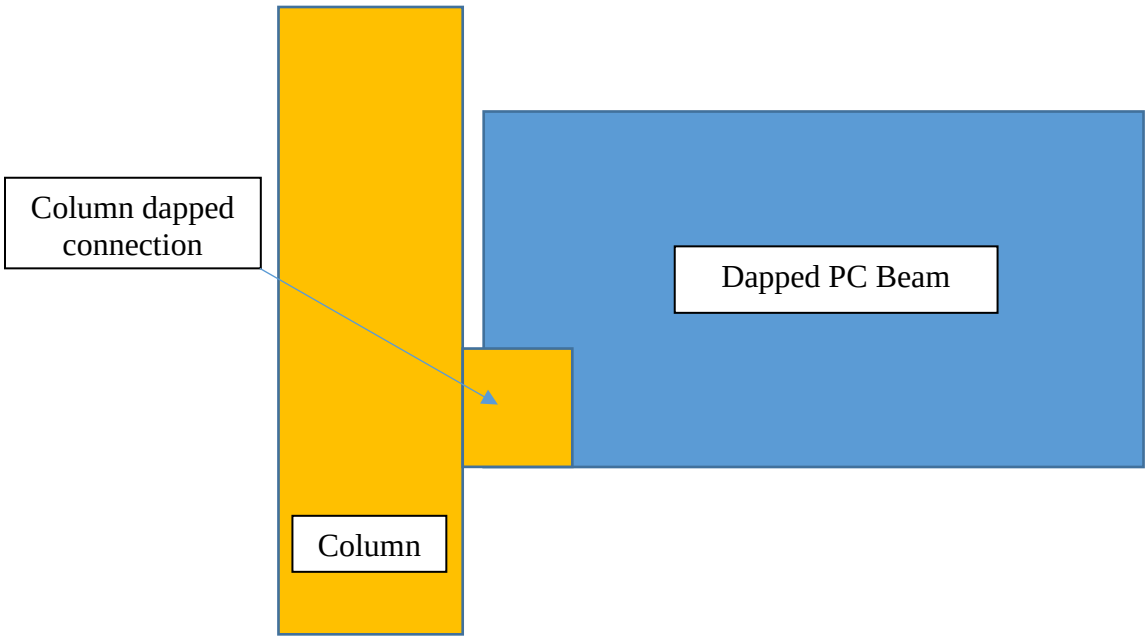

Figure 6.1 Representation of a beam dapped PC beam connection to column

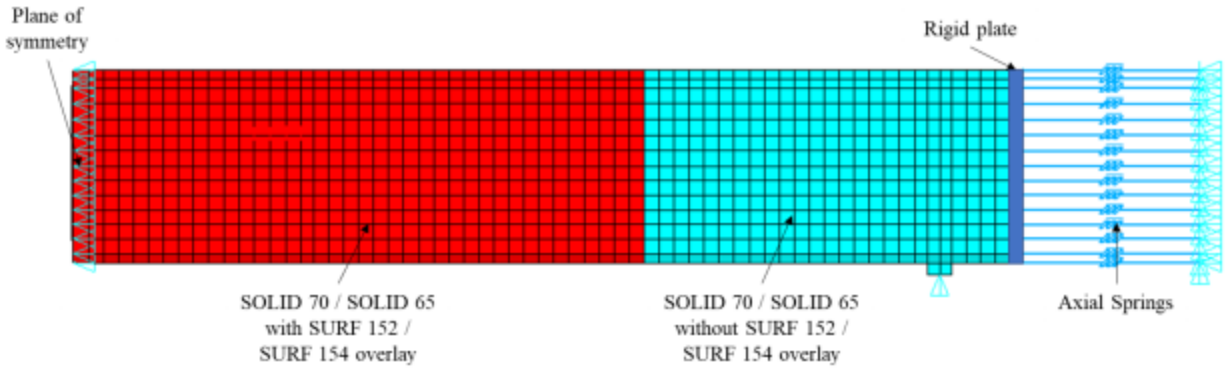

Figure 6.2 Discretization of PC beam using finite elements to perform thermo-mechanical analysis

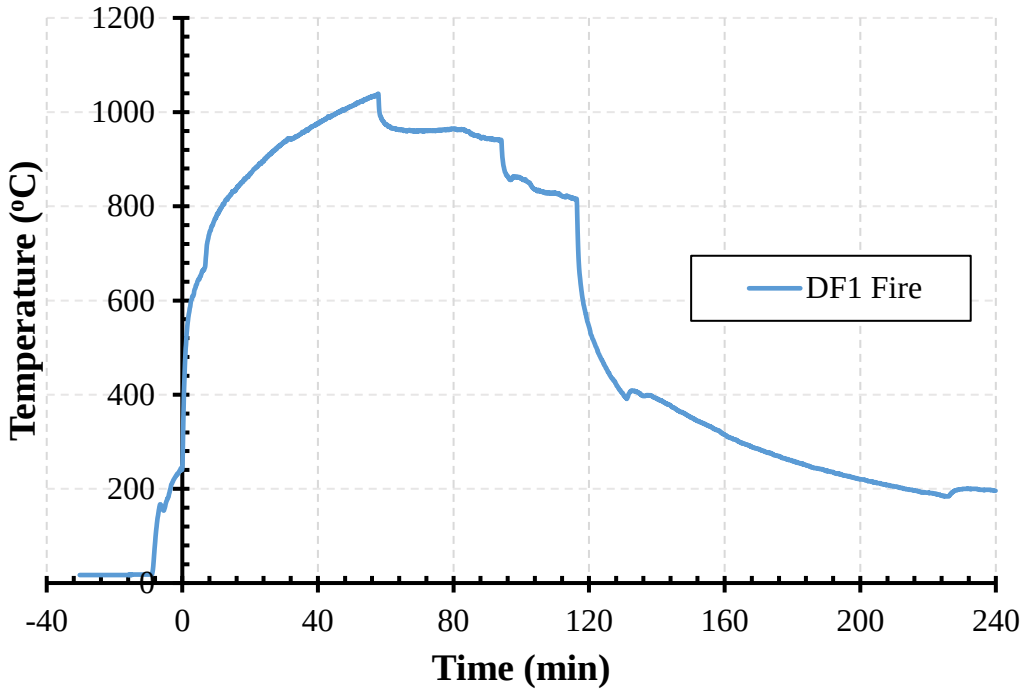

Figure 6.3 Time-temperature curve for realistic DF1 fire exposure used in the analysis

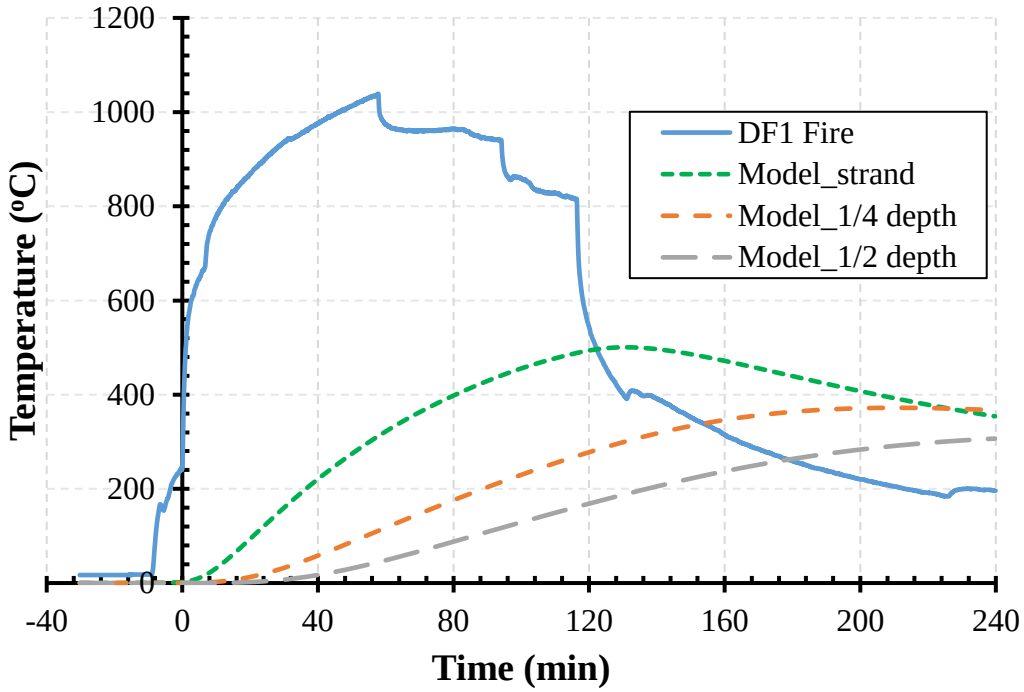

Figure 6.4 Progression of sectional temperatures in PC beam

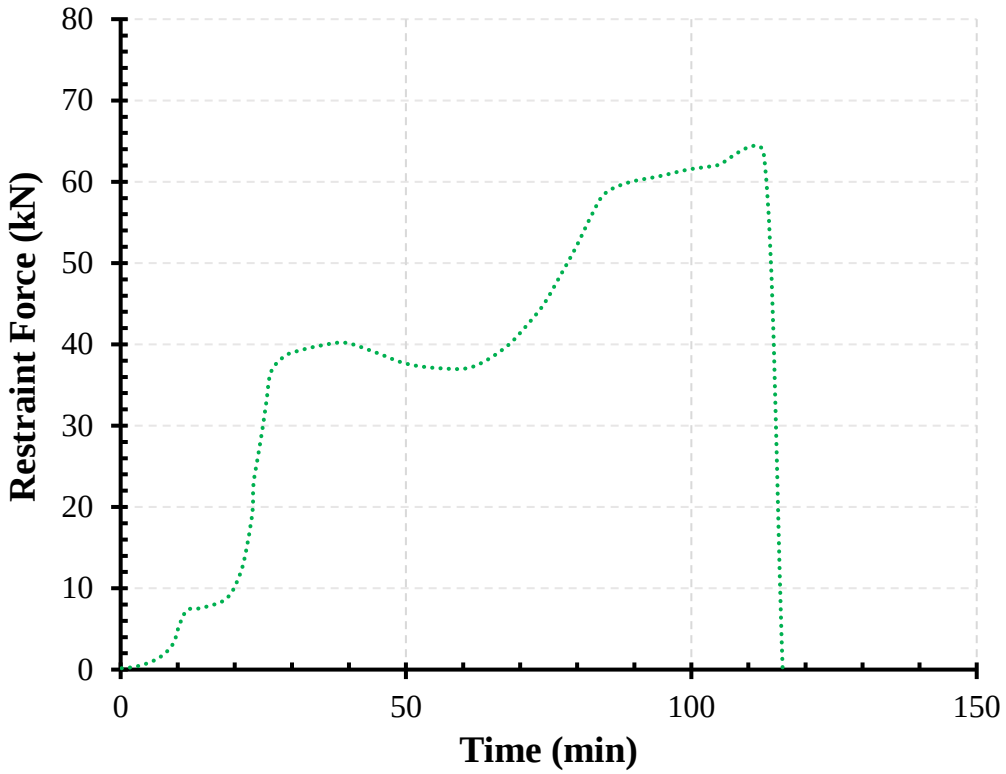

Figure 6.5 Progression of fire induced restraint force in PC beam under DF1 fire exposure

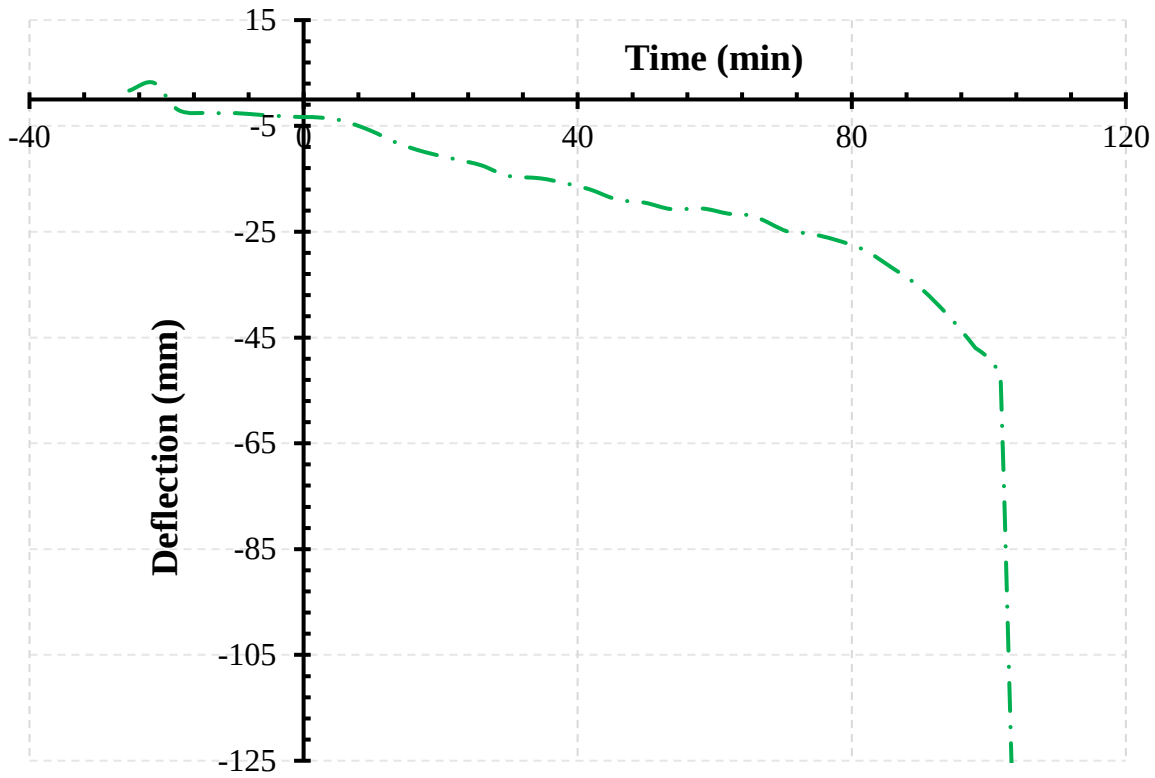

Figure 6.6 Progression of mid span deflection in PC beam under DF1 fire exposure

CHAPTER 7

7 Conclusions

7.1 General

The response of prestressed concrete (PC) beams under fire exposure is investigated as part of this research. A three-dimensional finite element based numerical model was developed for simulating the fire response of PC and RC beams under realistic fire, loading and restraint conditions. The developed numerical model accounts for the effect of critical governing factors including type of support, gap in connection, spalling in concrete, beam geometry, and material and geometric non-linearity. Specifically, the numerical model can capture the effect of fire induced restraint forces on structural response of a PC beam. Evolution of fire induced restraint forces is realized through idealized spring elements which can trace the magnitude and location of restraint forces for the entire duration of fire exposure. Also, fire induced spalling in HSC beams is accounted for through a simplified approach, and the model incorporates an adaptive temperature dependent failure envelope to capture cracking and crushing of concrete. To validate the numerical model, fire tests are undertaken on four PC beams under varying fire, loading, and restraint conditions. Data

generated from fire tests is utilized to validate the developed numerical model by comparing predicted and measured midspan deflections, fire induced restraint forces, and sectional temperatures. The validated numerical model is utilized to analyze a total of 76 PC beams under different end conditions, section types, and prestress. Based on the results from the parametric studies preliminary design recommendations are proposed for fire design of PC beams.

7.2 Key conclusions

Based on the research undertaken in this thesis, following conclusions can be made:

1. The current fire resistance provisions in codes and standards are prescriptive in nature and are based on standard fire tests, which do not account for the full effect of fire induced restraint forces. Significant fire induced restraint forces can develop in PC beams under restrained conditions, and the prescriptive codes may not yield realistic fire resistance assessment for restrained PC beams.
2. The proposed finite element based numerical model can predict the response of PC beams from preloading stage to failure under combined effects of fire and structural loading. The model can trace the evolution of fire induced restraint forces throughout the fire exposure duration.
3. RC beams are likely to experience a 5% to 20% higher level of fire induced restraint forces than the equivalent PC beams. The level of fire-induced restraint force that develops in the HSC PC beam is lower than a similar NSC PC beam because of the early failure in HSC beams which do not allow ample time for restraint forces to develop.
4. PC beams with gaps of more than 50 mm in the connection may not develop significant fire induced restraint forces as the beam’s thermal expansion may not be able to overcome the gap.

5. The evolution of restraint force may follow similar trends in PC and equivalent RC beams, however, fire-induced forces in PC beams are relatively less effective in increasing the fire resistance of the beam than as compared to the RC beams.
6. Currently, PC beam connections to framing structural elements (columns, walls etc.) are not specifically designed to withstand high level of restraint forces that may develop under fire exposure. This may lead to premature failure of the connections due to fire induced restraint forces.
7. Clear cover of 76 mm does not guarantee 4 hour fire rating (as recommended by most prescriptive codes and standards) for all PC beams under restrained or unrestrained conditions.

7.3 Research impact

Currently, PC beams are classified as restrained or unrestrained based on qualitative prescriptive guidelines, and then fire resistance rating of PC beams is predicted based on restraint classification, minimum beam width, and cover thickness to strands. This prescriptive approach for evaluating fire resistance of PC beams is based on limited standard fire tests and do not specifically account for realistic fire, loading and restraint conditions present in buildings. Also, there is no guidance in codes and standards to evaluate the magnitude and location of restraint forces. Therefore, prescriptive approaches may not yield realistic fire resistance assessment especially under restrained support conditions. On the other hand, the simplified rational design approaches, present in some codes, allow designers to calculate actual moment capacity of PC beam under fire exposure by incorporating temperature dependent material degradation into room temperature moment capacity equations (which are based on strain compatibility). However, such rational

design approaches do not account for full effects of fire induced restraint forces and therefore, cannot predict realistic fire resistance of restrained PC beams.

The validated numerical model in this study provides a numerical approach to predict the fire resistance of PC beams. The developed model accounts for critical factors governing fire resistance of PC beams, and therefore, can be used to predict fire resistance of PC beams under realistic fire, loading, and restraint conditions. Further, the numerical model can generate detailed fire response parameters which can enhance the understanding of the fire response of PC beams. Therefore, results from parametric studies conducted using the numerical model provide vital data on evolution of fire induced restraint forces; and also, on how these forces vary with support conditions, beam geometry, prestress, gap in connection, and material properties. These results provided basis for preliminary design recommendations which can improve the fire resistance assessment and our understanding on the fire response of restrained PC beams. Therefore, results from this thesis provide new insights on a less understood intricate problem.

7.4 Recommendations for future research

While this study developed an advanced numerical model to evaluate fire response of restrained and unrestrained PC beams, further research can be undertaken to improve some of the critical aspects on the response of restrained PC beams under varying design configurations. The following recommendations are made for future research in this area:

- In the current version of the model temperature dependent bond between rebars/strands and concrete is not specifically accounted for, therefore, degradation of bond between prestressing strands and concrete at elevated temperatures can be incorporated to better trace local stress transfer between strands and concrete.

- In the model, a simplified approach is adopted for predicting spalling. Advanced spalling model based on hygro-thermal-mechanical analysis can be incorporated to improve spalling predictions.
- The numerical model can be further extended to other PC structural members (such as hollowcore slabs, double-tee beams etc.) to account for the effect of fire induced restraint forces on their fire response.
- The current approach is member level only. The effect of fire induced restraint forces can be better understood through a system level analysis to capture the effect of fire induced restraint forces on the global structural response.

REFERENCES

[1] N. Brushlinsky, S. Sokolov, P. Wagner, B. Messerschmidt, World fire statistics, CTIF, International Association of Fire and Rescue Services, No. 27 (2022). Available at: https://www.ctif.org/sites/default/files/2022-08/CTIF_Report27_ESG_0.pdf (accessed 3 September 2022).

[2] Bulletin, World fire statistics, The Geneva Association, No. 29, (2014). Available at: www.genevaassociation.org/research-topics/world-fire-statistics-bulletin-no-29 (accessed 30 June 2019).

[3] GDP, World bank national accounts data, and OECD national accounts data files, (2018). Available at: https://data.worldbank.org/indicator/NY.GDP.MKTP.CD (accessed 3 September 2022).

[4] Eurocode 2, Design of concrete structures-part 1-2: general rules -structural fire design. European Committee for Standardization, London, (2004).

[5] ASTM E119, Standard Test Methods for Fire Tests of Building Construction and Materials, (2018).

[6] PCI Manual 124-18, Specification for fire resistance of precast/prestressed concrete. Precast Concrete Institute, Chicago, (2018).

[7] ACI Committee 216, ACI 216.1-14 Code requirements for determining fire resistance of concrete and masonry construction assemblies, American Concrete Institute, Farmington, MI, (2014).

[8] M.B.M. Dwaikat. Flexural response of reinforced concrete beams exposed to fire. PhD Thesis. East Lansing, MI: Michigan State University; 2009.

[9] M.B. Dwaikat, V.K.R.R. Kodur, Response of restrained concrete beams under design fire exposure, J. Struct. Eng. 135 (2009) 1408–1417. doi:10.1061/(ASCE)ST.1943-541X.0000058.

[10] G.L. Albuquerque, A.B. Silva, J.P.C. Rodrigues, V.P. Silva, Behavior of thermally restrained RC beams in case of fire, Eng. Struct. 174 (2018) 407–417. doi:10.1016/j.engstruct.2018.07.075.

[11] Eurocode 1, Actions on structures – Part 1-2: general actions – actions on structures exposed to fire, European Committee for Standardization, London, (2002).

[12] S. Fan, Y. Zhang, K.H. Tan, Experimental and analytical studies of reinforced concrete short beams at elevated temperatures, Eng. Struct. 212 (2020) 110445. doi:10.1016/j.engstruct.2020.110445.

[13] Y. Wang, G. Yuan, Z. Huang, J. Lyv, Z.Q. Li, T. yan Wang, Experimental study on the fire behaviour of reinforced concrete slabs under combined uni-axial in-plane and out-of-plane loads, Eng. Struct. 128 (2016) 316–332. doi:10.1016/j.engstruct.2016.09.054.

[14] Y. Wang, L.A. Bisby, T. yan Wang, G. Yuan, E. Baharudin, Fire behaviour of reinforced concrete slabs under combined biaxial in-plane and out-of-plane loads, Fire Saf. J. 96 (2018) 27–45. doi:10.1016/j.firesaf.2017.12.004.

[15] S. Banerji, V. Kodur, R. Solhmirzaei, Experimental behavior of ultra high performance fiber reinforced concrete beams under fire conditions, Eng. Struct. 208 (2020) 110316. doi:10.1016/j.engstruct.2020.110316.

[16] A. Al-Attar, M. Abdulrahman, H. Hamada, B. Tayeh, Investigating the behaviour of hybrid fibre-reinforced reactive powder concrete beams after exposure to elevated temperatures, J. Mater. Res. Technol. 9 (2019) 1966–1977. doi:10.1016/j.jmrt.2019.12.029.

[17] X. Hou, P. Ren, Q. Rong, W. Zheng, Y. Zhan, Comparative fire behavior of reinforced RPC and NSC simply supported beams, Eng. Struct. 185 (2019) 122–140. doi:10.1016/j.engstruct.2019.01.097.

[18] L. Jin, R. Zhang, G. Dou, X. Du, Fire resistance of steel fiber reinforced concrete beams after low-velocity impact loading, Fire Saf. J. 98 (2018) 24–37. doi:10.1016/j.firesaf.2018.04.003.

[19] A. Abbasi, P.J. Hogg, Fire testing of concrete beams with fibre reinforced plastic rebar, Compos. Part A Appl. Sci. Manuf. 37 (2006) 1142–1150. doi:10.1016/j.compositesa.2005.05.029.

[20] P. Turkowski, M. Łukomski, P. Sulik, P. Roszkowski, Fire Resistance of CFRP-strengthened Reinforced Concrete Beams under Various Load Levels, Procedia Eng. 172 (2017) 1176–1183. doi:10.1016/j.proeng.2017.02.137.

[21] Q. Xu, C. Han, Y.C. Wang, X. Li, L. Chen, Q. Liu, Experimental and numerical investigations of fire resistance of continuous high strength steel reinforced concrete T-beams, Fire Saf. J. 78 (2015) 142–154. doi:10.1016/j.firesaf.2015.09.001.

[22] B.I. Song, K. A. Giriunas, H. Sezen, Progressive collapse testing and analysis of a steel frame building, J. Constr. Steel Res. 94 (2014) 76–83. doi:10.1016/j.jcsr.2013.11.002.

[23] M.M. Raouffard, M. Nishiyama, Fire response of exterior reinforced concrete beam-column subassemblages, Fire Saf. J. 91 (2017) 498–505. doi:10.1016/j.firesaf.2017.03.054.

[24] A.H. Akca, N. Özyurt, Post-fire mechanical behavior and recovery of structural reinforced concrete beams, Constr. Build. Mater. 253 (2020) 119188. doi:10.1016/j.conbuildmat.2020.119188.

[25] C.J. Jiang, J.T. Yu, L.Z. Li, X. Wang, L. Wang, J.H. Liao, Experimental study on the residual shear capacity of fire-damaged reinforced concrete frame beams and cantilevers, Fire Saf. J. 100 (2018) 140–156. doi:10.1016/j.firesaf.2018.08.004.

[26] X. yan Shang, J. tao Yu, L. zhi Li, Z. dao Lu, Shear strengthening of fire damaged RC beams with stirrup reinforced engineered cementitious composites, Eng. Struct. 210 (2020) 110263. doi:10.1016/j.engstruct.2020.110263.

[27] G. Ba, J. Miao, W. Zhang, J. Liu, Influence of reinforcement corrosion on fire performance of reinforced concrete beams, Constr. Build. Mater. 213 (2019) 738–747. doi:10.1016/j.conbuildmat.2019.04.065.

[28] L.Z. Li, C.J. Jiang, B.Z. Liu, Z.D. Lu, Shear strengthening of fire-damaged reinforced concrete beams using bolted-side plating, Procedia Eng. 210 (2017) 186–195. doi:10.1016/j.proeng.2017.11.065.

[29] L.A. Ashton, H.L. Malhotra, The fire resistance of prestressed concrete beams, Department of scientific and industrial research and fire offices' committee joint fire research organization, (1953).

[30] J.V. Ryan, Fire resistance of prestressed concrete beams, National bureau of standards report, (1954).

[31] K. LaMalva, L. Bisby, J. Gales, T. Gernay, E. Hantouche, C. Jones, A. Morovat, R. Solomon, J. Torero, Rectification of "restrained vs unrestrained," Fire Mater. (2020) 1–11. doi:10.1002/fam.2771.

[32] X. Hou, V.K.R. Kodur, W. Zheng, Factors governing the fire response of bonded prestressed concrete continuous beams, Mater. Struct. Constr. 48 (2015) 2885–2900. doi:10.1617/s11527-014-0365-9.

[33] S.L. Selvaggio, A.C.C. Carlson, Effect of restraint on fire resistance of prestressed concrete, ASTM international, (1963).

[34] J.J. Franssen, A. Bruls, Design And Tests Of Prestressed Concrete Beams, Fire Saf. Sci. 5 (1997) 1081–1092. doi:10.3801/iafss.fss.5-1081.

[35] X. Hou, W. Zheng, K. V.K.R., Response of unbonded prestressed concrete continuous slabs under fire exposure, Eng. Struct. 56 (2013) 2139–2148. doi:10.1016/j.engstruct.2013.08.035.

[36] Y. Aimin, D. Yuli, G. Litang, Behavior of unbonded prestressed continuous concrete slabs with the middle and edge span subjected to fire in sequence, Fire Saf. J. 56 (2013) 20–29. doi:10.1016/j.firesaf.2012.10.023.

[37] D. Qin, P.K. Gao, F. Aslam, M. Sufian, H. Alabduljabbar, A comprehensive review on fire damage assessment of reinforced concrete structures, Case Stud. Constr. Mater. 16 (2022) e00843. doi:10.1016/j.cscm.2021.e00843.

[38] J. Cai, I. Burgess, R. Plank, A generalised steel/reinforced concrete beam-column element model for fire conditions, Eng. Struct. 25 (2003) 817–833. doi:10.1016/S0141-0296(03)00019-1.

[39] V.K.R. Kodur, P. Pakala, M.B. Dwaikat, Energy based time equivalent approach for evaluating fire resistance of reinforced concrete beams, Fire Saf. J. 45 (2010) 211–220. doi:10.1016/j.firesaf.2010.03.002.

[40] W.Y. Gao, J.G. Dai, J.G. Teng, G.M. Chen, Finite element modeling of reinforced concrete beams exposed to fire, Eng. Struct. 52 (2013) 488–501. doi:10.1016/j.engstruct.2013.03.017.

[41] F. Liao, Z. Huang, An extended finite element model for modelling localised fracture of reinforced concrete beams in fire, Comput. Struct. 152 (2015) 11–26. doi:10.1016/j.compstruc.2015.02.006.

[42] R.A. Hawileh, M. Naser, W. Zaidan, H.A. Rasheed, Modeling of insulated CFRP-strengthened reinforced concrete T-beam exposed to fire, Eng. Struct. 31 (2009) 3072–3079. doi:10.1016/j.engstruct.2009.08.008.

[43] A. Ahmed, V. Kodur, Effect of bond degradation on fire resistance of FRP-strengthened reinforced concrete beams, Compos. Part B Eng. (2011). http://www.sciencedirect.com/science/article/pii/S135983681000212X (accessed April 16, 2016).

[44] B. Yu, V.K.R. Kodur, Factors governing the fire response of concrete beams reinforced with FRP rebars, Compos. Struct. 100 (2013) 257–269. doi:10.1016/j.compstruct.2012.12.028.

[45] X. Lin, Y.X. Zhang, Nonlinear finite element analyses of steel/FRP-reinforced concrete beams in fire conditions, Compos. Struct. 97 (2013) 277–285. doi:10.1016/j.compstruct.2012.09.042.

[46] E. Nigro, G. Cefarelli, A. Bilotta, G. Manfredi, E. Cosenza, Guidelines for flexural resistance of FRP reinforced concrete slabs and beams in fire, Compos. Part B Eng. 58 (2014) 103–112. doi:10.1016/j.compositesb.2013.10.007.

[47] J.P. Firmo, M.R.T. Arruda, J.R. Correia, Numerical simulation of the fire behaviour of thermally insulated reinforced concrete beams strengthened with EBR-CFRP strips, Compos. Struct. 126 (2015) 360–370. doi:10.1016/j.compstruct.2015.02.084.

[48] M. Wu, S. Fan, H. Zhou, Y. Han, D. Liang, Experimental and numerical research on fire resistance of stainless steel-concrete composite beam, J. Constr. Steel Res. 194 (2022) 107342. doi:10.1016/j.jcsr.2022.107342.

[49] R. Kirthiga, S. Elavenil, A review on using inorganic binders in fiber reinforced polymer at different conditions to strengthen reinforced concrete beams, Constr. Build. Mater. 352 (2022) 129054. doi:10.1016/j.conbuildmat.2022.129054.

[50] I.C. Rosa, J.P. Firmo, J.R. Correia, Fire behaviour of GFRP-reinforced concrete slab strips. Effect of straight and 90° bent tension lap splices, Eng. Struct. 270 (2022). doi:10.1016/j.engstruct.2022.114904.

[51] D. Mirdan, A.R. Saleh, Case Studies in Construction Materials Flexural performance of reinforced concrete (RC) beam strengthened by UHPC layer, Case Stud. Constr. Mater. 17 (2022) e01655. doi:10.1016/j.cscm.2022.e01655.

[52] H. Zhou, H. Li, H. Qin, T. Liang, M.Z. Naser, Examining fire response of unilaterally concrete-reinforced web prestressed composite beams with corrugated webs, Eng. Struct. 274 (2023) 115194. doi:10.1016/j.engstruct.2022.115194.

[53] R. Li, M. Deng, H. Chen, Y. Zhang, Shear strengthening of RC shear-deficient beams with highly ductile fiber-reinforced concrete, Structures. 44 (2022) 159–170. doi:10.1016/j.istruc.2022.08.013.

[54] X. Lu, Z. Zhu, M. Mohibullah, K. Wang, Nonlinear analysis of flexural performance of reactive powder concrete beams reinforced with hybrid GFRP and steel bars, Case Stud. Constr. Mater. 17 (2022) e01450. doi:10.1016/j.cscm.2022.e01450.

[55] H. Jafarzadeh, M. Nematzadeh, Flexural strengthening of fire-damaged GFRP-reinforced concrete beams using CFRP sheet: Experimental and analytical study, Compos. Struct. 288 (2022) 115378. doi:10.1016/j.compstruct.2022.115378.

[56] K. Rajesh Kumar, R. Yuvanesh Kumar, Structural behaviour of deep beam using hybrid fiber reinforced concrete with M−sand, Mater. Today Proc. (2022). doi:10.1016/j.matpr.2022.07.097.

[57] C. Lu, Q. Cai, K. Xu, X. Sha, Y. Yan, Comparison of flexural behaviors between plain and steel-fiber-reinforced concrete beams with hybrid GFRP and steel bars, Structures. 43 (2022) 1–11. doi:10.1016/j.istruc.2022.06.037.

[58] D. Yang, S.S. Huang, F. Liu, H. Yang, Structural fire design of square tubed-reinforced-concrete columns with connection to RC beams in composite frames, J. Build. Eng. 57 (2022) 104900. doi:10.1016/j.jobe.2022.104900.

[59] V.K.R. Kodur, A. Agrawal, An approach for evaluating residual capacity of reinforced concrete beams exposed to fire, Eng. Struct. 110 (2016) 293–306. doi:10.1016/j.engstruct.2015.11.047.

[60] V.K.R. Kodur, A. Agrawal, Effect of temperature induced bond degradation on fire response of reinforced concrete beams, Eng. Struct. 142 (2017) 98–109. doi:10.1016/j.engstruct.2017.03.022.

[61] S. Ni, T. Gernay, Predicting residual deformations in a reinforced concrete building structure after a fire event, Eng. Struct. 202 (2020) 109853. doi:10.1016/j.engstruct.2019.109853.

[62] X. Li, X. Lu, J. Qi, Y. Bao, Flexural behavior of fire-damaged concrete beams repaired with strain-hardening cementitious composite, Eng. Struct. 261 (2022). doi:10.1016/j.engstruct.2022.114305.

[63] F. Dabbaghi, T.Y. Yang, A. Tanhadoust, S.B. Emadi, M. Dehestani, H. Yousefpour, Experimental and numerical investigation on post-fire seismic performance of light weight aggregate reinforced concrete beams, Eng. Struct. 268 (2022) 114791. doi:10.1016/j.engstruct.2022.114791.

[64] A.S. Abdulrahman, M.R.A. Kadir, Behavior and flexural strength of fire damaged high strength reinforced rectangular concrete beams after strengthening with CFRP laminates, Ain Shams Eng. J. 13 (2022) 101767. doi:10.1016/j.asej.2022.101767.

[65] B.A. Shehab, T. Ekmekyapar, Connection behaviour of through reinforced concrete beam to concrete-filled steel tube column after exposed to heating, Fire Saf. J. 133 (2022) 103666. doi:10.1016/j.firesaf.2022.103666.

[66] H. Vitorino, H. Rodrigues, C. Couto, Evaluation of post-earthquake fire capacity of a reinforced concrete one bay plane frame under ISO fire exposure, Structures. 23 (2020) 602–611. doi:10.1016/j.istruc.2019.12.009.

[67] Y. Wang, Y. Bu, Z. Huang, A. Gu, G. Han, X. Zhang, Y. Zhang, Y. Liu, Z. Chen, W. Guo, Experimental and numerical investigation on reinforced-concrete slab-beam assemblies exposed to extended and travelling fires, Eng. Struct. 264 (2022) 114430. doi:10.1016/j.engstruct.2022.114430.

[68] J. Melo, Z. Triantafyllidis, D. Rush, L. Bisby, T. Rossetto, A. Arêde, H. Varum, I. Ioannou, Cyclic behaviour of as-built and strengthened existing reinforced concrete columns previously damaged by fire, Eng. Struct. 266 (2022). doi:10.1016/j.engstruct.2022.114584.

[69] S. Liu, X. Wang, Y.M.S. Ali, C. Su, Z. Wu, Flexural behavior and design of under-reinforced concrete beams with BFRP and steel bars, Eng. Struct. 263 (2022) 114386. doi:10.1016/j.engstruct.2022.114386.

[70] P. Du, Y. Yang, K.H. Tan, Fire behaviour and design of hybrid fibre reinforced high-performance concrete columns subjected to uniaxial bending, Eng. Struct. 251 (2022) 113425. doi:10.1016/j.engstruct.2021.113425.

[71] N. Hua, N. Elhami Khorasani, A. Tessari, Numerical modeling of the fire behavior of reinforced concrete tunnel slabs during heating and cooling, Eng. Struct. 258 (2022) 114135. doi:10.1016/j.engstruct.2022.114135.

[72] Z. Li, T. Dong, F. Fu, K. Qian, Dynamic response of cross steel reinforced concrete filled steel tubular columns under impact under fire, J. Constr. Steel Res. 200 (2023) 107643. doi:10.1016/j.jcsr.2022.107643.

[73] W. Mao, W. Wang, K. Zhou, Fire performance on steel-reinforced concrete-filled steel tubular columns with fire protection, J. Constr. Steel Res. 199 (2022) 107580. doi:10.1016/j.jcsr.2022.107580.

[74] Z. Shao, X. Zha, C. Wan, Design method of fire-resistance capacity of reinforced-concrete-filled steel tube column under axial compression, Fire Saf. J. 129 (2022) 103572. doi:10.1016/j.firesaf.2022.103572.

[75] T. Eduardo, T. Buttignol, Case Studies in Construction Materials Analytical and numerical analyses of RC beams exposed to fire adopting a LITS trilinear constitutive law for concrete, Case Stud. Constr. Mater. 17 (2022) e01619. doi:10.1016/j.cscm.2022.e01619.

[76] L. Li, H. Wang, J. Wu, X. Du, X. Zhang, Y. Yao, Experimental and numerical investigation on impact dynamic performance of steel fiber reinforced concrete beams at elevated temperatures, J. Build. Eng. 47 (2022) 103841. doi:10.1016/j.jobe.2021.103841.

[77] Y. Chen, S. Zhang, Z. Chen, Experimental study on steel reinforced concrete T-section beam subjected to pure torsion and combined action of bending-torsion, Structures. 46 (2022) 1000–1015. doi:10.1016/j.istruc.2022.10.109.

[78] S.H. Ji, W. Da Wang, W. Xian, Impact and post-impact behaviours of steel-reinforced concrete-filled steel tubular columns after exposure to fire, Structures. 44 (2022) 680–697. doi:10.1016/j.istruc.2022.08.030.

[79] N. Hua, N. Elhami Khorasani, A. Tessari, R. Ranade, Experimental study of fire damage to reinforced concrete tunnel slabs, Fire Saf. J. 127 (2022) 103504. doi:10.1016/j.firesaf.2021.103504.

[80] V. Van Cao, H.B. Vo, L.H. Dinh, D. Van Doan, Experimental behavior of fire-exposed reinforced concrete slabs without and with FRP retrofitting, J. Build. Eng. 51 (2022) 104315. doi:10.1016/j.jobe.2022.104315.

[81] P. Kumar, G. Srivastava, Numerical modeling of structural frames with infills subjected to thermal exposure: State-of-the-art review, J. Struct. Fire Eng. 8 (2017) 218–237. doi:10.1108/JSFE-05-2017-0031.

[82] V.K.R. Kodur, P. Kumar, Rational design approach for evaluating fire resistance of hollow core slabs under vehicle fire exposure, PCI Convention, Denver, CO.2018.

https://www.pci.org/PCI_Docs/Convention-Papers/2018/9_Final_Paper.pdf (accessed June 15, 2018).

[83] M.B. Dwaikat, V.K.R. Kodur, A numerical approach for modeling the fire induced restraint effects in reinforced concrete beams, Fire Saf. J. 43 (2008) 291–307. doi:10.1016/j.firesaf.2007.08.003.

[84] V.K.R. Kodur, M.B. Dwaikat, Design equation for predicting fire resistance of reinforced concrete beams, Eng. Struct. 33 (2011) 602–614. doi:10.1016/j.engstruct.2010.11.019.

[85] B. Wu, J.Z. Lu, A numerical study of the behaviour of restrained RC beams at elevated temperatures, Fire Saf. J. 44 (2009) 522–531. doi:10.1016/j.firesaf.2008.10.006.

[86] S. Albrifkani, Y.C. Wang, Explicit modelling of large deflection behaviour of restrained reinforced concrete beams in fire, Eng. Struct. 121 (2016) 97–119. doi:10.1016/j.engstruct.2016.04.032.

[87] S. Albrifkani, Y.C. Wang, Behaviour of axially and rotationally restrained reinforced concrete beams in fire, Eng. Struct. 213 (2020) 110572. doi:10.1016/j.engstruct.2020.110572.

[88] V.K.R. Kodur, N.R. Hatinger, A performance-based approach for evaluating fire resistance of prestressed concrete double T-beams, J. Fire Prot. Eng. 21 (2011) 185–222. doi:10.1177/1042391511417795.

[89] N.M. Okasha, S. Pessiki, Restraint mechanisms in precast concrete double-tee floor systems subjected to fire, PCI J. 58 (2013) 95–110. doi:10.15554/pcij.06012013.95.110.

[90] R.W. Bletzacker, Fire resistance of protected steel beam floor and roof assemblies as affected by structural restraint, Symp. Fire Test Methods-Restraint Smoke 1966, ASTM STP 422, Ameri- Can Soc. Test. Mater. (1967) 63–90.

[91] V. Kodur, Properties of Concrete at Elevated Temperatures, ISRN Civ. Eng. 2014 (2014) e468510. doi:10.1155/2014/468510.

[92] A.M. Shakya. Flexural and shear response of precast prestressed concrete hollowcore slabs under fire conditions. PhD Thesis. East Lansing, MI: Michigan State University; 2016.

[93] ASCE, T. Lie, Structural Fire Protection, ASCE Comm. Fire Prot. Struct. Div. Am. Soc. Civ. Eng. New York, NY, USA. (1992).

[94] P. Kumar, V.K.R. Kodur, Response of prestressed concrete beams under combined effects of fire and structural loading, Eng. Struct. 246 (2021) 113025. doi:10.1016/j.engstruct.2021.113025.

[95] ACI Committee 318, ACI 318-14, Building code requirements for structural concrete, American Concrete Institute, Farmington, MI, (2014).

[96] V. Kodur, P. Kumar, M.M. Rafi, Fire hazard in buildings : review , assessment and strategies for improving fi re safety buildings, PSU Res. Rev. (2019). doi:10.1108/PRR-12-2018-0033.

[97] ANSYS, Mechanical APDL theory reference, Version 16.2, Canonsb. ANSYS, Inc. (2015).

[98] J. Purkiss, Fire safety engineering design of structures, Second Edition, Butterworth-Heinemann, 2007.

[99] P. Kumar, G. Srivastava, Effect of fire on in-plane and out-of-plane behavior of reinforced concrete frames with and without masonry infills, Constr. Build. Mater. 167 (2018) 82–95. doi:10.1016/j.conbuildmat.2018.01.116.

[100] P. Kumar, V.K.R. Kodur, Modeling the behavior of load bearing concrete walls under fire exposure, Constr. Build. Mater. 154 (2017) 993–1003. doi:10.1016/j.conbuildmat.2017.08.010.

[101] P. Kumar, V.K.R. Kodur, A rational approach for fire-resistance evaluation of double-tee, prestressed concrete slabs in parking structures, PCI Journal 65 (2020) 20–41.

[102] V. Kodur, M. Dwaikat, Fire-induced spalling in reinforced concrete beams, Proc. Inst. Civ. Eng. Struct. Build. 165 (2012) 347–359. doi:10.1680/stbu.11.00013.

[103] V. Kodur, S. Banerji, Modeling the fire-induced spalling in concrete structures incorporating hydro-thermo-mechanical stresses, Cem. Concr. Compos. 117 (2021) 103902. doi:10.1016/j.cemconcomp.2020.103902.

[104] S. Deeny, T. Stratford, R.P. Dhakal, P.J. Moss, A.H. Buchanan, Spalling of concrete: Implications for structural performance in fire, Futur. Mech. Struct. Mater. - Proc. 20th Australas. Conf. Mech. Struct. Mater. ACMSM20. 1 (2008) 231–235.

[105] R. Jansson, Fire Spalling of Concrete, KTH Architecture and the Built Environment, PhD Thesis, Stockholm, Sweden (2013).

[106] ISO834, Fire resistance tests – elements of building construction, Geneva, Switz. Int. Organ. Stand. (1975).

[107] P. Kumar, V.K.R. Kodur, Effect of fire-induced restraint forces on fire behavior of reinforced and prestressed concrete beams, Eng. Struct. 275 (2023) 115200. doi:10.1016/j.engstruct.2022.115200.

[108] PCI Handbook 8, PCI Design Handbook Precast and Prestressed Concrete, Chicago, IL, (2017).

APPENDIX A: DESIGN OF PC BEAMS FOR PARAMETRIC STUDIES

PC beams used in the parametric studies are designed for the room temperature as per the PCI Handbook [108] recommendations, and the details of the same are provided in this appendix. All PC and equivalent RC beams are designed using strain compatibility approach and their detailed design parameters are illustrated in Figures A.1 to A.8 with summary in Table A.1. For all 76 beams in parametric studies, compressive strength of concrete ($f_c{}'$) is kept at 7251.89 psi (50 MPa), and ultimate strength of prestressing strands (f_{pu}) is kept at 270 ksi (1861 MPa). The reinforcement and other details for PC beams can be referred to Chapter 5. For all 76 PC beams, appropriate prestress ratio was assigned, and a total prestress loss of 30000 psi was considered.

Then beams are designed using strain compatibility and rectangular equivalent compressive stress block for concrete as per PCI Handbook recommendations. First, the depth of equivalent rectangular compressive stress block, a, is calculated by the force equilibrium between tensile and compressive forces in the beam. The total compression and tension force in the beam, is given as:

$$C = 0.85 * f\_c\text{^}' * b * a + As\text{^}' * fy \quad \text{(A.1)}$$

$$T = A\_ps * f\_ps + A\_s * fy \quad \text{(A.2)}$$

Based on the force equilibrium, a compressive stress block (a) of 2.57 in generated a compression and tension force of 206 kips at a lever arm of 15”. For calculating the compression force, the neutral axis depth was calculated to calculate the strain at the top compression rebars to capture actual stress in holding rebars. Also, the strain in strands is checked to ensure that beam is designed as under reinforced, and the yielding of strands to ensure maximum stress in strands is achieved. Based on the moment capacity of the beam, and the load ratio, the applied loads are then calculated to achieve desired load ratio. For beams with Section 1 a live load of 3626 psf is needed in addition to the self-weight of the beam on the top beam width of 12 in to achieve a load ratio of 50%.

Then the shear capacity of the beam is checked to design appropriate shear reinforcement. The shear strength is calculated as below:

$$\phi V\_c = \phi(0.6\sqrt{(f\_c\text{^}')} + 700\ (V\_u\ d\_p)/M\_u\ \backslash)bd \leq \phi 5\sqrt{(f\_c\text{^}')}\ bd \qquad \text{(A.3)}$$

For most beams, the shear strength of the concrete alone was higher than the ultimate shear. Therefore, minimum shear reinforcement is provided as per PCI Handbook [108] recommendations. Also. To ensure that the beam satisfies the service requirements for stresses, top and bottom stresses are calculated, and as can be observed from the Figure A.1, these limits are within limits. More details on the exact design of all beams can be referred to the Figures A.1 to A.8.

Table A.1 Summary of PC beam capacity and applied loading

Beam Type	Beam Section[+]	Steel Reinforcement*	Moment Capacity (kN-m)	Applied Load (kN/m^2)
PC	12RB20	5 Φ12.7 mm strands with 2 Φ12.7 mm holder rebars	365	173.6
	12RB36		919	122.7
	16RB24	7 Φ12.7 mm strands with 2 Φ12.7 mm holder rebars	641	155.4
	16RB40		1443	113.6
	8RB20	3 Φ12.7 mm strands with 2 Φ12.7 mm holder rebars	220	155.8

*All beams constitute low relaxation prestressing strands with a tensile strength of 1861 MPa, all rebars have a tensile strength of 415 MPa

[+]All temperature dependent material properties are assigned as per Eurocode 2 recommendations

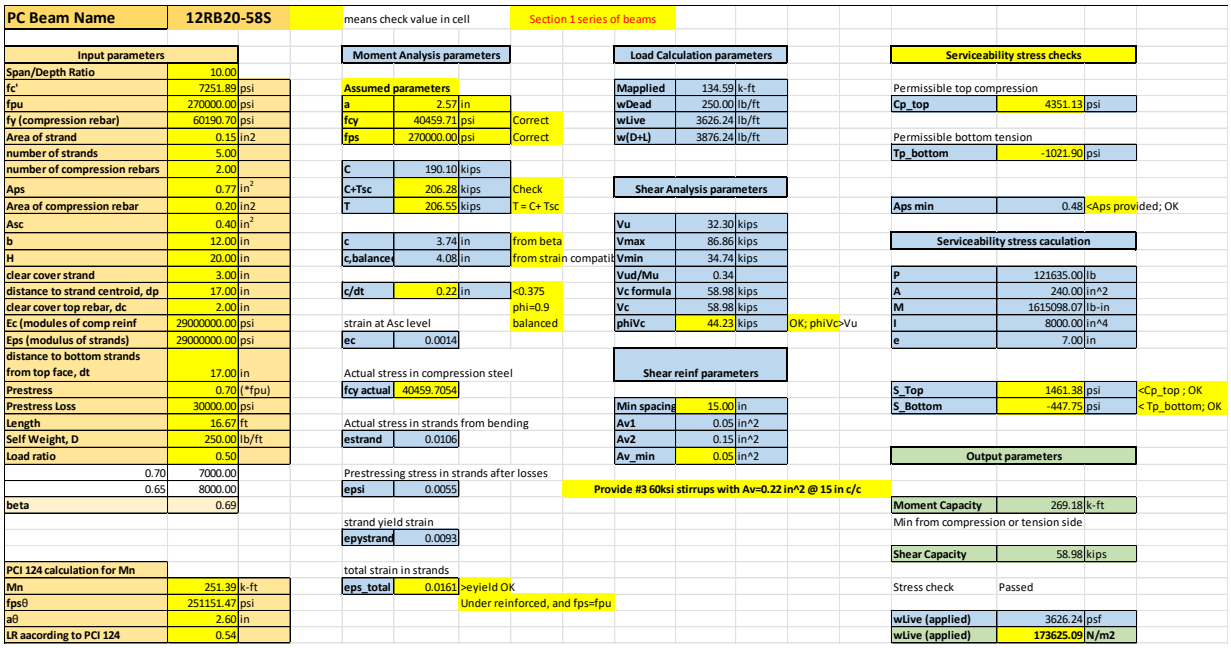

PC Beam Name	12RB20-58S		means check value in cell			Section 1 series of beams										
Input parameters			**Moment Analysis parameters**				**Load Calculation parameters**				**Serviceability stress checks**					
Span/Depth Ratio	10.00															
fc'	7251.89	psi	**Assumed parameters**				Mapplied	134.59	k-ft		Permissible top compression					
fpu	270000.00	psi	a	2.57	in		wDead	250.00	lb/ft		Cp_top	4351.13	psi			
fy (compression rebar)	60190.70	psi	fcy	40459.71	psi	Correct	wLive	3626.24	lb/ft							
Area of strand	0.15	in2	fps	270000.00	psi	Correct	w(D+L)	3876.24	lb/ft		Permissible bottom tension					
number of strands	5.00										Tp_bottom	-1021.90	psi			
number of compression rebars	2.00		C	190.10	kips											
Aps	0.77	in^2	C+Tsc	206.28	kips	Check	**Shear Analysis parameters**									
Area of compression rebar	0.20	in2	T	206.55	kips	T = C+ Tsc					Aps min	0.48	<Aps provided; OK			
Asc	0.40	in^2					Vu	32.30	kips							
b	12.00	in	c	3.74	in	from beta	Vmax	86.86	kips		**Serviceability stress caculation**					
H	20.00	in	c,balanced	4.08	in	from strain compatit	Vmin	34.74	kips							
clear cover strand	3.00	in					Vud/Mu	0.34			P	121635.00	lb			
distance to strand centroid, dp	17.00	in	c/dt	0.22	in	<0.375	Vc formula	58.98	kips		A	240.00	in^2			
clear cover top rebar, dc	2.00	in				phi=0.9	Vc	58.98	kips		M	1615098.07	lb-in			
Ec (modules of comp reinf	29000000.00	psi	strain at Asc level			balanced	phiVc	44.23	kips	OK; phiVc>Vu	I	8000.00	in^4			
Eps (modulus of strands)	29000000.00	psi	ec	0.0014							e	7.00	in			
distance to bottom strands from top face, dt	17.00	in	Actual stress in compression steel				**Shear reinf parameters**									
Prestress	0.70	(*fpu)	fcy actual	40459.7054							S_Top	1461.38	psi	<Cp_top ; OK		
Prestress Loss	30000.00	psi					Min spacing	15.00	in		S_Bottom	-447.75	psi	< Tp_bottom; OK		
Length	16.67	ft	Actual stress in strands from bending				Av1	0.05	in^2							
Self Weight, D	250.00	lb/ft	estrand	0.0106			Av2	0.15	in^2							
Load ratio	0.50						Av_min	0.05	in^2		**Output parameters**					
0.70	7000.00		Prestressing stress in strands after losses													
0.65	8000.00		epsi	0.0055			**Provide #3 60ksi stirrups with Av=0.22 in^2 @ 15 in c/c**									
beta	0.69										**Moment Capacity**	269.18	k-ft			
			strand yield strain								Min from compression or tension side					
			epystrand	0.0093												
											Shear Capacity	58.98	kips			
PCI 124 calculation for Mn			total strain in strands													
Mn	251.39	k-ft	eps_total	0.0161	>eyield OK						Stress check	Passed				
fpsθ	251151.47	psi			Under reinforced, and fps=fpu											
aθ	2.60	in									**wLive (applied)**	3626.24	psf			
LR aacording to PCI 124	0.54										**wLive (applied)**	**173625.09**	**N/m2**			

Figure A.1 Design of PC beams with Section 1 (12RB20)

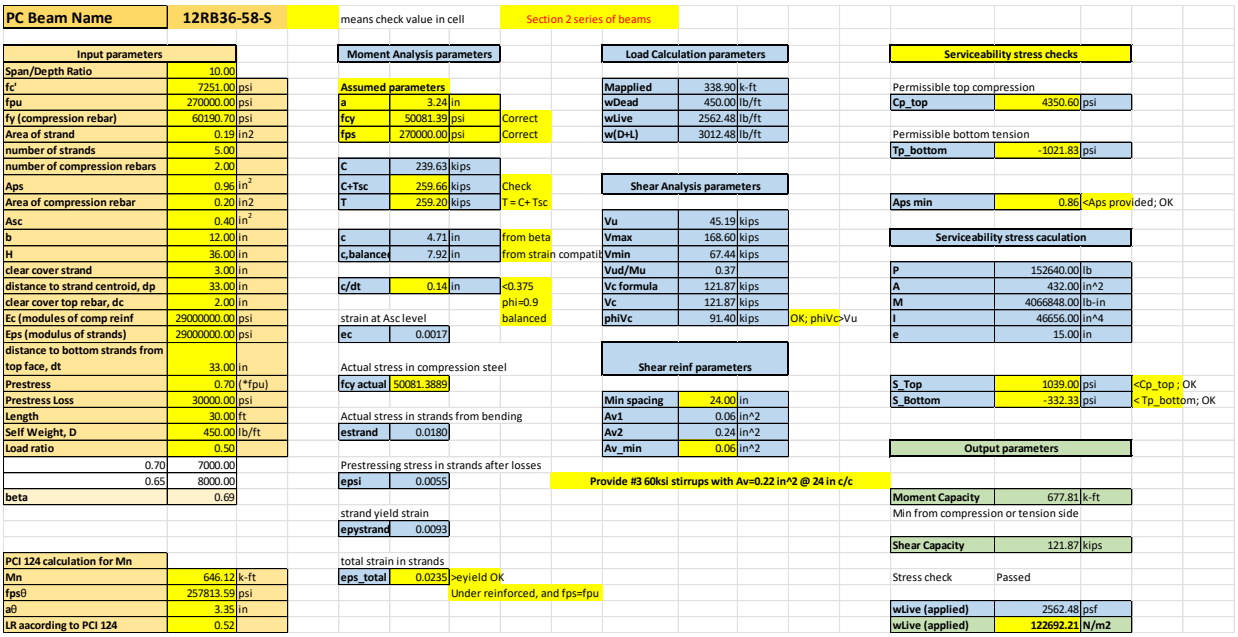

PC Beam Name	12RB36-58-S		means check value in cell			Section 2 series of beams													
Input parameters			**Moment Analysis parameters**				**Load Calculation parameters**						**Serviceability stress checks**						
Span/Depth Ratio	10.00																		
fc'	7251.00	psi	**Assumed parameters**				**Mapplied**	338.90	k-ft				Permissible top compression						
fpu	270000.00	psi	**a**	3.24	in		**wDead**	450.00	lb/ft				**Cp_top**	4350.60	psi				
fy (compression rebar)	60190.70	psi	**fcy**	50081.39	psi	Correct	**wLive**	2562.48	lb/ft										
Area of strand	0.19	in2	**fps**	270000.00	psi	Correct	**w(D+L)**	3012.48	lb/ft				Permissible bottom tension						
number of strands	5.00												**Tp_bottom**	-1021.83	psi				
number of compression rebars	2.00		**C**	239.63	kips														
Aps	0.96	in^2	**C+Tsc**	259.66	kips	Check	**Shear Analysis parameters**												
Area of compression rebar	0.20	in2	**T**	259.20	kips	T = C+ Tsc							**Aps min**	0.86	<Aps provided; OK				
Asc	0.40	in^2					**Vu**	45.19	kips										
b	12.00	in	**c**	4.71	in	from beta	**Vmax**	168.60	kips				**Serviceability stress caculation**						
H	36.00	in	**c,balance**	7.92	in	from strain compatil	**Vmin**	67.44	kips										
clear cover strand	3.00	in					**Vud/Mu**	0.37					**P**	152640.00	lb				
distance to strand centroid, dp	33.00	in	**c/dt**	0.14	in	<0.375	**Vc formula**	121.87	kips				**A**	432.00	in^2				
clear cover top rebar, dc	2.00	in				phi=0.9	**Vc**	121.87	kips				**M**	4066848.00	lb-in				
Ec (modules of comp reinf	29000000.00	psi	strain at Asc level			balanced	**phiVc**	91.40	kips	OK; phiVc>Vu			**I**	46656.00	in^4				
Eps (modulus of strands)	29000000.00	psi	**ec**	0.0017									**e**	15.00	in				
distance to bottom strands from top face, dt	33.00	in	Actual stress in compression steel				**Shear reinf parameters**												
Prestress	0.70	(*fpu)	**fcy actual**	50081.3889									**S_Top**	1039.00	psi	<Cp_top ; OK			
Prestress Loss	30000.00	psi					**Min spacing**	24.00	in				**S_Bottom**	-332.33	psi	< Tp_bottom; OK			
Length	30.00	ft	Actual stress in strands from bending				**Av1**	0.06	in^2										
Self Weight, D	450.00	lb/ft	**estrand**	0.0180			**Av2**	0.24	in^2										
Load ratio	0.50						**Av_min**	0.06	in^2				**Output parameters**						
0.70	7000.00		Prestressing stress in strands after losses																
0.65	8000.00		**epsi**	0.0055			**Provide #3 60ksi stirrups with Av=0.22 in^2 @ 24 in c/c**												
beta	0.69												**Moment Capacity**	677.81	k-ft				
			strand yield strain										Min from compression or tension side						
			epystrand	0.0093															
													Shear Capacity	121.87	kips				
PCI 124 calculation for Mn			total strain in strands																
Mn	646.12	k-ft	**eps_total**	0.0235	>eyield OK								Stress check	Passed					
fpsθ	257813.59	psi			Under reinforced, and fps=fpu														
aθ	3.35	in											**wLive (applied)**	2562.48	psf				
LR aacording to PCI 124	0.52												**wLive (applied)**	**122692.21**	**N/m2**				

Figure A.2 Design of PC beams with Section 2 (12RB36)

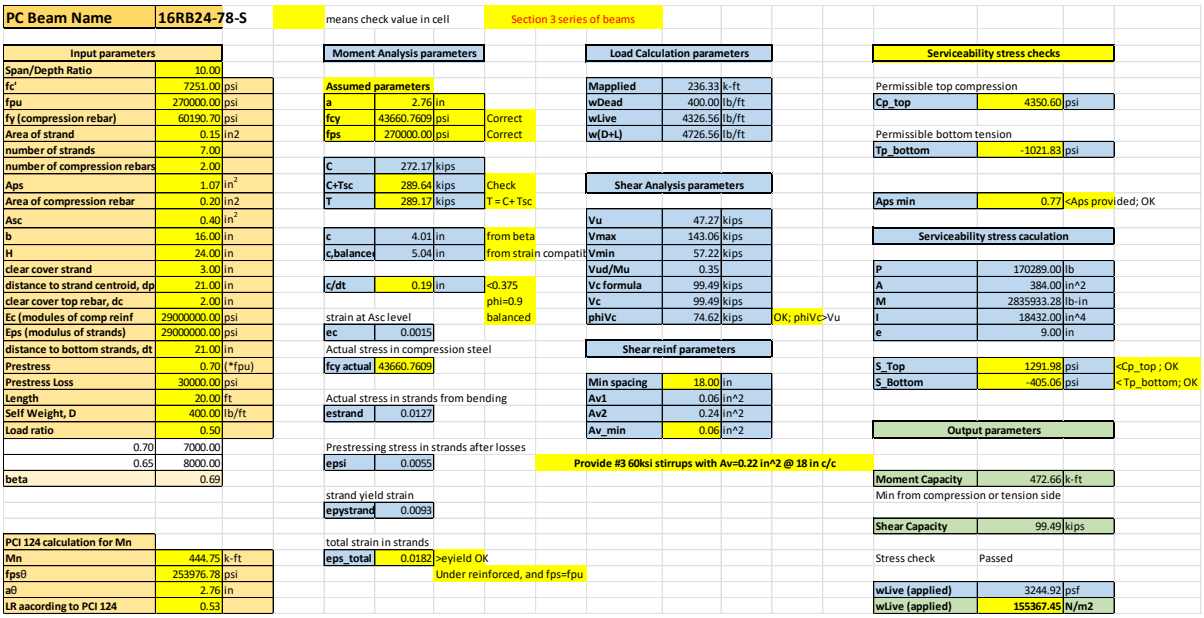

PC Beam Name	16RB24-78-S		means check value in cell			Section 3 series of beams												
Input parameters			**Moment Analysis parameters**				**Load Calculation parameters**						**Serviceability stress checks**					
Span/Depth Ratio	10.00																	
fc'	7251.00	psi	**Assumed parameters**				Mapplied	236.33	k-ft				Permissible top compression					
fpu	270000.00	psi	a	2.76	in		wDead	400.00	lb/ft				Cp_top	4350.60	psi			
fy (compression rebar)	60190.70	psi	fcy	43660.7609	psi	Correct	wLive	4326.56	lb/ft									
Area of strand	0.15	in2	fps	270000.00	psi	Correct	w(D+L)	4726.56	lb/ft				Permissible bottom tension					
number of strands	7.00												Tp_bottom	-1021.83	psi			
number of compression rebars	2.00		C	272.17	kips													
Aps	1.07	in^2	C+Tsc	289.64	kips	Check	**Shear Analysis parameters**											
Area of compression rebar	0.20	in2	T	289.17	kips	T = C+ Tsc							Aps min	0.77	<Aps provided; OK			
Asc	0.40	in^2					Vu	47.27	kips									
b	16.00	in	c	4.01	in	from beta	Vmax	143.06	kips				**Serviceability stress caculation**					
H	24.00	in	c,balanced	5.04	in	from strain compatit	Vmin	57.22	kips									
clear cover strand	3.00	in					Vud/Mu	0.35					P	170289.00	lb			
distance to strand centroid, dp	21.00	in	c/dt	0.19	in	<0.375	Vc formula	99.49	kips				A	384.00	in^2			
clear cover top rebar, dc	2.00	in				phi=0.9	Vc	99.49	kips				M	2835933.28	lb-in			
Ec (modules of comp reinf	29000000.00	psi	strain at Asc level			balanced	phiVc	74.62	kips	OK; phiVc>Vu			I	18432.00	in^4			
Eps (modulus of strands)	29000000.00	psi	ec	0.0015									e	9.00	in			
distance to bottom strands, dt	21.00	in	Actual stress in compression steel				**Shear reinf parameters**											
Prestress	0.70	(*fpu)	fcy actual	43660.7609									S_Top	1291.98	psi	<Cp_top ; OK		
Prestress Loss	30000.00	psi					Min spacing	18.00	in				S_Bottom	-405.06	psi	< Tp_bottom; OK		
Length	20.00	ft	Actual stress in strands from bending				Av1	0.06	in^2									
Self Weight, D	400.00	lb/ft	estrand	0.0127			Av2	0.24	in^2									
Load ratio	0.50						Av_min	0.06	in^2				**Output parameters**					
0.70	7000.00		Prestressing stress in strands after losses															
0.65	8000.00		epsi	0.0055			**Provide #3 60ksi stirrups with Av=0.22 in^2 @ 18 in c/c**						Moment Capacity	472.66	k-ft			
beta	0.69												Min from compression or tension side					
			strand yield strain															
			epystrand	0.0093														
													Shear Capacity	99.49	kips			
PCI 124 calculation for Mn			total strain in strands															
Mn	444.75	k-ft	eps_total	0.0182	>eyield OK								Stress check	Passed				
fpsθ	253976.78	psi			Under reinforced, and fps=fpu													
aθ	2.76	in											wLive (applied)	3244.92	psf			
LR aacording to PCI 124	0.53												wLive (applied)	155367.45	N/m2			

Figure A.3 Design of PC beams with Section 3 (16RB24)

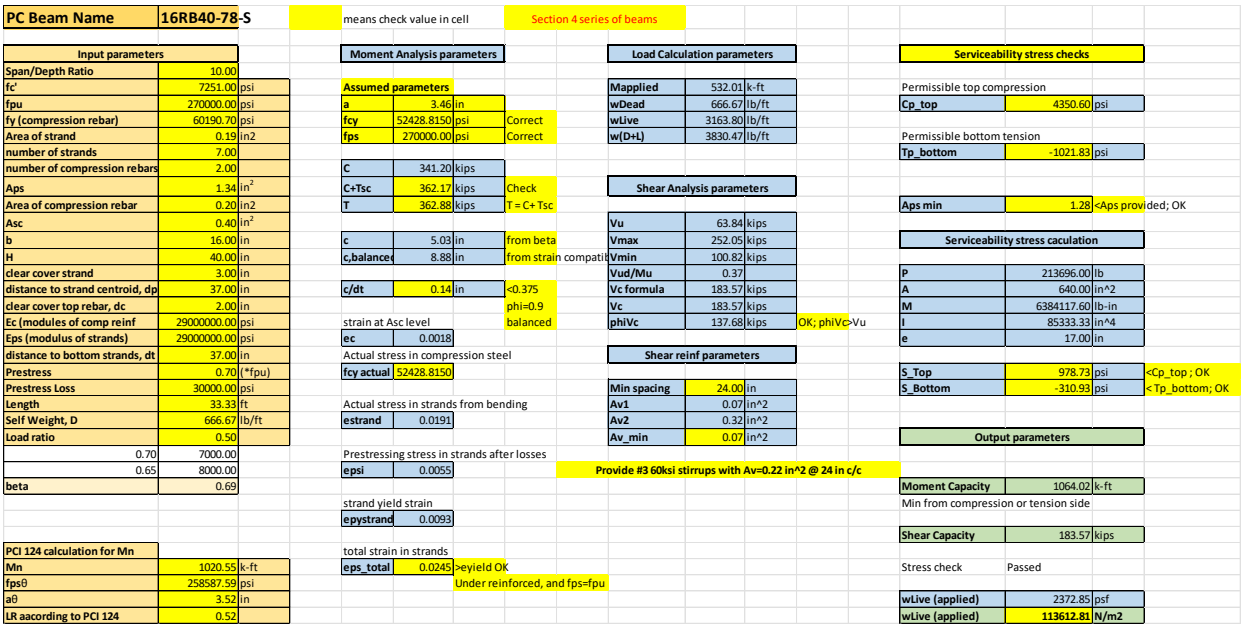

PC Beam Name	16RB40-78-S		means check value in cell			Section 4 series of beams											
Input parameters			**Moment Analysis parameters**				**Load Calculation parameters**						**Serviceability stress checks**				
Span/Depth Ratio	10.00																
fc'	7251.00	psi	**Assumed parameters**				Mapplied	532.01	k-ft				Permissible top compression				
fpu	270000.00	psi	a	3.46	in		wDead	666.67	lb/ft				Cp_top	4350.60	psi		
fy (compression rebar)	60190.70	psi	fcy	52428.8150	psi	Correct	wLive	3163.80	lb/ft								
Area of strand	0.19	in2	fps	270000.00	psi	Correct	w(D+L)	3830.47	lb/ft				Permissible bottom tension				
number of strands	7.00												Tp_bottom	-1021.83	psi		
number of compression rebars	2.00		C	341.20	kips												
Aps	1.34	in^2	C+Tsc	362.17	kips	Check	**Shear Analysis parameters**										
Area of compression rebar	0.20	in2	T	362.88	kips	T = C+ Tsc							Aps min	1.28	<Aps provided; OK		
Asc	0.40	in^2					Vu	63.84	kips								
b	16.00	in	c	5.03	in	from beta	Vmax	252.05	kips				**Serviceability stress caculation**				
H	40.00	in	c,balance	8.88	in	from strain compatit	Vmin	100.82	kips								
clear cover strand	3.00	in					Vud/Mu	0.37					P	213696.00	lb		
distance to strand centroid, dp	37.00	in	c/dt	0.14	in	<0.375	Vc formula	183.57	kips				A	640.00	in^2		
clear cover top rebar, dc	2.00	in				phi=0.9	Vc	183.57	kips				M	6384117.60	lb-in		
Ec (modules of comp reinf	29000000.00	psi	strain at Asc level			balanced	phiVc	137.68	kips	OK; phiVc>Vu			I	85333.33	in^4		
Eps (modulus of strands)	29000000.00	psi	ec	0.0018									e	17.00	in		
distance to bottom strands, dt	37.00	in	Actual stress in compression steel				**Shear reinf parameters**										
Prestress	0.70	(*fpu)	fcy actual	52428.8150									S_Top	978.73	psi	<Cp_top ; OK	
Prestress Loss	30000.00	psi					Min spacing	24.00	in				S_Bottom	-310.93	psi	< Tp_bottom; OK	
Length	33.33	ft	Actual stress in strands from bending				Av1	0.07	in^2								
Self Weight, D	666.67	lb/ft	estrand	0.0191			Av2	0.32	in^2								
Load ratio	0.50						Av_min	0.07	in^2				**Output parameters**				
0.70	7000.00		Prestressing stress in strands after losses														
0.65	8000.00		epsi	0.0055			**Provide #3 60ksi stirrups with Av=0.22 in^2 @ 24 in c/c**										
beta	0.69												**Moment Capacity**	1064.02	k-ft		
			strand yield strain										Min from compression or tension side				
			epystrand	0.0093													
													Shear Capacity	183.57	kips		
PCI 124 calculation for Mn			total strain in strands														
Mn	1020.55	k-ft	eps_total	0.0245	>eyield OK								Stress check	Passed			
fpsθ	258587.59	psi			Under reinforced, and fps=fpu												
aθ	3.52	in											**wLive (applied)**	2372.85	psf		
LR aacording to PCI 124	0.52												**wLive (applied)**	**113612.81**	**N/m2**		

Figure A.4 Design of PC beams with Section 3 (16RB40)

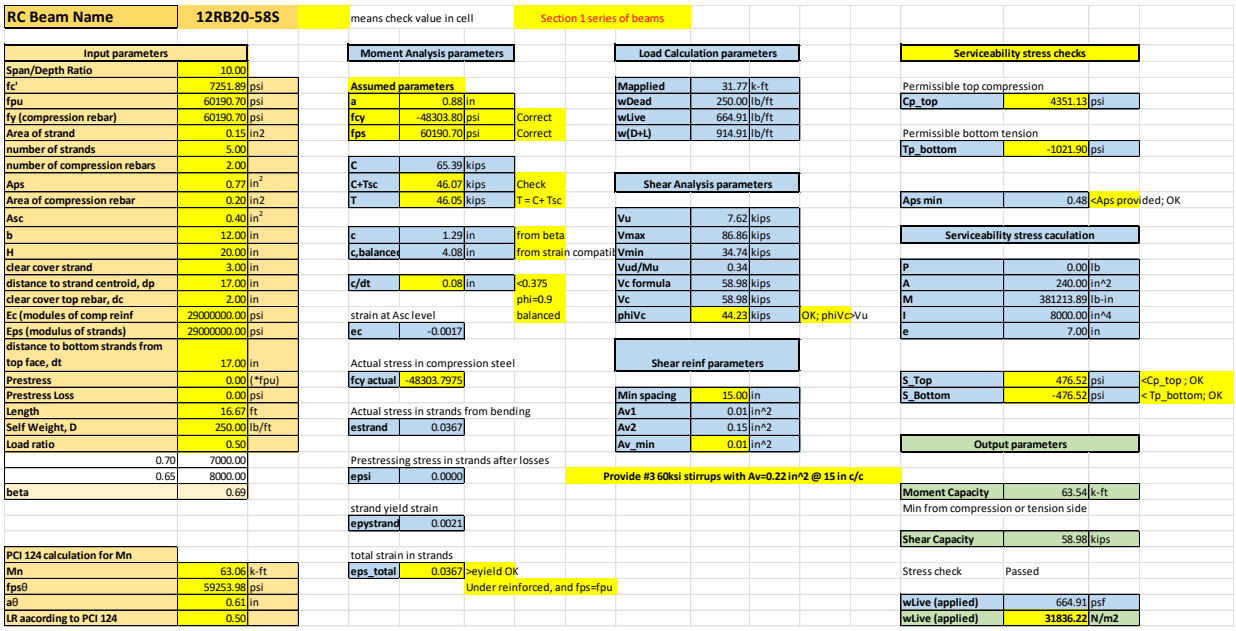

RC Beam Name	12RB20-58S		means check value in cell			Section 1 series of beams									
Input parameters			**Moment Analysis parameters**				**Load Calculation parameters**				**Serviceability stress checks**				
Span/Depth Ratio	10.00														
fc'	7251.89	psi	**Assumed parameters**				**Mapplied**	31.77	k-ft		Permissible top compression				
fpu	60190.70	psi	**a**	0.88	in		**wDead**	250.00	lb/ft		**Cp_top**	4351.13	psi		
fy (compression rebar)	60190.70	psi	**fcy**	-48303.80	psi	Correct	**wLive**	664.91	lb/ft						
Area of strand	0.15	in2	**fps**	60190.70	psi	Correct	**w(D+L)**	914.91	lb/ft		Permissible bottom tension				
number of strands	5.00										**Tp_bottom**	-1021.90	psi		
number of compression rebars	2.00		**C**	65.39	kips										
Aps	0.77	in^2	**C+Tsc**	46.07	kips	Check	**Shear Analysis parameters**								
Area of compression rebar	0.20	in2	**T**	46.05	kips	T = C+ Tsc					**Aps min**	0.48	<Aps provided; OK		
Asc	0.40	in^2					**Vu**	7.62	kips						
b	12.00	in	**c**	1.29	in	from beta	**Vmax**	86.86	kips		**Serviceability stress caculation**				
H	20.00	in	**c,balance**	4.08	in	from strain compatil	**Vmin**	34.74	kips						
clear cover strand	3.00	in					**Vud/Mu**	0.34			**P**	0.00	lb		
distance to strand centroid, dp	17.00	in	**c/dt**	0.08	in	<0.375	**Vc formula**	58.98	kips		**A**	240.00	in^2		
clear cover top rebar, dc	2.00	in				phi=0.9	**Vc**	58.98	kips		**M**	381213.89	lb-in		
Ec (modules of comp reinf	29000000.00	psi	strain at Asc level			balanced	**phiVc**	44.23	kips	OK; phiVc>Vu	**I**	8000.00	in^4		
Eps (modulus of strands)	29000000.00	psi	**ec**	-0.0017							**e**	7.00	in		
distance to bottom strands from top face, dt	17.00	in	Actual stress in compression steel				**Shear reinf parameters**								
Prestress	0.00	(*fpu)	**fcy actual**	-48303.7975							**S_Top**	476.52	psi	<Cp_top ; OK	
Prestress Loss	0.00	psi					**Min spacing**	15.00	in		**S_Bottom**	-476.52	psi	< Tp_bottom; OK	
Length	16.67	ft	Actual stress in strands from bending				**Av1**	0.01	in^2						
Self Weight, D	250.00	lb/ft	**estrand**	0.0367			**Av2**	0.15	in^2						
Load ratio	0.50						**Av_min**	0.01	in^2		**Output parameters**				
0.70	7000.00		Prestressing stress in strands after losses												
0.65	8000.00		**epsi**	0.0000			**Provide #3 60ksi stirrups with Av=0.22 in^2 @ 15 in c/c**								
beta	0.69										**Moment Capacity**	63.54	k-ft		
			strand yield strain								Min from compression or tension side				
			epystrand	0.0021											
											Shear Capacity	58.98	kips		
PCI 124 calculation for Mn			total strain in strands												
Mn	63.06	k-ft	**eps_total**	0.0367	>eyield OK						Stress check	Passed			
fpsθ	59253.98	psi			Under reinforced, and fps=fpu										
aθ	0.61	in									**wLive (applied)**	664.91	psf		
LR aacording to PCI 124	0.50										**wLive (applied)**	**31836.22**	**N/m2**		

Figure A.5 Design of equivalent RC beams with Section 1 (12RB20)

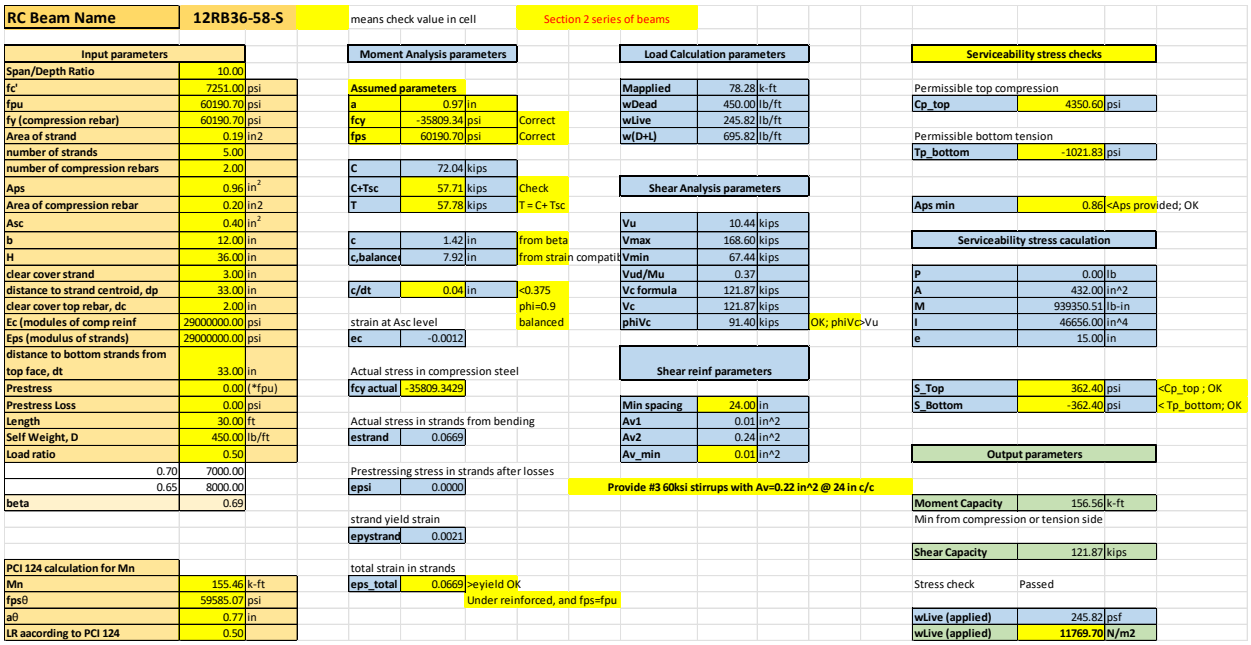

RC Beam Name	12RB36-58-S		means check value in cell			Section 2 series of beams													
Input parameters			**Moment Analysis parameters**				**Load Calculation parameters**						**Serviceability stress checks**						
Span/Depth Ratio	10.00																		
fc'	7251.00	psi	**Assumed parameters**				**Mapplied**	78.28	k-ft				Permissible top compression						
fpu	60190.70	psi	a	0.97	in		**wDead**	450.00	lb/ft				**Cp_top**	4350.60	psi				
fy (compression rebar)	60190.70	psi	fcy	-35809.34	psi	Correct	**wLive**	245.82	lb/ft										
Area of strand	0.19	in2	fps	60190.70	psi	Correct	**w(D+L)**	695.82	lb/ft				Permissible bottom tension						
number of strands	5.00												**Tp_bottom**	-1021.83	psi				
number of compression rebars	2.00		C	72.04	kips														
Aps	0.96	in^2	C+Tsc	57.71	kips	Check	**Shear Analysis parameters**												
Area of compression rebar	0.20	in2	T	57.78	kips	T = C+ Tsc							**Aps min**	0.86	<Aps provided; OK				
Asc	0.40	in^2					**Vu**	10.44	kips										
b	12.00	in	c	1.42	in	from beta	**Vmax**	168.60	kips				**Serviceability stress caculation**						
H	36.00	in	c,balanced	7.92	in	from strain compatibi	**Vmin**	67.44	kips										
clear cover strand	3.00	in					**Vud/Mu**	0.37					**P**	0.00	lb				
distance to strand centroid, dp	33.00	in	c/dt	0.04	in	<0.375	**Vc formula**	121.87	kips				**A**	432.00	in^2				
clear cover top rebar, dc	2.00	in				phi=0.9	**Vc**	121.87	kips				**M**	939350.51	lb-in				
Ec (modules of comp reinf	29000000.00	psi	strain at Asc level			balanced	**phiVc**	91.40	kips	OK; phiVc>Vu			**I**	46656.00	in^4				
Eps (modulus of strands)	29000000.00	psi	ec	-0.0012									**e**	15.00	in				
distance to bottom strands from top face, dt	33.00	in	Actual stress in compression steel				**Shear reinf parameters**												
Prestress	0.00	(*fpu)	fcy actual	-35809.3429									**S_Top**	362.40	psi	<Cp_top ; OK			
Prestress Loss	0.00	psi					**Min spacing**	24.00	in				**S_Bottom**	-362.40	psi	< Tp_bottom; OK			
Length	30.00	ft	Actual stress in strands from bending				**Av1**	0.01	in^2										
Self Weight, D	450.00	lb/ft	estrand	0.0669			**Av2**	0.24	in^2										
Load ratio	0.50						**Av_min**	0.01	in^2				**Output parameters**						
0.70	7000.00		Prestressing stress in strands after losses																
0.65	8000.00		epsi	0.0000			**Provide #3 60ksi stirrups with Av=0.22 in^2 @ 24 in c/c**												
beta	0.69												**Moment Capacity**	156.56	k-ft				
			strand yield strain										Min from compression or tension side						
			epystrand	0.0021															
													Shear Capacity	121.87	kips				
PCI 124 calculation for Mn			total strain in strands																
Mn	155.46	k-ft	eps_total	0.0669	>eyield OK								Stress check	Passed					
fpsθ	59585.07	psi			Under reinforced, and fps=fpu														
aθ	0.77	in											**wLive (applied)**	245.82	psf				
LR aacording to PCI 124	0.50												**wLive (applied)**	**11769.70**	**N/m2**				

Figure A.6 Design of equivalent RC beams with Section 2 (12RB36)

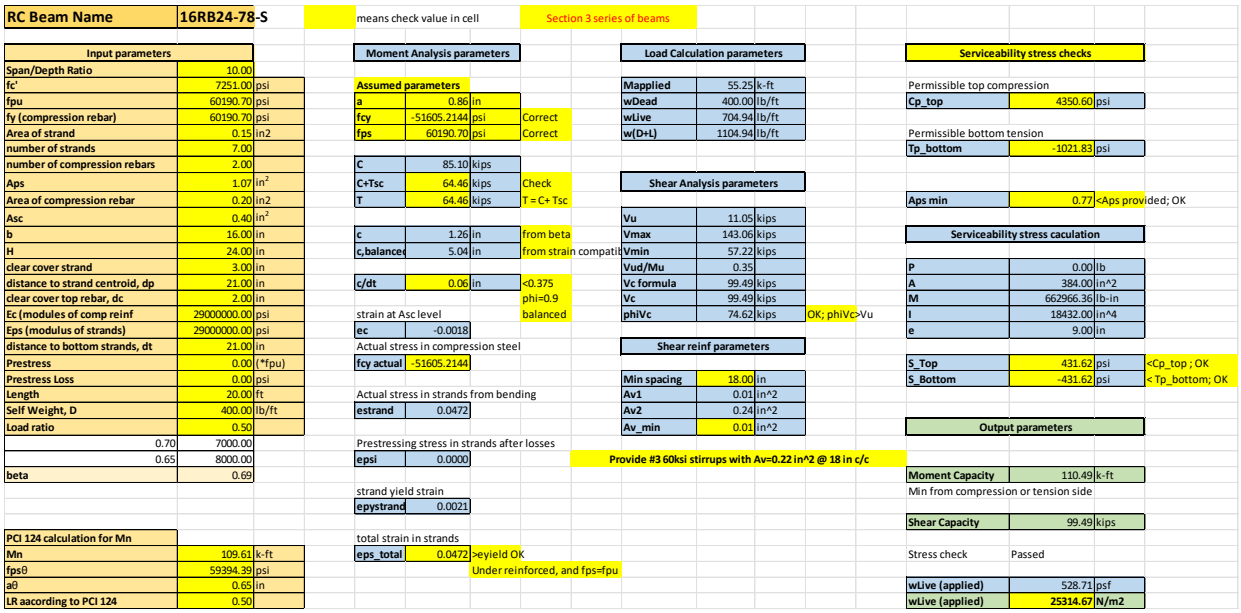

RC Beam Name	16RB24-78-S		means check value in cell			Section 3 series of beams											
Input parameters			**Moment Analysis parameters**				**Load Calculation parameters**					**Serviceability stress checks**					
Span/Depth Ratio	10.00																
fc'	7251.00	psi	**Assumed parameters**				Mapplied	55.25	k-ft			Permissible top compression					
fpu	60190.70	psi	a	0.86	in		wDead	400.00	lb/ft			Cp_top	4350.60	psi			
fy (compression rebar)	60190.70	psi	fcy	-51605.2144	psi	Correct	wLive	704.94	lb/ft								
Area of strand	0.15	in2	fps	60190.70	psi	Correct	w(D+L)	1104.94	lb/ft			Permissible bottom tension					
number of strands	7.00											Tp_bottom	-1021.83	psi			
number of compression rebars	2.00		C	85.10	kips												
Aps	1.07	in^2	C+Tsc	64.46	kips	Check	**Shear Analysis parameters**										
Area of compression rebar	0.20	in2	T	64.46	kips	T = C+ Tsc						Aps min	0.77	<Aps provided; OK			
Asc	0.40	in^2					Vu	11.05	kips								
b	16.00	in	c	1.26	in	from beta	Vmax	143.06	kips			**Serviceability stress caculation**					
H	24.00	in	c,balanced	5.04	in	from strain compatit	Vmin	57.22	kips								
clear cover strand	3.00	in					Vud/Mu	0.35				P	0.00	lb			
distance to strand centroid, dp	21.00	in	c/dt	0.06	in	<0.375	Vc formula	99.49	kips			A	384.00	in^2			
clear cover top rebar, dc	2.00	in				phi=0.9	Vc	99.49	kips			M	662966.36	lb-in			
Ec (modules of comp reinf	29000000.00	psi	strain at Asc level			balanced	phiVc	74.62	kips	OK; phiVc>Vu		I	18432.00	in^4			
Eps (modulus of strands)	29000000.00	psi	ec	-0.0018								e	9.00	in			
distance to bottom strands, dt	21.00	in	Actual stress in compression steel				**Shear reinf parameters**										
Prestress	0.00	(*fpu)	fcy actual	-51605.2144								S_Top	431.62	psi	<Cp_top ; OK		
Prestress Loss	0.00	psi					Min spacing	18.00	in			S_Bottom	-431.62	psi	< Tp_bottom; OK		
Length	20.00	ft	Actual stress in strands from bending				Av1	0.01	in^2								
Self Weight, D	400.00	lb/ft	estrand	0.0472			Av2	0.24	in^2								
Load ratio	0.50						Av_min	0.01	in^2			**Output parameters**					
0.70	7000.00		Prestressing stress in strands after losses														
0.65	8000.00		epsi	0.0000			**Provide #3 60ksi stirrups with Av=0.22 in^2 @ 18 in c/c**										
beta	0.69											Moment Capacity	110.49	k-ft			
			strand yield strain									Min from compression or tension side					
			epystrand	0.0021													
												Shear Capacity	99.49	kips			
PCI 124 calculation for Mn			total strain in strands														
Mn	109.61	k-ft	eps_total	0.0472	>eyield OK							Stress check	Passed				
fpsθ	59394.39	psi			Under reinforced, and fps=fpu												
aθ	0.65	in										wLive (applied)	528.71	psf			
LR aacording to PCI 124	0.50											wLive (applied)	25314.67	N/m2			

Figure A.7 Design of equivalent RC beams with Section 3 (16RB24)

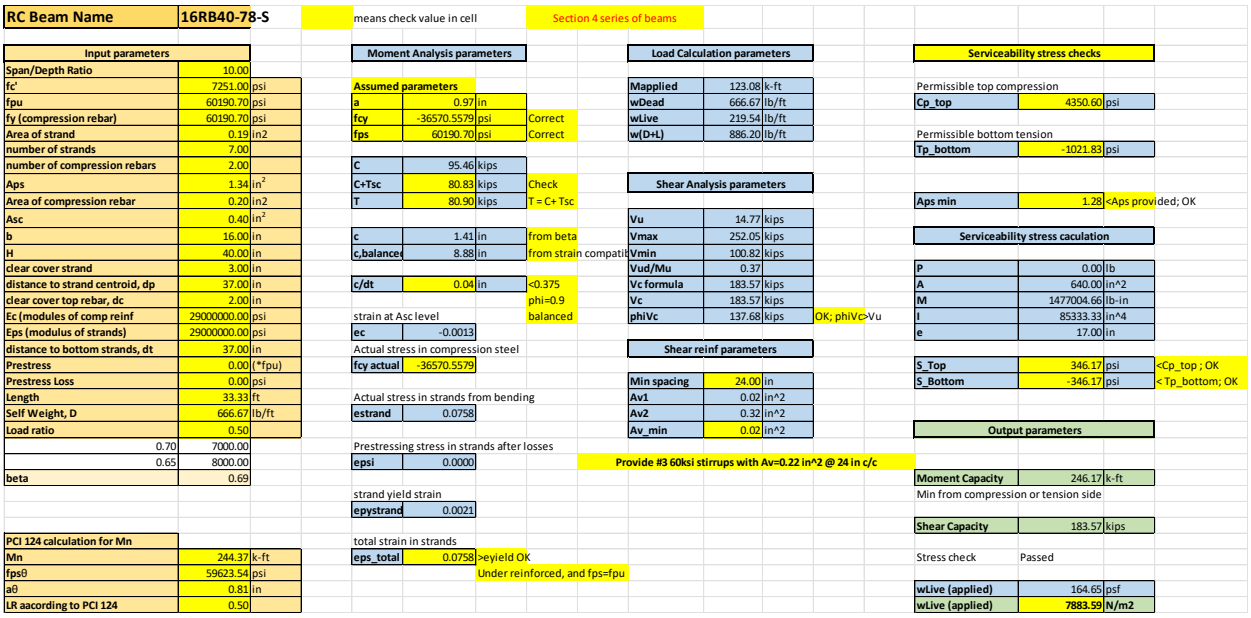

RC Beam Name	16RB40-78-S		means check value in cell			Section 4 series of beams											
Input parameters			**Moment Analysis parameters**				**Load Calculation parameters**						**Serviceability stress checks**				
Span/Depth Ratio	10.00																
fc'	7251.00	psi	**Assumed parameters**				**Mapplied**	123.08	k-ft				Permissible top compression				
fpu	60190.70	psi	**a**	0.97	in		**wDead**	666.67	lb/ft				**Cp_top**	4350.60	psi		
fy (compression rebar)	60190.70	psi	**fcy**	-36570.5579	psi	Correct	**wLive**	219.54	lb/ft								
Area of strand	0.19	in2	**fps**	60190.70	psi	Correct	**w(D+L)**	886.20	lb/ft				Permissible bottom tension				
number of strands	7.00												**Tp_bottom**	-1021.83	psi		
number of compression rebars	2.00		**C**	95.46	kips												
Aps	1.34	in^2	**C+Tsc**	80.83	kips	Check	**Shear Analysis parameters**										
Area of compression rebar	0.20	in2	**T**	80.90	kips	T = C+ Tsc							**Aps min**	1.28	<Aps provided; OK		
Asc	0.40	in^2					**Vu**	14.77	kips								
b	16.00	in	**c**	1.41	in	from beta	**Vmax**	252.05	kips				**Serviceability stress caculation**				
H	40.00	in	**c,balanced**	8.88	in	from strain compatit	**Vmin**	100.82	kips								
clear cover strand	3.00	in					**Vud/Mu**	0.37					**P**	0.00	lb		
distance to strand centroid, dp	37.00	in	**c/dt**	0.04	in	<0.375	**Vc formula**	183.57	kips				**A**	640.00	in^2		
clear cover top rebar, dc	2.00	in				phi=0.9	**Vc**	183.57	kips				**M**	1477004.66	lb-in		
Ec (modules of comp reinf	29000000.00	psi	strain at Asc level			balanced	**phiVc**	137.68	kips	OK; phiVc>Vu			**I**	85333.33	in^4		
Eps (modulus of strands)	29000000.00	psi	**ec**	-0.0013									**e**	17.00	in		
distance to bottom strands, dt	37.00	in	Actual stress in compression steel				**Shear reinf parameters**										
Prestress	0.00	(*fpu)	**fcy actual**	-36570.5579									**S_Top**	346.17	psi	<Cp_top ; OK	
Prestress Loss	0.00	psi					**Min spacing**	24.00	in				**S_Bottom**	-346.17	psi	< Tp_bottom; OK	
Length	33.33	ft	Actual stress in strands from bending				**Av1**	0.02	in^2								
Self Weight, D	666.67	lb/ft	**estrand**	0.0758			**Av2**	0.32	in^2								
Load ratio	0.50						**Av_min**	0.02	in^2				**Output parameters**				
0.70	7000.00		Prestressing stress in strands after losses														
0.65	8000.00		**epsi**	0.0000			**Provide #3 60ksi stirrups with Av=0.22 in^2 @ 24 in c/c**										
beta	0.69												**Moment Capacity**	246.17	k-ft		
			strand yield strain										Min from compression or tension side				
			epystrand	0.0021													
													Shear Capacity	183.57	kips		
PCI 124 calculation for Mn			total strain in strands														
Mn	244.37	k-ft	**eps_total**	0.0758	>eyield OK								Stress check	Passed			
fpsθ	59623.54	psi			Under reinforced, and fps=fpu												
aθ	0.81	in											**wLive (applied)**	164.65	psf		
LR aacording to PCI 124	0.50												**wLive (applied)**	**7883.59**	**N/m2**		

Figure A.8 Design of equivalent RC beams with Section 4 (16RB40)

APPENDIX B: IDEALIZATION OF CONNECTION FOR PARAMETRIC STUDIES

The connections used in the parametric studies are idealized using the simplified spring framework discussed in Section 4.4. For simplicity, column sizes at the connections are assumed to have the same width as beams for all idealized connections. The stiffness parameters for all beams are illustrated in Figures B.1 to B.4.

PC Beam	12RB20-58S	
b	3.05E-01	m
H	5.08E-01	m
Aps	4.94E-04	m2
Asc	2.58E-04	m2
Es	2.00E+11	Pa
Ec	2.91E+10	Pa
Beam Length	5.08E+00	m
%steel	4.85E-03	
%concrete	9.95E-01	

Column	12 x 12	in
Column	0.305 x 0.305	m
b	0.305	m
H	0.305	m
Ec	2.91E+10	Pa
Lc	4.50E+00	m

A	1.55E-01	m2
E(composite)	2.99E+10	Pa
B_Iy	1.20E-03	m4
C_Iz	7.21E-04	m4

Simply supported	KB1	KB2	KB3	KB4	KC1	KC2	Total	
N/m		9.11E+08			2.84E+06	2.84E+06	9.17E+08	N/m
							9.17E+02	kN/mm

Moment resisting	KB1	KB2	KB3	KB4	KC1	KC2	Total	
N/m		9.11E+08	3.28E+06	3.28E+06	2.84E+06	2.84E+06	9.24E+08	N/m
							9.24E+02	kN/mm

number of springs, n	1	
K1	5678739.43	N/m
K2	917007534.26	N/m

C1 and C2 are assumed to have same length

Figure B.1 Design of idealized spring connection for beams with Section 1 (12RB20)

PC Beam	12RB36-58-S	
b	3.05E-01	m
H	9.14E-01	m
Aps	6.19E-04	m2
Asc	2.58E-04	m2
Es	2.00E+11	Pa
Ec	2.91E+10	Pa
Beam Length	9.14E+00	m
%steel	3.15E-03	
%concrete	9.97E-01	

Column	12 x 12	in
Column	0.305 x 0.305	m
b	0.305	m
H	0.305	m
Ec	2.91E+10	Pa
Lc	4.50E+00	m

A	2.79E-01	m2
E(composite)	2.96E+10	Pa
B_Iy	2.16E-03	m4
C_Iz	7.21E-04	m4

Simply supported

	KB1	KB2	KB3	KB4	KC1	KC2	Total	
N/m		9.02E+08			2.81E+06	2.81E+06	9.08E+08	N/m
							9.08E+02	kN/mm

Moment resisting

C1 and C2 are assumed to have length

	KB1	KB2	KB3	KB4	KC1	KC2	Total	
N/m		9.02E+08	1.00E+06	1.00E+06	2.81E+06	2.81E+06	9.10E+08	N/m
							9.10E+02	kN/mm

number of springs, n	1	
K1	5623371.01	N/m
K2	908066594.68	N/m

Figure B.2 Design of idealized spring connection for beams with Section 2 (12RB36)

PC Beam	16RB24-78-S	
b	4.06E-01	m
H	6.10E-01	m
Aps	6.91E-04	m2
Asc	2.58E-04	m2
Es	2.00E+11	Pa
Ec	2.91E+10	Pa
Beam Length	6.10E+00	m
%steel	3.83E-03	
%concrete	9.96E-01	

Column	16 x 16	in
Side	16	in
b	0.4064	m
H	0.4064	m
Ec	2.91E+10	Pa
Lc	4.50E+00	m

A	2.48E-01	m2
E(composite)	2.97E+10	Pa
B_Iy	3.41E-03	m4
C_Iz	2.27E-03	m4

Simply supported	KB1	KB2	KB3	KB4	KC1	KC2	Total	
N/m		1.21E+09			8.90E+06	8.90E+06	1.23E+09	N/m
							1.23E+03	kN/mm

Moment resisting	KB1	KB2	KB3	KB4	KC1	KC2	Total	
N/m		1.21E+09	5.37E+06	5.37E+06	8.90E+06	8.90E+06	1.24E+09	N/m
							1.24E+03	kN/mm

C1 and C2 are assumed to have same length

number of springs, n	1	
K1	17795889.42	N/m
K2	1225793697.91	N/m

Figure B.3 Design of idealized spring connection for beams with Section 3 (16RB24)

PC Beam	16RB40-78-S	
b	4.06E-01	m
H	1.02E+00	m
Aps	8.67E-04	m2
Asc	2.58E-04	m2
Es	2.00E+11	Pa
Ec	2.91E+10	Pa
Beam Length	1.02E+01	m
%steel	2.73E-03	
%concrete	9.97E-01	

Column	16 x 16	in
Side	16	in
b	0.4064	m
H	0.4064	m
Ec	2.91E+10	Pa
Lc	4.50E+00	m

A	4.13E-01	m2
E(composite)	2.95E+10	Pa
B_Iy	5.68E-03	m4
C_Iz	2.27E-03	m4

number of springs, n	1	
K1	17682768.57	N/m
K2	1218001852.13	N/m

Simply supported	KB1	KB2	KB3	KB4	KC1	KC2	Total	
N/m		1.20E+09			8.84E+06	8.84E+06	1.22E+09	N/m
							1.22E+03	kN/mm

Moment resisting	KB1	KB2	KB3	KB4	KC1	KC2	Total	
N/m		1.20E+09	1.92E+06	1.92E+06	8.84E+06	8.84E+06	1.22E+09	N/m
							1.22E+03	kN/mm

C1 and C2 are assumed to have same length

Figure B.4 Design of idealized spring connection for beams with Section 4 (16RB40)

APPENDIX C: BEAM CONDITIONS UNDER FIRE TESTS

Several pictures were taken during fire tests to monitor the progression of spalling. Few of these images are included here from casting of the beams to failure stage.

Figure C.1 Installation of thermocouples in PC beams at key locations

Figure C.2 Installation of strain gauges in PC beams at key locations

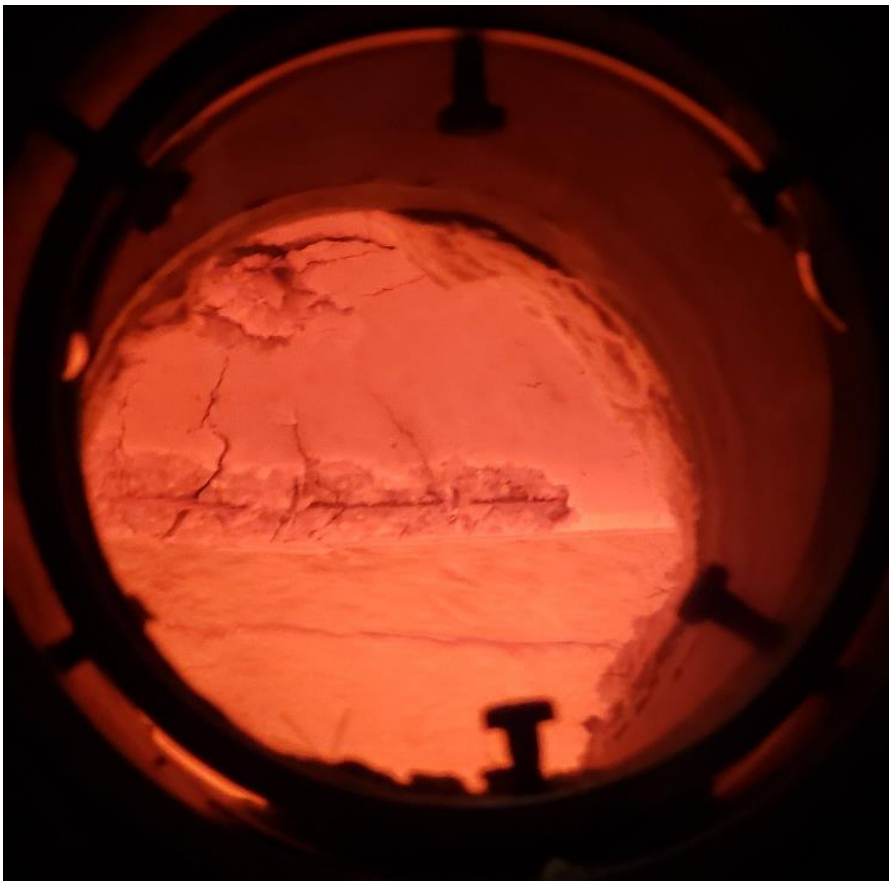

Figure C.3 Cracking and crushing of concrete in beam N1 during failure

Figure C.4 Cracking and crushing of concrete in beam N1R after failure

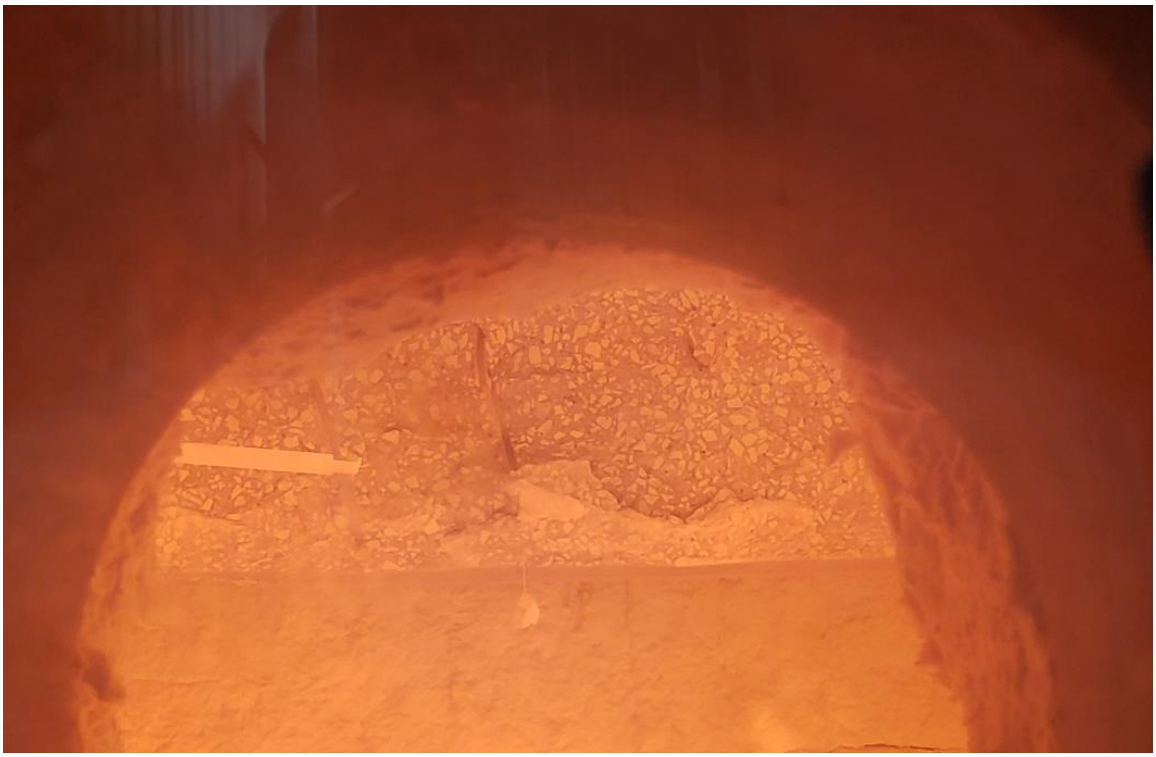

Figure C.5 Cracking and crushing of concrete in beam H1 at 40 minutes of fire exposure

Figure C.6 Cracking and crushing of concrete in beam H1R at 40 minutes of fire exposure